University of Glasgow | College of Medical, Veterinary & Life Sciences

The role of the human Discs large homologue-1 (Dlg1) in the Connexin 43 (Cx43) lifecycle and wound healing in keratinocytes

Harry Scott

BSc

Submitted in the fulfilment of the requirements for the Degree of Doctor of Philosophy

MRC-Centre for Virus Research

School of Infection and Immunity

College of Medical, Veterinary and Life Sciences

University of Glasgow

December 2023

Abstract

Gap junctions, which are formed by connexin proteins, are responsible for direct intercellular communication between adjacent cells by allowing the exchange of ions, metabolites, secondary messengers and microRNAs. Through this function, gap junctions are essential in maintaining homeostasis. Connexin 43 (Cx43) is a ubiquitous member of the gap junction family of proteins, being expressed in a diverse range of cells such as keratinocytes, cardiomyocytes and neurons. Alterations in Cx43 expression and function are associated with various disease states, including chronic non-healing wounds, which do not progress through the normal stages of wound healing in an orderly fashion. Chronic wounds are especially prevalent in patients suffering from diabetes and impose a massive economic and health burden worldwide, partially due to a lack of effective treatment options.

Discs large protein was originally discovered in *Drosophila* and acts as a tumour suppressor. The mammalian homologue of Discs large, human Discs large homologue-1 (Dlg1), is a cell polarity and scaffolding protein which has previously been shown to interact with Cx43 *in vitro* in various epithelial cell lines and *in vivo* in human cervical mucosal epithelial tissue. The interaction of Cx43 and Dlg1 was further investigated in this study.

In order to determine the role of Dlg1 in the Cx43 lifecycle, Dlg1 was depleted in HaCaT cells, a human epithelial cell line. Knockdown of Dlg1 decreased Cx43 on the plasma membrane and reduced overall Cx43 protein levels, but had no effect on Cx43 mRNA levels, indicating that Dlg1 has an important function in the Cx43 lifecycle. Cx43 colocalisation with a marker of the endoplasmic reticulum also decreased, while association with the lysosomes and, particularly, the Golgi increased, revealing Dlg1 depletion causes accumulation of Cx43 in these subcellular compartments. Treatment of cells with a lysosomal inhibitor resulted in a higher fold increase in Cx43 levels in siDlg1-treated cells compared

to mock-treated cells, suggesting increased Cx43 degradation through this pathway in cells where Dlg1 is knocked down. Depletion of Dlg1 also caused significantly reduced gap junctional intercellular communication between cells, signifying that Dlg1 controls gap junctional signalling. Based on these data, Dlg1 is suggested to be involved in forward trafficking of Cx43 to the plasma membrane or stabilisation of Cx43 at the plasma membrane, or perhaps a combination of the two.

Due to its role in maintaining Cx43 at the plasma membrane, it was hypothesised that removal of Dlg1 may improve wound healing rates, as Cx43 is frequently upregulated in cells at the wound edge of chronic wounds. Therefore, scratch wound assays were carried out on HaCaT cells with and without siDlg1 treatment. Surprisingly, Dlg1 depletion resulted in reduced wound closure rates due to an inhibition of cell proliferation, demonstrating that Dlg1 has other crucial functions in the cell which outweigh the benefit gained by removal of Cx43 from the plasma membrane. Cx43 and Dlg1 were also observed to colocalise in live cell wound closure experiments using HEK293 cells, with both proteins being detected at the cell membrane and at the tips of cellular protrusions of cells migrating into the wound area. The localisation of the two proteins was also investigated in diabetic and non-diabetic human skin in immunofluorescence experiments. The two proteins were found to colocalise at the plasma membrane of cells in different sublayers of the epidermis and colocalisation was additionally observed in dermal cells and adipocytes, suggesting the interaction is conserved in a range of cell types.

Finally, the interaction between the Cx43 C-terminal tail and Dlg1 SH3/HOOK/pGUK domains was investigated through the use of AlphaFold, which modelled the interaction of the two proteins. Three potential sites of interaction with the Dlg1 SH3/HOOK/pGUK domains were observed within the Cx43 C-terminus. Expression vectors for the Cx43 C-terminus (and deletions of putative interaction sites) and Dlg1 SH3/HOOK/pGUK were designed for experimental testing to confirm the accuracy of the AlphaFold model. Further

experiments involving these recombinant proteins will reveal the molecular determinants of Cx43/Dlg1 interaction, as well as whether phosphorylation affects the interaction.

Overall, this thesis builds on previous work on the Cx43/Dlg1 interaction, further defining the role of Dlg1 in the Cx43 lifecycle. It also provides the first demonstration that Dlg1 is an important component of the normal wound healing process in keratinocytes and defines three potential interaction sites with Dlg1 within the Cx43 C-terminus. Future research will determine whether disruption of the Cx43/Dlg1 interaction can improve wound healing rates and therefore whether the interaction may be a viable therapeutic target.

Table of Contents

List of Tables

List of Figures

Publications

The human discs large protein 1 interacts with and maintains connexin 43 at the plasma membrane in keratinocytes. **Scott, H.**, Dong, L., Stevenson, S., MacDonald, A.I., Srinivasan, S., Massimi, P., Banks, L., Martin, P.E., Johnstone, S.R., Graham, S.V. J Cell Sci (2023) 136 (11).

https://doi.org/10.1242/jcs.259984

Acknowledgment

I would firstly like to say a massive thank you to my supervisors, Prof Sheila Graham and Dr Patricia Martin. I have been extremely lucky to benefit from their knowledge and advice throughout this project. I am also grateful to Prof Malcolm Hodgins for the keen insight he has provided during this time.

I would also like to acknowledge the current and past members of the Graham group, including Andy, Anna, Ilaria, Chris and Maddie. I am incredibly grateful to be able to work in such a positive, helpful and friendly environment. This especially applies to Andy and Anna, whose help and advice has been appreciated immensely over the last three years. I am grateful to Sanzida for her contribution to this project. Thank you to the members of the histopathology service and to Colin for his patience with microscopy-related issues. Thank you to Amit for her advice on protein expression and purification. Thank you to Max for his help with the Incucyte. Thanks also to Marino, Boatemaa and Kate at Glasgow Caledonian University for their help with various projects.

I am grateful to both the friends I have met through this project and those outside of it for their support. Thanks to Matt, who provided useful advice on AlphaFold. Special thanks to Kerr, who is a great friend and also happens to have access to a 3D printer. Finally, thank you to my family for their continuous encouragement and to Kira, who has been endlessly supportive throughout this project and who I appreciate more each day.

Author's Declaration

I declare that, except where explicit reference is made to the contribution of others, that this Thesis is a result of my own work carried out at the University of Glasgow and at Glasgow Caledonian University. This work has not been submitted for any other degree at the University of Glasgow or any other institution. All external sources have been accordingly referenced.

Printed Name: HARRY SCOTT

Signature:

Abbreviations

ΔΔCt- Delta delta cycle threshold

ΔCt- Delta cycle threshold

2xYT- 2x yeast extract tryptone

AKT- Protein kinase B

AP-1- Activator protein-1

AP-2- Adapter protein complex-2

APC- Adenomatous polyposis coli

Arf6- ADP-ribosylation factor 6

ATP- Adenosine triphosphate

Ca^{2+}- Calcium ion

CaMKII- Calcium-calmodulin dependent protein kinase II family

CASK- Calcium/calmodulin dependent serine protein kinase

CBX- Carbenoxolone

CDK- Cylcin-dependent kinase

cDNA- Complementary DNA

CIP75- Connexin 43 interacting protein of 75kDa

Co-IP- Coimmunoprecipitation

Crb- Crumbs protein

CV- Coefficient of variance

Cx43- Connexin 43

DAPI- 4',6-diamidino-2-phenylindole

DFU- Diabtetic foot ulcer

dH_2O- Distilled H_2O

Dlg1/SAP97- Discs large homologue-1/Synapse associated protein 97

DMEM- Dulbecco's modified eagle's medium

DMSO- Dimethylsulfoxide

DTT- Dithiothreitol

EB1- End binding 1

EDTA- Ethylenediaminetetraacetic acid

EEA1- Early endosome antigen 1

ER- Endoplasmic reticulum

ERAD- Endoplasmic reticulum associated degradation

ERGIC- ER-Golgi intermediate compartment

Esp15- Epidermal growth factor receptor pathway substrate 15

FBS- Fetal bovine serum

FFPE- Formlain-fixed paraffin-embedded

FRET- Fluorescence resonance energy transfer

GAPDH- Glyceraldehyde 3-phosphate dehydrogenase

GFP- Green fluorescent protein

GJA1- Gap junction alpha 1

GJA1-11k- Gap junction alpha 11kDa

GJA1-20k- Gap junction alpha 20kDa

GJIC- Gap junctional intercellular communication

GST- Glutathione S-transferase

GTEx- Genotype-Tissue Expression

GUK- Guanylate kinase domain

HEK293- Human embryonic kidney cells

HPV- Human papillomavirus

IGF-1- Insulin-like growth factor-1

IgG- Immunoglobulin G

IL-10- Interleukin-10

JAK/STAT- Janus kinase/signal transducers and activators of transcription

JNK kinase- c-Jun N-terminal kinase

K^+- Potassium ion

L27- Lin2/Lin7

LAMP-2- Lysosome-associated membrane glycoprotein-2

LDS- lithium dodecyl sulfate

Lgl- Lethal giant larvae

M1- Manders' colocalisation coefficient

MAGUK- Membrane associated guanylate kinase

MAPK- Mitogen-activated protein kinase

MES- 2-ethanesulfonic acid

MgCl- Magnesium chloride

$MgSO_4$- Magnesium sulfate

MMC- Mitomycin C

MMP- Matrix metalloproteinase

MST- Microscale thermophoresis

mTOR- mammlian target of raamycin

MTT- (3-(4,5-Dimethylthiazol-2-yl)-2,5-Diphenyltetrazolium Bromide

NAD^+- Nicotinamide adenine dinucleotide

NEDD4- Neural precursor cell-expressed developmentally downregulated gene 4

NH_4Cl- Ammonium chloride

NIKS- Normal immmortal keratinocytes

NMDA- N-methyl-D-aspartate

NMR- Nuclear magnetic resonance

ODDD- Oculo-dento-digital dysplasia

PAE- Predicted aligned error

Par- Partitioning defective

PBS- Phosphate-buffered saline

PBST- PBS Tween

PCR- Polymerase chain reaction

PDZ- Postsynaptic density protein of 95 kDa (PSD95), *Drosophila* disc large tumor suppressor (Dlg), and zonula occludens-1 protein (ZO-1)

PFA- Paraformaldehyde

PKC- Protein kinase C

PLA- Proximity ligation assay

pLDDT- Predicted local distance difference test

PSF- Polypyrimidine tract-binding protein-associated splicing factor

PTEN- Phosphatase and tensin homolog

pTM- predicted Template modelling

qRT-PCR- quantitative Reverse transcription PCR

Rab11- Ras-related protein 11

Rab5- Ras-related protein 5

RhoG- Ras-homology growth-related

RT- Room temperature

RWD- Relative wound density

SEC- Size exclusion chromatography

SGEF- SH3-containing guanine nucleotide exchange factor

SH3- Src homology 3

siRNA- small interfering RNA

SP-1- Specificity protein-1

Src- Proto-oncogene tyrosine-protein kinase Src

STAT3- Signal transducer and activator of transcription 3

TGFβ- Transforming growth factor β

TGN- *Trans*-Golgi network

TNT- Tunnelling nanotube

VEGF- Vascular endothelial growth factor

W12T- W12 tumour

Wnt- Wingless-related integration site

ZO-1- Zonula occludens-1

αCT1- Alpha carboxyl-terminus 1

Chapter 1: Introduction

1.1 Function of the Skin in Health and Disease

The skin acts as a crucial barrier against the external environment. The role of this barrier is to protect the body against external threats including pathogens, UV light, temperature extremes and mechanical trauma (Abdo, Sopko and Milner, 2020). The skin is composed of three compartments: the hypodermis, dermis and epidermis. The hypodermis and dermis are made up of connective tissue, while the epidermis is mainly composed of keratinocytes in five distinct ascending sublayers: stratum basale, stratum spinosum, stratum granulosum, stratum lucidum (only present in thick skin such as palms and soles) and stratum corneum (Randall Wickett and Visscher, 2006). As keratinocytes ascend from the stratum basale towards the upper layers, they follow a terminal differentiation pathway, eventually resulting in cell death to form part of the stratum corneum and subsequent shedding from the top of the epidermis (Abdo *et al.*, 2020).

Alterations in normal skin physiology are associated with many different pathologies, including chronic inflammatory conditions such as non-healing wounds, atopic dermatitis and psoriasis. The presentation of such conditions is largely heterogeneous but often includes itchiness and swelling. Skin diseases tend to involve a complex interplay of genetic and environmental factors. In particular, dysregulation of the immune system is an important driver of skin pathology, with autoimmunity being implicated in many different skin diseases (Ávalos-Díaz and Esparza, 2013). In addition to the symptoms of the disease itself, patients suffering from skin diseases are predisposed to mental health conditions and skin infections. This, in addition to the massive global health and economic burden imposed by skin diseases and their treatment emphasises the importance of skin research (Hay *et al.*, 2014).

1.2 The Epidermal Wound Healing Process

Repair of the skin whenever breached is essential in order to protect against pathogens and restore homeostasis. The wound healing process is comprised of four main overlapping processes: haemostasis, inflammation, proliferation and maturation. A summary of the normal wound healing timeline is shown in **Figure 1.1.** Directly following injury, the process of haemostasis begins in order to prevent haemorrhage. Constriction of surrounding blood vessels to restrict blood flow to the affected area is one of the initial events in this stage. Through the detection of exposed collagen fibres caused by the injury, circulating platelets adhere to the damaged surface and begin to aggregate, which will eventually cause the formation of a fibrin clot to prevent further haemorrhage. Detection of damaged collagen also causes the platelets to become activated, which promotes release of a variety of signals and growth factors that ultimately promote wound healing. Examples of these factors include ADP and fibrinogen, which participate in a positive feedback loop to allow recruitment and activation of greater numbers of platelets. Platelet activation also causes release of epidermal growth factor, transforming growth factor ß (TGFß) and calcium, which plays a key role in promoting coagulation (Golebiewska and Poole, 2015). A further role of the aggregation of platelets is to form an extracellular matrix scaffold for immune cells, which are crucial to remove pathogens in the following stages of wound healing.

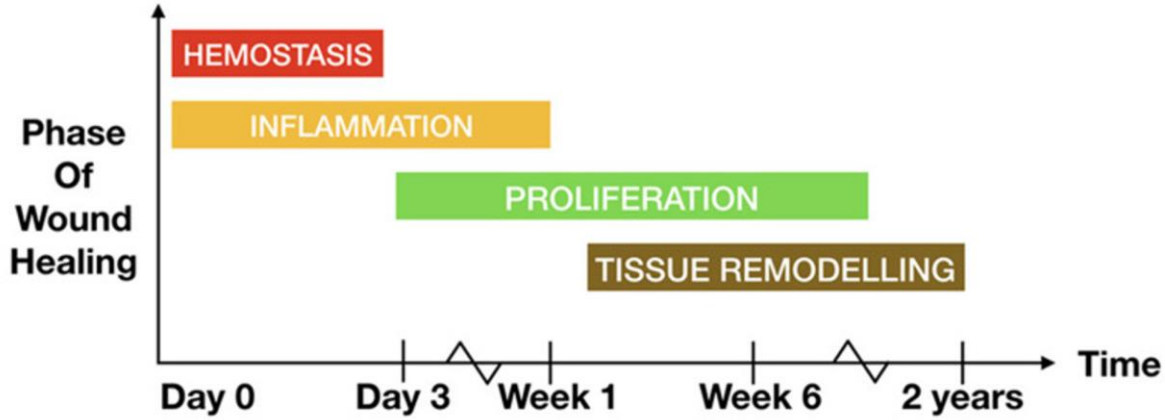

Figure 1.1: Timeline of normal wound healing events. The wound healing process is separated into 4 main stages: haemostasis (red), inflammation (yellow), proliferation (green) and tissue remodelling (brown). Stage of wound healing is shown on the y-axis, time is shown on the x-axis. Several stages overlap in time. Adapted from Opneja, Kapoor and Stavrou, 2019.

Neutrophils are the first circulating inflammatory cells to reach a wound site and are recruited through certain chemokines secreted by keratinocytes and fibroblasts in response to wounding (MacLeod and Mansbridge, 2016). These immune cells are involved in defence against pathogens through the release of antimicrobial peptides, proteases and reactive oxygen species (Wilgus, Roy and McDaniel, 2013). These proteases include certain matrix-metalloproteases (MMPs) such as MMP-8, which digest damaged type I collagen found in the wound area (Cabral-Pacheco *et al.*, 2020). Neutrophils also cause amplification of the immune response via release of inflammatory factors that recruit other immune cells to the affected area such as monocytes, which then undergo differentiation to become macrophages. These macrophages are responsible for phagocytosis of both invading pathogens and neutrophils, which undergo apoptosis following completion of their role. Following successful clearance of pathogens, macrophages progress from a pro-inflammatory phase to an anti-inflammatory phase, releasing anti-inflammatory molecules such as IL-10 (Murray and Wynn, 2011). A portion of the macrophages will undergo apoptosis as with neutrophils. This is a key regulatory phase in wound healing, as failure to progress past the inflammatory phase is associated with chronic inflammation and stalling of the wound healing process (Schilrreff and Alexiev, 2022).

The proliferation phase of wound healing overlaps with the preceding inflammatory phase, with some factors released by anti-inflammatory macrophages encouraging the proliferation of keratinocytes and fibroblasts, as well as the creation of new blood vessels via the process of angiogenesis. These include TGFß, insulin-like growth factor (IGF-1) and vascular endothelial growth factor (VEGF) (Krzyszczyk *et al.*, 2018). A crucial component of the proliferative phase is replacement of the fibrin clot formed in the initial stages with granulation tissue, which is composed of fibroblasts, blood vessels, newly-synthesised collagen, neutrophils and macrophages (Landén, Li and Ståhle, 2016). This stage is largely dependent on fibroblast migration from the dermis into the wound area, where these cells proliferate and deposit extracellular matrix components. The new granulation tissue more closely mimics unwounded skin through some structural and functional qualities not observed in the fibrin clot. Re-epithelialisation is the other major component of the proliferation phase and is orchestrated by keratinocytes of the wound-edge, which begin to proliferate and migrate into the wound to facilitate wound closure. Migration of wound-edge keratinocytes usually occurs first out of these two processes and is stimulated by a lack of contact inhibition which usually restricts migration. This is then followed by proliferation of keratinocytes of the basal layer 2-3 days after initial wounding to repopulate the area (Landén *et al.*, 2016).

The final stage of wound healing is the remodelling phase, which begins two to three weeks after wounding and can last upwards of a year depending on environmental and genetic factors (Gonzalez *et al.*, 2016). The main purpose of this stage is to recover tensile strength and return the wounded area to a similar state to unwounded tissue. This involves constant remodelling of the granulation tissue, resulting in scar formation and a decrease in cell and blood capillary density. A major focus of this stage also hinges on replacement of type III collagen (which is deposited in the early stages of wound healing) with type I collagen, which is the main collagen type found in unwounded skin (Schultz *et al.*, 2011). This eventually results in scar tissue which retains most of the tensile strength of unwounded tissue, although full strength is never recovered due to factors such as altered orientation of collagen fibres (Marshall *et al.*, 2018).

1.3 Chronic Wound Healing

When the wound healing process does not progress as normal, chronic non-healing wounds can develop. Chronic wounds are defined as any wound that does not progress through the stages of wound healing in a predictable amount of time (Iqbal *et al.*, 2017), instead tending to remain in a state of prolonged inflammation with low levels of associated growth factors (Yamakawa and Hayashida, 2019) and high levels of matrix metalloproteinases (MMPs) (Lobmann *et al.*, 2002). Chronic wounds are frequently observed in patients with diabetes, a condition that has a multifactorial impact on the wound healing process through peripheral neuropathy and vascular disease, among other properties (Dinh and Veves, 2005). Diabetic patients are estimated to have a lifetime risk of 25% of developing a diabetic foot ulcer (DFU), a form of chronic wound (Boulton and Whitehouse, 2020). In ~25% of DFU cases, surgical amputation of the affected limb is required, leading to an increased risk of mortality in the years following (Chang and Nguyen, 2021). Management and treatment of wounds currently represents a massive burden on both global finances and health, with an estimated annual cost of £8.3B in the UK alone in the year 2017-2018 (Guest, Fuller and Vowden, 2020). Much of this cost stems from the limited efficacy of current treatments, which often require a prolonged treatment period and are ineffective at preventing recurrence. This, coupled with the ageing population and the fact that the incidence of diabetes is predicted to rise sharply over the next few decades, cements chronic wounds as an area of research requiring new and improved treatment options (Becker, Thrasivoulou and Phillips, 2012).

1.4 Introduction to Connexin 43 and Structure

Mammalian cell to cell junctions are crucial sites of interaction between cells and can be broadly separated into three main types: anchoring, tight and gap junctions. Anchoring junctions (which include adherens junctions, desmosomes

and hemidesmosomes) are involved in tethering of the cell cytoskeleton to the cytoskeleton of adjacent cells or the extracellular matrix. Tight junctions are instead responsible for maintaining apicobasal polarity of cells and forming impermeable areas between adjacent cells to prevent free diffusion of macromolecules through the extracellular space (Zihni *et al.*, 2016). Finally, the gap junction family of proteins constitute one of the major forms of cell-cell signalling via the creation of direct intercellular channels between adjacent cells. Gap junction channels are composed of transmembrane connexin proteins, such as Connexin 43 (Cx43), which congregate at discrete regions of the plasma membrane to form areas known as gap junction plaques. Formation of gap junction channels permits the sharing of various factors of <1kDa in size, including ions, metabolites, secondary messengers and microRNAs (Aasen *et al.*, 2019a). Through this role, connexins are known to impact many fundamental processes, including tissue homeostasis, apoptosis, cell proliferation and differentiation (Gao *et al.*, 2021; Au *et al.*, 2020).

There are currently 21 known connexin genes in humans, which are split into subgroups depending on genetic similarity. These subgroups are: alpha, beta, gamma, delta and epsilon (Vinken, 2015). For example, as the first alpha connexin protein described, Cx43 protein is coded for by the *GJA1* gene. *GJA1* consists of two exons (the first being untranslated) separated by an 11kb intron, with the second exon singularly containing the sequence coding for full-length Cx43 protein (Pace *et al.*, 2019). A single promoter region has been described for the human *GJA1* gene, containing binding sites for AP-1 and SP-1 transcription factors (Oyamada, Takebe and Oyamada, 2013). In this investigation, the Cx43 protein name is primarily used in place of the *GJA1* gene name.

Connexin proteins are named according to their respective molecular weights and have surprisingly short half-lives compared to other transmembrane proteins, being between 1-4 h (Berthoud *et al.*, 2004). The turnover rate of connexins can vary depending on cell type, with early pulse-chase experiments

being instrumental in demonstrating the rapid turnover of these proteins (Laird, Puranam and Revel, 1991). All connexins share the same basic structure **(**

Figure 1.2), containing cytoplasmic N- and C-termini, four α-helical transmembrane domains, two extracellular loops and a cytoplasmic loop (Laird, 2006). All connexins possess a certain degree of structural homology, with the N-terminus, as well as the transmembrane domains and the extracellular loops being well-conserved between the different connexin family members, with some variation in the cytoplasmic loop which is involved in channel gating (Xu *et al.*, 2012). However, most of the heterogeneity between the different connexins is contained within the cytoplasmic C-terminal tail, which is longer in the alpha subgroup (including Cx43) and therefore allows interaction with many other proteins both prior to, and following transport of the protein to the plasma membrane (Leithe, Mesnil and Aasen, 2018). This means that connexin functions can be roughly divided into two main sections of channel-dependent and channel-independent roles, with each of these contributing to the diverse processes connexins can influence.

Gap junction formation begins with oligomerisation of six individual connexin proteins during trafficking to the plasma membrane to form a connexon, which on docking with an opposing connexon on a neighbouring cell creates a fully functional gap junction channel **(**

Figure 1.2). There is a level of variety in this process, as connexons can be formed of either six of the same connexin protein (homomeric), or different compatible types of connexins (heteromeric). This diversity is conserved at the channel level, where docking connexons may be identical (homotypic) or varied (heterotypic) based on compatibility (Koval, 2006). Different connexin proteins can alter various properties of the overall gap junction channel they are part of, including channel permeability and gating, which results in a complex system allowing fine-tuned control over gap junction signalling. There are however

some limits to this variation, such as alpha and beta connexins being unable to form heteromeric connexons (Koval, Molina and Burt, 2014). In addition to forming gap junctions, individual connexons localised to the plasma membrane can act as hemichannels which communicate with the extracellular environment, releasing factors such as ATP and NAD^+ (Bruzzone *et al.*, 2001; Cotrina *et al.*, 1998). Hemichannels are usually closed but are induced to open under conditions of cell stress (Wang *et al.*, 2013). Connexin function is further modulated through the existence of many different post-translational modifications that can affect protein function, particularly phosphorylation and ubiquitination (Solan and Lampe, 2009; Totland *et al.*, 2020).

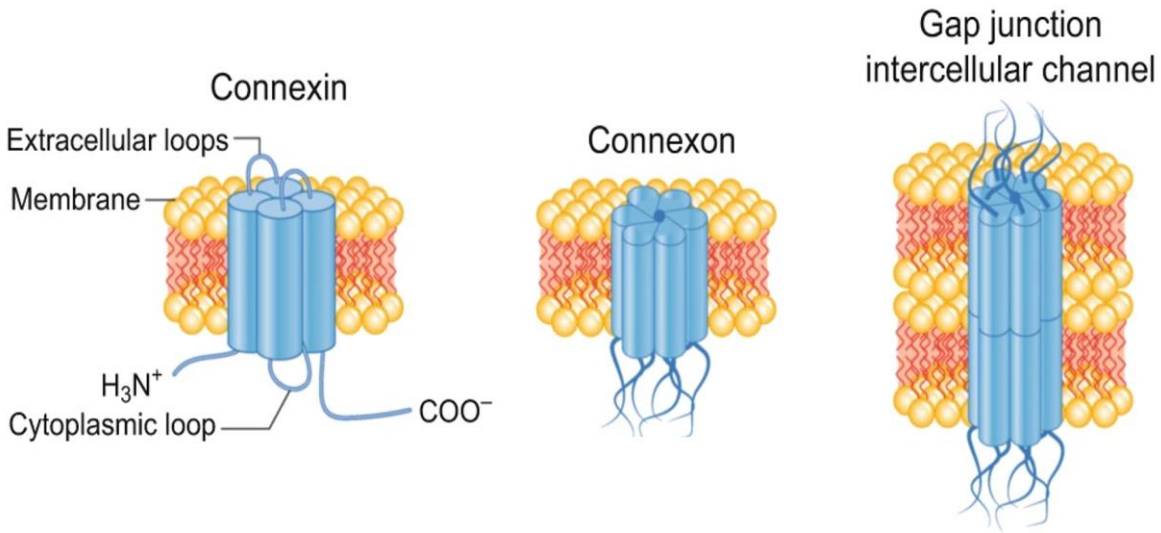

Figure 1.2: General structure of individual connexin protein, a connexon and a gap junction intercellular channel. Connexin 43 contains four α-helical transmembrane domains, two extracellular loops, a cytoplasmic loop and cytoplasmic N- and C-termini. A connexon is formed of six connexin proteins, which can be either homomeric or heteromeric depending on individual connexin protein compatibility. Individual connexons inserted into the plasma membrane can also act as hemichannels to release certain factors to the extracellular environment. Docking of two apposing connexons on the surfaces of different cells causes formation of a fully functional gap junction channel. Adapted from Aasen *et al.*, 2019.

Cx43 is a 382 amino acid long protein and is the most well-documented member of the connexin family in humans, owing to its important functions and its possession of the widest connexin expression profile in the human body (Zhang

and Cui, 2017). Cx43 is known to be expressed in a diverse range of cells, which includes keratinocytes (Kamibayashi *et al.*, 1993), cardiomyocytes (Beyer, Paul and Goodenough, 1987), neurons (Nadarajah *et al.*, 1997) and retinal glial cells (Goodenough, Goliger and Paul, 1996). Within the tissues these cells make up, Cx43 has been shown to be play roles in wound healing, propagating the action potential between cardiomyocytes and facilitating electrical synapse formation between neurons.

In addition to its role as a channel-forming protein, Cx43 possesses channel-independent functions which are mainly enabled through interaction of the cytoplasmic C-terminal tail with a diverse range of other proteins. Study of these channel-independent roles is complicated by the modulation of Cx43 through post-translational modifications, particularly phosphorylation, which controls interactions between Cx43 and other proteins, as well as interactions which are necessary for its normal lifecycle as a channel-forming protein. Phosphorylation of Cx43 is achieved through many different kinases, including protein kinase C (PKC) and MAP kinase (MAPK) (Axelsen *et al.*, 2013). The existence of six internal translation sites within the *GJA1* gene coding for Cx43 further complicates matters. These internal translation sites produce various sizes of N-terminally truncated Cx43 protein lacking the complete transmembrane domains of the full-length protein **(Figure 1.3)**. These isoforms are increasingly being recognised to have distinct functions from full-length Cx43, with the most prominent, GJA1-20k, interestingly being involved in forward trafficking of full-length Cx43 to the plasma membrane (Smyth and Shaw, 2013; Basheer *et al.*, 2017). This role has been found to be reliant on GJA1-20k stabilising polymerised actin to allow subsequent trafficking of Cx43-containing vesicles. A further isoform, GJA1-11k, localises to the nucleus and inhibits cell cycle progression (Epifantseva *et al.*, 2020). The levels at which each of these internal translation sites are utilised, which is controlled by the mTOR pathway (Smyth and Shaw, 2013), constitutes a further regulatory mechanism of Cx43 (Leithe *et al.*, 2018).

The importance of connexin function is best emphasised through the phenotypes of patients with mutated connexin proteins, which can range from

nonsyndromic/syndromic deafness to cardiopathies and cataracts (García *et al.*, 2016). Many different mutations in Cx43 specifically are associated with oculodentodigital dysplasia (ODDD), which is a mostly autosomal dominant inherited disease affecting the eyes, teeth and digits (McLachlan *et al.*, 2008). This disease frequently presents as syndactyly/camptodactyly and/or craniofacial abnormalities, demonstrating the necessity of proper Cx43 function.

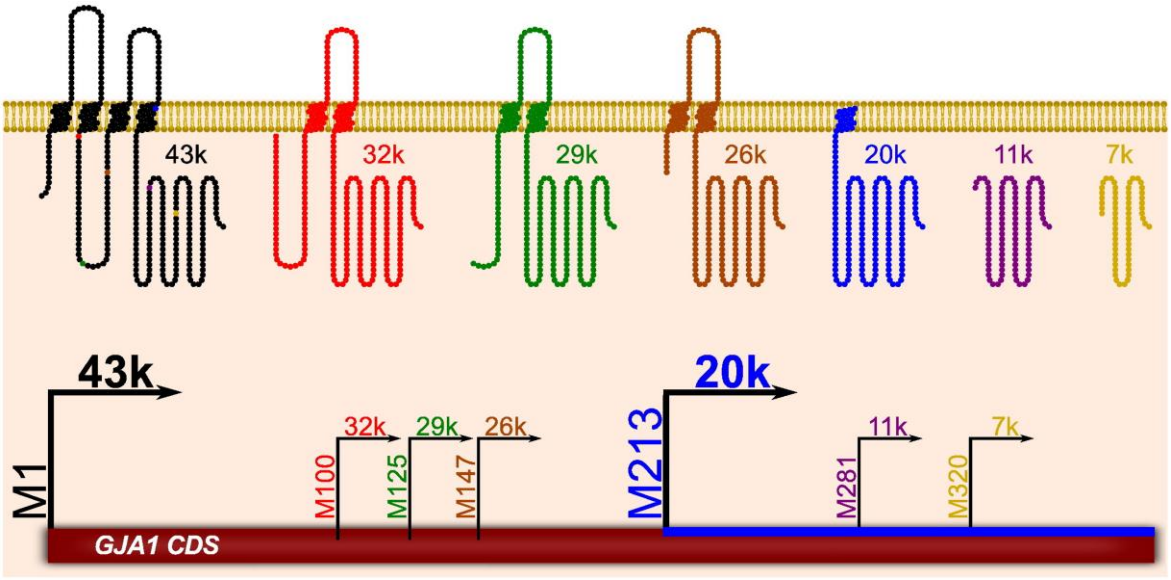

Figure 1.3: N-terminally truncated isoforms of Cx43 resulting from internal translation initiation sites in the GJA1 gene. Isoforms are named according to their predicted molecular weights which are shown in Da (e.g. GJA1-32k=32kDa). Methionine translation initiation sites on the GJA1 gene are shown in the lower half. GJA1-20k and GJA1-11k have been shown to have distinct functions from full-length Cx43. Adapted from Leithe *et al.*, 2018.

1.5 Cx43 in Epidermal Wound Healing

Of the 21 known connexin genes in humans, at least 10 are expressed in the skin (Cx26, Cx30, Cx30.3, Cx31, Cx31.1, Cx32, Cx37, Cx40, Cx43, and Cx45), with known roles in keratinocyte migration, proliferation and differentiation (Zhou and Jiang, 2014; Di *et al.*, 2001). Expression of the connexin protein family

members varies depending on the sublayer of the epidermis (Di *et al.*, 2001) **(Figure 1.4A)**. For example, Cx26 is expressed within the spinous and granular layers (Garcia-Vega *et al.*, 2021), while Cx43, the most well-documented connexin in the skin, is expressed mainly in the basal and spinous layers, as well as the dermis (Salomon *et al.*, 1994). There is little expression of connexins in the cornified layer. These differences in expression may be due to, or be involved in controlling the stage of the differentiation pathway that the cells in each layer reside in (Langlois *et al.*, 2007).

Unsurprisingly given their roles in many fundamental cellular processes, significant changes in the expression patterns of connexins occur over the course of normal epidermal wound healing **(Figure 1.4B)**. These changes are specific to each connexin family member, further emphasising the diverse range of connexin functions. Within the first 24h after a wound is sustained, Cx30/Cx26 levels are enhanced and expression is expanded to include all nucleated layers of the epidermis (Kretz *et al.*, 2003), while Cx43, Cx31 and Cx31.1 levels decrease in cells of the wound-edge (Brandner *et al.*, 2004; Coutinho *et al.*, 2003). Despite this, Cx43 expression is maintained in cells that are distant from the wound-edge and is even upregulated in dermal fibroblasts (Coutinho *et al.*, 2003). This suggests that Cx43 impacts the wound healing process in distinct ways depending on cell type. These observations led to the proposal that Cx43 expression may be down-regulated in keratinocytes of the wound-edge to allow migration into the wound area to promote closure. Supporting this theory, inducible deletion of the Cx43 coding region in a transgenic mouse model resulted in increased wound closure rates (Kretz *et al.*, 2003). Additionally, targeting Cx43 expression using both antisense oligodeoxynucleotides and siRNA demonstrated increased keratinocyte migration (Mori *et al.*, 2006; Faniku *et al.*, 2018). Further studies which reduced plasma membrane levels of Cx43 through the use of connexin mimetic peptides showed an increase in keratinocyte and fibroblast migration rates (Wright *et al.*, 2009; Faniku *et al.*, 2018). As these mimetic peptides target Cx43 plasma membrane localisation rather than expression, it was suggested that Cx43 removal in cells of the wound-edge may be to restrict channel-dependent functions, rather than channel-independent

functions which rely on interactions with other proteins. Cx43 levels begin to increase around 48h after wounding and return to normal following closure of the wound (Coutinho *et al.*, 2003). In addition to Cx43 expression levels, phosphorylation status also appears to play an important early role in wound healing, with sequential phosphorylation of S373, S279/S282 and S368 being associated with initial growth of gap junction plaques and subsequent internalisation of Cx43 (Solan and Lampe, 2018). Changes in Cx43 phosphorylation during wounding also differ between sublayers of the epidermis, as phosphorylation on serine residue 368 is increased in cells of the basal layer 24h after wounding, while simultaneously being almost undetectable in the other layers of the epidermis (Richards *et al.*, 2004). Phosphorylation of S368 has been tied to a reduction in gap junctional signalling, which may indicate Cx43 phosphorylated on S368 is involved in proliferation of basal keratinocytes through a channel-independent function. As with unphosphorylated Cx43 expression, this change is transient, with levels returning to normal 72h after wounding (Richards *et al.*, 2004).

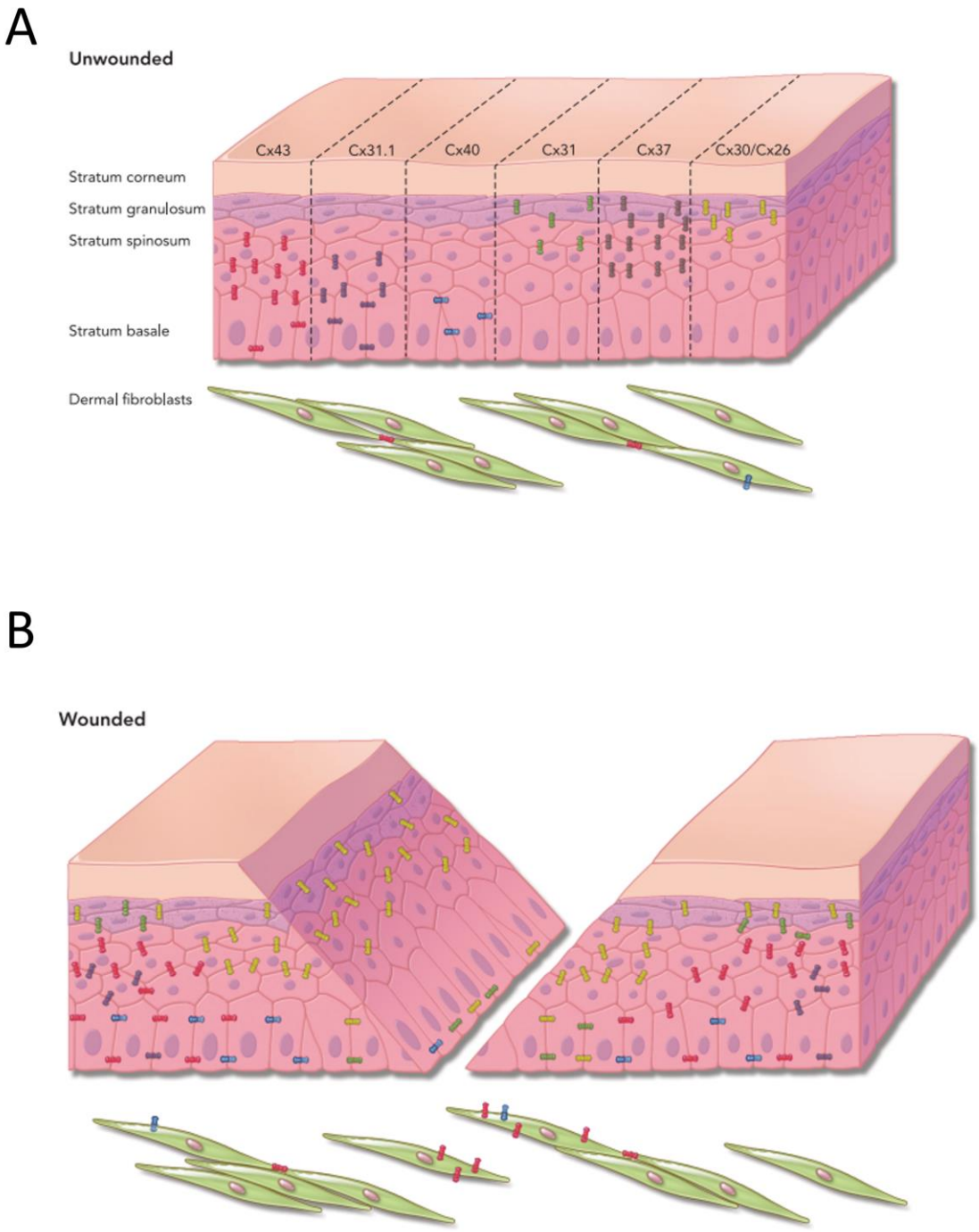

Figure 1.4: Expression patterns of connexin proteins in the epidermis under unwounded (A) and wounded conditions (B). (A) Connexin expression in unwounded epidermal layers and the dermis. Individual gap junctions are shown as coloured channels between cells. Cx43=red, Cx31.1=purple, Cx40=blue, Cx31=green, Cx37=grey and Cx30/Cx26=yellow. Layers of the epidermis are shown on the left-hand side. Adapted from Churko and Laird, 2013. **(B)** Connexin expression is altered in wounded epidermal layers and dermis. Layers and connexin colours are as shown in **(A)**.

1.6 Cx43 in Chronic Epidermal Wound Healing

Compared to normal wound healing progression, chronic wounds are associated with altered expression of a variety of factors. These include upregulation of MMPs (Lobmann *et al.*, 2002) and downregulation of various keratins, including keratin 6 and keratin 17 (Charles *et al.*, 2008), which are usually upregulated during wound healing and are associated with activation of wound-edge keratinocytes (Mazzalupo *et al.*, 2003). In contrast to the normal wound healing process, Cx43 is upregulated in wound-edge cells of chronic wounds (Brandner *et al.*, 2004). Such upregulation has been shown for various types of chronic wound, including venous leg, diabetic foot and pressure ulcers (Sutcliffe et al., 2015a). This emphasises the importance of downregulation of Cx43 in cells of the wound-edge to promote normal wound healing. Due to studies showing that targeting of Cx43 leads to faster wound healing in both normal (Qiu *et al.*, 2003) and chronic wounds (Ghatnekar *et al.*, 2015), Cx43 has become a promising therapeutic target to improve wound healing rates, with one treatment currently undergoing a phase III clinical trial (Montgomery *et al.*, 2018). Existing strategies to target Cx43 in wound healing are discussed further in **Chapter 4**.

1.7 The Interactions of Cx43

Due to the ~150aa long cytoplasmic C-terminal tail of Cx43, interaction with a large number of other proteins is possible **(**
Figure 1.5), massively expanding the functions of Cx43. Many of these interactions are involved in the normal lifecycle of Cx43 (for a full description of the lifecycle see **Chapter 3**). An important example of this is the interaction with both α- and ß-tubulin, which may have several functions (Giepmans *et al.*, 2001b). While not a requirement for localisation of Cx43 to the plasma membrane, a certain proportion of Cx43 is trafficked to the cell surface via the microtubule network and interaction with tubulin may be involved in direct targeting of Cx43 to adherens junctions (Johnson *et al.*, 2002; Shaw *et al.*, 2007). This form of direct targeting is likely reliant on export from the Golgi in

vesicles and trafficking along microtubules through interaction with cargo receptors such as consortin and motor proteins such as kinesin (Epifantseva and Shaw, 2018; del Castillo *et al.*, 2010). There is also some evidence that interaction of Cx43 and tubulin aids stabilisation of the microtubule network in cells communicating via gap junctions (Giepmans, Verlaan and Moolenaar, 2009). Interaction with tubulin is surprisingly specific to Cx43 within the connexin family, as other members do not possess the binding site located between residues 234-243 (Giepmans *et al.*, 2001b). Binding of the two proteins has also been found to be regulated through post-translational modifications, with phosphorylation at residue Y247 abolishing the interaction (Saidi Brikci-Nigassa *et al.*, 2012).

The carboxyl terminal tail of Cx43 also interacts with Drebrin, which is an F-actin binding protein with two main isoforms produced from a single gene. One of these isoforms, Drebrin A, is expressed primarily in the brain, while Drebrin E is expressed more widely, including in the skin (Shirao and Sekino, 2017). Interaction between Drebrin E and Cx43 was originally confirmed in murine brain tissue and was shown to be important for stabilisation of Cx43 in gap junctions, as knockdown of Drebrin via siRNA resulted in relocation of Cx43 from the cell membrane to the cytoplasm, as well as an increase in Cx43 degradation (Butkevich *et al.*, 2004). Drebrin has since been shown to aide trafficking of Cx43 to the plasma membrane by indirectly tethering it to F-actin, with the main Drebrin binding site of Cx43 being located between residues 264-275 (Ambrosi *et al.*, 2016). As this region is targeted by other Cx43-interacting proteins such as c-Src, which can cause internalisation of Cx43 through phosphorylation of several sites on the carboxyl tail including Y265 (Giepmans *et al.*, 2001a), it is suggested that Drebrin may stabilise Cx43 at the cell membrane through steric inhibition of these interactions.

The most well-characterised interaction of Cx43 is with the zonula occludens-1 protein (ZO-1) (Toyofuku *et al.*, 1998). ZO-1 is a member of the membrane associated guanylate kinase (MAGUK) family of proteins, which share a modular

structure including one or several postsynaptic density protein of 95kDa/*Drosophila* Discs large tumour suppressor/ZO-1 (PDZ) domains, a Src-homology 3 (SH3) domain and a guanylate kinase-like (GUK) domain (Te Velthuis, Admiraal and Bagowski, 2007) **(**Error! Reference source not found.**)**. Through interactions with diverse protein partners, MAGUK proteins have roles in cell polarity, signal transduction and junctional communication between cells (Reissner and Missler, 2014). In particular, ZO-1 is involved in the formation of tight junctions between epithelial cells, acting as a molecular scaffold for other tight junction proteins (McNeil, Capaldo and Macara, 2006). However, it has also been shown that ZO-1 plays a key role in the regulation of Cx43 gap junctions (Hunter, Jourdan and Gourdie, 2003). The interaction between ZO-1 and Cx43 takes place through interaction of the ZO-1 second PDZ domain with the extreme C-terminal amino acids of Cx43 and has been found to negatively regulate the incorporation of newly-synthesised Cx43 into gap junctional plaques (Giepmans and Moolenaar, 1998; Rhett, Jourdan and Gourdie, 2011). Rhett and colleagues showed that disruption of this interaction via either siRNA targeting of ZO-1 or a Cx43 mimetic peptide which binds to the PDZ2 domain of ZO-1 resulted in larger gap junction plaques and increased gap junctional communication, thus providing a direct mechanism of modulating gap junctional communication between cells.

A

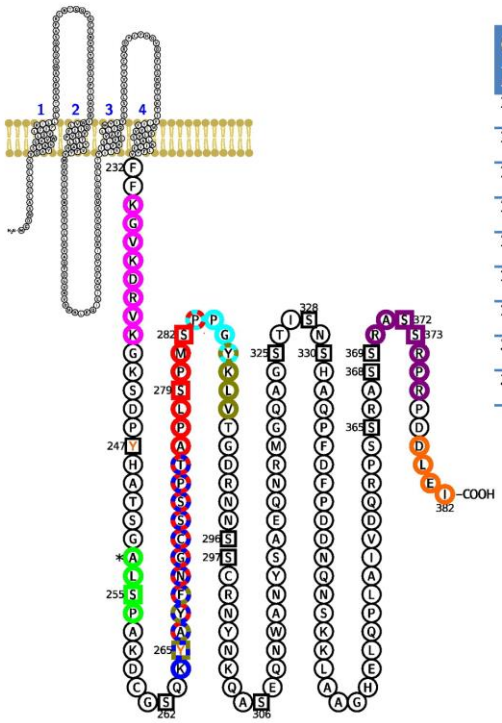

B

Cx43 Sequence Binding Domain	Binding protein
^{234}KGVKDRVKGK^{243}	Tubulin
^{253}PLSP^{256}	CIP85*
^{264}KYAYFNGCSSPT^{275}	Drebrin**
^{265}YAYF^{268}	µ2 subunit of AP-2
^{266}AYFNGCSSPTAPLSPMSP^{283}	c-Src/PTEN/Csk
^{283}PPGY^{286}	NEDD4
^{286}YKLV^{289}	µ2 subunit of AP-2
^{370}RASSRPR^{376}	14-3-3***
^{379}DLEI^{382}	ZO-1****

Figure 1.5: The sequence of the Cx43 C-terminus and sites of interaction with binding partners. (A) Topographical representation of Cx43 protein inserted in the plasma membrane. Amino acid residues are shown as circles with one-letter abbreviations. The Cx43 cytoplasmic C-terminus is enlarged and colour-coded to denote residues involved in interaction with certain binding partners. Combinations of colours indicate overlapping binding regions between several proteins. Pink=tubulin, lime green=CIP85, dark blue=Drebrin, olive=AP-2 red=c-Src/PTEN/Csk, cyan=NEDD4, purple=14-3-3, orange=ZO-1 **(B)** Corresponding table of the Cx43 interaction sites with other proteins. Adapted from Leithe, Mesnil and Aasen, 2018.

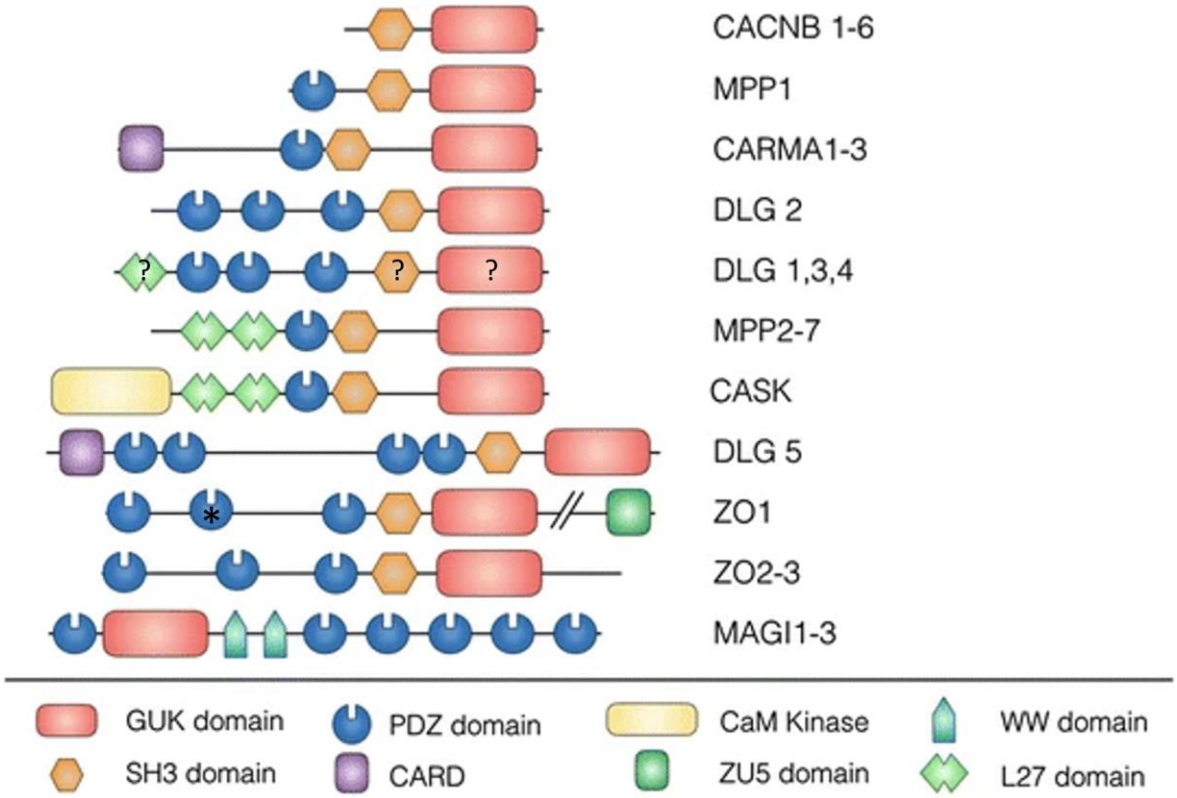

Figure 1.6: The domain structure of MAGUK protein family members. CACNB=Calcium Voltage-Gated Channel Auxiliary Subunit Beta 1, MPP=MAGUK P55 Scaffold Protein, CARMA=CARD recruited membrane associated protein, DLG=Discs large, CASK=calcium/calmodulin-dependent serine protein kinase, ZO-1 zonula occludens, MAGI=Membrane-associated guanylate kinase inverted. Red rounded rectangles=GUK domain, blue indented circles=PDZ domains, yellow rounded rectangles=CaM kinase domains, turquoise arrow=WW domains, orange hexagon=SH3 domain, purple squares=CARD domain, green squares=ZU5 domain, light green indented diamond=L27 domains. ?= Domains of Dlg1 which may interact with Cx43, other members of the Dlg1 family are not known to interact with Cx43. *= PDZ2 domain of ZO-1 which interacts with Cx43. Adapted from Oliva and Sierralta, 2018.

1.8 Human Discs Large Homologue-1 (Dlg1)

In addition to ZO-1, Cx43 has been found to interact with a further MAGUK protein, human Discs large homologue-1 (Dlg1) (MacDonald *et al.*, 2012). Dlg1 (also known as synapse-associated protein 97 or SAP97) is a key regulator of epithelial cell polarity and signal transduction and localises to areas of cell-cell contact. Recruitment to these sites is directed by E-cadherin and is required for adherens junction formation (Laprise, Viel and Rivard, 2004; Reuver and Garner, 1998). Dlg1 protein is encoded by the *DLG1* gene and maintains the core MAGUK structure of a PDZ, SH3 and inactive GUK domain, however it also contains an additional 2 PDZ domains (for a total of 3) and an L27 domain **(**Error! Reference source not found.**)**. The PDZ, SH3 and GUK domains all serve as regions for protein-protein interactions, with these being joined by linker regions which confer flexibility and allow the protein to act as a molecular scaffold for other proteins. An important regulatory area known as the HOOK region lies between the SH3 and GUK domains and has been implicated in mediating interaction of the SH3 and GUK domains to modulate Dlg1 function (Reissner and Missler, 2014). The N-terminal L27 domain is only present in certain MAGUK family members and controls subcellular localisation of Dlg1 and homo/heterodimerisation with itself and other L27-containing MAGUK proteins (Nakagawa *et al.*, 2004; Wu *et al.*, 1998). Upon original characterisation of the human protein, at least four Dlg1 isoforms were reported to be generated through alternative splicing (Lue *et al.*, 1994). Further research revealed at least six insertions in the Dlg1 protein exist across two main sites (Mori *et al.*, 1998). The first of these is between the L27 and PDZ1 domains (I1A and I1B) and these insertions have been found to regulate multimerisation of Dlg1 and interaction with other SH3 domain-containing proteins through the formation of SH3-binding motifs. The second site is located between the SH3 and GUK domains (I2, I3, I4 and I5), with I2 being shown to target Dlg1 to the nucleus, while I3 instead targets Dlg1 to sites of cell-cell contact. In contrast, the functions of the I4 and I5 insertions remain unclear (McLaughlin *et al.*, 2002). Dlg1 protein can also be produced with certain combinations of these insertions, with expression of all isoforms varying based on the tissue type (Mori *et al.*, 1998).

Preliminary knowledge of Dlg1 came from studies of its *Drosophila* homologue, Dlg. In these investigations, Dlg was highlighted as a tumour suppressor protein, as mutation of the *DLG* gene resulted in uncontrolled proliferation and tumour formation (Woods and Bryant, 1989). Dlg was also shown to be required for establishment of correct apicobasal polarity in *Drosophila* epithelial cells (Woods *et al.*, 1996). While only one *DLG* gene exists in *Drosophila*, five are present in humans (*DLG1*, *DLG2*, *DLG3*, *DLG4* and *DLG5*), with a level of functional redundancy proposed due to the proteins being highly related (Andolfi, Tiribelli and Pascut, 2022). Importantly however, the proteins differ in their subcellular localisation in mammalian epithelial cells, suggesting they likely have diverse functions (Van Campenhout *et al.*, 2011).

One of the main roles of Dlg1 is to function together with the Scribble and Lethal giant larvae (Lgl) proteins as part of the Scribble polarity module, which is crucial for the establishment and maintenance of correct apicobasal polarity. The three proteins localise to the basolateral domain of epithelial cells to regulate cell polarity, proliferation and junction formation, while other protein complexes such as Crumbs (Crb) and partitioning-defective (Par) localise to the apical domain and maintain polarity in this area (Su *et al.*, 2012). Mutation of any of the three members of the Scribble polarity module in Drosophila leads to a similar phenotype of loss of cell organisation and changes to cell shape, suggesting they act together to maintain polarity (Bilder, Li and Perrimon, 2000).

As with *Drosophila* Dlg, Dlg1 has been reported to have a tumour suppressor function through its interactions with APC and PTEN proteins (Makino *et al.*, 1997; Sotelo *et al.*, 2012). PTEN functions as a phosphatase and targets phosphoinositide 3-kinase (3IPK) to regulate downstream targets of this pathway such as mammalian target of rapamycin (mTOR) (Song, Salmena and Pandolfi, 2012). APC instead inhibits the Wnt signalling pathway through interaction with ß-catenin (Aoki and Taketo, 2007). Further indirect evidence for a tumour suppressor function comes in the form of Dlg1 being targeted by several

oncogenic viruses, including human T-cell leukaemia virus and adenovirus type 9 (James and Roberts, 2016). Dlg1 is also targeted by the oncogenic E6 protein of certain high-risk human papillomaviruses (HPVs) (Thomas *et al.*, 2016; Vande Pol and Klingelhutz, 2013), which are the primary cause of cervical cancer but also cause other cancers of the anogenital region, as well as cancers of the head and neck (Graham, 2017). Despite these data for a tumour suppressor function, some evidence also exists for an oncogenic role of Dlg1 in promoting cell invasion (Massimi *et al.*, 2012), suggesting the function of Dlg1 as a tumour suppressor/oncogene is likely context dependent.

1.9 Previous Work on the Cx43/Dlg1 Interaction

The interaction between Cx43 and Dlg1 was initially discovered through tandem mass spectrometry analysis of rat kidney cells (Singh and Lampe, 2003). This interaction was of interest in HPV-associated cancer, as gap junctional communication is frequently disrupted during cancer progression (including cervical cancer) and the HPV oncogenic E6 protein targets Dlg1 for degradation via the proteasome (Gardiol *et al.*, 1999; Aasen *et al.*, 2019a). In order to study gap junctional communication during the different stages of HPV-associated cancer progression, the Graham group utilised the immortal but untransformed W12NT cervical epithelial cell line, which harbours integrated HPV16 DNA and was originally derived from the W12E parent cell line from a patient with low-grade cervical intraepithelial neoplasia (Sterling *et al.*, 1990). Selection of cells with a transformed phenotype through culturing of W12NT cells in basic media lacking normal supplements resulted in the generation of the W12T cell line, which exhibit increased E6 expression relative to W12NT cells (Aasen *et al.*, 2003). Coimmunoprecipitation experiments subsequently demonstrated that Cx43 and Dlg1 could interact in both the W12NT and W12T cell lines **Table 1.1** (MacDonald *et al.*, 2012). Macdonald and colleagues also found that Cx43 and Dlg1 colocalised at the cell membrane in untransformed cells, with both proteins relocating to the cytoplasm in transformed cells. This effect was specific to Cx43, as Cx26 and Cx30 plasma membrane localisation was unaffected by the

transformation process, presumably due to their short carboxyl termini and lack of binding domains. Further work by the Graham group confirmed that the interaction was conserved *in vivo* in normal cervical mucosal epithelial tissue by proximity ligation assay and also showed that HPV E6 was responsible for controlling Cx43 distribution in transformed cells (Sun *et al.*, 2015). Depletion of E6 via siRNA in transformed cells resulted in redistribution of both Cx43 and Dlg1 to the cell membrane. Furthermore, expression of HPV E6 containing a mutated Dlg1-binding motif in HPV-negative cells did not cause relocation of Cx43/Dlg1 to the cytoplasm, suggesting the interaction between E6 and Dlg1 was necessary to induce Cx43 relocation. This led to the proposal that Cx43, Dlg1 and E6 may exist as a complex in these cells.

Having established the importance of the Cx43/Dlg1 interaction in HPV-positive cancer cell lines, the Graham group next explored whether the interaction was conserved *in vitro* in HPV-negative cells. This involved use of three different human cell lines: HaCaT (immortalised keratinocytes), HEK293 (human embryonic kidney cells) and NIKS (normal immortal keratinocytes). Coimmunoprecipitation experiments showed that Cx43 and Dlg1 interact in each of these cell lines, emphasising the importance of the interaction in normal epithelial cells **(Table 1.1)** (Dong, 2021).

Previous studies have also worked towards defining the molecular determinants of the Cx43/Dlg1 interaction. Given the well-established interaction between the Cx43 extreme C-terminus and the PDZ2 domain of a related MAGUK protein, ZO-1, it was presumed that Cx43 and Dlg1 may interact in a similar fashion. However, studies of Dlg1 interaction with a different connexin, Cx32, found that the C-terminal tail of Cx32 bound to the SH3/HOOK/GUK domains of Dlg1 (Duffy *et al.*, 2007). This suggested that the regions involved in Dlg1/Cx43 interaction may be distinct from those which are crucial for ZO-1/Cx43 interaction. Indeed, the terminal 5 amino acids of Cx43, essential for ZO-1 interaction, were found to be dispensable for binding to Dlg1 (MacDonald *et al.*, 2012). Instead, the Cx43 C-terminus was observed to bind to both the N-terminus (residues 1-122) and the

C-terminus (residues 560-911) of Dlg1, suggesting multiple interaction sites and a distinct interaction from Cx43/ZO-1. Further research showed through deletion mutations that a Dlg1 binding site was contained within residues 348-377 of Cx43 (Dong, 2021). Given that Cx43 binds both the N- and C-termini of Dlg1, there are also likely additional interaction sites yet to be defined. The effect of mutations at specific residues of Cx43 to mimic unphosphorylated serine were also investigated. Results from this showed that mutation of certain sites (S255, S262, S279, S368 and S373) inhibited the interaction with Dlg1, while mutation of S282 conversely enhanced the interaction (Dong, 2021). This suggests a complex relationship between Cx43 post-translational modifications and interaction with Dlg1.

While significant progress has been made on understanding the specifics of the Cx43/Dlg1 interaction, several questions remain unaddressed. For example, the specific function of Dlg1 during the normal lifecycle of Cx43 is yet to be fully elucidated. The role of Dlg1 in wound healing requires further study and it is also currently unknown whether the interaction between Cx43 and Dlg1 is conserved in human skin. Finally, the exact binding sites of Cx43 and Dlg1 are unknown. Therefore, this investigation sought to further investigate the Cx43/Dlg1 interaction.

Table 1.1: Properties of epithelial cell lines where the Cx43/Dlg1 interaction has been previously studied

Cell Line	Cancer Status	HPV Status	Reference
HaCaT	Non-cancerous	-ve	Dong, 2021
HEK293	Non-cancerous	-ve	Dong, 2021
NIKS	Non-cancerous	-ve	Dong, 2021
W12NT (W12G)	Non-cancerous	+ve	Macdonald *et al.*, 2012
W12T (W12GPXY)	Cancerous	+ve	Macdonald *et al.*, 2012
C33a	Cancerous	-ve	Sun *et al.*, 2015
C33aE6	Cancerous	E6 expressing	Sun *et al.*, 2015

1.10 Aims

The present gaps in knowledge this thesis aims to address are as follows:

Aim 1: Investigate how the Cx43 lifecycle is altered *in vitro* in cells where Dlg1 has been depleted.

- Assess whether Cx43 mRNA levels are altered when Dlg1 is knocked down.
- Analyse changes in Cx43 protein subcellular localisation when Dlg1 is depleted.
- Investigate changes in Cx43 degradation when Dlg1 is knocked down.
- Establish whether Dlg1 knockdown affects other junctional structures/cell membrane integrity.
- Determine whether Dlg1 controls gap junctional communication.
- Define the specific role of Dlg1 in the Cx43 lifecycle.

Aim 2: Determine the role of Dlg1 in the wound healing process/keratinocyte migration and proliferation.

- Evaluate the effectiveness of a 3D printed wound mask in reducing variation between individual scratch wounds.
- Determine how Dlg1 knockdown affects wound closure in scratch assays and assess whether any observed change is due to an effect on cell proliferation and/or migration.
- Observe how Cx43 and Dlg1 move and colocalise in live cell scratch wound experiments.
- Establish whether the interaction between Cx43 and Dlg1 is conserved in skin tissue keratinocytes/dermal cells/adipocytes and whether this is altered in diabetic skin.

Aim 3: Identify the molecular determinants of the Cx43/Dlg1 interaction.

- Use AlphaFold modelling software to predict potential interaction sites of Cx43 and Dlg1.
- Using information from this AlphaFold model, produce recombinant Cx43 and Dlg1 protein and determine the regions of Cx43 which are required for interaction with Dlg1.
- Investigate the effect of Cx43 mutations mimicking phosphorylation of certain residues on the Cx43/Dlg1 interaction.

Chapter 2: Materials and Methods

2.1 Materials

2.1.1 Bacterial Cells

The following bacterial cell lines were utilised in this study:

- Stellar competent *E. coli* cells used for maintenance of recombinant plasmid DNA were obtained from Takara Bio (Takara, CA, USA, 638951).
- BL21 Gold *E. coli* cells used for expression of recombinant proteins were kindly gifted from Dr Amit Meir, MRC-University of Glasgow Centre for Virus Research, Glasgow, UK.

2.1.2 Cell Lines

The following cell lines were utilised in this study:

- HaCaT cells- human spontaneously immortalised HPV-negative keratinocytes (Boukamp *et al.*, 1988). (https://cls.shop/HaCaT/300493).
- HEK293 cells- human embryonic kidney cells, HPV-negative (ATCC, https://www.atcc.org/products/crl-1573).
- W12T cells (previously referred to as W12GPXY)- transformed and invasive HPV16-positive human cervical epithelial cells (Aasen *et al.*, 2003).
- HeLa Ohio- Human cervical cancer cells, HPV18-positive (Sigma, Poole, UK, https://www.sigmaaldrich.com/GB/en/product/sigma/cb_84121901).

2.1.3 Antibodies

Primary antibodies used in immunofluorescence and western blot experiments are summarised in **Table 2.1**. Secondary antibodies used are shown in **Table 2.2**. Cx43 antibody was kindly gifted by Dr Edward Leithe, Oslo University Hospital, Norway (Rivedal *et al.*, 1996).

Table 2.1: Information on primary antibodies used in this investigation, including application, species, dilution and manufacturer

Antibody	Application	Species	Dilution	Manufacturer	Reference Number
Cx43	IF/WB	Rabbit	1:1000 (1:500 for skin tissue)	N/A (Rivedal *et al.*, 1996)	N/A
Dlg1	IF/WB	Mouse	1:250 (1:50 for skin tissue)	Santa Cruz Biotechnology	sc-9961
GAPDH	WB	Mouse	1:1000	Meridian Life Sciences	18L34316
ß-catenin	IF	Mouse	1:200	BD Transduction Laboratories	610154
Calnexin-1	IF	Rabbit	1:100	Enzo Life Sciences	ADI-SPA-860
58K	IF	Mouse	1:100	Abcam	ab27043
Cytopainter Golgi Staining Kit	IF	N/A	Manufacturer's Instructions	Abcam	ab139483
EEA1	IF	Mouse	1:200	Abcam	ab15846
LAMP-2	IF	Mouse	1:100	Proteintech	66301-1-Ig
ZO-1	IF	Mouse	1:500	ThermoFisher Scientific	610966
Rabbit IgG	IF	Rabbit	1ug/ml	Abcam	Ab37415
GST	WB	Rabbit	1:1000	Sigma	G7781
FLAG	WB	Mouse	1:1000	Sigma	F3165

Table 2.2: Information on secondary antibodies used in this investigation, including application, species, dilution and manufacturer

Antibody	Application	Species	Dilution	Manufacturer	Reference Number
Alexa Fluor 488 (anti-mouse/rabbit)	IF	Donkey	1:500	Life Technologies	A21202/A21206
Alexa Fluor 594 (anti-rabbit/mouse)	IF	Donkey	1:500	Life Technologies	A21207/ A-11032
Dylight 680 (anti-rabbit)	WB	Goat	1:2000	ThermoFisher Scientific	35568
Dylight 800 (anti-mouse)	WB	Goat	1:2000	ThermoFisher Scientific	SA535521

2.1.4 Plasmids

- The pegfp-C1 mammalian expression plasmid containing the sequence coding for rat Dlg1 with a GFP-tag on the N-terminus was kindly gifted by Dr Lawrence Banks and Dr Miranda Thomas, International Centre for Genetic Engineering and Biotechnology, Trieste, Italy (Marziali *et al.*, 2017).
- The pmCherry-N1 plasmid containing sequence coding for human Cx43 with a C-terminal mCherry-tag was previously generated in the Graham lab by Andrew Stevenson, MRC-University of Glasgow Centre for Virus Research, Glasgow, UK.
- The pFLAG3xCMV10 plasmid containing the sequence coding for the human Cx43 C-terminus (aa236-382) which was used for site-directed mutagenesis and expression studies in mammalian cells was previously generated in the Graham lab by Dr Li Dong and Andrew Stevenson, MRC-University of Glasgow Centre for Virus Research, Glasgow, UK.

2.1.5 Primers and Probes

Primers and probes used for the amplification and detection of Cx43 and GAPDH in RT-qPCR are shown in **Table 2.3**. The primers used to amplify sequences to be cloned into the pGEX2T vector for expression of recombinant protein in bacterial cells are shown in **Table 2.4**. The primers used to amplify sequences to be included in the pFLAG3xCMV10 vector for recombinant protein expression in mammalian cells are shown in **Table 2.5**.

Table 2.3: Primers and probes for the amplification and detection of Cx43 and GAPDH in RT-qPCR

Target	Primer/Probe	Sequence
Cx43	Forward	5'-CTGGGTCCTGCAGATCATATTT-3'
	Reverse	5'-GGCAACCTTGAGTTCTTCCT-3'
	Probe-FAM	5'-CCCACACTCTTGTACCTGGCTCAT-3'
GAPDH	Forward	5'-GAAGGTGAAGGTCGGAGT-3'
	Reverse	5'-GAAGATGGTGATGGGATTTC-3'
	Probe-HEX	5'-CAAGCTTCCCGTTCTCAGCC-3'

Table 2.4: Primer sequences for bacterial cell expression studies

Target	Fwd /Rv	Sequence
pGEX2T	Fwd	5'-CCGGGAATTCATCGTGACTGACT-3'
	Rv	5'-GGATCCACGCGGAACCAGA-3'
Cx43 C-terminus (aa232-382)	Fwd	5'-GTTCCGCGTGGATCCTTCTTCAAGGGCGTTAAGGATCGG-3'
	Rv	5'-ACGATGAATTCCCGGCTAGATCTCCAGGTCATCAGGCC-3'
Cx43 C-terminus Deletion A (Δ263-274)	Fwd	5'-GTGGGTCTACCGCTCCCCTCTCGCCTATG-3'
	Rv	5'-GAGCGGTAGACCCACAGTCTTTGGCAGG-3'
Cx43 C-terminus Deletion B (Δ302-310)	Fwd	5'-GCAATTACGCTAATTACAGTGCAGAACAAAATC-3'
	Rv	5'-AATTAGCGTAATTGCGGCAAGAAGAATTG-3'
Cx43 C-terminus Deletion C (Δ372-379)	Fwd	5'-GTCGTGCCCTGGAGATCTAGCCGGGAATTCA-3'
	Rv	5'-TCTCCAGGGCACGACTGCTGGCTCT-3'
Dlg1 SH3/ HOOK/ pGUK (aa569-764)	Fwd	5'-GTTCCGCGTGGATCCATTAGTTCAGGGTCAGGTTCTCT-3'
	Rv	5'-ACGATGAATTCCCGGTCAAGTCACAAAATGATAATCTCTT-3'

ZO-1 PDZ2 (aa150-312)	Fwd	5’-GTTCCGCGTGGATCCAGGAGTGAGAAGATTTGGCCGA-3’
	Rv	5’-ACGATGAATTCCCGGTCACCGGCTGCGGCGGGGA-3’

Table 2.5: Primer sequences for mammalian cell expression studies

Target	Fwd/Rv	Sequence
Cx43 C-terminus Deletion D (Δ296-330)	Fwd	5’-GAAACAATCATGCACAGCCTTTTGATTTCCC-3’
	Rv	5’-GTGCATGATTGTTTCTGTCGCCAGTAACC-3’
S255E	Fwd	5’-TGCGCTGGAACCTGCCAAAGACTGTGGGTC-3’
	Rv	5’-GCAGGTTCCAGCGCACCACTGGTCGC-3’
S262E	Fwd	5’-CTGTGGGGAACAAAAATATGCTTATTTCAATGGCT-3’
	Rv	5’-TTTTGTTCCCCACAGTCTTTGGCAGG-3’
S279E	Fwd	5’-TCCCCTCGAACCTATGTCTCCTCCTGGGTACAAG-3’
	Rv	5’-ATAGGTTCGAGGGGAGCGGTTGGTGAG-3’
S282E	Fwd	5’-GCCTATGGAACCTCCTGGGTACAAGCTGG-3’
	Rv	5’-GGAGGTTCCATAGGCGAGAGGGGAGCG-3’
S368E	Fwd	5’-CAGAGCCGAAAGTCGTGCCAGCAGCAGACC-3’
	Rv	5’-CGACTTTCGGCTCTGCTTGAAGGTCGCT-3’
S373E	Fwd	5’-TGCCAGCGAAAGACCTCGGCCTGATGACC-3’
	Rv	5’-GGTCTTTCGCTGGCACGACTGCTGGC-3’
Y265E	Fwd	5’-TCAAAAAGAAGCTTATTTCAATGGCTGCTCC-3’
	Rv	5’-TAAGCTTCTTTTTGAGACCCACAGTCTTTGGC-3’
Y265F	Fwd	5’-TCAAAAATTTGCTTATTTCAATGGCTGCTCC-3’
	Rv	5’-TAAGCAAATTTTTGAGACCCACAGTCTTTGGC-3’

2.1.6 Kits

Kits used in this study are summarised in **Table 2.6**.

Table 2.6: Kits used in this study

Kit	Manufacturer	Reference Number
RNeasy	Qiagen	74104
Maxima™ First Strand cDNA Synthesis	ThermoFisher Scientific	K1641
NucleoSpin™ Gel and PCR Clean-up Kit	Macherey-Nagel	740609.50
In-Fusion® HD Cloning Kit	Takara	638945

2.1.7 Human tissues

Formalin-fixed human abdominal skin tissue blocks from six patients (three diabetic, three non-diabetic) taken during replacement of breast tissue following mastectomy, were obtained with ethical permission (GCU Skin Tissue Bank, REC Reference 21-WS-0088, in association with NHS GG&C Biorepository) (https://www.gcu.ac.uk/aboutgcu/academicschools/hls/research/researchgroups/molecularmechanismsoflongtermconditions/gcuskinresearchtissuebank).
Informed consent was obtained for all tissue donors, and all clinical investigations were conducted according to the principles expressed in the Declaration of Helsinki.

2.2 Methods

2.2.1 Cell Culture

HaCaT, HEK293, W12T and HeLa Ohio cells were cultured in Dulbecco's Modified Eagle's Medium (DMEM) (Gibco, Renfrew, UK, ref no 31966-021) containing 10 % (v/v) FBS (Gibco, Renfrew, UK, ref no 10270-106) and 1 % (v/v) penicillin-streptomycin (Gibco, Renfrew, UK, ref no 15140-122). Cells were maintained in a humidified incubator with 5 % CO_2 at 37 °C. Cell were detached from plates using 0.05 % trypsin-EDTA (Gibco Renfrew, UK, ref no 25300-054) and passaged three times a week at either 1:5 or 1:10 dilution depending on growth rate.

2.2.2 Cell Treatments

For siRNA transfections, cells were cultured as described above in either 6 or 12-well plates until they reached 30-50 % confluency, at which point transfection with siRNA against Dlg1 (ON-TARGETplus SMARTpool siRNA, Dharmacon, L-009415-00-0010) or control oligonucleotides (siGLO, Dharmacon, D-001630-01-0) was carried out using Lipofectamine RNAiMax transfection reagent (ThermoFisher Scientific, 13778075). siRNA sequences targeting Dlg1 are shown in **Table 2.7**. Briefly, siRNAs and 2.5 µl lipofectamine per sample (5 µl when using 40 nM siRNA) were diluted in Opti-MEM medium (Gibco, 31985070) before addition of lipofectamine to each siRNA tube. Transfection mixes were incubated at RT for 15 min before being added to wells. The final concentration of siRNA in each well was 20 nM or 40 nM. siGLO control oligonucleotide was used as a non-target oligonucleotide and to assess transfection efficiency.

Lysosomal inhibition was carried out by treatment of cells with 10 mM NH_4Cl (Sigma) for 8 h at 37 °C.

For determination of optimum mitomycin C (MMC) concentration for HaCaT scratch wound assays, HaCaT cells were treated with final concentrations of MMC (Sigma, M4287) ranging from 4 x 10^2 - 4 x 10^{-5} μg/ml and incubated for 5 minutes. Cells were then washed twice in PBS and incubated in fresh media for 24 h at 37 °C. Medium was collected and floating cells were counted using a haemocytometer.

For MTT assay following MMC treatment, MTT powder (Abcam, Cambridge, UK, ab146345) was dissolved in PBS to a concentration of 5 mg/ml and filter sterilised. MMC treatment was carried out as above in a 96-well plate. Medium was removed following 24 h incubation and 50 µl MTT substrate, as well as 50 µl fresh media were added to each well. 50 µl MTT and 50 µl media were also added to wells containing no cells for background signal controls. The plate was incubated at 37 °C for a further 3 h. To dissolve formazan crystals formed by MTT, 150 µl DMSO (Sigma, D1435) was then added to each well and the plate was wrapped in foil to protect from light before being placed on a rotating orbital shaker for 15 min. Following dissolution of formazan crystals, absorbance was measured at a wavelength of 595 nm by a Multiskan™ FC Microplate Photometer (ThermoFisher Scientific, 11590685). Background values from wells containing only 50 µl MTT + 50 µl media were subtracted from test samples. Values were then normalised against control HaCaT cells to give final results.

Table 2.7: ON-TargetplusSMARTpool siDlg1 target sequences

siDlg1 SMARTpool Target Sequences siRNA No.	Target Sequence
J-0009415-05	GAUCGUAUUAUAUCGGUAA
J-0009415-06	CCAUAGAACGGGUUAUUAA
J-0009415-07	GUACUGGUCAACACAGAUA
J-0009415-08	AAAACGAGAUUAUGAGGUA

2.2.3 Preparation of Cell Stocks

Cells were removed from the culture vessel using trypsin as described in **Section 2.2.1**. Cells were counted using a haemocytometer and centrifuged at 1000 rpm for 5 min. Supernatant was removed and the cell pellet was resuspended in media + 10 % (v/v) DMSO (Sigma) to give a concentration of 1 x 10^6 cells/ml. Cells were stored in 1 ml aliquots at -80 °C overnight before being moved to a liquid nitrogen tank for long-term storage.

2.2.4 Protein extract preparation and western blotting

Plates containing cells were placed on ice and washed twice in ice-cold PBS before being lysed in NuPAGE™ lithium dodecyl sulfate (LDS) sample buffer (Invitrogen). Protein extracts were syringe-passaged through a 22-gauge needle 10 times then sonicated in a Sonibath (Kerry Ultrasonics, Hitchin, UK) for 30 s, followed by 30 s resting on ice 3 times. The samples were boiled at 100 °C for 5 min before loading on a 12 % NuPAGE gel (Invitrogen) and electrophoresed at 200 V for 45 min in 1× MES buffer (NuPAGE MES Running Buffer 20x, ThermoFisher, NP0002). Proteins were transferred to a nitrocellulose membrane using an iBlot™2 transfer system (Invitrogen, IB22001) and iBlot™2 Gel Transfer Stacks (Invitrogen, IB23001) as per the manufacturer's instructions. Membranes were blocked in 5 % (w/v) milk powder (Marvel, Tesco, UKFF005MC) in PBST (PBS containing 0.1 % (v/v) Tween 20) at room temperature with rotation for 1 h. Blots were incubated with primary antibodies **(Table 2.1)** diluted in PBST with 5 % (w/v) milk powder with rotation for 1 h at RT or overnight at 4°C. The blots were washed three times in PBST for 5 min. They were then placed in tubes containing secondary antibodies diluted in PBST 5 % (w/v) milk powder and incubated with rotation for 1 h **(Table 2.2)**. Tubes were wrapped in tinfoil during this stage to protect from light. Blots were washed 3 times in PBST for 5 min before imaging using a LI-COR Odyssey imager (LI-COR Biosciences, NE, U.S.A.). Signal intensity for Cx43 and Dlg1 bands was quantified and normalised against the signal for GAPDH loading control.

2.2.5 qRT-PCR and analysis

Dlg1 depletion in HaCaT cells was carried out as in **Section 2.2.2**. RNA was prepared from siRNA-transfected cells using a Qiagen RNeasy extraction kit (Qiagen, Manchester, UK) exactly as described in the manufacturer's protocol. cDNA was synthesised using a Maxima cDNA synthesis kit (ThermoFisher Scientific, UK) with DNase digestion according to the manufacturer's protocol. Cx43 and GAPDH primer and probe sets are shown in **Table 2.3** (Eurofins, Livingston, UK). Fluorescent reporters were FAM for Cx43 and HEX for GAPDH. The final concentrations of primer and probe in each reaction were 900 nM and 100 nM respectively. qRT-PCR was carried out using an ABI 7500 Real Time PCR System (ThermoFisher Scientific) with the following conditions: 1 cycle of 50 °C for 2 min, 1 cycle of 95 °C for 3 min, then 40 cycles of 95 °C for 10 s followed by 60 °C for 1 min. GAPDH was included for each sample as an internal control gene. Each sample was run in triplicate. ΔCt values were calculated as the difference in Ct between internal control GAPDH and Cx43 Ct values. ΔΔCt values were then calculated as the difference in ΔCt between control-treated cells and 20 nM siDlg1-treated cells. The average expression ratio of Cx43 cDNA in cells depleted of Dlg1 compared to control-treated cells was then calculated as $2^{-\Delta\Delta Ct}$.

2.2.6 Confocal immunofluorescence microscopy and quantification

Cells were grown on sterile 13 x 13 mm coverslips until 90% confluent, then washed twice with PBS. For Cx43 and LAMP-2 colocalisation, cells were fixed with 4 % (w/v) paraformaldehyde (PFA) for 15 min at room temperature. For all other experiments, cells were fixed with 100 % ice-cold methanol for 10 min at 4 °C. Cells were permeabilised in acetone for 1 min followed by three 5 min washes in PBS and incubation at room temperature for 1h with PBS 10 % (v/v) donkey serum to block. Primary antibodies **(Table 2.1)** were diluted using PBS 5 % (v/v) donkey serum and incubated for either 1h at room temperature or overnight at 4 °C. Coverslips were washed five times with PBS. Alexa Fluor

secondary antibodies **(Table 2.2)** were diluted in PBS 5 % (v/v) donkey serum and added to the coverslips for 1h, protected from light. Coverslips were washed 5 times in PBS, followed by one wash in distilled (d)H_2O. Coverslips were mounted on glass slides with ProLong™ Gold Antifade Mountant with DAPI (Invitrogen, P36935). Control samples which were incubated with secondary antibodies but no primary antibodies were included in each experiment. For experiments focusing on colocalisation of Cx43 and Calnexin-1, both primary antibodies were derived from rabbits, which can generate cross-signal through secondary antibodies targeting both primary antibodies. Therefore, sequential staining was carried out. Samples were incubated with Cx43 primary antibody followed by incubation with secondary antibody Alexa Fluor 594. Samples were then blocked in PBS 10 % (v/v) donkey serum for a further 1 h before incubation with Calnexin-1 primary antibody, followed by incubation with secondary antibody Alexa Fluor 488. In this experiment, an extra control sample was included without Calnexin-1 primary antibody incubation to assess if cross-signal was generated through Alexa Fluor 488 binding to Cx43 primary antibody.

For staining of paraffin-embedded human skin tissue, sections on slides were de-paraffined, and antigen retrieval was performed using sodium citrate (10 mM, pH 6.0). Sections were then washed gently in PBS before blocking for 1 h as above. Incubation with Cx43 (1:500) and Dlg1 (1:50) **(Table 2.1)** primary antibodies was carried out overnight at 4 °C. Subsequent steps were performed as above. Control samples including secondary antibodies with no primary antibodies were included, with an additional control of 1 µg/ml rabbit IgG in place of primary antibody. Samples were examined using a Zeiss LSM 710 confocal microscope (Zeiss, Oberkochen, Germany) and Zen black software (Zeiss) was used for capturing images.

Quantification of colocalisation was performed using Zen blue software (Zeiss). As Cx43 signal levels were expected to vary between untreated and siRNA-treated cells, threshold setting and colocalisation measurements were selected to be as independent of signal intensity as possible, while allowing an appropriate background signal level to be set. Thresholds for colocalisation were

set using single stains of Cx43, calnexin-1, LAMP-2, Golgi Tracker, 58K and EEA1 imaged in both red and green channels under the same conditions as in the test samples. Cells were outlined using the Zeiss software drawing tool, and Manders' colocalisation coefficient (M1) was measured for each outlined cell (Manders et al., 1993); 50 individual cells were analysed for each treatment group.

Quantification of the proportion of total Cx43 on the plasma membrane was performed using ImageJ/Fiji® software (Schindelin *et al.*, 2012). Using the free-hand drawing tool, two outlines were created for each cell, one surrounding the entire cell and the other covering the cell minus the plasma membrane (as indicated by ß-catenin plasma membrane staining). The proportions of Cx43 staining were analysed using integrated density values obtained from each of these outlines. To account for background signal, three areas with no Cx43 staining were selected in each image and the average value of these areas were subtracted from the raw values. Cx43 signal level on the plasma membrane was calculated by subtracting the value of the outline not containing the plasma membrane from the outline containing the plasma membrane. The resulting value was then divided by the value of the outline covering the entire cell to give the proportion of total cellular Cx43 on the plasma membrane; 50 individual cells were analysed for each treatment group.

2.2.7 Parachute assay

Parachute assays were based on the previously described technique (Donnelly *et al.*, 2012). A summary of the parachute assay procedure is shown in **Figure 2.1**. Donor cells (three plates of HaCaT cells, one plate of HeLa Ohio cells) were grown in 60 mm plates until they reached 30–50 % confluence, at which point one plate of HaCaT cells was treated with siRNA targeting Dlg1. Cells were incubated for a further 24 h before being treated with 2.5 µM calcein-AM (ThermoFisher Scientific, C1300MP) diluted in PBS plus 1 mM Ca^{2+} at 37 °C for 30 min with gentle rocking every 5 min. Calcein-AM is a membrane permeable compound which is converted intracellularly into green fluorescent calcein

(molecular weight = 623 Da), which can pass through gap junctions. Cells were washed three times in PBS plus 1 mM Ca^{2+} and incubated at 37 °C for 30 min in fresh medium. Following this, donor cells were washed twice and incubated with 1 µM CellTracker™ CM-DiI (molecular weight = 1051.5 Da) (ThermoFisher Scientific, C7000) for 5 min at 37 °C after which they were wrapped in tinfoil to protect from light and incubated for a further 15 min at 4 °C. CM-DiI is a red fluorescent dye that binds to intracellular membranes and cannot freely diffuse through gap junctions due to its size, therefore allowing distinction of red and green 'donor' cells from green 'acceptor' cells. Cells were washed three times and trypsinised before being pelleted by centrifugation at 283 g for 5 min. Cells were resuspended and pelleted as before and then resuspended and counted. Carbenoxolone (50 µM) (CBX; Sigma, C4790-1G) was added to HaCaT cells from one of the donor plates and incubated for 30 min to block communication through gap junctions. Donor cells (HaCaT cells, HaCaT cells + siDlg1, HaCaT cells + CBX, HeLa Ohio Cells) were 'parachuted' onto 80 % confluent 'acceptor' HaCaT cells (cultured in a 12-well plate) at a donor:acceptor cell ratio of 1:20. Each condition was run in triplicate. Cells were incubated at 37 °C for 4 h 30 min to allow dye transfer to take place followed by imaging on an AMG EVOS imaging microscope at 20x magnification (Invitrogen). Gap junctional communication was assessed as the average number of acceptor cells receiving dye from a donor cell (total number of acceptor cells receiving calcein green dye from a directly adjacent donor cell divided by total number of donor cells). Each group was then normalised to the control HaCaT cell group to give final values. At least 140 donor cells were analysed per treatment group.

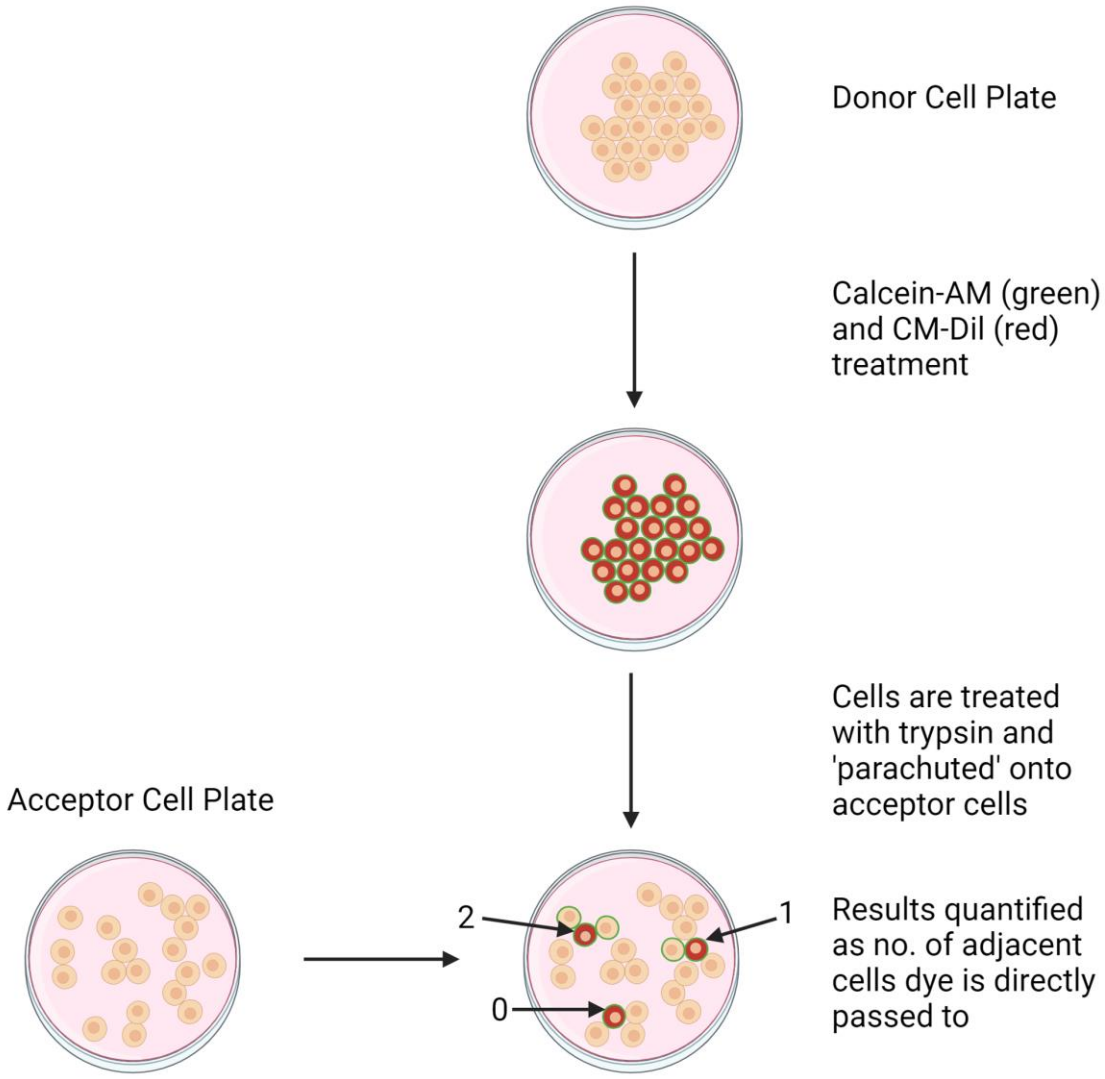

Figure 2.1: Parachute assay protocol. Donor cells (HaCaT cells, HaCaT+siDlg1, HaCaT+CBX or HeLa Ohio cells) are treated with Calcein-AM (green) and CM-Dil (red). Calcein is capable of being passed through gap junctions, while CM-Dil becomes trapped within the cell. This allows donor cells (green+red) to be distinguished from acceptor cells (green). Note that this figure does not accurately portray the cellular distribution of the dyes and the cells are only coloured to differentiate between labelled and unlabelled cells. Donor cells are treated with trypsin and 'parachuted' onto HaCaT acceptor cells at a donor:acceptor ratio of 1:20. Following incubation for 4 h 30 min, results are quantified as the number of adjacent acceptor cells dye is directly passed to from donor cells. Examples of quantification are shown. Figure made using Biorender.

2.2.8 Quantification of Cell Confluence following Depletion of Dlg1

Assessment of cell confluence after siDlg1 treatment was performed using an Incucyte® S3 Live-Cell Analysis System (Sartorius, Göttingen, Germany), which is an insert for a cell incubator which is able to take images of cells while maintaining normal incubator conditions. HaCaT cells were seeded at a density of 5 x 10^3 cells per well in an Incucyte® Imagelock 96-well Plate (Sartorius) and incubated for 24 h at 37 °C. Imagelock plates contain markings which allow consistent orientation of the plate within the live-cell analysis system and imaging of the same area of cells at each individual timepoint. siRNA treatments were carried out as described above and the plate was immediately transferred to the live-cell analysis system for imaging. Images were captured every 2 h, with the final timepoint being at 96 h.

Quantification of cell confluence was performed using the Incucyte® Base Analysis Software (Sartorius). Values were collated and exported to calculate average confluence values for each treatment group at each timepoint.

2.2.9 Design of a 3D-printed Wound Mask for use in *in vitro* 2D Scratch Wound Experiments

For use in 2D wound healing experiments, a wound mask to cover a 35 mm plate was designed using NX10 software (Siemens, Munich, Germany) **(Figure 2.2A)** before being exported and processed using Ultimaker Cura software (Ultimaker, Utrecht, Netherlands) to create code for 3D printing. The mask was printed using an Ultimaker S5 3D printer (Ultimaker). The gap in the mask was designed to allow a sterile 200 µl pipette tip through with minimal room for movement to limit variation in wound size **(Figure 2.2B-D)**.

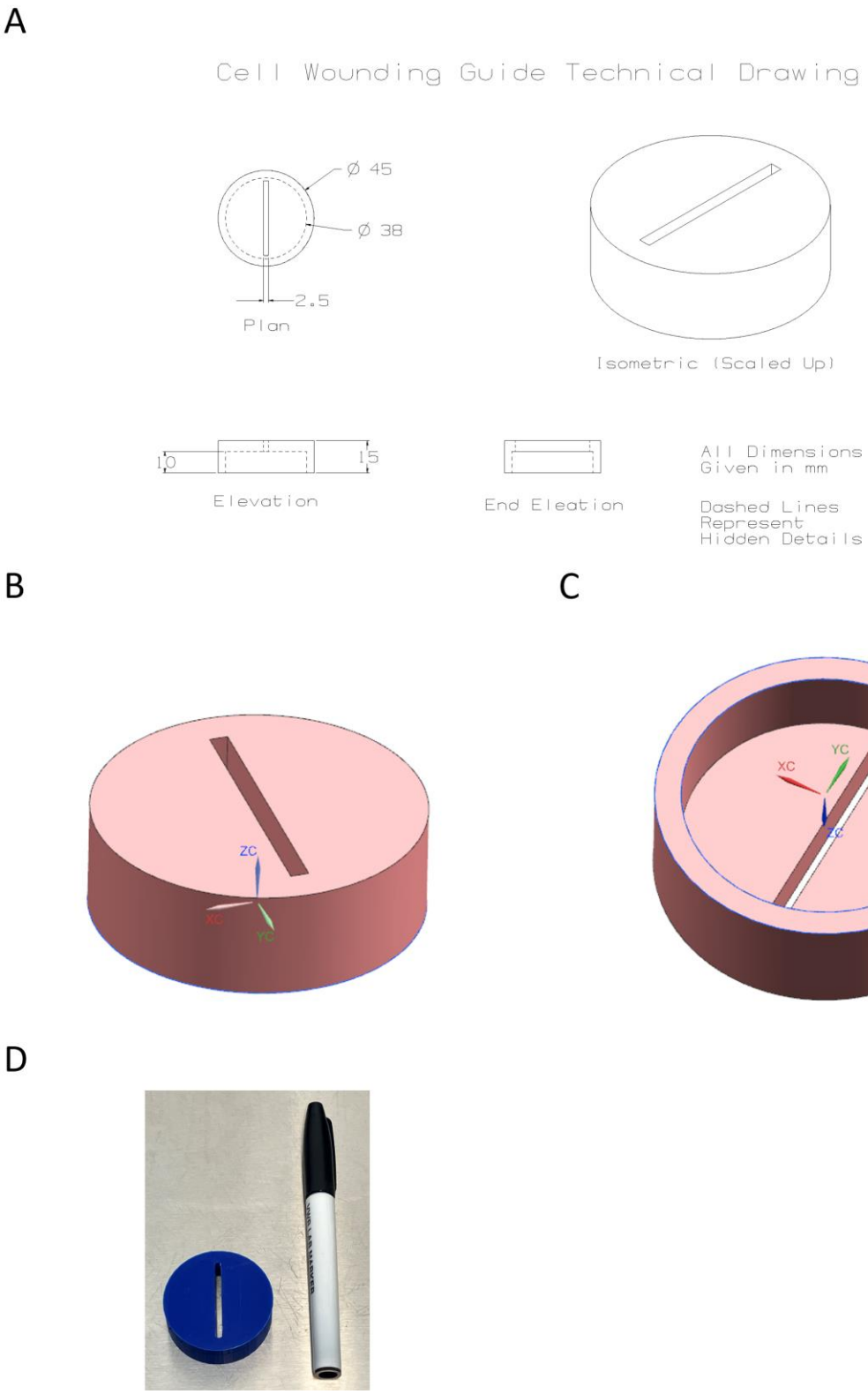

Figure 2.2: A 3D-printed wound mask for use in scratch wound assays. (A) Technical drawing of the 3D-printed wound mask from various angles, with dimensions shown in mm. Dashed lines represent hidden details. **(B)** and **(C)** 3D renders of the wound mask in an upright and upturned position respectively. The wound mask is placed over a 35mm cell culture dish in the orientation of **(B)** and a 200µl pipette tip is inserted through the gap of the top face of the mask for wounding. **(D)** Top view of the final wound mask with a marker pen for scale.

2.2.10 Scratch Wound Assay

For experiments utilising the 3D-printed wound mask, HaCaT, HEK293 and W12T cells were seeded in 35 mm plates at a density that would allow them to reach 100 % confluence in 24 h (0.6 x 10^6), or 4 h/8 h (1.2 x 10^6 cells) in experiments to assess impact of cell-cell attachment on wound variability. Cells were wounded using a sterile Starlab 200 µl pipette tip either free-hand or by placing the wound mask over the plate and using it to guide the pipette tip. Cell medium was removed and cells were washed twice in PBS before adding fresh media. Scratch wounds were immediately imaged using an EVOS™ M5000 microscope (Invitrogen). Wound size and variation were evaluated using the ImageJ/Fiji® Wound Healing Size plugin tool produced by Suarez-Arnedo et al. (Suarez-Arnedo *et al.*, 2020; Schindelin *et al.*, 2012). This tool is capable of measuring both average wound size and standard deviation of size within the wound.

For scratch wound experiments using the Incucyte® S3 Live-Cell Analysis System (Sartorius), 0.4 x 10^6 HaCaT cells were seeded in each well of a 6-well plate. There were four treatment groups, HaCaT control, 20 nM siDlg1-treated, 40 nM siDlg1-treated and 100 nM ZPC-treated. ZPC is a stable analogue of the GAP27 Cx43 mimetic peptide (molecular weight = 795.92 Da, formulation priority Zealand Pharma IP 068-DK-NOR-01). Following 24 h incubation, siRNA treatment was carried out as described above. Three biological replicates were included in each treatment group. Cells were then incubated for a further 20 h before being transferred to wells of a Incucyte® Imagelock 96-well Plate (Sartorius) at a fixed cell density of 0.08 x 10^6 cells per well. Cells were incubated for 4 h to allow attachment to the plate. 30 min prior to reaching the 4 h mark, the ZPC group was treated with 100 nM ZPC. In mitomycin C-treated groups, MMC was added to a final concentration of 4 x 10^{-2} µg/ml 5 min prior to wounding. Wounds were created using the Incucyte® Woundmaker Tool (Sartorius), which is a device composed of a tray plate and a plate containing 96 pins. The 96-well plate lid was removed and the plate was placed in the tray, with the pin board positioned over the wells. The button on the pin board was then pressed down to move the

pins across the cell monolayer, creating wounds in each well of the plate. Cell medium was removed and cells were washed twice using PBS before adding fresh media. ZPC was again added to the ZPC-treated group to a final concentration of 100 nM and the plate was placed in the live-cell analysis system for imaging. Images of initial wound area were captured and subsequently images were taken in each well every 2 h. The final timepoint was 48 h post-wounding.

Quantification of wound area in all wells at each timepoint was performed using the Incucyte® Scratch Wound Analysis Software Module (Sartorius). Use of the Incucyte Woundmaker Tool occasionally resulted in the generation of an uneven wound where a much larger area of cells was removed than intended. Wells containing these wounds were excluded from further analysis. Relative wound density % (RWD %) values were exported and average RWD % was calculated for each treatment group at each timepoint.

2.2.11 AlphaFold Models

AlphaFold2 models were generated using an AlphaFold CoLab online server: https://colab.research.google.com/github/sokrypton/ColabFold/blob/main/beta/AlphaFold2_advanced.ipynb (Jumper *et al.*, 2021). Steps were followed in a sequential fashion as listed on the server. For individual models, full amino acid sequences for Cx43 (1-382) or Dlg1 (1-904) were entered into the sequence input field. For the complex model, the sequences for the Cx43 C-terminus (232-382) and Dlg1SH3/HOOK/pGUK (569-764) were entered together separated by a colon to allow them to be modelled as a complex. Five models were generated for each input sequence, with a maximum number of 3 recycles (no. of times structure is fed back into neural network to alter structure prediction). Models were ranked according to their predicted template modelling (pTM) scores, which is a measure of the structural congruence of the model (Zhang and Skolnick, 2004). The top-ranked models of Cx43, Dlg1 and the two proteins together were evaluated in this investigation. In addition to protein models, plots of pLDDT (per-residue confidence score, from 0 being low confidence to

100 being high confidence) and PAE values (confidence in the placement of domains relative to other domains in a 3D space, from 0 being low error to 30 being high error) were generated for each model. Results were exported to Chimera X software for analysis (Pettersen *et al.*, 2021). Domains of each protein were coloured according to the UniprotKB annotation system for each protein (Vasudevan *et al.*, 2011). Contacts were set at a maximum distance of 4Å between atoms, which is generally accepted to be an appropriate limit on contacts (Furmanová *et al.*, 2018; Ofran and Rost, 2003; Zubek *et al.*, 2015).

2.2.12 Bacterial Cell Culture and Buffers

Stellar competent *E. coli* cells and BL21 Gold *E. coli* cells were used for plasmid maintenance and GST-tagged recombinant protein expression respectively. L-broth (10 g NaCl, 16 g Bactopeptone, 5 g yeast extract in 1 litre H_2O, pH 7.5) and agar plates made of 1.5% (w/v) agar in L-Broth were used to grow bacteria. Where necessary, 100 µg/ml ampicillin was added to agar plates or broth. Autoinduction of protein expression in BL21 Gold *E. coli* cells was carried out using autoinduction media composed of 2xYT media (16 g tryptone, 10 g yeast extract, 5 g NaCl in 1 litre H_2O) supplemented with 1 ml 1 M $MgSO_4$, 20 ml 50 x 5052, 50 ml 20x NPS and 1 ml ampicillin.

For recombinant protein purification, breaking buffer was composed of 4 mM MgCl, 1 mM DTT (ThermoFisher, 20290), 0.1 mg/ml lysozyme (ThermoFisher, J60701.03), 20 µl DNase (ThermoFisher, EN0521) and one cOmplete™ mini protease inhibitor cocktail tablet for every 10 ml buffer (Sigma, 04693124001). Binding buffer was PBS, 1 mM DTT. Elution buffer was 50 mM Tris, 10 mM glutathione (Sigma, G4251-1G), 0.15 M NaCl, 1 mM DTT. Buffers were adjusted to pH 7.0 for Cx43 purification.

2.2.13 Preparation of Bacterial Stocks

Bacterial stocks were prepared by adding 500 µl 50% glycerol (Sigma, G5516) to 500 µl bacterial cell culture. Bacterial stocks were stored at -80 °C.

2.2.14 Generation of pGEX-2T Plasmids Containing Sequences of Interest

Primers for the Cx43 C-terminus, Dlg1 SH3/HOOK domain and ZO-1 PDZ2 domain were designed using the In-Fusion Primer Design Tool (https://www.takarabio.com/learning-centers/cloning/primer-design-and-other-tools) **(Table 2.4)**. Previously designed primers to amplify and sequence the pGEX-2T vector were also utilised. Desired fragments were amplified from HaCaT cell DNA extracts using appropriate primers and the following conditions; 35 cycles of 98 °C for 10 s, 55 °C for 5 s, 72 °C for 5 s per kilobase. PCR products were then purified using a NucleoSpin™ Gel and PCR Clean-up Kit (Macherey-Nagel, Düren, Germany) according to the manufacturer's instructions. Size of PCR products was checked by gel electrophoresis before cloning of fragments into the pGEX-2T vector using an In-Fusion® HD Cloning Kit (Takara Bio) according to the manufacturer's instructions.

2.2.15 PCR-mediated Site Directed Mutagenesis

For expression of recombinant protein in bacterial cells, the pGEX-2T-Cx43 C-terminus plasmid was used as the template for PCR-mediated site directed mutagenesis with primers designed as above to delete interaction regions A, B and C **(Table 2.4)**. Conditions for PCR reactions were as above. Following PCR, parental DNA was degraded by Dpn1 (ThermoFisher ER1701) treatment for 15 min at 37 °C. Amplification of products was checked via gel electrophoresis, however these PCRs were unsuccessful.

For expression of recombinant protein in mammalian cells, the pFLAG3xCMV10-Cx43 C-terminus plasmid was used as the template for PCR-mediated site directed mutagenesis with primers designed as above to delete the entire main α-helix of Cx43 (Deletion D) as well as to cause substitution mutations of residues of interest **(Table 2.5)**. Following PCR, parental DNA was degraded by Dpn1 (ThermoFisher) treatment for 15 min at 37˚C.

2.2.16 Stellar *E. coli* Transformation and Sequencing of Cloned DNA Fragments

pGEX-2T and pFLAG3xCMV10 vectors containing sequences of interest were transformed into stellar competent *E. coli* cells according to instructions from the manufacturer (Takara Bio, Shiga, Japan). Transformation reactions were incubated on agar plates overnight at 37 ˚C containing 100 µg/ml ampicillin to select transformed cells. Resulting colonies were grown in 5 ml liquid culture containing 100 µg/µl ampicillin overnight with shaking at 220 rpm before DNA extraction. PCR was performed for the fragment of interest and PCR product size was confirmed by gel electrophoresis. Plasmid DNA was also sent to Eurofins for sequencing (Eurofins, Livingston, UK).

2.2.17 Expression of recombinant protein in BL21 *E. coli* cells

Plasmids containing successfully sequenced PCR fragments were transformed into BL21 Gold *E. coli* cells. DNA (~50 ng) was added to 50 µl *E.coli* cells and incubated on ice for 30 min. Transformation reactions were heat-pulsed at 42 ˚C in a water bath for 20 s and immediately placed back on ice for 2 min, followed by addition of 450 µl of SOC media (which was preheated to 42 ˚C) to each transformation reaction. Reactions were incubated at 37 ˚C for 1 h with shaking at 220 rpm. Cells were concentrated by centrifugation at 200 g for 5 min before plating of 20 µl transformation reaction + 80 µl H_2O on an agar plate containing 100 µg/ml ampicillin. Plates were incubated overnight at 37 ˚C.

For expression of recombinant GST-tagged protein, a single colony was picked from each transformation plate and grown in 5 ml LB broth overnight at 37 °C with rotation at 220 rpm. As an uninduced control sample, 500 µl of overnight culture was collected and pelleted at 14,000 rpm for 1 min. Supernatant was discarded and the cell pellet was frozen at -20 °C. For induced samples, overnight culture was diluted in autoinduction media 1:50 to a final volume of 5 ml. Samples were incubated overnight at either 20 °C or 24 °C with shaking at 220 rpm (maximum 16 h). Bacterial cells were pelleted by centrifugation of 1.5 ml culture at 14,000 rpm for 1 min. Medium was removed and bacterial cells were lysed in 300 µl breaking buffer for 30 min. Samples were centrifuged at 14,000 rpm for 25 min and supernatant containing protein was moved to a fresh tube. LDS sample buffer (Invitrogen) was added to supernatant tubes and samples were boiled for 3 min at 100 °C prior to gel electrophoresis. Success of induction and purification were confirmed by western blotting with an anti-GST antibody.

2.2.18 Glutathione Affinity Chromatography

For production of a sufficient quantity of recombinant protein to purify by glutathione affinity chromatography, the above protocol for recombinant protein expression was scaled up to a 1L culture. BL21 Gold *E. coli* containing the plasmid for expressing the Cx43 C-terminus were incubated at 20 °C with shaking at 220 rpm overnight. Bacterial cells were pelleted at 14,000 rpm for 1 min and the pellet was transferred to a new tube. The cell pellet was resuspended in 100 ml breaking buffer and incubated with rotation for 30 min at 4 °C. Sample was then sonicated on ice for 3 min in cycles of 10 s on, 10 s off before centrifugation at 21,000 rpm for 30 min to pellet cell debris. The sample, as well as binding and elution buffers were filtered and degassed. Glutathione affinity chromatography was performed using a GSTrap 1 ml column (Cytiva, MA, USA, GE17-5281-01) according to the manufacturer's instructions. Flow rates of sample onto column/elution flow rates were 0.7 ml/min and eluted sample was collected in 1.5 ml fractions. Fractions were run on a gel and subsequently stained with Coomassie brilliant blue G-250 (Sigma). Briefly, following

electrophoresis, the gel was transferred to a container and incubated for 1 h with Coomassie solution (0.05 % (w/v) Coomassie brilliant blue R-250 (Sigma, 1125530025), 50 % v/v methanol, 10 % v/v acetic acid, 40% H_2O) with rotation. Coomassie solution was then removed and the gel was incubated for a further 1 h with destaining solution (10 % v/v methanol, 10 % v/v acetic acid, 80 % H_2O) with gentle rotation. Fractions containing recombinant Cx43 C-terminus were pooled for size exclusion chromatography.

2.2.19 Size Exclusion Chromatography

Appropriate Cx43 C-terminus fractions from glutathione affinity chromatography were concentrated using a 6 ml Vivaspin®, 10 kDa MWCO polyethersulfone tube (Sigma, GE28-9323-63). The sample was then loaded onto a Superdex 200 increase column (Cytiva, 28990944). Size exclusion chromatography was performed according to the manufacturer's instructions. Fractions were run on a gel and stained with Coomassie brilliant blue dye and protein levels were measured using a Nanodrop One (Thermo). Fractions containing Cx43 C-terminus were frozen in liquid nitrogen and stored at -80 °C.

2.2.20 Transfection of HEK293 Cells with Cx43 C-terminal Mutant Constructs

HEK293 cells were cultured in 6 well-plates until reaching 80% confluency. Cx43 C-terminus construct DNA (1 µg) and 2.5 µl lipofectamine 2000 (ThermoFisher, 11668030) were each diluted in separate tubes of 250 µl Opti-MEM media (Gibco) and incubated for 5 min at RT. DNA and lipofectamine tubes were combined and incubated for 20 min at RT. Transfection mix (500 µl) was added to each well and cells were incubated for 48 h at 37 °C. Cells were lysed and protein expression was checked by western blot using the protocol described above.

2.2.21 Live Cell Experiments

HEK293 cells in a 35 mm plate were transfected as above using 1 µg Cx43-mCherry, 1 µg Dlg1-GFP DNA and 5 µl lipofectamine 2000. Cells were incubated for 24 h at 37 °C followed by scratch wounding using the wound mask as described above. Cells were then moved to the environmental chamber of a Zeiss Axio Observer Z1 microscope (Zeiss) which had been pre-incubated at 37 °C 5% CO_2. Images were captured every 10 min for a period of 66 h, at which point wound closure was almost 100%.

2.2.22 Statistical Analysis

An unpaired two-tailed t-test was used to assess significance in the colocalisation analyses. For western blots, Dlg1 and Cx43 values were normalised to GAPDH for each sample. For the lysosomal inhibition experiment, significance was assessed using a two-tailed Mann–Whitney U-test. For qRT-PCR, an unpaired two-tailed t-test was performed on $2^{-\Delta\Delta Ct}$ values to assess significance. For the parachute assay, results were expressed as the average number of acceptor cells receiving dye from a directly adjacent donor cell. Significance was assessed using a Kruskal–Wallis test followed by Dunn's post-hoc test to determine differences between the individual treatment groups. Data shown are the result of at least three biological replicates.

For the comparison of scratch wounds made either free-hand or using the 3D-printed wound mask at different timepoints, an unpaired two-tailed t-test was performed to assess significance. Analysis of knockdown of Dlg1 in scratch wound assays was performed using a Kruskal-Wallis test followed by Dunn's post-hoc test. This test was also used for experiments testing the effect of Dlg1 knockdown on cell proliferation. For the determination of mitomycin C concentration for use in scratch wound assays, a one-way ANOVA was performed followed by Tukey's test to determine differences between the individual treatment groups.

Chapter 3: The Role of Dlg1 in the Cx43 Lifecycle

3.1 Introduction

3.1.1 The Connexin 43 Lifecycle

The Cx43 lifecycle begins with transcription of mRNA from the *GJA1* gene. Like other connexins, Cx43 mRNA is translated on the ribosomes, then co-translationally inserted into the membrane of the endoplasmic reticulum (ER) **(Figure 3.1)** (Segretain and Falk, 2004). During this stage, folding of connexin proteins occurs, with regulatory mechanisms in place to remove any misfolded connexin proteins that could lead to dysfunctional gap junctional intercellular signalling (Epifantseva and Shaw, 2018). Following folding checks, connexins are trafficked in vesicles through the ER-Golgi intermediate compartment (ERGIC). Early post-translational modification of Cx43 can occur in the ER or the Golgi in the form of phosphorylation (Puranam, Laird and Revel, 1993). Despite this, the majority of Cx43 post-translational modifications take place later in the lifecycle and phosphorylation at this stage is not known to be required for oligomerisation or delivery to the plasma membrane (Dunham *et al.*, 1992). Oligomerisation to form connexons also occurs in the ERGIC for most connexins, however Cx43 atypically oligomerises later in the *trans*-Golgi network (TGN) (Koval, 2006). The reason for this discrepancy between Cx43 and other connexins is currently unknown, however one theory proposes that this is to regulate heteromeric connexon formation (Hesketh, Van Eyk and Tomaselli, 2009).

Connexons are mainly targeted to the plasma membrane to fringes of areas containing gap junctions and then diffuse laterally along the plasma membrane to join plaque edges (Lauf *et al.*, 2002). The degree to which connexins are delivered to specific areas of the cell membrane following export from the TGN is currently subject to some debate, with certain groups arguing that the rapid

turnover time of connexins points to targeted delivery to specific sites at the cell membrane, rather than random accumulation in plaques over time (Epifantseva and Shaw, 2018). Evidence to support this comes in the form of several microtubule-related proteins, such as EB1, being required for efficient trafficking of Cx43 to the plasma membrane (Smyth and Shaw, 2013). Disruption of microtubules via nocodazole treatment also impaired connexin vesicle movement and gap junctional communication (Martin *et al.*, 2001). In this model, Cx43 exits the Golgi in vesicles and can bind directly to tubulin through the Cx43 C-terminus. Tubulin itself is anchored to adherens junctions through ß-catenin, allowing quick transportation of Cx43 to areas adjacent to gap junction plaques (Shaw *et al.*, 2007). Drebrin is also involved in this stage of the trafficking pathway by directly binding the Cx43 C-terminus and attaching it to actin filaments, acting together with tubulin to tether Cx43 to the cytoskeleton (Ambrosi *et al.*, 2016). On reaching the plasma membrane, Cx43 interacts with ZO-1, which as previously mentioned negatively regulates the incorporation of newly synthesised Cx43 into gap junction plaques (Giepmans and Moolenaar, 1998; Rhett *et al.*, 2011). Once inserted into the plasma membrane, hemichannel and gap junctional activity are regulated by many different environmental factors, with hemichannels remaining closed under normal conditions (Wang *et al.*, 2013). Intracellular calcium (Ca^{2+}) levels are an important regulator of gap junctional signalling (Loewenstein, Nakas and Socolar, 1967), with higher Ca^{2+} levels causing decreased gap junctional communication through binding of calmodulin to the cytoplasmic loop and C-terminus of Cx43 (and other connexins) which results in channel closure (Zheng *et al.*, 2020). Other factors affecting channel opening include pH and transjunctional voltage (Peracchia, 2004).

As with other stages of the lifecycle, internalisation and degradation of gap junctions is an efficient process. Gap junctions are internalised from the cell membrane as double-membraned organelles termed annular gap junctions or connexosomes, which surprisingly can consist of cell membranes containing entire gap junctions from the two communicating cells, as opposed to lone connexons from a single cell (Jordan *et al.*, 2001). There is some evidence that connexosomes can recycle back to the plasma membrane following

internalisation (Carette *et al.*, 2015), however the majority eventually fuse with lysosomes to facilitate digestion of the protein. Cx43 internalised from gap junctions can also be degraded by the proteasome (Leithe and Rivedal, 2004a).

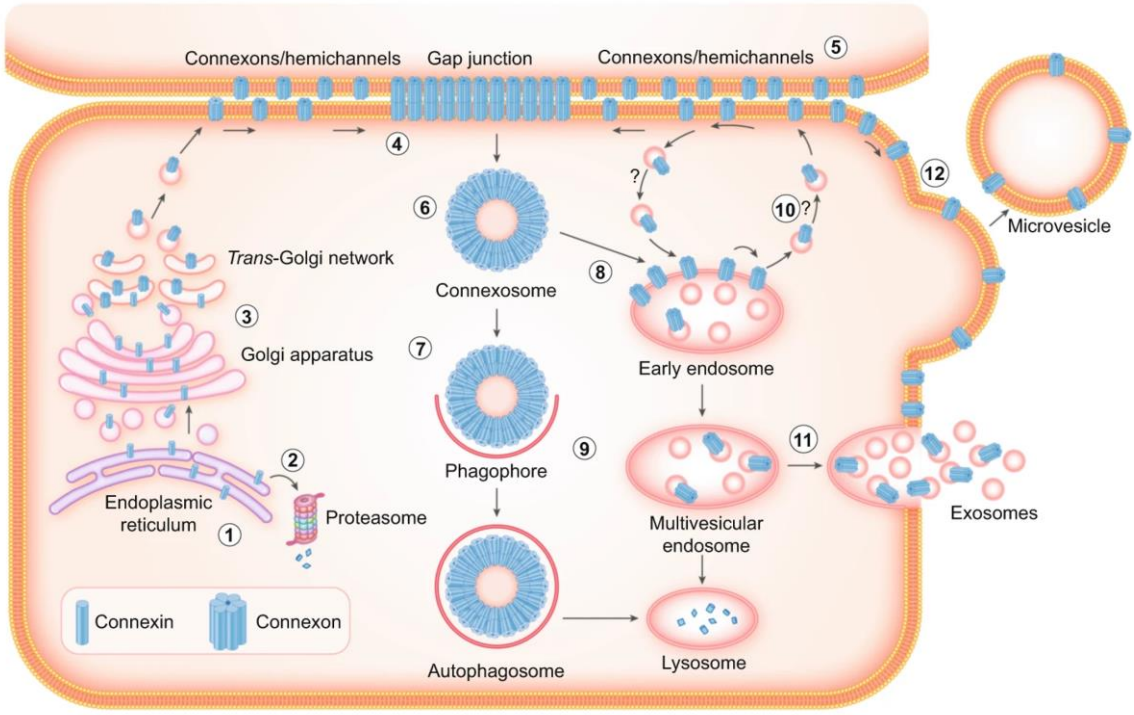

Figure 3.1: The general lifecycle of connexins. **1**: Nascent connexin protein is co-translationally inserted into the endoplasmic reticulum. **2**: A portion of newly-synthesised connexins are degraded by the proteasome following interaction with CIP75 and other mechanisms. **3**: Connexins oligomerise to form connexons in either the ER-Golgi intermediate compartment (most connexins) or the *trans*-Golgi network (Cx43). Trafficking of Cx43 is partially dependent on microtubules and motor proteins. **4**: Upon reaching the plasma membrane, connexons are incorporated into gap junction plaques where they dock with compatible connexons on apposing cells and form fully functional intercellular channels. **5**: Alternatively, connexons can exist as lone hemichannels which open under stress to release factors such as ATP and NAD^+ **6**: Full gap junctions are regularly removed from the membrane via endocytosis, which produces double-membraned connexosomes. **7**: Connexosomes can be degraded by autophagy. **8**: In a separate pathway, connexosomes can be remodelled into early endosomes **9**: Connexons follow the lysosomal pathway and are degraded. **10**: Occasionally, connexons may be recycled to the membrane from endosomes. **11**: Endosomes containing connexons may fuse with the plasma membrane to release exosomes into the extracellular environment. **12**: The membrane may also bud outwards from the cell to form extracellular microvesicles containing connexons. Adapted from Aasen *et al.*, 2019.

3.1.2 Control of Cx43 mRNA Transcription

Due to the short half-life of connexins (1-4 h) and the dynamic control of their activity, their expression is unsurprisingly tightly regulated by many different factors at three broad levels; transcription, translation and post-translational (Aasen *et al.*, 2019a). At the transcriptional level, the adherens junction protein ß-catenin promotes transcription of Cx43 from the *GJA1* gene directly by localising to the nucleus as part of the Wnt signalling pathway (Ai *et al.*, 2000). ß-catenin also interacts with Cx43 at gap junction sites, which is thought to sequester ß-catenin and prevent nuclear translocation, creating a negative feedback loop of Cx43 transcription (Spagnol *et al.*, 2018). On the other hand, there is also some evidence that under certain conditions Cx43 hemichannels can promote Cx43 gene expression through activation of JNK kinase in a positive feedback loop (Li *et al.*, 2013). Cx43 mRNA expression is also increased following activation of the JAK/STAT pathway, where phosphorylated STAT3 protein localises to the nucleus and promotes transcription of the *GJA1* gene (Ozog *et al.*, 2004). The JAK/STAT pathway plays a key role in a variety of processes, including but not limited to cell migration, proliferation and differentiation (Rawlings, Rosler and Harrison, 2004). The pathway is also involved in promoting inflammation in response to viral infection (Ezeonwumelu, Garcia-Vidal and Ballana, 2021). Further important transcription factors regulating Cx43 mRNA expression include activator protein-1 (AP-1) and specificity protein-1 (SP-1) (Echetebu *et al.*, 1999; Geimonen *et al.*, 1996).

As with other genes, histone modifications and DNA methylation are additional factors which can affect Cx43 mRNA transcription (Vinken, 2016). Acetylation of histones has been demonstrated to contribute to Cx43 mRNA transcription, as inhibition of histone deacetylases in prostate epithelial cells increased Cx43 transcription (Hernandez *et al.*, 2006). In contrast, the majority of studies on *GJA1* gene methylation, which is mainly associated with transcriptional repression, have focussed on cancer cells (Yi *et al.*, 2007). This means it is currently unknown to what degree this mechanism is employed to augment Cx43 mRNA transcription in normal cells. As with all forms of Cx43 regulation, the

effects of these modifications are likely to be highly dependent on cell-type and cancer status.

3.1.3 Control of Cx43 mRNA Translation

Recent work has shown that following transcription, Cx43 mRNA is regulated by several additional factors. MicroRNAs (miRNAs), a class of non-coding RNAs that bind to the 3' region of target mRNAs and inhibit translation or promote degradation, are important controllers of Cx43 expression (Oyamada *et al.*, 2013). Regulation of Cx43 in this fashion has been implicated in several types of cancer, including melanoma (Wang et al., 2019) and prostate cancer (Li *et al.*, 2012). Further regulation occurs through six internal translation sites within the *GJA1* gene which produce various sizes of N-terminally truncated Cx43 protein with distinct functions from full-length Cx43 (see **Chapter 1**) (Epifantseva *et al.*, 2020).

3.1.4 Post-translational control of Cx43 Protein

Cx43 protein can be degraded through the proteasomal, endosomal/lysosomal or autophagy pathways (Totland *et al.*, 2020). As mentioned previously, a certain portion of newly synthesised Cx43 will be misfolded and subsequently degraded due to quality checks within the ER. An example of such a check is through interaction with connexin-interacting protein of 75kDa (CIP75), which is a member of the ubiquitin-like ubiquitin-associated domain family of proteins and interacts preferentially with misfolded Cx43 (Li *et al.*, 2008), promoting its exit from the ER and subsequent ER-associated degradation (ERAD) via the proteasome (Su *et al.*, 2014). This process is unusual in that it does not involve ubiquitination of Cx43, while ERAD of other connexin proteins does (Gemel *et al.*, 2014). While this is currently the most well-defined mechanism of Cx43 ERAD, other mechanisms also contribute to degradation via this pathway.

Degradation of Cx43 through the lysosomal pathway in the stages before reaching the plasma membrane has also been reported (Qin *et al.*, 2003).

As with almost all sections of the Cx43 lifecycle, internalisation of gap junctions is influenced through post-translational modifications, which include phosphorylation (Solan and Lampe, 2014), ubiquitination (Totland *et al.*, 2020), SUMOylation (Kjenseth *et al.*, 2012) and acetylation (Meraviglia *et al.*, 2015). Phosphorylation on specific residues of Cx43 (mainly in the C-terminus) is associated with reduced gap junctional communication, with examples of interacting kinases being MAPK (Warn-Cramer *et al.*, 1998) and PKC (Lampe *et al.*, 2000). The oncogenic Src kinase protein also inhibits gap junctional communication through phosphorylation at residues Y247 and Y265 (Toyofuku *et al.*, 2001). In contrast, phosphorylation at other amino acid residues by different kinases such as AKT is associated with increased stabilisation of gap junctions (Dunn *et al.*, 2012). Ubiquitination also plays a critical role in Cx43 degradation and has been associated with channel closure/internalisation (Leithe and Rivedal, 2004a) and trafficking from early endosomes to lysosomes (Leithe *et al.*, 2009). An example of an E3 ubiquitin ligase enzyme that interacts with Cx43 is Nedd4, which ubiquitinates Cx43 in gap junctions in a phospho-dependent manner (Leykauf *et al.*, 2006), with this modification subsequently promoting recruitment of other factors such as Esp15 to allow internalisation of Cx43 (Girão, Catarino and Pereira, 2009). Cx43 is mainly monoubiquitinated as opposed to polyubiquitinated (Leith and Rivedal, 2004).

Despite the vast number of studies contributing to knowledge of the Cx43 lifecycle over the last few decades, many details remain to be elucidated. For example, the role that Dlg1 plays in the Cx43 lifecycle is incompletely understood. The interaction between the two proteins is known to play a significant role in human epithelial cell lines (Dong, 2021) and also in human papillomavirus (HPV)-associated cancer, with the oncogenic E6 protein targeting Dlg1 for degradation via the proteasome and thereby decreasing Cx43 levels (Sun *et al.*, 2015). However, no work to date has focused on defining the specific section of the Cx43 lifecycle that Dlg1 controls in normal epithelial cells. In this

chapter, the effect of depleting Dlg1 via siRNA is assessed in a human spontaneously immortalised HPV-negative keratinocyte cell line (HaCaT), both in terms of Cx43 levels/localisation and gap junctional communication/cell membrane integrity. This work provides insight into what stage(s) of the Cx43 lifecycle Dlg1 participates in.

Aims:

- Determine the effect of siRNA targeting Dlg1 on Cx43 mRNA and protein levels.
- Investigate the role of Dlg1 in the Cx43 lifecycle through immunofluorescence experiments to determine localisation of Cx43 when Dlg1 is depleted.
- Quantify how Cx43 is degraded when Dlg1 is depleted.
- Assess whether knockdown of Dlg1 results in changes to cellular junctions or cell membrane integrity.
- Evaluate whether Dlg1 controls gap junctional intercellular communication.

3.2 Knockdown of Dlg1 reduces Cx43 protein levels but does not affect Cx43 mRNA levels

Previous work has shown that knockdown of Dlg1 via 40nM siRNA results in reduced Cx43 protein at the cell membrane and lower levels of both Dlg1 and Cx43 protein in HaCaT, HEK293, NIKS and NIKS16 keratinocyte cell lines (MacDonald et al., 2012; Dong, 2021). As the focus of this study was to define the role of Dlg1 in the Cx43 lifecycle in normal human keratinocytes, HaCaT cells were selected and used for all experiments in this chapter. It was frequently observed during previous studies that Cx43 was difficult to visualise by immunofluorescence in siDlg1 cells due to removal of 72% of the total Cx43 protein (Dong, 2021). Therefore, for investigations into the localisation of Cx43 in Dlg1-depleted cells it was decided that 20nM of siRNA should be used instead

of the previous 40nM concentration. Consequently, it was important to quantify whether 20nM siRNA retained the ability to effectively knock down Dlg1 and if there was any effect on Cx43 protein levels. To address this, a western blot was performed with cell lysates from HaCaT cells treated with 20nM siDlg1 and protein levels were compared to cells transfected with an unrelated oligonucleotide, siGLO **(**Error! Reference source not found.**A)**. Levels of Cx43 and Dlg1 were normalised to GAPDH as a protein loading control. While Cx43 can produce several protein bands on western blots due to different phosphorylation states, these bands are not consistently detected in HaCaT cells and therefore only the base P0 Cx43 band was quantified in this study. Dlg1 also produced several protein bands, which likely represent the different isoforms of Dlg1 generated through alternative splicing (discussed in **Chapter 1, Section 1.8)**, as has been previously observed in keratinocytes (Roberts *et al.*, 2007). As these bands are consistently detected in HaCaT cells, all Dlg1 bands were quantified. The results show that Dlg1 level was reduced by 42% in 20nM siDlg1 cells, with Cx43 levels also being reduced by 28% **(**Error! Reference source not found.**B-C)**. This finding, in addition to the previous data using 40nM siRNA raised the question of whether Dlg1 controls Cx43 mRNA expression. To answer this question, quantitative reverse-transcriptase PCR was carried out on extracts of HaCaT cells which had been treated with 20nM of siRNA against Dlg1 **(**Error! Reference source not found.**D)**. mRNA levels were expressed as the fold change in Cx43 mRNA relative to the change in GAPDH mRNA (as described in **Chapter 2, Section 2.2.5**). These results were then normalised to control-treated cells. No significant difference was observed between control-treated cells and cells treated with 20nM siDlg1, suggesting that Dlg1 does not control Cx43 mRNA expression and therefore loss of Cx43 is at the protein level.

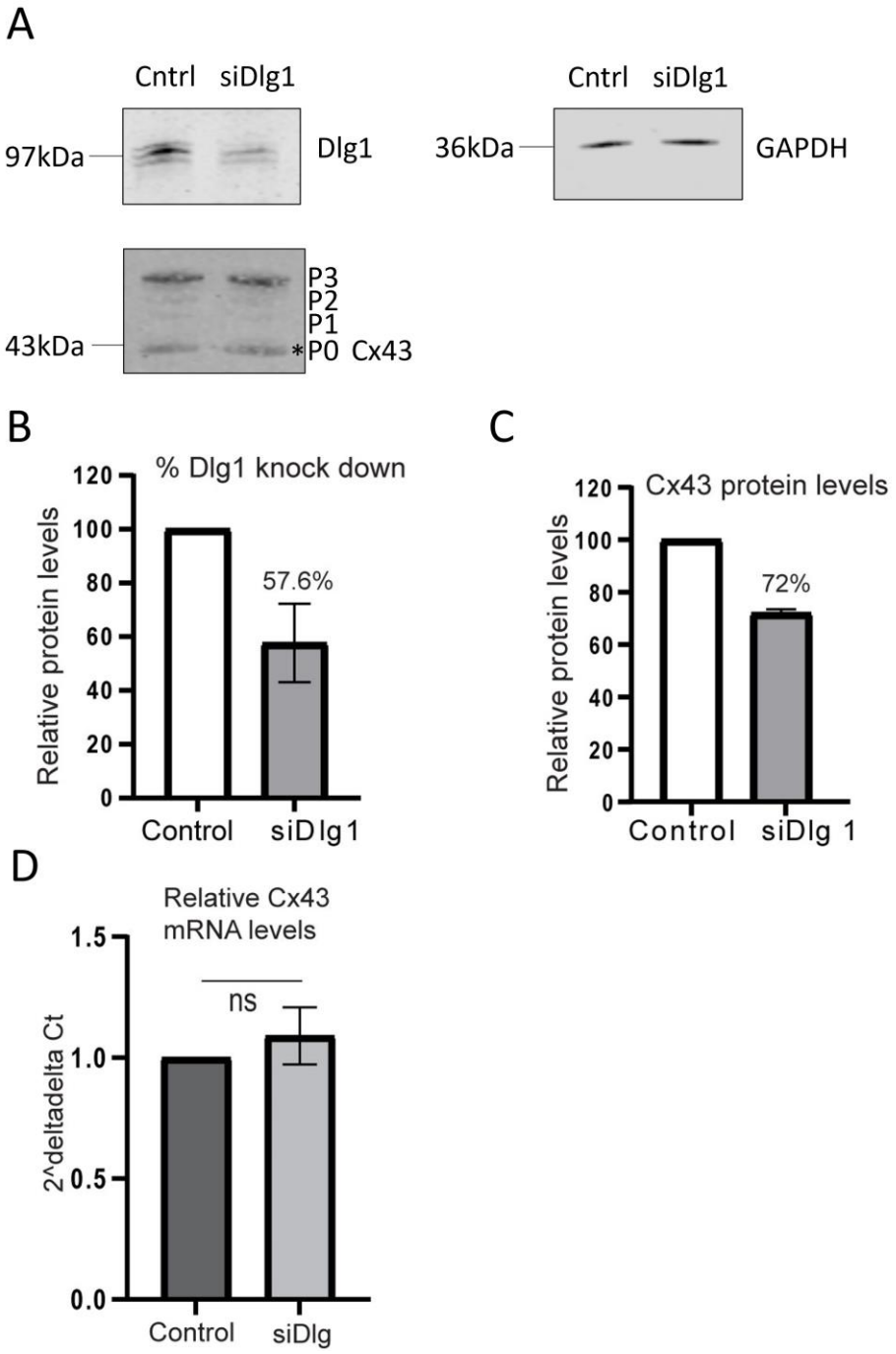

Figure 3.2: Treatment of HaCaT cells with 20nM siRNA targeting Dlg1 results in lower protein levels of Cx43 and Dlg1 but no changes to Cx43 mRNA levels. **(A)** Representative western blot of Cx43, Dlg1 and GAPDH loading control levels following treatment with 20nM siDlg1. Phosphorylation states of Cx43 protein bands are indicated by P0, P1, P2 and P3. As phosphorylation bands are not reliably detected in HaCaT cells, only the P0 band was quantified (indicated by asterisk). **(B-C)** Quantification of results from **(A)** for Dlg1 and Cx43 respectively. Cx43 and Dlg1 levels are normalised against GAPDH levels and then further normalised against control-treated cells. Graphs show the mean±s.d from three separate experiments. **(D)** qRT-PCR analysis shows no change in Cx43 mRNA levels following 20nM siDlg1 treatment. Results are shown as changes in Cx43 mRNA relative to changes in GAPDH mRNA and normalised to control-treated cells ($2^{-\Delta\Delta Ct}$). Graph shows the mean±s.d from three separate experiments. ns=p>0.05. Significance was assessed by a two-tailed unpaired t-test.

3.3 Knockdown of Dlg1 results in altered Cx43 localisation

While knockdown of Dlg1 is well-documented to result in reduced Cx43 plasma membrane localisation (MacDonald et al., 2012; Dong, 2021), this effect has not been quantified previously. Therefore, using confocal microscopy, the levels of Cx43 on the cell membrane in mock-treated and 20nM siDlg1 HaCaT cells were assessed using ß-catenin as a marker of the plasma membrane **(Figure 3.3A)**. Consistent with its role as an adherens junction protein, ß-catenin localised to sites of cell-cell contact in both mock-treated and siDlg1-treated cells **(Figure 3.3A, middle panels)**. In agreement with previous data, less Cx43 was evident on the cell membrane of siDlg1 cells, instead being mainly localised to the cytoplasm **(Figure 3.3A, left panels)**. Using ImageJ software, the total proportion of Cx43 present on the cell membrane was then determined for each cell and compared for the two treatment groups, with 50 cells being included in each group **(Figure 3.3B)**. Importantly, as this method considers the proportion of total cellular Cx43 on the plasma membrane, as opposed to the raw Cx43 signal levels on the plasma membrane, the inherently lower levels of Cx43 present in siDlg1 cells are controlled for. The results showed a significant decrease in the proportion of Cx43 on the cell membrane from 54% in mock-treated cells to 38% in siDlg1-treated cells, representing a relative reduction of 29% less Cx43 membrane staining compared to mock-treated cells. Together with previous data, this further demonstrates the importance of Dlg1 in the Cx43 lifecycle, as knockdown of Dlg1 restricts a portion of Cx43 from localising to the cell membrane.

As Cx43 was reduced at the cell membrane upon depletion of Dlg1, it was logical to determine whether this reduction was associated with accumulation of Cx43 in other subcellular compartments. Therefore, knockdown of Dlg1 was performed as before and colocalisation of Cx43 with markers of various organelles were assessed using Manders colocalisation coefficient. The first marker used in comparison of mock-treated and siDlg1 samples was Calnexin-1,

which is a marker of the ER **(Figure 3.4A, middle panels)**. As before, Cx43 mainly localised to the cell membrane in mock-treated cells **(Figure 3.4A, top left panel)** but was relocated to the cytoplasm in siDlg1-treated samples **(Figure 3.4A, bottom left panel)**, with Calnexin-1 displaying perinuclear staining characteristic of the ER in both treatment groups. A limited amount of colocalisation was observed between the two proteins in both mock-treated and siDlg1-treated samples, with no clear visual change in overlap in the siDlg1-treated cells. Quantification of these results by calculating the proportion of Cx43 that colocalised with Calnexin-1 per cell revealed there was a small but significant decrease in the overlap of the two signals in siDlg1-treated cells, which was reduced from 24% to 18% **(Figure 3.4B)**. This illustrates that Cx43 is not localised to the ER in cells where Dlg1 is depleted.

Next, the colocalisation of Cx43 with 58K (also known as p58 or p58K), a marker of the Golgi, was determined using the same approach **(Figure 3.5A)**. 58K staining was more diffuse than Calnexin-1 staining, with brighter regions in the perinuclear area typical of the Golgi, and some wider cytoplasmic staining **(Figure 3.5A, middle panels)**. In these samples an increase in colocalisation of Cx43 with 58K in siDlg1-treated cells compared to mock-treated cells was observed **(Figure 3.5A, right panels)**. This was confirmed by quantification, which demonstrated there was a significant increase from 29% colocalisation in mock-treated cells to 49% colocalisation in siDlg1 cells **(Figure 3.5B)**. This finding was also recapitulated using a direct Golgi staining kit **(Figure 3.6)**. Compared with 58K, direct Golgi staining was less diffuse and was mainly limited to the perinuclear region in both mock-treated and siDlg1-treated cells **(Figure 3.6A, middle panels)**. An increase in colocalisation between the Golgi and Cx43 in siDlg1-treated cells was evident **(Figure 3.6A, right panels)**, which was confirmed by quantification to be a significant increase from 30% colocalisation in mock-treated cells to 56% in siDlg1-treated cells **(Figure 3.6B)**. These results indicate that an increased proportion of Cx43 resides in the Golgi of siDlg1-treated cells.

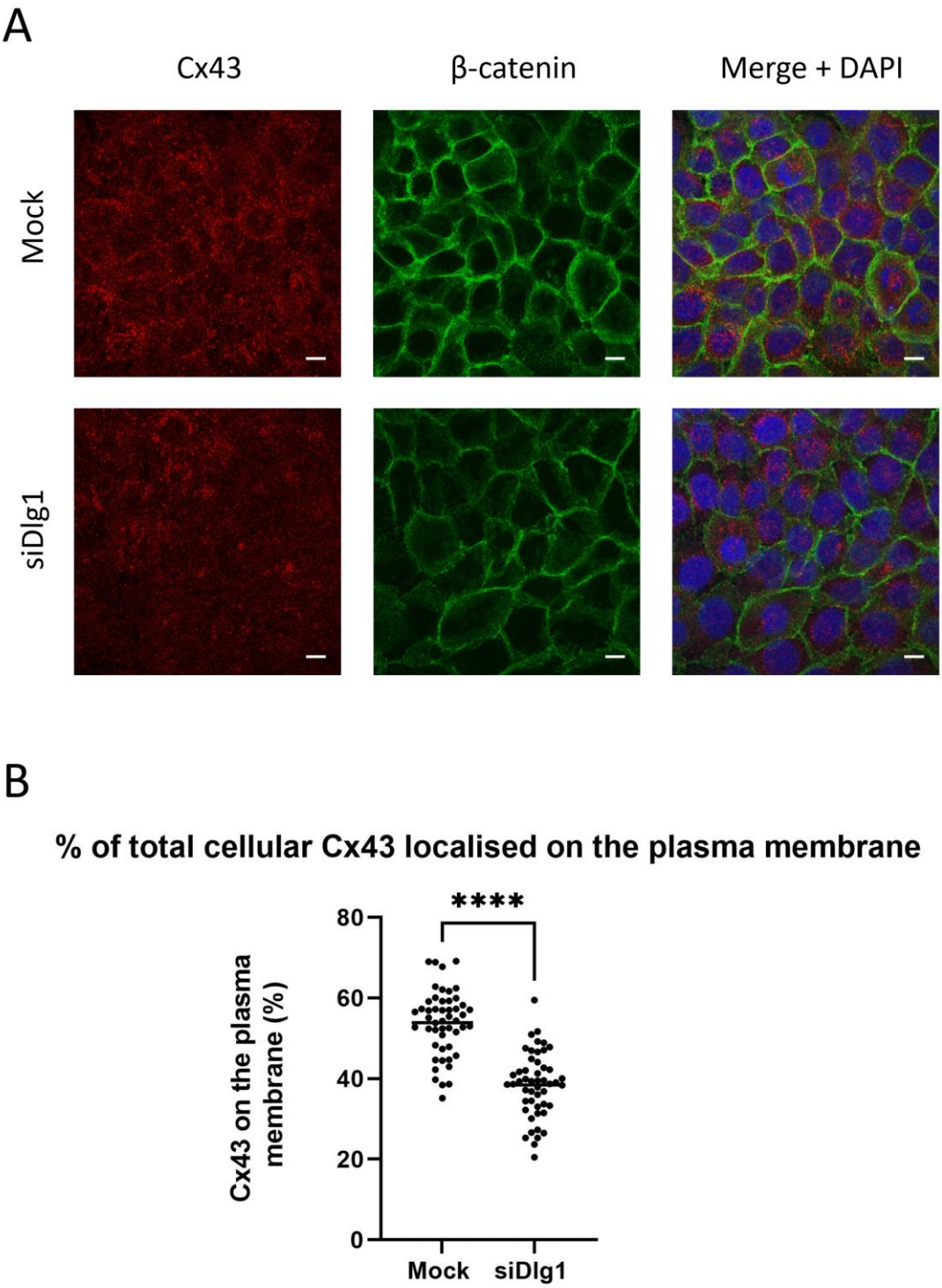

Figure 3.3: Assessment of plasma membrane levels of Cx43 following 20nM siDlg1 treatment. (A) Immunofluorescent staining of Cx43 (red) and β-catenin (green) in mock-treated and siDlg1 HaCaT cells. Blue staining denotes cell nuclei. Images are representative of three separate experiments. Scale bars=10μm. **(B)** Quantification of **(A)**. The proportion of Cx43 on the plasma membrane was assessed in cells from three biological replicates (mock replicate 1 24 cells, replicate 2 16 cells, replicate 3 10 cells; siDlg1 replicate 1 22 cells, replicate 2 11 cells, replicate 3 17 cells), with a final combined total of 50 cells being considered for each treatment group. Graph shows each cell as an individual data point. Horizontal line=mean. ****=$p<0.0001$. Significance was assessed by a two-tailed unpaired t-test.

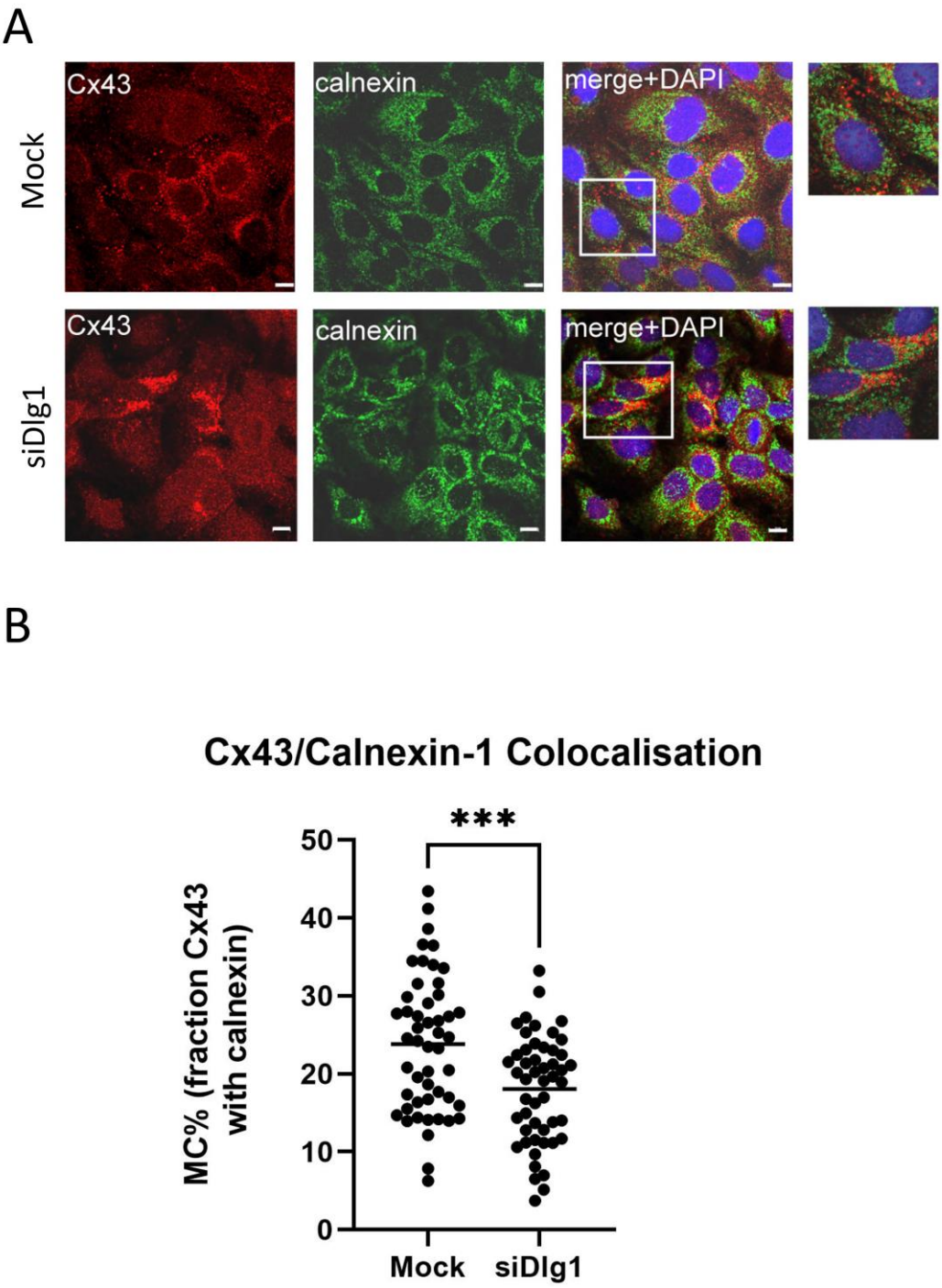

Figure 3.4: Cx43 colocalisation with Calnexin-1, a marker of the endoplasmic reticulum, is significantly decreased following 20nM siDlg1 treatment. (A) Immunofluorescent staining of Cx43 (red) and Calnexin-1 (green) in mock-treated and siDlg1 HaCaT cells. Blue staining denotes cell nuclei. Areas enclosed by white boxes are shown enlarged on the right-hand side. Images are representative of three separate experiments. Scale bars=10μm. **(B)** Quantification of **(A)**. Manders' colocalisation coefficient was calculated for cells from three biological replicates (mock replicate 1 18 cells, replicate 2 17 cells, replicate 3 15 cells; siDlg1 replicate 1 21 cells, replicate 2 13 cells, replicate 3 16 cells), with a final combined total of 50 cells being considered for each treatment group. Graph shows each cell as a single data point. Horizontal line=mean. ***=$p<0.001$. Significance was assessed by a two-tailed unpaired t-test.

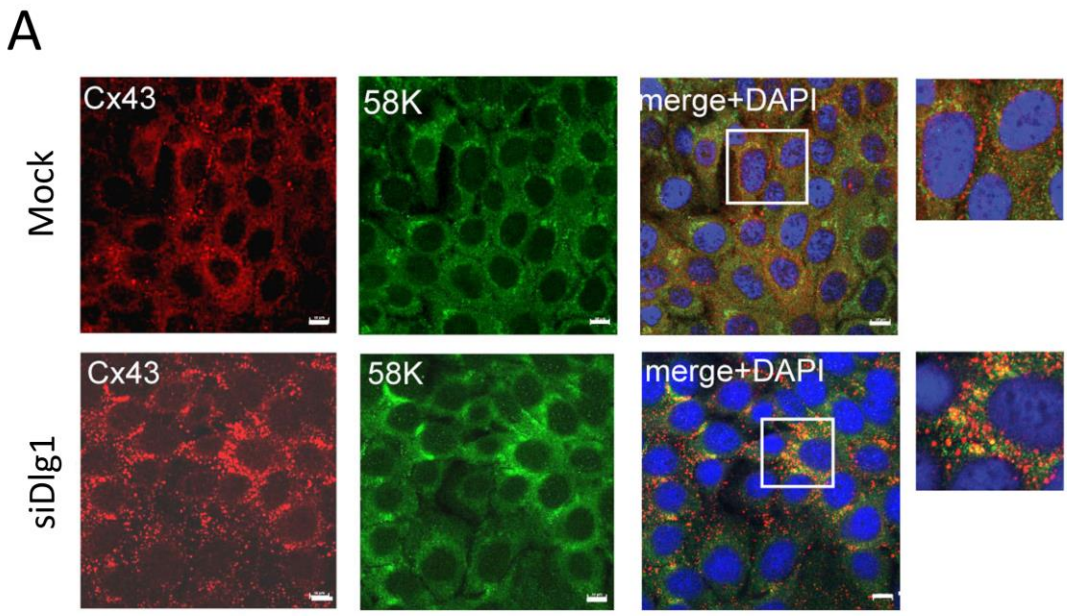

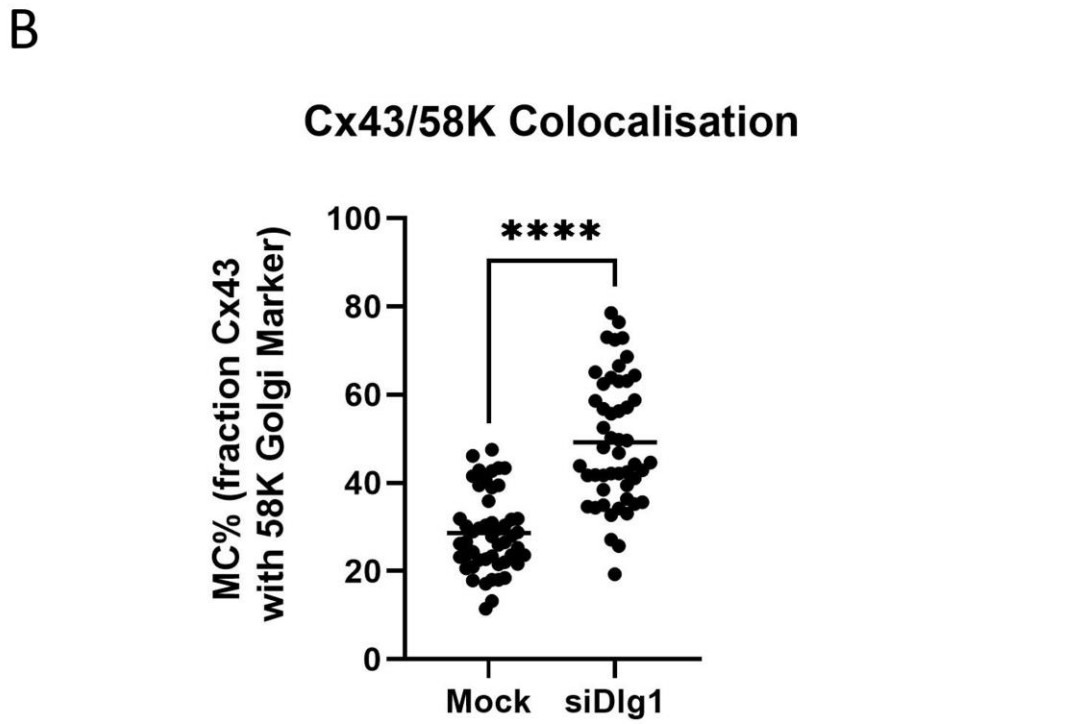

Figure 3.5: Cx43 colocalisation with 58K, a marker of the Golgi, is significantly increased following 20nM siDlg1 treatment. (A) Immunofluorescent staining of Cx43 (red) and 58k (green) in mock-treated and siDlg1 HaCaT cells. Blue staining denotes cell nuclei. Areas enclosed by white boxes are shown enlarged on the right-hand side. Images are representative of three separate experiments. Scale bars=10μm. **(B)** Quantification of **(A)**. Manders' colocalisation coefficient was calculated for cells from three biological replicates (mock replicate 1 15 cells, replicate 2 18 cells, replicate 3 17 cells; siDlg1 replicate 1 15 cells, replicate 2 23 cells, replicate 3 12 cells), with a final combined total of 50 cells being considered for each treatment group. Graph shows each cell as a single data point. Horizontal line=mean. ****=$p<0.0001$. Significance was assessed by a two-tailed unpaired t-test.

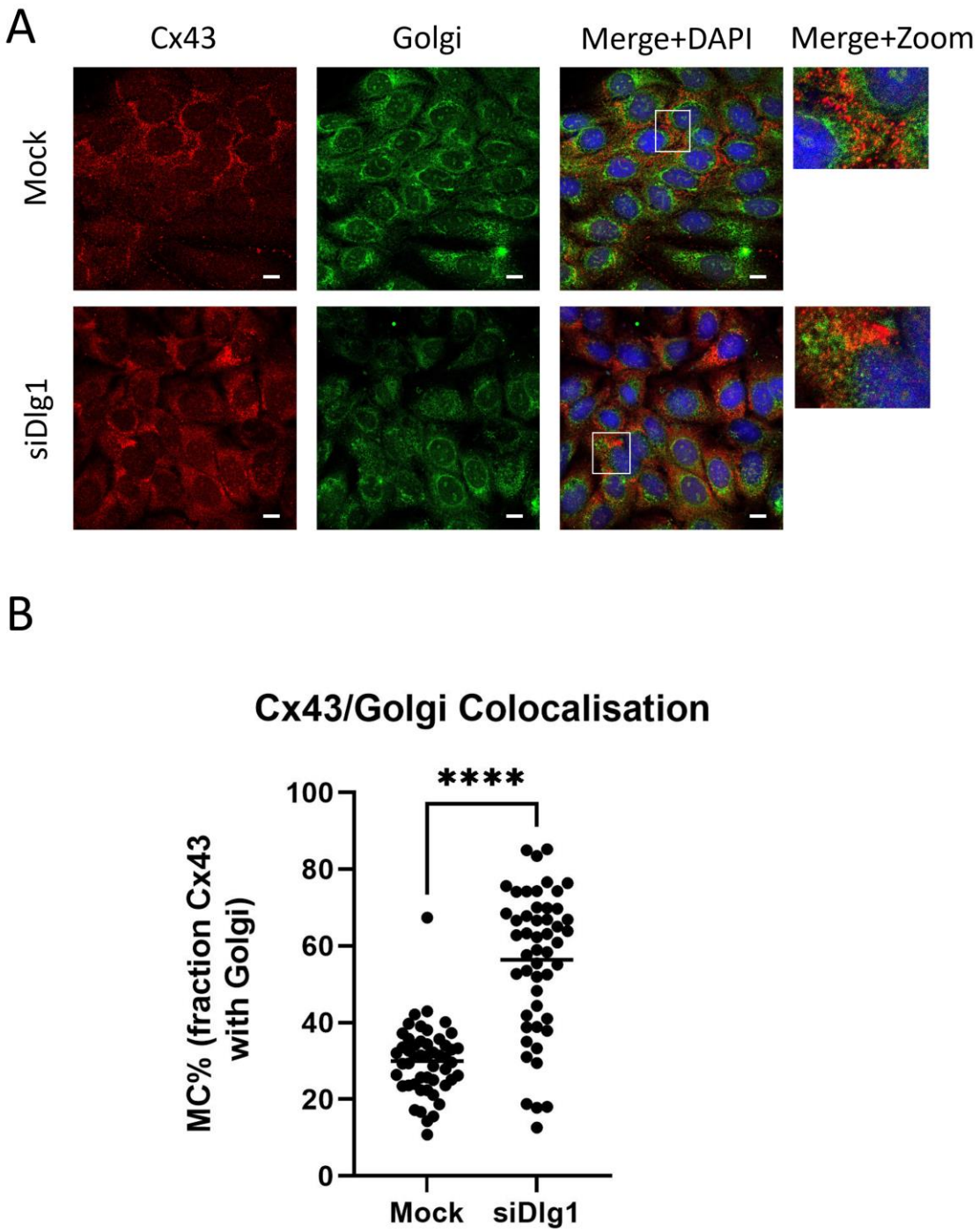

Figure 3.6: Cx43 colocalisation with the Golgi (as stained by Cytopainter) is significantly increased following 20nM siDlg1 treatment. (A) Immunofluorescent staining of Cx43 (red) and the Golgi (green) in mock-treated and siDlg1 HaCaT cells. Blue staining denotes cell nuclei. Areas enclosed by white boxes are shown enlarged on the right-hand side. Images are representative of three separate experiments. Scale bars=10μm. **(B)** Quantification of **(A)**. Manders' colocalisation coefficient was calculated for cells from three biological replicates (mock replicate 1 22 cells, replicate 2 10 cells, replicate 3 18 cells; siDlg1 replicate 1 19 cells, replicate 2 18 cells, replicate 3 13 cells), with a final combined total of 50 cells being considered for each treatment group. Graph shows each cell as a single data point. Horizontal line=mean. ****=$p<0.0001$. Significance was assessed by a two-tailed unpaired t-test.

Due to the reduced level of Cx43 protein in siDlg1-treated cells, it was of interest to study the proportion of Cx43 localised to organelles associated with Cx43 internalisation and degradation. Therefore, the colocalisation between Cx43 and early endosome antigen-1 (EEA1) was assessed **(Figure 3.7A).** EEA1 was observed throughout the cell in both treatment groups **(Figure 3.7A, middle panels)**. No clear change was visible in colocalisation between control-treated and siDlg1-treated cells **(Figure 3.7A, right panels)**. Surprisingly, quantification of these results showed there was a significant decrease in colocalisation between the two proteins from 5.4% in control-treated cells to 0.9% in siDlg1-treated cells **(Figure 3.7B)**. This suggests that less Cx43 is present in the early stages of the endosomal/lysosomal pathway in siDlg1 cells. However, compared to the other markers used in this study, the staining with the EEA1 antibody was of a lower quality and therefore these data were somewhat equivocal.

Finally, the proportion of Cx43 localised to a later stage of the degradation pathway, the lysosomes, was determined using lysosome-associated membrane protein 2 (LAMP2) as a marker **(Figure 3.8A)**. Lysosomal staining was very diffuse, with some brighter spots around the perinuclear region observed in both treatment groups **(Figure 3.8A, middle panels)**. Overlap between Cx43 and LAMP2 in all samples was low **(Figure 3.8A, right panels)**, with only 1.8% of Cx43 colocalising with LAMP2 in mock-treated cells **(Figure 3.8B)**. Colocalisation in siDlg1-treated cells was also very low at just 2.6%. While this difference was minor, it represents a ~50% increase in the proportion of Cx43 localised to the lysosomes in siDlg1-treated samples **(Figure 3.8C)**, suggesting that more Cx43 is degraded through the lysosomal pathway in these cells.

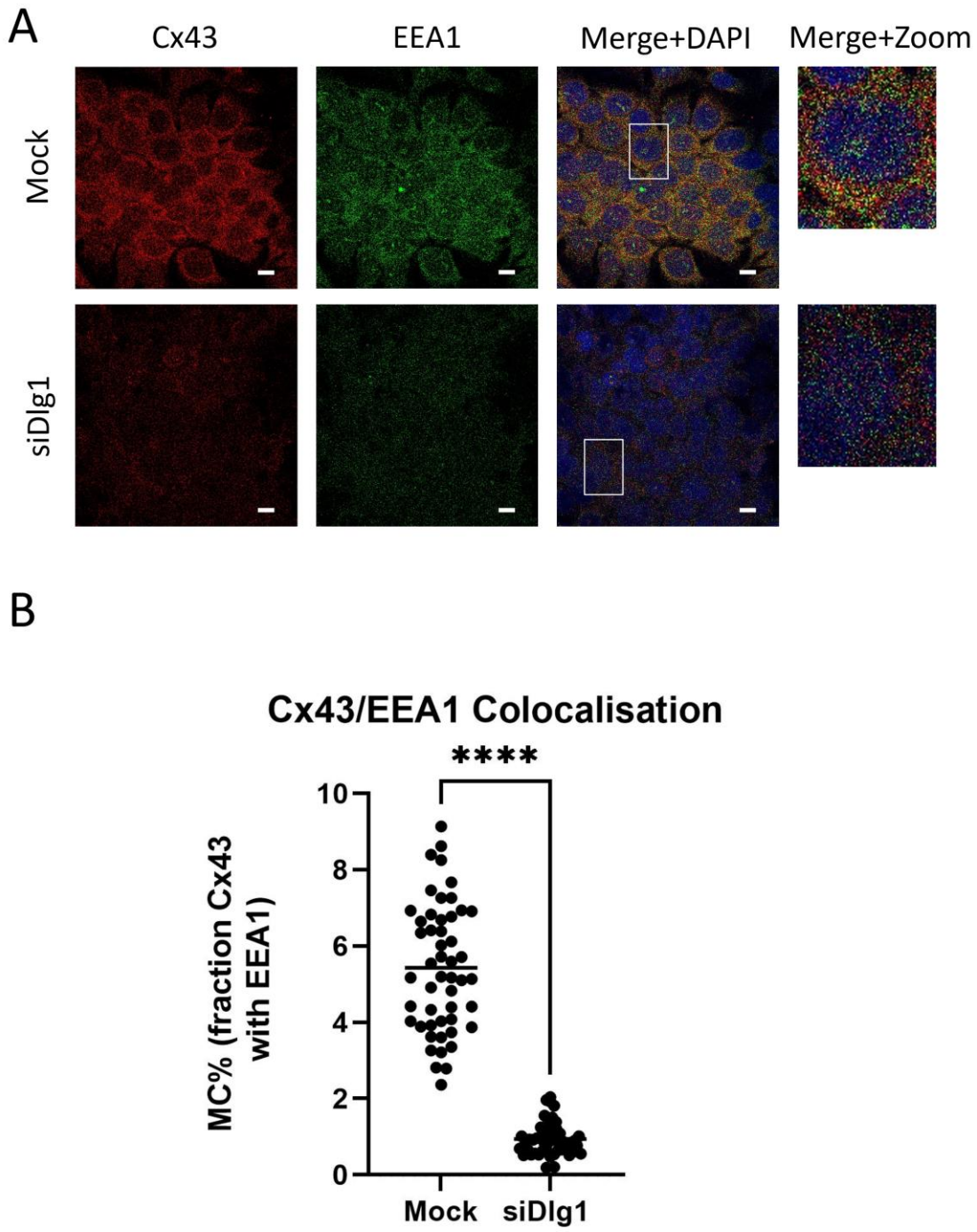

Figure 3.7: Cx43 colocalisation with EEA1, a marker of endosomes is significantly decreased following 20nM siDlg1 treatment. (A) Immunofluorescent staining of Cx43 (red) and the EEA1 (green) in mock-treated and siDlg1 HaCaT cells. Blue staining denotes cell nuclei. Areas enclosed by white boxes are shown enlarged on the right-hand side. Images are representative of three separate experiments. Scale bars=10μm. **(B)** Quantification of **(A)**. Manders' colocalisation coefficient was calculated for cells from three biological replicates (mock replicate 1 19 cells, replicate 2 15 cells, replicate 3 16 cells; siDlg1 replicate 1 14 cells, replicate 2 22 cells, replicate 3 14 cells), with a final combined total of 50 cells being considered for each treatment group. Graph shows each cell as a single data point. Horizontal line=mean. ****=$p<0.0001$. Significance was assessed by a two-tailed unpaired t-test.

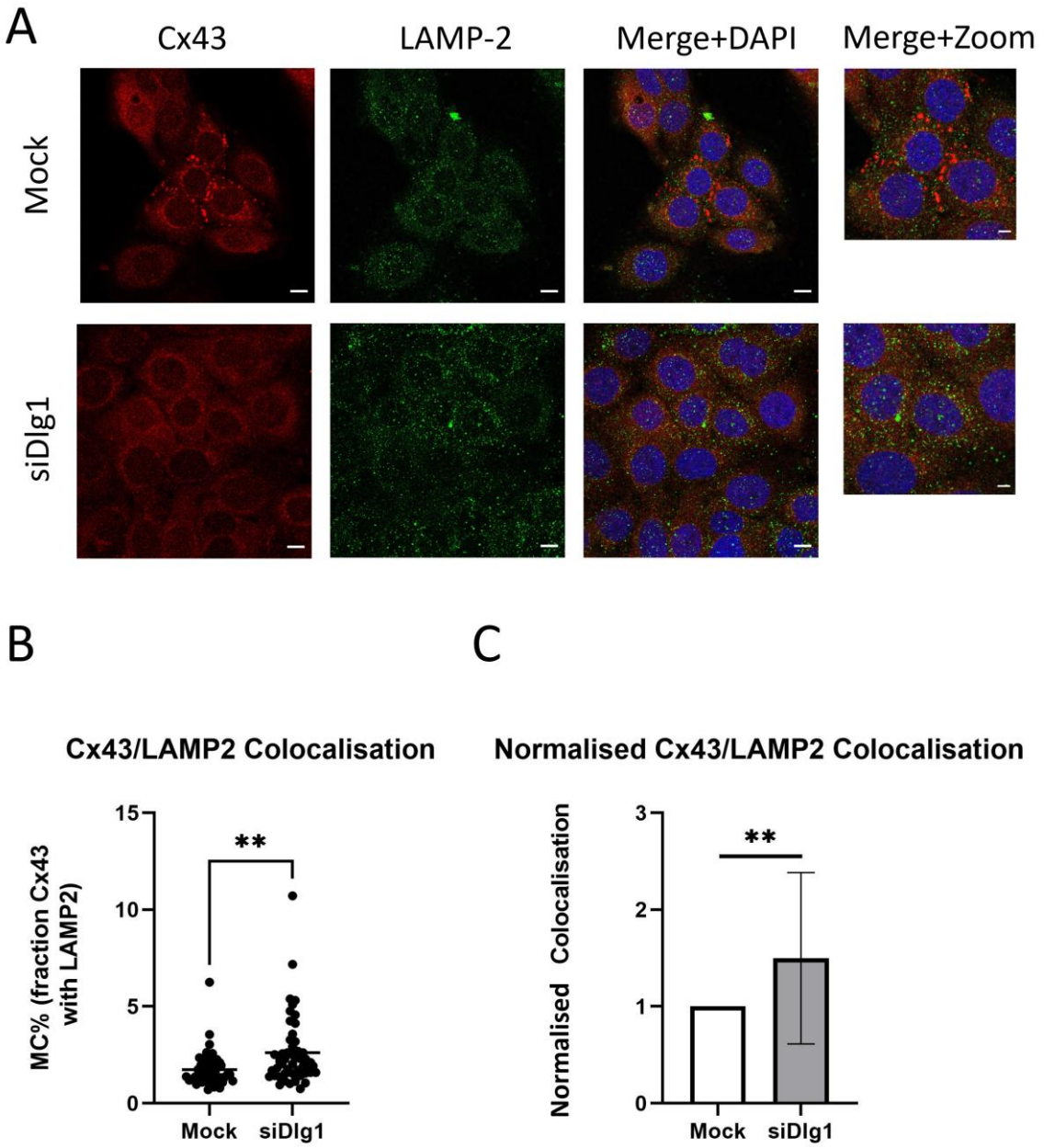

Figure 3.8: Cx43 colocalisation with LAMP2, a marker of lysosomes is significantly increased following 20nM siDlg1 treatment. (A) Immunofluorescent staining of Cx43 (red) and the LAMP2 (green) in mock-treated and siDlg1 HaCaT cells. Blue staining denotes cell nuclei. Areas enclosed by white boxes are shown enlarged on the right-hand side. Images are representative of three separate experiments. Scale bars=10μm. **(B)** Quantification of **(A)**. Manders' colocalisation coefficient was calculated for cells from three biological replicates (mock replicate 1 23 cells, replicate 2 10 cells, replicate 3 17 cells; siDlg1 replicate 1 11 cells, replicate 2 16 cells, replicate 3 23 cells) with a final combined total of 50 cells being considered for each treatment group. Graph shows each cell as a single data point. Horizontal line=mean. **(C)** Results of **(B)** normalised to mock-treated cells. Error bar=±s.d.. **=$p<0.01$. Significance was assessed by a two-tailed unpaired t-test.

3.4 Dlg1 knockdown results in increased lysosomal degradation of Cx43

Previous work by the Graham group demonstrated that Cx43 is mainly degraded through the lysosomal pathway and not the proteasomal pathway in normal HaCaT cells, as treatment with NH_4Cl (inhibitor of the lysosomal pathway (Misinzo, Delputte and Nauwynck, 2008)) increased Cx43 levels while treatment with MG132 (inhibitor of the proteasomal pathway) had no effect (Dong, 2021). In this study, it was suggested that due to the increased proportion of Cx43 localised to the lysosomes in siDlg1-treated cells, increased lysosomal degradation of Cx43 may be taking place. Therefore, a western blot was carried out to investigate Cx43 and Dlg1 levels in mock-treated or siDlg1-treated HaCaT cells which had additionally been treated with 10mM NH_4Cl **(Figure 3.9A)**. siGlo-treated samples were included as a non-target oligonucleotide transfection control. There was a clear increase in Cx43 levels in the NH_4Cl-treated group compared to the no treatment group for mock-treated, siGlo and siDlg1-treated cells **(Figure 3.9A)**, suggesting that blocking the lysosomal pathway prevented degradation of Cx43. This difference was not observed for Dlg1. As before, knockdown of Dlg1 resulted in decreased levels of both Cx43 and Dlg1 protein. Stronger bands for Cx43 were present in the siDlg1+NH_4Cl-treated group compared to the siDlg1-treatment only group. Quantification of these results via analysis in ImageJ confirmed that Cx43 levels were significantly higher in NH_4Cl-treated cells in both the mock-treated and siDlg1 groups **(Figure 3.9B)**. Interestingly however, treatment with NH_4Cl in the siDlg1-treated group restored Cx43 protein to 1.81 fold mock-treated -NH_4Cl levels, which was very similar to the 1.67 fold difference observed between the mock-treated +NH_4Cl group and the mock-treated -NH_4Cl group. This meant that there was a larger fold change in Cx43 protein levels between the siDlg1-treatment only group and the siDlg1 +NH_4Cl-treated group than there was between the mock-treated only group and the mock-treated +NH_4Cl-treated groups (1.7x difference compared to 2.8x difference). In agreement with the immunofluorescence data **(Figure 3.8A-C)**, these results strongly suggest that more Cx43 is degraded through the lysosomal pathway in siDlg1 cells and therefore treatment with NH_4Cl blocks this effect.

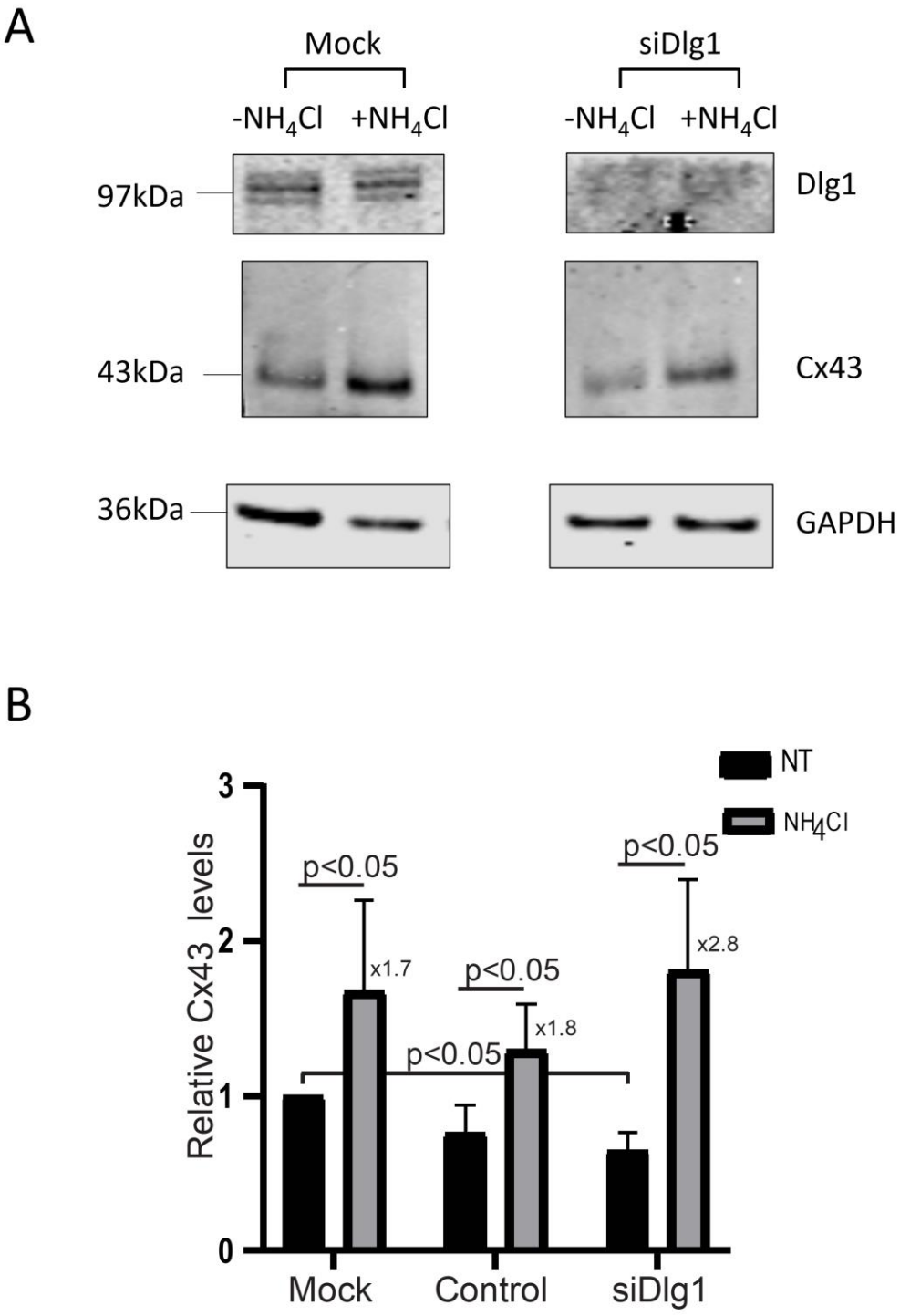

Figure 3.9: Degradation of Cx43 through the lysosomal pathway is increased in siDlg1 cells. (A) Western blots of HaCaT cell extracts showing Dlg1 and Cx43 levels +/- 24h 20nM siDlg1 treatment and +/- 8h 10mM NH_4Cl treatment (lysosomal pathway inhibitor). GAPDH was included as a loading control. **(B)** Quantification of Cx43 levels from **(A)**. Results are normalised to GAPDH expression and then normalised to mock no treatment Cx43 levels. NT=No treatment. Control samples were treated with 40nM siGlo as a transfection control. Multiplication symbols represent the fold change in Cx43 levels between NT and NH_4Cl for each group. Results are representative of three separate experiments. $p<0.05$ where shown. Significance was assessed by a two-tailed Mann-Whitney U-test.

3.5 Dlg1 knockdown does not affect adherens and tight junction formation or cell membrane integrity

As a key cell polarity and scaffolding protein, depletion of Dlg1 may be expected to result in changes to cell shape and cell membrane integrity, which could account for the differences in Cx43 localisation observed in this investigation. To test this, further immunofluorescence staining was carried out using Calnexin-1 to determine any apparent differences in distribution of this protein **(Figure 3.10A)**. No changes were detected in Calnexin-1 localisation following siDlg1 treatment, which was localised to the perinuclear region **(Figure 3.10A, left hand panels)**. This suggests that intracellular membranes are unaffected by knockdown of Dlg1. Next, staining of the adherens junction protein, ß-catenin, was compared in mock-treated and siDlg1-treated cells **(Figure 3.10A, middle panels)**. In both groups, ß-catenin localised mainly to sites of cell-cell contact, which is consistent with its role as a junctional protein (Spagnol *et al.*, 2018). Lastly, the distribution of ZO-1, a tight junction protein which is structurally related to Dlg1 and interacts with Cx43 at the cell membrane, was investigated **(Figure 3.10B)**. As with the other markers, no difference was noted in ZO-1 distribution on Dlg1 knockdown, which was localised to the plasma membrane in both groups. Taken together, these data indicate that membrane integrity, as well as adherens and tight junction formation, are maintained under conditions where Dlg1 is depleted. This means changes in Cx43 localisation are due to a specific effect of Dlg1 on the Cx43 lifecycle.

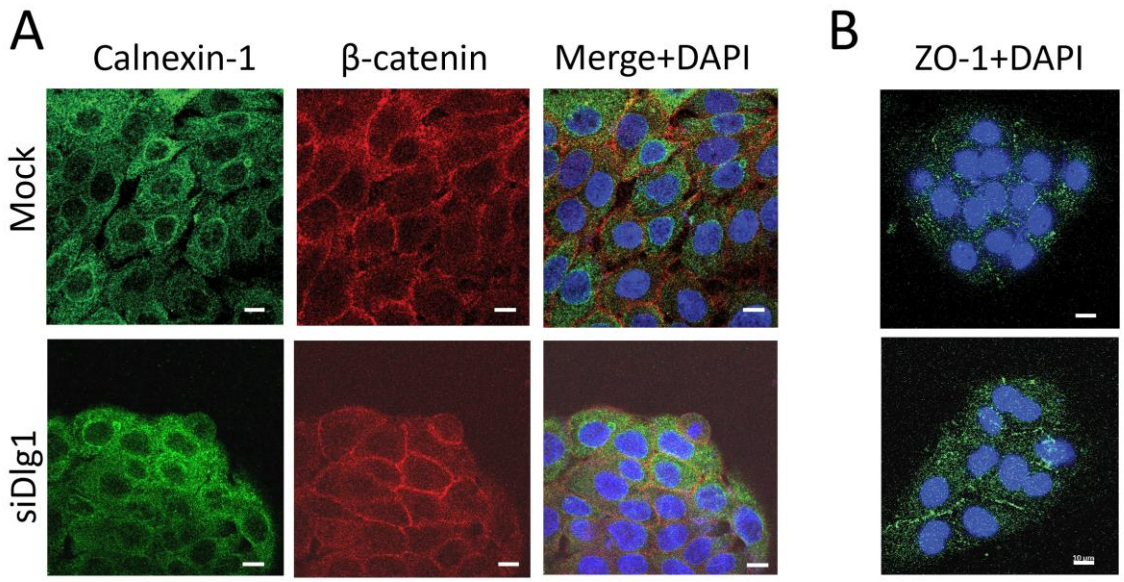

Figure 3.10: Knockdown of Dlg1 with 20nM siDlg1 does not affect cell shape or cell membrane integrity. (A) Immunofluorescent staining of Calnexin-1 (green) and ß-catenin (red) in mock-treated and siDlg1 HaCaT cells. **(B)** Immunofluorescent staining of ZO-1 (green). Blue staining denotes cell nuclei. Images are representative of three separate experiments. Scale bars=10μm.

3.6 Dlg1 controls gap junctional communication

As reduced levels of Cx43 protein are found on the cell membrane of siDlg1-treated cells, it was important to address whether Dlg1 controlled gap junctional communication. To address this, a parachute assay was performed (Donnelly *et al.*, 2012). Briefly, a parachute assay requires two groups of cells: 'donor' and 'acceptor' cells. Donor cells are treated with a dye, in this case calcein-AM, which is a cell-permeable molecule that upon entering cells is cleaved to produce fluorescent calcein. Once cleaved, calcein is no longer able to diffuse out of the cell but can spread to other cells via gap junctions (molecular weight = 623 Da). In contrast, acceptor cells are unstained. Donor cells are then removed from their original culture vessel and 'parachuted' onto acceptor cells at a given donor: acceptor cell ratio and dye spread is assessed after a period of 4h 30min. Donor cells with intact gap junctions should therefore be observed to have increased dye spread to acceptor cells compared to cells which are

deficient in gap junctional signalling. For a full description of this procedure, see **Chapter 2, Section 2.2.7**.

In this study, donor cells were either mock-treated HaCaT cells, 40nM siDlg1-treated cells, HaCaT cells which had been treated with 50μM of carbenoxolone (CBX), a general gap junction inhibitor, or HeLa Ohio cells, which are deficient in gap junctional signalling (Elfgang *et al.*, 1995). In contrast, acceptor cells were kept constant as untreated HaCaT cells. siDlg1 was used at 40nM in this experiment to observe the effect of removal of a greater portion of Dlg1 and consequently, Cx43 protein (73% and 72% decrease in cellular levels) (Dong, 2021). Clear spread of calcein green dye from the original donor cells to acceptor cells was apparent in the mock-treated group, implying that functional gap junctional channels were formed between the HaCaT cells **(Figure 3.11A)**. This was in contrast to the siDlg1-treated, CBX-treated and HeLa Ohio cells, which had greatly reduced dye transfer **(Figure 3.11B-D)**. These results were quantified as the average number of acceptor cells receiving dye directly from a given donor cell. At least 140 individual donor cells were analysed for each treatment group. These values were then normalised to the mock-treated HaCaT group to give a relative measure of gap junctional communication **(Figure 3.11E)**. The data show that 40nM siDlg1 treatment significantly reduced the average number of acceptor cells to receive dye, with a reduction of 55% compared to mock-treated cells. This was comparable to the inhibitory effect of CBX treatment, which caused a 65% reduction in dye spread between cells. In keeping with the inability to form gap junctions, HeLa Ohio cells exhibited an 85% reduction in dye spread compared to mock-treated cells. Overall, these results demonstrate that Dlg1 is an important positive regulator of gap junctional communication in epithelial cells and therefore depletion of Dlg1 results in vastly reduced gap junctional communication.

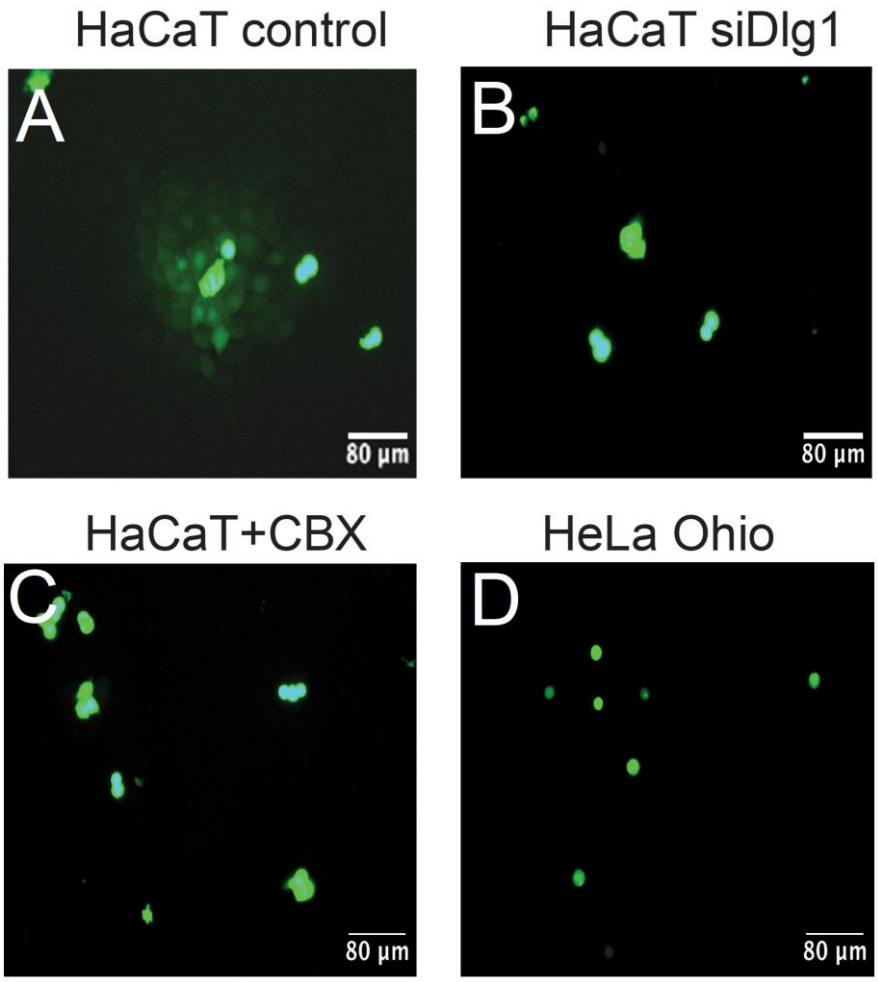

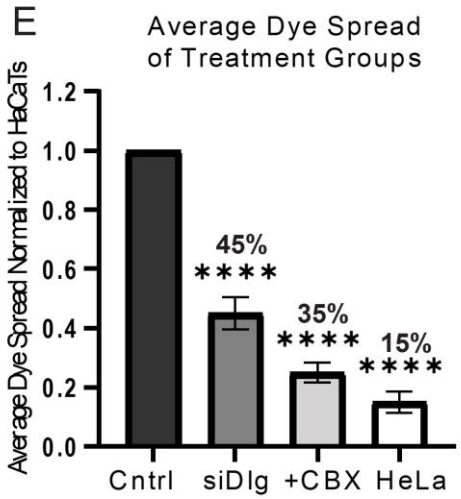

Figure 3.11: Knockdown of Dlg1 through 40nM siDlg1 treatment significantly reduces gap junction intercellular communication by parachute assay in HaCaT cells. (A-D) Representative images of calcein dye transfer from donor **(A)** HaCaT control cells, **(B)** HaCaT siDlg1 cells, **(C)** HaCaT cells+carbenoxolone to block gap junctions and **(D)** HeLa Ohio cells to HaCaT acceptor cells. **(E)** Quantification of the average number of acceptor cells receiving calcein dye from each donor cell, normalised to HaCaT control cells. At least 140 individual donor cells were analysed for each treatment group. ****=p<0.0001. Significance was assessed using a Kruskal-Wallis test followed by Dunn's post-hoc test.

3.7 Discussion

As a critical cell-cell communication protein with a high turnover rate, Cx43 interacts with, and is regulated by, a myriad of other proteins during its lifecycle. Dlg1 has previously been shown to interact with Cx43 in several keratinocyte cell lines *in vitro* and cause a reduction in Cx43 protein levels when depleted through siRNA treatment (Dong, 2021). Due to previous difficulties visualising residual Cx43 in immunofluorescence experiments where Dlg1 was knocked down, it was necessary for the concentration of siRNA targeting Dlg1 to be reduced from 40nM to 20nM in this investigation. Despite this reduction, 20nM of siRNA resulted in decreased levels of both Dlg1 (42% reduction) and Cx43 (28% reduction). The decrease in Cx43 protein levels in siDlg1 cells raised the question of whether Dlg1 could control Cx43 mRNA levels. While Dlg1 has not been reported to have direct transcriptional activity, it is capable of localising to the nucleus and binding to proteins such as protein-associated splicing factor (PSF) in HEK293 cells, which is involved in transcription and mRNA processing (Sabio *et al.*, 2010). Dlg1 also controls expression of certain schizophrenia risk-associated genes in mice hippocampi (Gupta *et al.*, 2018). In this study, mRNA levels of Cx43 in HaCaT cells remained unchanged following Dlg1 treatment, meaning the loss of Cx43 was at the protein level alone. This strongly indicates that Dlg1 has a functional role in the Cx43 lifecycle following production of Cx43 protein.

Under baseline conditions, Cx43 is mainly degraded through the lysosomal pathway and not the proteasomal pathway in HaCaT cells (Dong, 2021). Here, it was revealed that lysosomal inhibition resulted in a larger increase in Cx43 levels in siDlg1 cells than in mock-treated cells. Immunofluorescence data similarly showed a ~50% increase in Cx43 colocalisation with the lysosomes in siDlg1 cells. Taken together, these results indicate that Cx43 degradation through the lysosomal pathway is increased when Dlg1 is depleted. Degradation through this pathway can take place either following translocation of Cx43 from

the ER/Golgi to lysosomes (Qin *et al.*, 2003) or following internalisation of Cx43 from the plasma membrane (Berthoud *et al.*, 2004).

Treatment with 20nM siDlg1 resulted in a relative reduction of 29% in Cx43 localised to the plasma membrane compared to mock-treated cells. This shows that even at lower concentrations, siRNA against Dlg1 results in a significant drop in Cx43 plasma membrane levels. In addition, Dlg1 was shown to control gap junctional intercellular communication, as 40nM siDlg1 treatment reduced dye spread between HaCaT cells by 55%. The finding that dye spread in siDlg1-treated cells was comparable to that of cells treated with a general gap junction blocker (carbenoxolone) emphasises the importance of Dlg1 in normal gap junction function. It is currently unknown whether Dlg1 controls plasma membrane localisation of other connexin proteins, however it is known to interact with at least one other connexin protein family member in Cx32 (Duffy *et al.*, 2007). While the effect of Dlg1 depletion on Cx32 levels and localisation is yet to be determined, interestingly Cx32-null mice display reduced Dlg1 protein. It would be worthwhile to examine whether a similar decrease in Dlg1 takes place on knockdown of Cx43.

Next, as Cx43 has been reported to localise to the cytoplasm in siDlg1-treated cells, the subcellular localisation of Cx43 was assessed in these cells. The results of this section are summarised in **Figure 3.12**. Firstly, a modest decrease in Cx43 association with the ER was observed. This suggests that knockdown in Dlg1 is not likely to result in any changes to Cx43 trafficking through the ER. However, significantly increased association of Cx43 with two individual markers of the Golgi was detected, meaning Cx43 accumulates in this compartment following Dlg1 depletion. There could be several possible explanations for this finding, with one being that alterations in Cx43 localisation are due to overall changes in cell membrane and junctional integrity caused by knockdown of Dlg1. However, there was no apparent change in these factors in this study as localisation of Calnexin-1 (ER), β-catenin (adherens junctions) and ZO-1 (tight junctions) were unaffected by Dlg1 knockdown. This was surprising in the case of β-catenin given that Dlg1 has previously been reported to be required for

formation of adherens junctions (Laprise *et al.*, 2004). It is possible that at lower levels of knockdown HaCaT cells retain enough Dlg1 protein for proper adherens junction formation, or alternatively cells are able to compensate for the loss of Dlg1 through other proteins. Despite no obvious changes to general cell shape in siDlg1-treated cells in this study, it would also be useful to clarify this experimentally in the future. This could be performed using image analysis software such as FlowShape (van Bavel, Thiels and Jelier, 2023). Given the lack of difference in the markers above, the changes in Cx43 localisation in siDlg1 cells are likely due to a specific effect of Dlg1 on the Cx43 protein lifecycle. This leads to two main hypotheses for the role of Dlg1, with the more straightforward theory being that Dlg1 is involved in forward trafficking of Cx43 from the Golgi to the plasma membrane. In support of this, Dlg1 is a cytoskeletal protein and is involved in the polymerisation of actin (Round *et al.*, 2005), also interacting indirectly with microtubules (Asaba *et al.*, 2003). This means that Dlg1 could help tether Cx43 to the cytoskeleton, allowing it to undergo efficient, targeted delivery to adherens junctions. Furthermore, Dlg1 is involved in the forward trafficking of other membrane proteins (Fourie, Li and Montgomery, 2014), indicating it may perform a similar role in Cx43 trafficking. On the other hand, the lack of colocalisation between Cx43 and Dlg1 in the cytoplasm suggests that interaction may be limited to the cell membrane in regular keratinocytes.

The second potential role of Dlg1 is in stabilisation of Cx43 at the plasma membrane. The C-terminus of Cx43, which binds the N- and C-termini of Dlg1 (MacDonald *et al.*, 2012) as well as other proteins, has been previously shown to be responsible for the stability of Cx43 gap junctions (Stout, Snapp and Spray, 2015). In this working model, loss of Dlg1 leads to Cx43 internalisation from the plasma membrane and recycling to the Golgi, where a portion is subsequently exported and degraded through the lysosomal pathway. Recycling of a different cell membrane protein to the Golgi, E-cadherin, has been documented under conditions where Scribble, a PDZ polarity protein which can complex with Dlg1, is knocked down (Lohia, Qin and Macara, 2012). This model is intriguing, as retrieval and maintenance of a Golgi-localised pool of Cx43 under conditions where stabilisation at the cell membrane is disrupted could allow rapid reformation of gap junctions on return to homeostasis. Indeed, gap junctions are

known to be swiftly reestablished even in the presence of a protein synthesis inhibitor, probably due to the recycling of connexosomes to the cell membrane (Tadvalkar and Pinto da Silva, 1983). This Golgi-localised pool of Cx43 could therefore comprise an additional method of gap junction reestablishment following disruption of certain factors such as Dlg1. Drebrin, an actin-binding protein, has also been implicated in stabilisation of Cx43 at the cell membrane (Butkevich *et al.*, 2004). Butkevich and colleagues knocked down Drebrin via siRNA, which resulted in reduction of Cx43 protein and cell membrane localisation. While colocalisation of Cx43 and the Golgi was not specifically addressed, the remaining Cx43 protein was localised to the perinuclear region of knockdown cells, which could feasibly represent the Golgi. Proteins recycled from the plasma membrane are usually internalised as endosomes which then undergo retrograde transport (Seaman, 2012). It would therefore be expected that Cx43 would display increased association with markers of early endosomes when Dlg1 is depleted, however this was not the case in this study. Given the diffuse cellular distribution of EEA1 observed in this investigation, the validity of these data are questionable. Examination of Cx43 colocalisation with a further marker of early endosomes, such as Rab5 (Shearer and Petersen, 2019), would be of benefit in determining whether this is an EEA1-specific effect.

It is also feasible that Dlg1 is involved in both forward trafficking and stabilisation of Cx43 at the plasma membrane. As neither model fits the entirety of the current data, further work is needed to definitively address which of these roles Dlg1 carries out. Experiments utilising endocytosis inhibitors, such as dynasore, could prove useful in this context (Smyth *et al.*, 2010). For example, if the proportion of Cx43 on the plasma membrane remains similar when treated with dynasore following siDlg1 treatment, it would suggest that Dlg1 functions in forward trafficking of Cx43 rather than stabilisation at the plasma membrane. Additionally, colocalisation of Cx43 with markers of recycling endosomes, such as Rab11 (Grant and Donaldson, 2009) or Arf6 (Kobayashi and Fukuda, 2013) should be investigated to determine whether there is an increase on depletion of Dlg1.

Work from this chapter was collated and published in Journal of Cell Science under the title 'The human discs large protein 1 interacts with and maintains connexin 43 at the plasma membrane in keratinocytes' (Scott *et al.*, 2023) (see paper bound with thesis, https://doi.org/10.1242/jcs.259984).

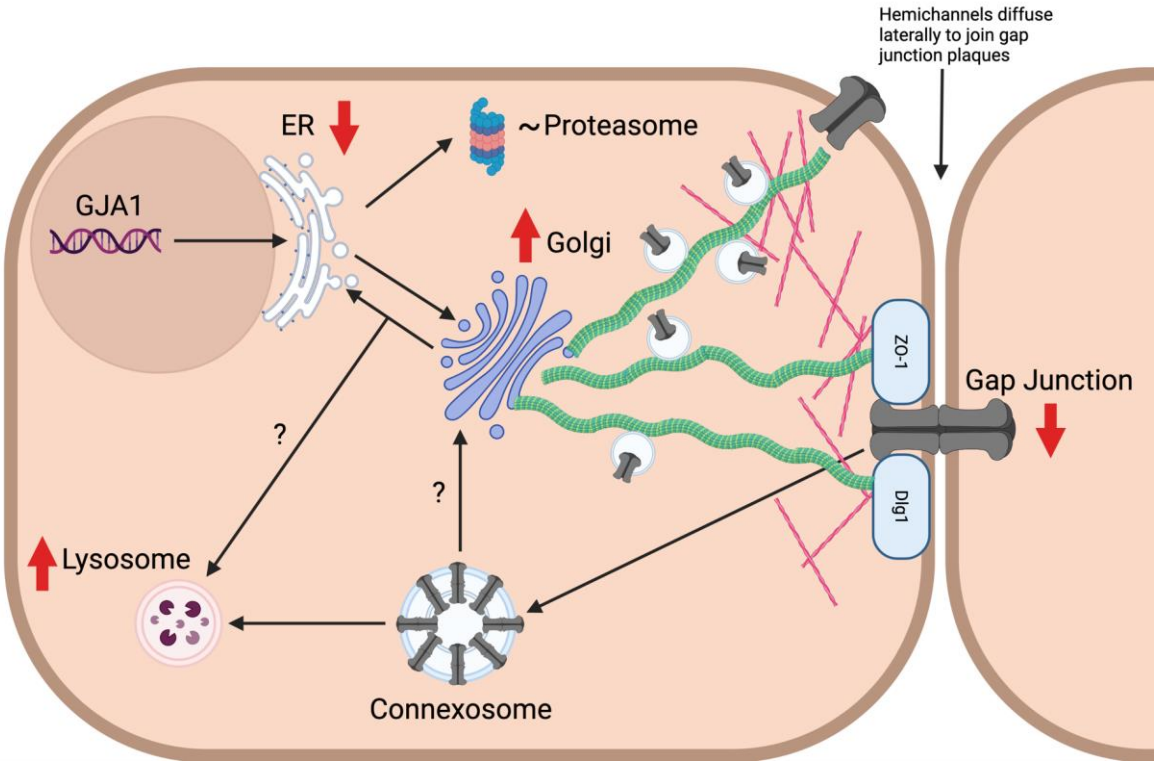

Figure 3.12: Summary of changes to the Cx43 lifecycle when Dlg1 is knocked down. Black arrows indicate the regular path of Cx43. Red arrows indicate increased (up)/decreased (down) levels of Cx43 in each stage of the lifecycle. GJA1 is the Cx43 gene. Microtubules are shown in green. Actin filaments are shown in pink. Connexons/hemichannels and gap junctions are shown in grey. Vesicles are shown as circles. Figure was produced in Biorender.

Chapter 4: The role of Dlg1 in Wound Healing and Keratinocyte Proliferation/Migration

4.1 Introduction

4.1.1 Scratch Wound Assay as a Technique to Study Wound Healing

Within the dermatological field, many different methods have been employed in order to study the process of *ex vivo* wound healing using 2D and 3D cell model approaches, all of these relying on the generation of a cell-free area ('wound') that adjacent cells will respond to and attempt to fill. These techniques range from relatively simple assays, such as the scratch wound assay, to far more complex methods using 3D organotypic cultures or *ex vivo* skin models (Masson-Meyers *et al.*, 2020). While the more sophisticated methods may be used in scenarios where accurately replicating the exact conditions of the skin is paramount, the scratch wound assay has remained the most popular method of studying wound healing. This is largely due to scratch assays being relatively easy to perform, typically involving use of a pipette tip or scalpel to remove cells from a certain area of the culture vessel. This results in an inexpensive assay requiring very little in the way of lab resources or technical expertise, with the option to develop a relatively high-throughput assay which has proved useful in drug discovery (Hulkower and Herber, 2011).

While the scratch assay has been extremely valuable for generating basic research data on the effect of many proteins and drugs in wound healing, there are certain aspects of the technique which result in considerable variation between any two given wounds. These include variations in the force applied by the researcher through the instrument used to create the wound, the angle at which the instrument is held and the steadiness of the researcher's hand as the

wound is made. These conditions have all been shown previously to affect wound geometry and therefore migration rates of cells into the wound, impacting the overall wound healing process (Fenu *et al.*, 2019). While several research groups and commercial companies have attempted to mitigate these issues in the past, the solutions presented often have a high associated cost or require less standard lab equipment, such as lasers (Tamada *et al.*, 2007). Therefore, there remains a need for low-cost approaches to improve standardisation of scratch wound assays.

4.1.2 Previous Work on the Expression of Cx43 in Wound Healing

Immediately following damage to the skin, the process of wound healing is triggered in order to prevent blood loss/infections and restore homeostasis (as discussed in **Chapter 1, Section 1.2**). One of the main aims of this study was to identify the role that Dlg1 plays during this process in keratinocytes, particularly due to its ability to control Cx43 plasma membrane localisation **(Chapter 3)**, which is elevated in cells of the wound edge in chronic non-healing wounds (Brandner *et al.*, 2004). Such work on the basic function of Dlg1 may eventually support the development of future therapeutics to improve wound healing rates, either by targeting Dlg1 directly or by targeting the Cx43/Dlg1 interaction.

Much like their differing expression profiles in the sublayers of the epidermis, connexins have been found to follow diverse expression patterns during wound healing, suggesting that they play distinct roles in this process. As the most widely expressed connexin in the skin, much of the work carried out on the role of connexins in epidermal wound healing has focused on Cx43. During the initial stages of epidermal wound healing in rodents, Cx43 is rapidly downregulated in keratinocytes of the wound edge, as well as cells further back from the wound, with this change being observed as early as 2h post-wounding (Goliger and Paul, 1995). This loss in expression is maintained as wound healing progresses, with the most pronounced differences observed at 24h post-wounding, where Cx43 is vastly reduced in cells of the wound edge and the surrounding area compared to

unwounded tissue, before expression returns to normal in cells of the basal layer around 48h post-wounding. Conversely, at 96h post-wounding, Cx43 is upregulated, with expression observed in most sublayers of the epidermis. This is then followed by downregulation and return to normal expression levels seven days after wounding (Coutinho *et al.*, 2003).

4.1.3 Cx43 as a Therapeutic Target in Chronic Wounds

Following the finding that Cx43 is downregulated in keratinocytes proximal to the wound in the early wound healing process (Goliger and Paul, 1995), an inducible Cx43 knockout mouse model was used to demonstrate that removal of Cx43 could improve wound closure rate (Kretz *et al.*, 2003). In contrast to acute wound healing, chronic wounds, which don't follow the typical progression of wound healing and instead remain in an inflammatory state, strongly express Cx43 in cells of the wound edge as well as further back from the wound (Brandner *et al.*, 2004). These observations led to the identification of Cx43 as a strong candidate for therapeutic targeting. Initial experiments in mice proved this to be the case, with inhibition of Cx43 expression via topical application of an antisense oligodeoxynucleotide not only improving wound healing rates in both excisional and incisional wounds but also reducing scar formation (Qiu *et al.*, 2003). Further research in this area explored the effect of Cx43 mimetic peptides, which represent a second strategy to study Cx43 in wound healing (with antisense oligonucleotides being the first). Connexin mimetic peptides function through their complementarity to the sequence of Cx43 **(Figure 4.1)**. For example, the peptide GAP27 mimics the second extracellular loop region of Cx43 (aa201-211) and will bind to this area, thereby forcing the closure of Cx43 hemichannels within minutes through a mechanism which is yet to be completely defined (Evans and Leybaert, 2009). After a period of 30 minutes, the peptide may additionally permeate the space within gap junction channels and inhibit gap junctional communication (Evans, Bultynck and Leybaert, 2012). Interestingly, GAP27-treatment results in phosphorylation of the Cx43 residue serine 368, which may also be involved in the inhibition of gap junctional communication (Pollok et al., 2011). GAP27 has been more recently shown to

improve wound healing rates in keratinocytes, causing an increase in cell migration but no changes in cell proliferation (Faniku *et al.*, 2018; Wright *et al.*, 2012). While useful for experimental research, GAP27 is unstable and its therapeutic potential is therefore limited. In search of a stable analogue of GAP27, the Martin lab at Glasgow Caledonian University, in collaboration with Zealand Pharma (Denmark), screened a variety of connexin mimetic peptides. One of these 'ZPC' was found to be more stable than GAP27 and effectively inhibited connexin hemichannel and gap junction function, in addition to enhancing scratch wound closure in primary keratinocytes isolated from both normal and diabetic individuals (Faniku, 2018, ZPC formulation priority Zealand Pharma). A patent for this compound is filed and awaits additional exploration. A further mimetic peptide, alpha connexin carboxyl terminus 1 (αCT1), mimics the terminal 9 amino acids of the Cx43 C-terminus (aa374-382) and therefore inhibits the interaction between Cx43 and ZO-1, as well as potentially affecting other interactions at the extreme C-terminal end of Cx43. αCT1 has proven extremely effective in promoting wound healing *in vivo* and reducing scar formation, leading to its use in a phase III clinical trial (Montgomery *et al.*, 2018) (https://clinicaltrials.gov/study/NCT02667327). In addition to their therapeutic potential, these mimetic peptides have the added benefit of targeting Cx43 channel function rather than expression, which is useful experimentally in terms of untangling the complexities of Cx43 channel-forming functions vs non-channel functions, with these diverse functions potentially playing different roles during wound healing. It is important to note that the therapeutic potential of Cx43 is not limited to wound healing and it may additionally be a valuable target in certain types of cancer and cardiac disease (Laird and Lampe, 2018).

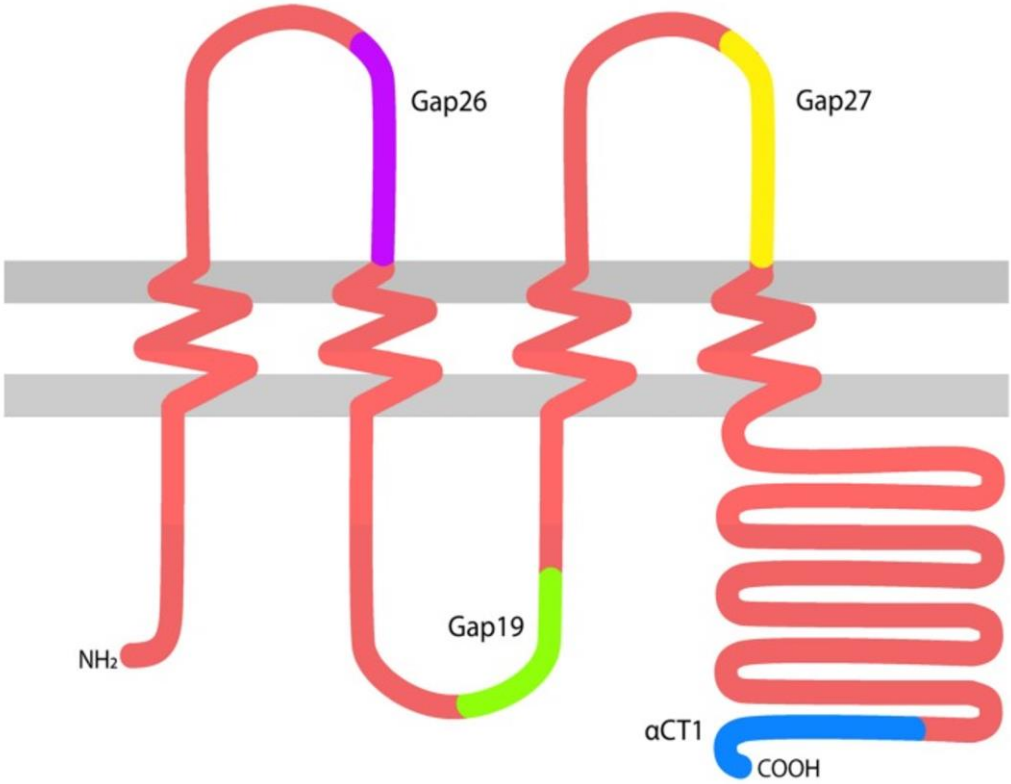

Figure 4.1: Existing mimetic peptides targeting Cx43. Full-length Cx43 (red) is shown inserted into the plasma membrane (grey horizontal lines). NH_2=N-terminus, COOH=C-terminus. Areas which mimetic peptides have been derived from are highlighted in different colours, purple=Gap26, green=Gap19, yellow=Gap27 and blue=αCT1. Gap26 and Gap27 mimic extracellular loops 1 and 2 respectively, while Gap19 mimics the cytoplasmic loop and αCT1 mimics the terminal 9 amino acids of the cytoplasmic C-terminus. Adapted from Montgomery *et al.*, 2018.

4.1.4 Existing Knowledge on the Role of Dlg1 in Wound Healing

Compared to the wealth of knowledge on Cx43, very little is known about the role of Dlg1 during the wound healing process. Due to its function as part of the Scribble polarity complex in addition to its interactions with PTEN and APC to inhibit cell cycle progression in epithelial cells (Sotelo *et al.*, 2012), it seems likely that Dlg1 would have some function in wound healing. In support of this idea, O'Neill and colleagues previously demonstrated that Dlg1 is involved in promoting cell migration during wound healing in mouse primary astrocyte cultures through interaction of the third PDZ domain of Dlg1 with Protein Kinase C α (PKCα). Depletion of Dlg1 via siRNA knockdown in H1703 cells (a squamous lung cancer cell line) resulted in 20% less coverage of the wound area at a time

of 16h post-wounding compared to control siRNA treatment (O'Neill *et al.*, 2011). The authors also demonstrated that Dlg1 could promote cell invasion in several cancerous epithelial cell lines, raising questions as to whether it could stimulate cell migration in normal keratinocytes. Based on the gaps in current knowledge, further study of the role of Dlg1 in epithelial wound healing is necessary.

4.1.5 Previous Study of the Cx43/Dlg1 Interaction

The interaction between Cx43 and Dlg1 has been previously studied in a variety of cultured cell lines including both cancerous and untransformed cells. Firstly, the interaction was investigated in HPV-positive cervical epithelial cell lines (MacDonald *et al.*, 2012), before shifting towards HPV-negative cell lines to provide information on the importance of the interaction outside of cancer (Dong 2021). In addition, the Cx43/Dlg1 interaction has also been confirmed in human HPV-negative primary cervical mucosal epithelial cells via proximity ligation assay, demonstrating the functional significance of the Cx43/Dlg1 complex both *in vitro* and *in vivo* (Sun *et al.*, 2015). As the importance of Cx43 during the course of epidermal wound healing is well-documented, it is crucial to establish if this interaction is conserved *in situ* in human skin tissue and may contribute to this process, particularly as the role of Dlg1 in wound healing remains understudied. This represents a gap in the wound healing field, as Dlg1 is a known tumour suppressor protein in Drosophila and is also a suspected tumour suppressor in humans (Sotelo *et al.*, 2012). This, coupled with results of the previous chapter demonstrating the role of Dlg1 in controlling Cx43 plasma membrane localisation **(Chapter 3)** highlights the potential of Dlg1 as a therapeutic target in chronic non-healing wounds. Intuitively, knocking-down Dlg1 would be expected to result in an increase in cell proliferation due to the loss of its interaction with APC and PTEN, which arrests the cell cycle in G_1/G_2 phases (Brandmaier, Hou and Shen, 2017). In addition, the depletion of Dlg1 would limit Cx43 plasma membrane localisation, which would be expected to have a similar effect to targeting Cx43 directly in non-healing wounds as previous treatments have (Montgomery *et al.*, 2018; Wright *et al.*, 2009; Pollok

et al., 2011; Faniku *et al.*, 2018), resulting in increased migration of cells into the wound area and potentially improved wound healing rates. Taken together, Dlg1 and the Cx43/Dlg1 interaction are promising preliminary therapeutic targets and consequently the role that Dlg1 plays in wound healing is an important area of research.

Aims:

- Evaluate the use of a 3D-printed wound mask in standardisation of scratch wound assays.
- Determine the optimum concentration of mitomycin C for use in preventing cell proliferation in HaCaT cell wound assays.
- Through siRNA depletion, assess the role of Dlg1 in wound healing in a keratinocyte cell line (HaCaT cells) and whether this role is through an effect on cell migration and/or cell proliferation.
- Investigate the molecular dynamics of Cx43 and Dlg1 in fluorescent live-cell experiments.
- Determine if the interaction between Cx43 and Dlg1 is conserved in adult human skin (keratinocytes/dermal cells/adipocytes) and assess whether there are differences in protein levels/localisation between diabetic and non-diabetic samples.

4.2 A 3D-printed wound mask reduces variation within and between *in vitro* scratch wound assays

Due to some of the associated issues with traditional scratch wound assays outlined in **Section 4.1.1**, a 3D-printed wound mask was generated in an attempt to increase standardisation of wound healing experiments in this study. The wound mask is circular in shape and was designed to fit around a 35mm cell culture dish, with a 2.5mm wide gap in the middle of the mask matching the width of a 200µl pipette tip, allowing the tip to follow a linear path as the

wound is created and therefore minimising variation in the wound width and orientation (for technical detail see **Chapter 2, Section 2.2.9**).

To test whether the 3D-printed wound mask was capable of reducing variation between scratch wounds, wounds were created in three different cell lines (HaCaT, HEK293 and W12T) either free-hand or using the wound mask **(**Error! Reference source not found.**A)**. The width of the wound as well as the standard deviation of the width were measured using the wound healing plugin tool for Image J (Suarez-Arnedo *et al.*, 2020). Variance in wounds was determined using the coefficient of variation (CV) ([standard deviation/mean]x100) **(**Error! Reference source not found.**B,C)**.

Overall, the coefficient of variation both within (variation of wound size within an individual wound) and between wounds (variation of wound size between various wounds) was low across the groups, however some differences were observed between cell lines. W12T cell wounds had the lowest variation between wounds **(**Error! Reference source not found.**B)** (CV of 1.89% FH vs 3.11% W), while HEK293 cell wounds had the lowest variation within wounds **(**Error! Reference source not found.**C)** (CV of 3.82% FH vs 2.71% W). In contrast, higher variation was observed in the HaCaT cell wound group (CV of 14.82% FH vs 11.71% W between wounds and 5.07% FH vs 5.17% W within wounds). For both measures, in most cases the wounds made with the wound mask showed reduced variation compared to free-hand wounded samples, although this difference was only significant when comparing variation within wounds in the W12T cells (CV of 2.27% vs 6.39%). This could reflect differences in the cell lines (i.e. W12T tumour cells vs untransformed HaCaT and HEK293 cells) which can affect the uniformity of a wound on generation.

An important factor when considering the creation of a uniform scratch wound is the degree of attachment between individual cells of the confluent monolayer. In the experiment above, where cells were scratched 24h after seeding, detachment of sheets of cells was frequently observed in the highly adherent

HaCaT and HEK293 groups on wounding, often leading to uneven wounds **(**Error! Reference source not found.**D)**. This effect was noticeably absent in the W12T cells, which as a tumour cell line are deficient in cell-cell contacts. As the only significant difference between the 3D-printed wound mask and free-hand wounds was observed in the W12T cells, it was possible that cell-cell contacts in the other cell lines were obscuring the benefit of using the 3D-printed wound mask. To address this, HaCaT cells were seeded at a fixed density of $1x10^6$ cells and wounded at timepoints of 4h or 8h post-seeding either free-hand or using the 3D-printed wound mask to compare with the existing 24h post-seeding data **(Figure 4.3A-C)**. The results generally showed that both within and between wounds, as time of wounding post-seeding increased, the coefficient of variation also increased, supporting the theory that reduced time for formation of cell-cell contacts between cell seeding and wounding is beneficial for standardisation of scratch wound assays. While no significant differences were noted when using the 3D-printed wound mask compared to creating wounds free-hand, at the 4h wounding timepoint the mask reduced variation both between and within wounds. This effect was especially pronounced in the between wounds groups, where the CV more than halved from 11.16% to 4.61%. Surprisingly, this effect was reversed for the 8h timepoint, where use of the 3D-printed wound mask was associated with increased variation compared to free-hand wounds, again particularly between wounds. The cell-cell attachment issue commonly seen in the 24h post-seeding wound groups was also observed in one of the wounds made at 8h post-seeding **(Figure 4.3D)**, adding further evidence that this problem was incubation time-dependent.

Overall, these data suggest that wound generation shortly after cell-seeding was favourable in terms of reducing variation both between and within scratch wounds. Despite the lack of a significant difference between the 3D-printed wound mask and free-hand groups in most cell lines and timepoints included in these two experiments, the majority of these data support a slight reduction in variation of wounds (which was already low in this study) when using the wound mask. Importantly, there were no drawbacks associated with use of the mask. Based on these results, the wound mask was used in future experiments where applicable.

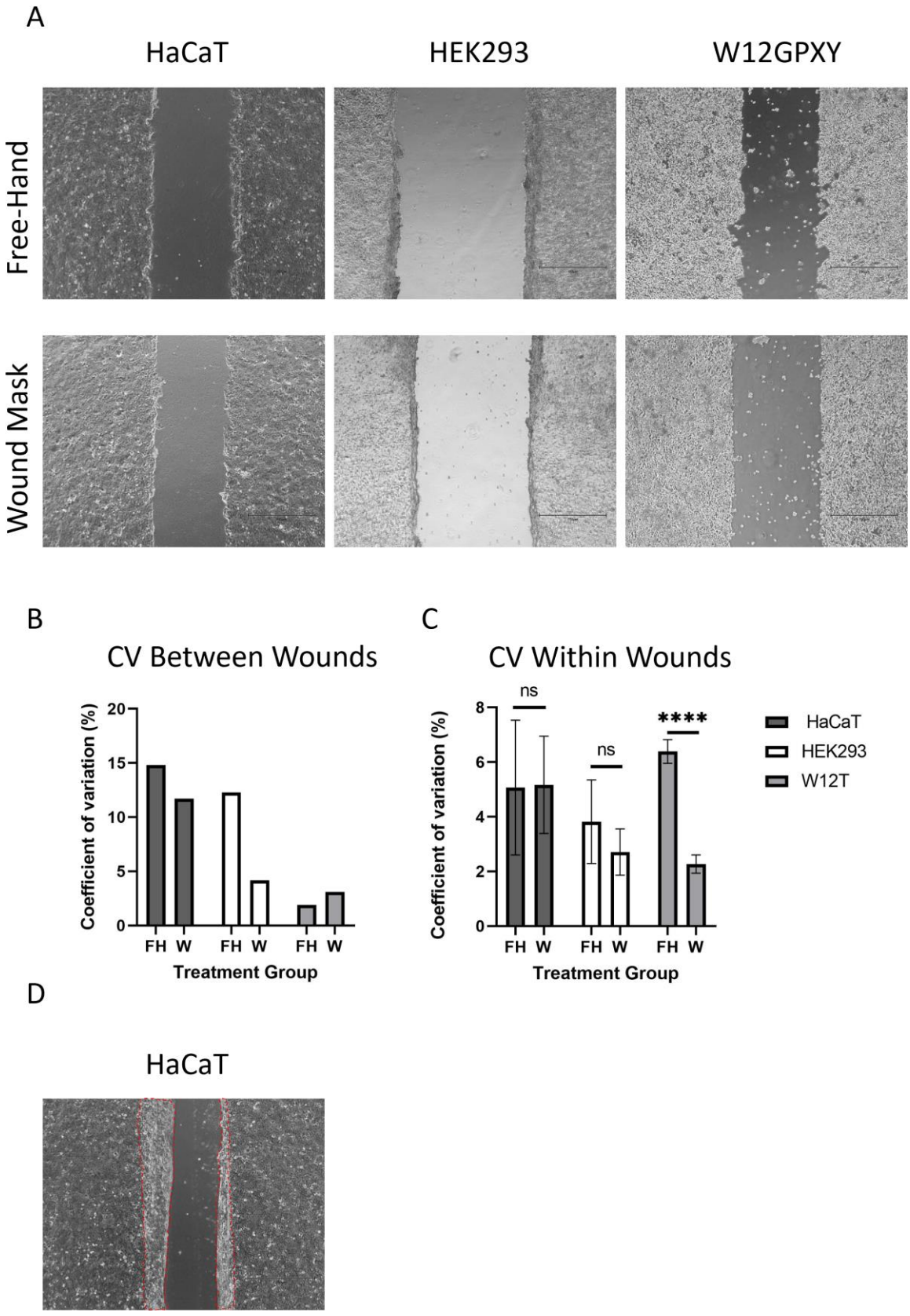

Figure 4.2: Evaluation of the effectiveness of a 3D-printed wound mask in reducing variation between and within scratch wounds in various cell lines. (A) Representative images of scratch wounds of HaCaT, HEK293 and W12GPXY cells immediately following wounding with a 200µl pipette tip free-hand or using

the wound mask. Five plates of cells were wounded for each cell line in each group. Scale bar=750μm. **(B-C)** Quantification of coefficient of variance, CV, in free-hand, FH, and wound mask, W, groups between and within wounds respectively in HaCaT, HEK293 and W12GPXY cells (Graph shows mean, n=5 per treatment group). Statistical testing and error bars representing s.d. are not shown for **(B)** as it represents a comparison between the 5 separate wounds and therefore only one CV value is generated following analysis. Significance in **(C)** was assessed using an unpaired t-test (****=$p<0.0001$). Graph shows mean±s.d. **(D)** Example of uneven wound generated due to extensive cell-cell attachment. Red dotted line indicates area where cells are not attached to plate following wounding but remain connected to other cells in a 'sheet' that folds over on itself to create an uneven wound area. Scale bars=750μm.

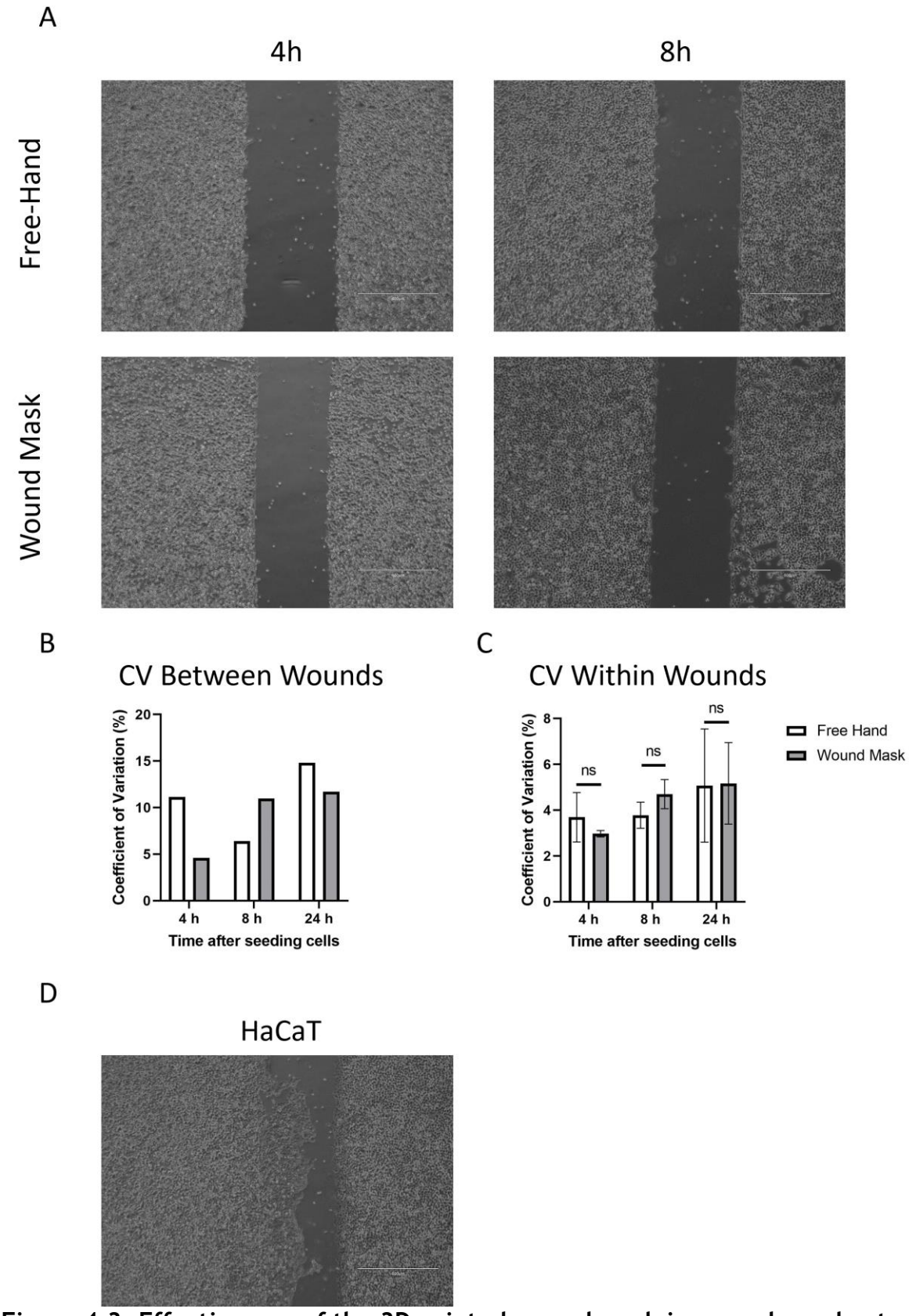

Figure 4.3: Effectiveness of the 3D-printed wound mask in wounds made at different timepoints after cell seeding. (A) Representative images of scratch wounds made free-hand or with the wound mask 4 and 8h after seeding of HaCaT cells. Scale bar=750µm. **(B-C)** Quantification of coefficient of variance,

CV, at different times after cell seeding in free-hand and wound mask groups between and within wounds respectively in HaCaT cells (Graph shows mean, n=5 per treatment group at each timepoint). Error bars representing s.d. are not shown for **(B)** as it represents a comparison between the 5 separate wounds and therefore only one CV value is generated following analysis. Significance in **(C)** was assessed using an unpaired t-test. Graph shows mean±s.d. **(D)** One of the ten total wounds created at 8h post-cell seeding showed signs of extensive cell-cell attachment as was frequently observed in wounds made 24h post-cell seeding. Scale bars=750μm.

4.3 Knockdown of Dlg1 inhibits wound healing

To analyse the impact of Dlg1 during the wound healing process, a series of scratch wound assays using HaCaT cells were performed using an Incucyte wound-maker tool and immediately imaged using an Incucyte live cell analyser unit. This technique has several advantages over other methods, including standardisation of wound angle, force exerted through wounding instrument and automated quantification of wound areas (Radstake *et al.*, 2023). These images were then analysed downstream to provide metrics such as relative wound density (RWD), which is a percentage value representing the relative density of cells within the wound compared to outside of the wound. This measure is seen as preferable to traditional wound confluence measurements as it is self-normalising for differences in cell density between samples. HaCaT cells with and without 24h 20nM or 40nM siRNA treatment against Dlg1 were wounded and images were captured of the wells every hour. HaCaT cells pre-treated for 30 minutes with 100nM ZPC (Zealand Pharma) were also included as a positive control (Faniku, 2018; Martin P, personal communication). ZPC is a stable analogue of the Cx43 mimetic peptide GAP27 which has previously been shown to improve scratch wound healing rates (Faniku *et al.*, 2018). Images were collated and analysed to provide measurements of relative wound density at different timepoints.

Observationally it appeared that ZPC-treated cells were the fastest in wound closure, followed by control cells, 20nM siDlg-treated cells and finally 40nM siDlg-treated cells **(Figure 4.4, video files are also available attached to thesis)**. When comparing the relative wound densities during the early stages of wound healing (0-2h), little difference was observed between the treatment groups, indicating that events early on in wound healing are not drastically altered in cells treated with siDlg1 or ZPC **(Figure 4.5A)**. However, by 4 h post-wounding there was a marked difference between ZPC-treated cells, mock treated cells and siDlg1-treated cells. As expected, ZPC-treated samples had a higher RWD at this timepoint (20.7%), while interestingly siDlg1-treated cells

(20nM 16.6%, 40nM 14.7%) exhibited reduced RWD compared to control HaCaT cells (19.6%), suggesting wound healing was inhibited. This inhibition was dose dependent, with 20nM-treated cells having higher RWD compared to 40nM-treated cells. The gap between these treatment groups continued to widen between 4-8h post-wounding, implying Dlg1 depletion had a cumulative deleterious effect on the wound healing process. The largest differences between the treatment groups were observed at 24h post-wounding (48h post-siRNA treatment), where 40nM siDlg1-treated cells had a 15.4% lower RWD compared to control cells (51.7% vs 67.1%), with ZPC-treated cells having a 7.5% higher RWD compared to control (74.6% vs 67.1%) **(Figure 4.5B)**. The relative wound densities of the treatment groups then converged slightly up to the final timepoint of 48h post-wounding (72h post-siRNA treatment), however the dose-dependent effect on siDlg1-treated cells was still evident compared to control cells. When comparing the control HaCaT cell group to the 40nM siDlg1-treated group, a significant effect was first observed at 4h post-wounding ($p<0.01$) and then continuing on throughout the rest of the experiment timepoints **(Figure 4.5C)**. While 100nM ZPC treatment improved relative wound density compared to control cells, this effect was not found to be significant, which may reflect the lower replicate number for this treatment group **(Figure 4.5D)**. The lack of significant effect could also be due an insufficient dose of ZPC, as parallel experiments with 100μM ZPC-treated HaCaT cells showed significantly faster wound closure compared to control-treated cells (Martin, unpublished data).

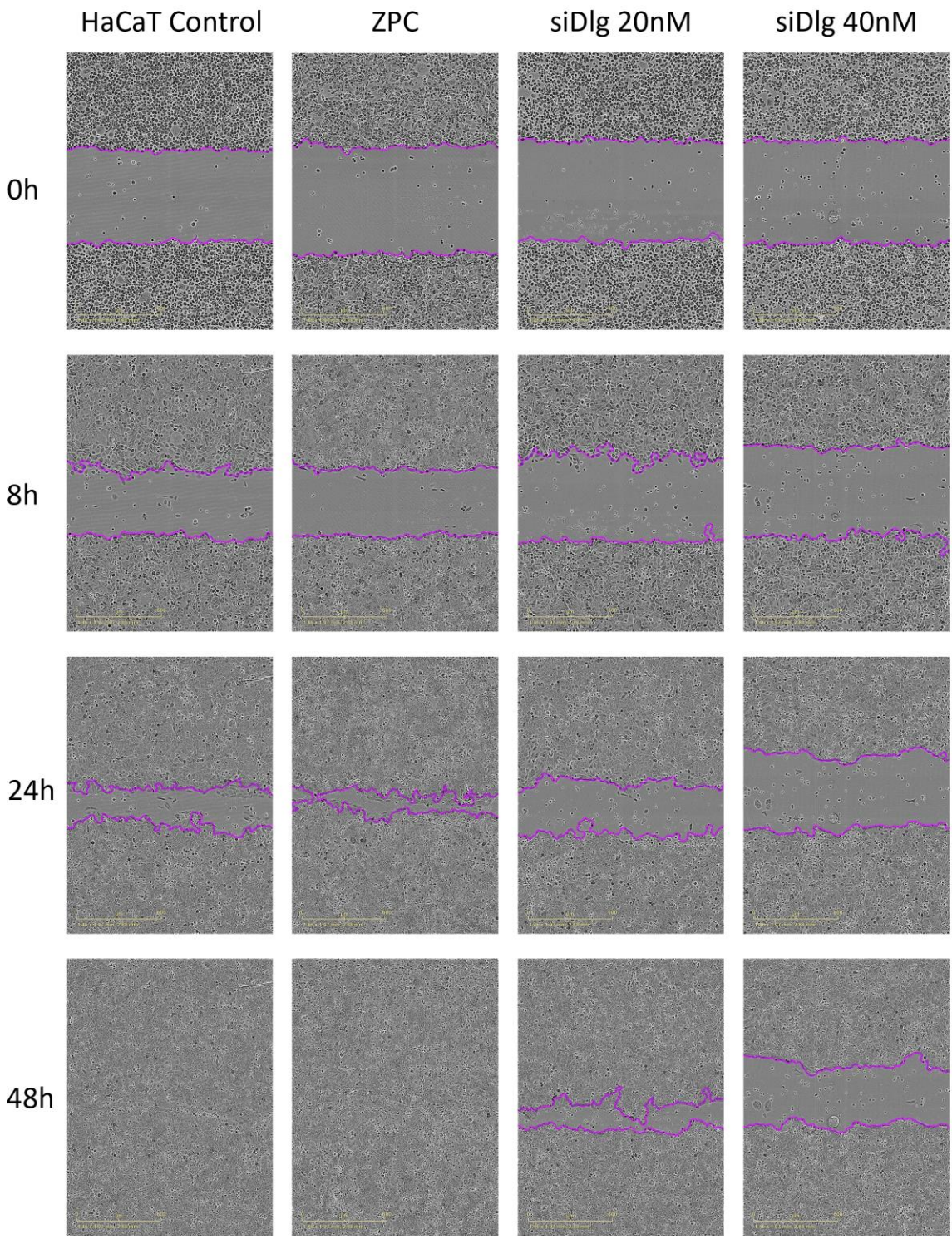

Figure 4.4: Representative images of HaCaT cells filling wounds created by an Incucyte WoundMaker at different timepoints. Treatment groups are 100nM ZPC, 20 and 40nM siDlg1. HaCaT Control are untreated samples for comparison. ZPC treatment group was made up of three biological replicates with three technical replicates of each for a total of nine samples. HaCaT Control, 20 and 40nM siDlg groups were made up of six biological replicates made up of three technical replicates each for a total of 18 samples. Timepoints are shown on the left-hand side. Purple line highlights the wound area at each given timepoint as determined by the Incucyte analysis software. Scale bars=600µm.

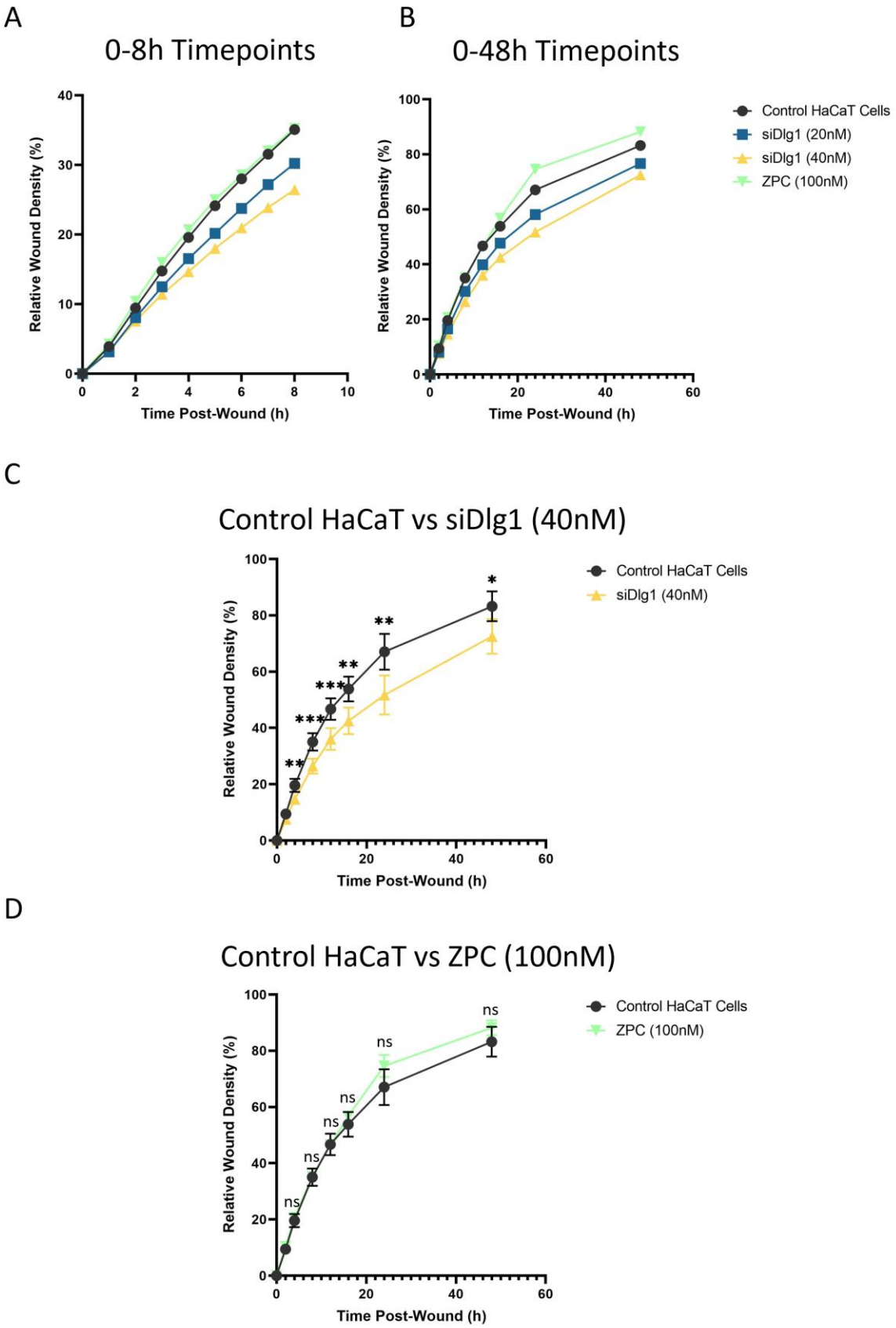

Figure 4.5: Quantification of HaCaT scratch wound assay. (A) RWD% of treatment groups at early timepoints (0-8h) **(B)** RWD% of treatment groups (0-48h). **(C)** RWD% showing Control HaCaT had a significantly higher relative wound density than siDlg1 (40nM) at various timepoints (*=p<0.05, **=p<0.01, ***=p<0.001). Graph shows mean±s.d. Statistical significance was assessed using

a Kruskal-Wallis test followed by Dunn's post-hoc test. **(D)** RWD% showing ZPC had a higher relative wound density than Control HaCaT. Graph shows mean±s.d. ZPC treatment group was made up of three biological replicates with three technical replicates of each for a total of nine samples. HaCaT Control, 20 and 40nM siDlg groups were made up of six biological replicates made up of three technical replicates each for a total of 18 samples.

4.4 Knockdown of Dlg1 inhibits cell proliferation in unwounded HaCaT cells

Cell proliferation and migration are both important drivers of the wound healing process, with cell migration being the major determinant of epidermal wound healing rate under normal circumstances (Martin, 1997). With the significant difference between relative wound density observed in control HaCaT cells compared to 40nM siDlg1-treated samples, it was crucial to determine whether this result was due to an effect on cell proliferation, cell migration, or a combination of the two. To address this, it was first important to clarify whether knockdown of Dlg1 affected cell proliferation in unwounded cells. For this, an MTT assay was performed on HaCaT cells treated with siDlg1 for 24h and OD_{595} values were collected as a measurement of cell proliferation **(Figure 4.6)**. As in **Chapter 3**, siGlo samples were included as a non-target oligonucleotide transfection control. Results for all treatment groups were normalised to control HaCaT cell samples. The results showed that treatment with 40nM siGlo resulted in a decrease of 12% in cell proliferation, however this difference was not significant. Treatment with 20nM siDlg1 also caused a very small decrease of 4% in OD_{595} value relative to control cells, suggesting this treatment had little effect on cell proliferation. This was in contrast to 40nM siDlg1 treatment, which resulted in a 25% decrease compared to control cells. This change was significant compared to both control HaCaT cells and 20nM siDlg1-treated cells, implying that siRNA against Dlg1 causes a dose-dependent inhibition of cell proliferation.

To confirm the anti-proliferative effect of treating HaCaT cells with siDlg1, a cell proliferation assay was carried out using an Incucyte live cell analyser unit as before **(Figure 4.7)**. Using an Incucyte software analysis module, confluence of cells was quantified over time and compared between treatment groups **(Figure 4.7A)**. Cell confluence was found to be almost identical between control HaCaT cells and cells which had been mock transfected by adding Opti-MEM serum-free media, with both groups reaching 90% confluence at the 36h timepoint. Cells treated with 40nM siGlo displayed slightly lower cell confluence

compared to control HaCaT cells, reaching 90% confluency at the 42h timepoint. This effect was again not found to be significant. Results from these control samples suggest that the conditions of transfection alone did not significantly alter cell proliferation. As with the previous experiment, a dose-dependent decrease in cell confluence was observed for cells treated with 20nM (90% confluence at 48h timepoint) and 40nM siDlg1 (90% confluence at 54h timepoint). While the previous experiment suggested siGlo treatment affected cell proliferation more than 20nM siDlg1 treatment, this finding was reversed here, with 20nM siDlg1-treated samples possessing lower cell confluence than 40nM siGlo-treated samples. Comparison of control HaCaT cells with each of the 20nM/40nM siDlg1-treated groups revealed a significant difference between the two groups at the 36h, 42h and 48h timepoints **(Figure 4.7B,C)**. Normalisation of each treatment group to control HaCaT cells showed that the maximum effect of siDlg1 was observed at the 42h timepoint, where there was a 7% decrease in cell confluence in the 20nM siDlg1-treated group and a 10% decrease in the 40nM siDlg1-treated group **(Figure 4.7D)**. This effect was diminished at later timepoints, which may reflect degradation of the siRNA.

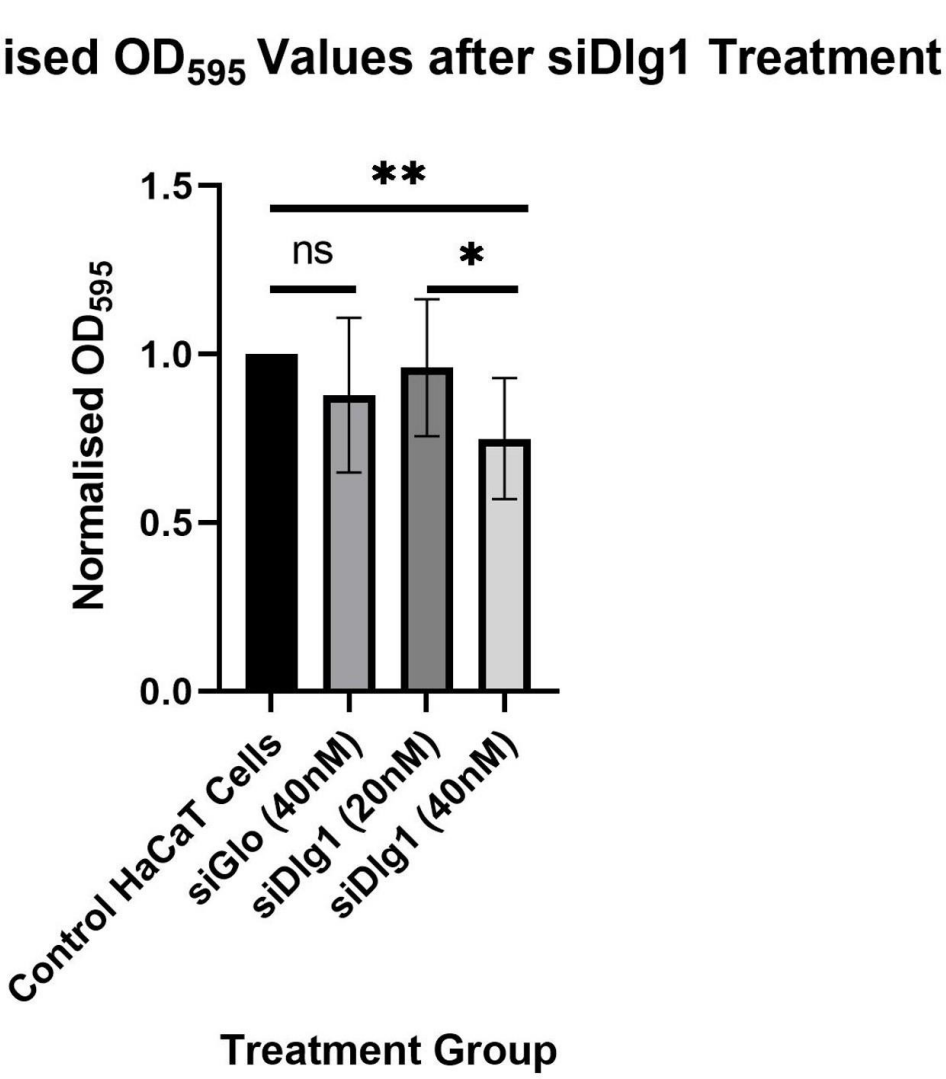

Figure 4.6: MTT assay of HaCaT cells treated with siRNA targeting Dlg1. Cells were transfected with siRNA 24h after seeding and were incubated for a further 24h. MTT solution was added and cells were incubated for 3h at 37°C. Following dissolution of MTT formazan crystals, OD_{595} values were read in a plate reader. Values were normalised against control HaCaT cells. siGlo samples were included to test the effect of transfection of an unrelated oligonucleotide. 12 samples were included for each treatment group, with a separate transfection being carried out for each sample. Graph shows mean±s.d. *=$p<0.05$, **=$p<0.01$. Statistical significance was assessed using a Kruskal-Wallis test followed by Dunn's post-hoc test.

A

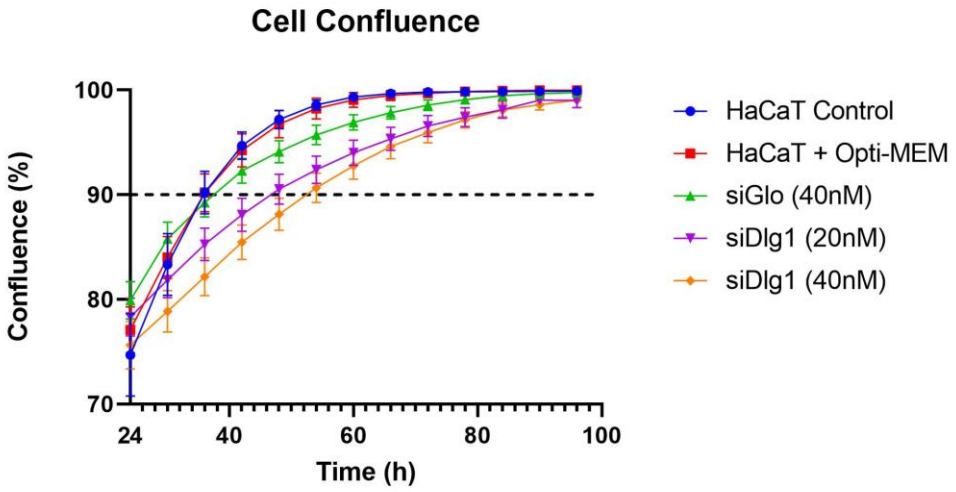
Cell Confluence
Confluence (%)
Time (h)
HaCaT Control
HaCaT + Opti-MEM
siGlo (40nM)
siDlg1 (20nM)
siDlg1 (40nM)

B

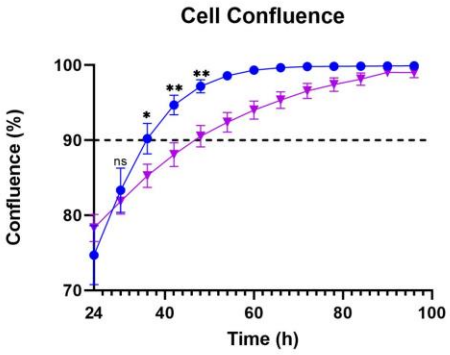
Cell Confluence
Confluence (%)
Time (h)

C

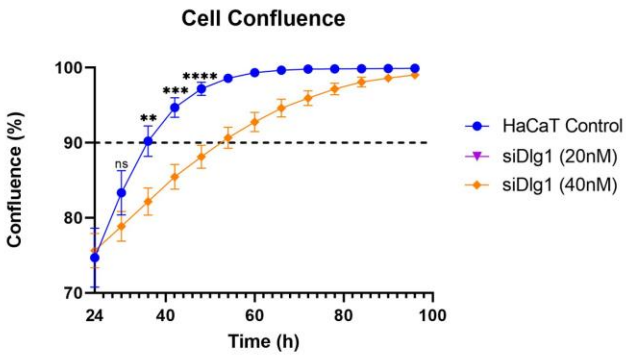
Cell Confluence
Confluence (%)
Time (h)
HaCaT Control
siDlg1 (20nM)
siDlg1 (40nM)

D

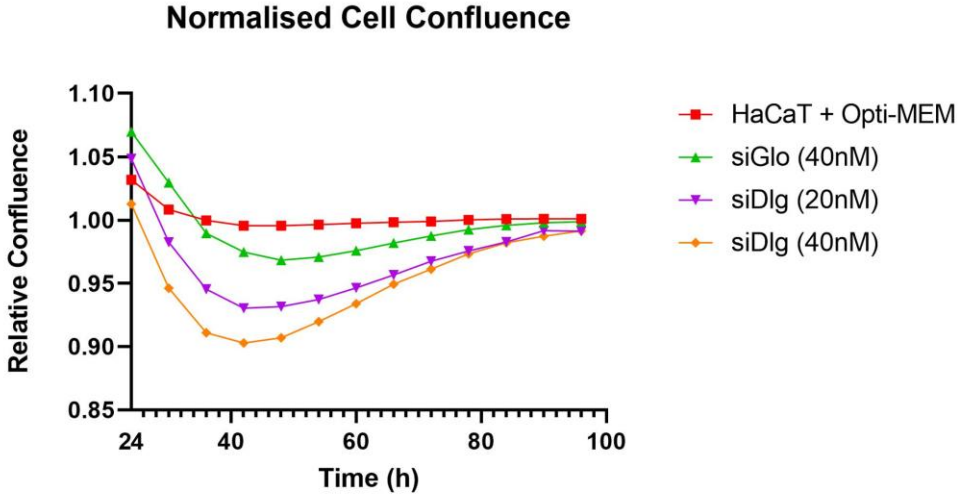
Normalised Cell Confluence
Relative Confluence
Time (h)
HaCaT + Opti-MEM
siGlo (40nM)
siDlg (20nM)
siDlg (40nM)

Figure 4.7: siDlg1 treatment inhibits cell proliferation in HaCaT cells. (A) Confluence % of treatment groups over time. Measurements are shown from 24h timepoint which represents 24h post-siRNA transfection. HaCaT+Opti-MEM group was included to test the effect of serum-free media on cell proliferation. siGlo samples were included to test the effect of transfection of an unrelated oligonucleotide on cell proliferation. Graph shows mean±s.d. 12 samples were included for each treatment group, with a separate transfection being carried out for each sample. **(B)** and **(C)** Cell confluence is significantly lower in 20nM siDlg1-treated cells **(B)** and 40nM siDlg1-treated cells **(C)** compared to control HaCaT cells at various timepoints. ns=not significant, **=p<0.01, ***=p<0.001, ****=p<0.0001. Statistical analysis was not carried out on timepoints after 48h due to the control group becoming almost 100% confluent. Statistical significance was assessed using a Kruskal-Wallis test followed by Dunn's post-hoc test. **(D)** Normalised cell confluence of treatment groups over time. Groups are normalised to control HaCaT cells.

4.5 Determination of mitomycin C concentration for use in HaCaT cell scratch wound assays

Having established that depletion of Dlg1 results in decreased cell proliferation in unwounded HaCaT cells, it was important to confirm if this effect was responsible for the reduced wound healing rates shown in cells treated with siDlg1. Mitomycin C (MMC) is a drug which, through its ability to cross-link DNA complementary strands, prevents cell division of cultured cells and is used in combination with other treatments for specific types of cancer therapy (Gad, 2014). MMC is commonly used in scratch wound assays to restrict cell proliferation, removing this as a variable so that observed differences between treatment groups result from differences in cell migration. However, cell toxicity is an important factor to consider in MMC treatments, meaning the appropriate MMC concentration must be determined for each given cell line. Little literature exists on the toxicity of MMC in HaCaT cells, however one study using clinical concentrations of MMC found that a 5 minute treatment with $4x10^{2}$ and $4x10^{1}\mu g/ml$ caused a dramatic decline in cell number over a 3 day time period (Wang *et al.*, 2012). For use in scratch wound assays, a concentration of MMC which effectively inhibits cell proliferation while causing minimal toxicity is required. Based on this, a dilution series of MMC from $4x10^{1}$-$4x10^{-4}\mu g/ml$ was prepared and used to treat HaCaT cells for a period of 5 minutes. Following this, cells were washed twice, incubated for 24h in fresh media and subsequently media was collected for a floating cell count to assess toxicity **(Figure 4.8A)**. A large number of floating cells were observed in cells treated with $4x10^{1}\mu g/ml$ MMC, indicating cell death due to toxicity of the MMC. By comparison, progressively less floating cells were present in the $4x10^{0}$ and $4x10^{-1}\mu g/ml$ treatment groups, with this effect mostly levelling out at lower concentrations. These data suggest a dose-dependent toxic effect of MMC on HaCaT cells at higher concentrations, which subsides at concentrations of $4x10^{0}\mu g/ml$ or lower, meaning MMC at this level may cause negligible cell death.

A further experiment to determine the optimum concentration of MMC for HaCaT cell scratch assays was carried out in the form of an MTT assay **(Figure**

4.8B). Here, treatments with MMC and 24h incubation in fresh media were performed as before followed by addition of MTT and further incubation for 3h. Formazan crystals were then dissolved using DMSO and subsequent readings were taken at a wavelength of 595nm to determine cell viability. In this test, a wider dilution range of MTT was employed ($4x10^{2}$-$4x10^{-5}$μg/ml) to more accurately capture the range of effect of MMC on cell viability. Control samples were included where the MTT assay was performed prior to MMC treatment of test samples, representing the number of viable cells in test samples before addition of MMC. Results of test samples were then normalised against these control values to give a measure of viable cells in comparison to the starting number of cells, with a value of 1 signifying an identical quantity of viable cells before and after 24h incubation following MMC treatment.

Drastically reduced cell viability was apparent at a concentration of $4x10^{2}$μg/ml MMC, with cell viability reduced by 71% compared to control samples. By comparison, cell viability was massively improved in cells treated with $4x10^{1}$μg/ml MMC, a trend which continued with the next dilutions in the series before levelling off around $4x10^{-1}$μg/ml, which was the first group in the dilution series to exceed a normalised OD_{595} value of 1. At the more dilute concentrations, the effect of the MMC appeared to wear off, with cell viability beginning to increase beyond a value of 1. Overall from these experiments, the lowest concentration of MMC which blocked cell proliferation without affecting cell viability was $4x10^{-2}$μg/ml and therefore this concentration of MMC was used in future experiments.

A

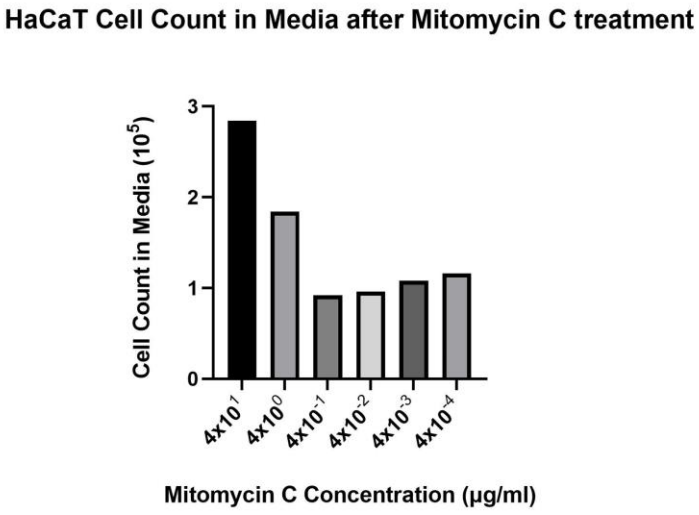

B

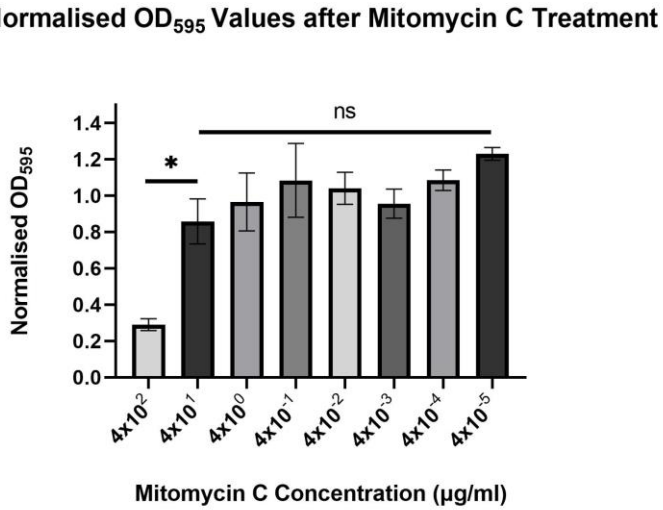

Figure 4.8: **Assessment of optimum concentration of mitomycin C for use in HaCaT scratch wound assays. (A)** Floating cell count following mitomycin C treatment. HaCaT cells were treated with various concentrations of mitomycin C for 5 minutes, washed twice with PBS and incubated in fresh media for 24h at 37°C. Media was collected and the number of floating cells was calculated n=1 for each treatment. **(B)** MTT assay of HaCaT cells following mitomycin C treatment. HaCaT cells were treated as in (A), however after 24h incubation MTT solution was added and plates were incubated for 3h at 37°C. Following dissolution of MTT formazan crystals, OD_{595} values were read in a plate reader. Control HaCaT cells were seeded at the same cell density as test samples and used in MTT assay without 24h incubation as a baseline. Test samples were normalised to control values to give a measure of viable cells compared to the time of cell seeding i.e. a reading of 1=equal number of viable cells before/after mitomycin C treatment and incubation. Graph shows mean±s.d. n=3 for each treatment group. Statistical significance was assessed using a one-way ANOVA followed by Tukey's test.

4.6 Reduced wound healing rate in siDlg1-treated cells is due to inhibition of proliferation and not migration

With the optimum concentration of mitomycin C determined above, a further scratch wound assay was carried out as before with the inclusion of a 5 minute pre-treatment with $4x10^{-2}\mu g/ml$ mitomycin C in order to block cell proliferation and assess changes in cell migration alone **(Figure 4.9**, **video files are also available attached to thesis)**. Several differences were observed when comparing the MMC groups with the previous scratch wound assay. As expected, relative wound densities for the MMC-treated groups were lower than the non-MMC groups, representing the contribution of cell proliferation to the wound healing process **(Figure 4.10A)**. At the final timepoint, 100nM ZPC-treated cells had the highest RWD as before (68.7%), followed closely by the 20nM siDlg1-treated group (66.9%), then closely again the 40nM siDlg1-treated group (63.4%) and the control HaCaT group (61.6%) **(Figure 4.10B)**. A surprising finding from this experiment was that between 2-12h post-wounding, cells treated with 20nM siDlg1 had a slightly higher relative wound density than ZPC-treated cells. At the 16h timepoint, 20nM siDlg1-treated cells had an identical relative wound density value to ZPC-treated cells (40.8%), followed by control cells (35.9%), then finally by 40nM siDlg1-treated cells (34.1%). Another apparent difference from the previous experiment was that there was less distinction between 40nM siDlg1-treated cells and control HaCaT cells, which was exemplified by the lack of a significant difference between the groups at any timepoint during the experiment (44.7%/44.3% vs 51.7%/67.1% at 24h timepoint) **(Figure 4.10C)**. Indeed, at the final timepoint of 48h, both siDlg1-treated groups had a higher relative wound density than the control cells, though this difference was minimal. In contrast, the ZPC-treated cells maintained the highest relative wound density overall, with a similar disparity between this and control cells as was observed in the previous experiment (53.9%/44.7% vs 74.6%/67.1% at 24h timepoint) **(Figure 4.10D)**. This suggests the effect of ZPC is conserved irrespective of cell division and therefore is due to increased cell migration, which is supported by previous studies on the mimetic peptide predecessor to ZPC, GAP27 (Faniku *et al.*, 2018). This differed from siDlg1 treatment, where

cell migration was seemingly unaffected compared to control cells, meaning the differences observed when comparing relative wound density of control and siDlg1-treated cells in the previous experiment were due to a decrease in cell proliferation.

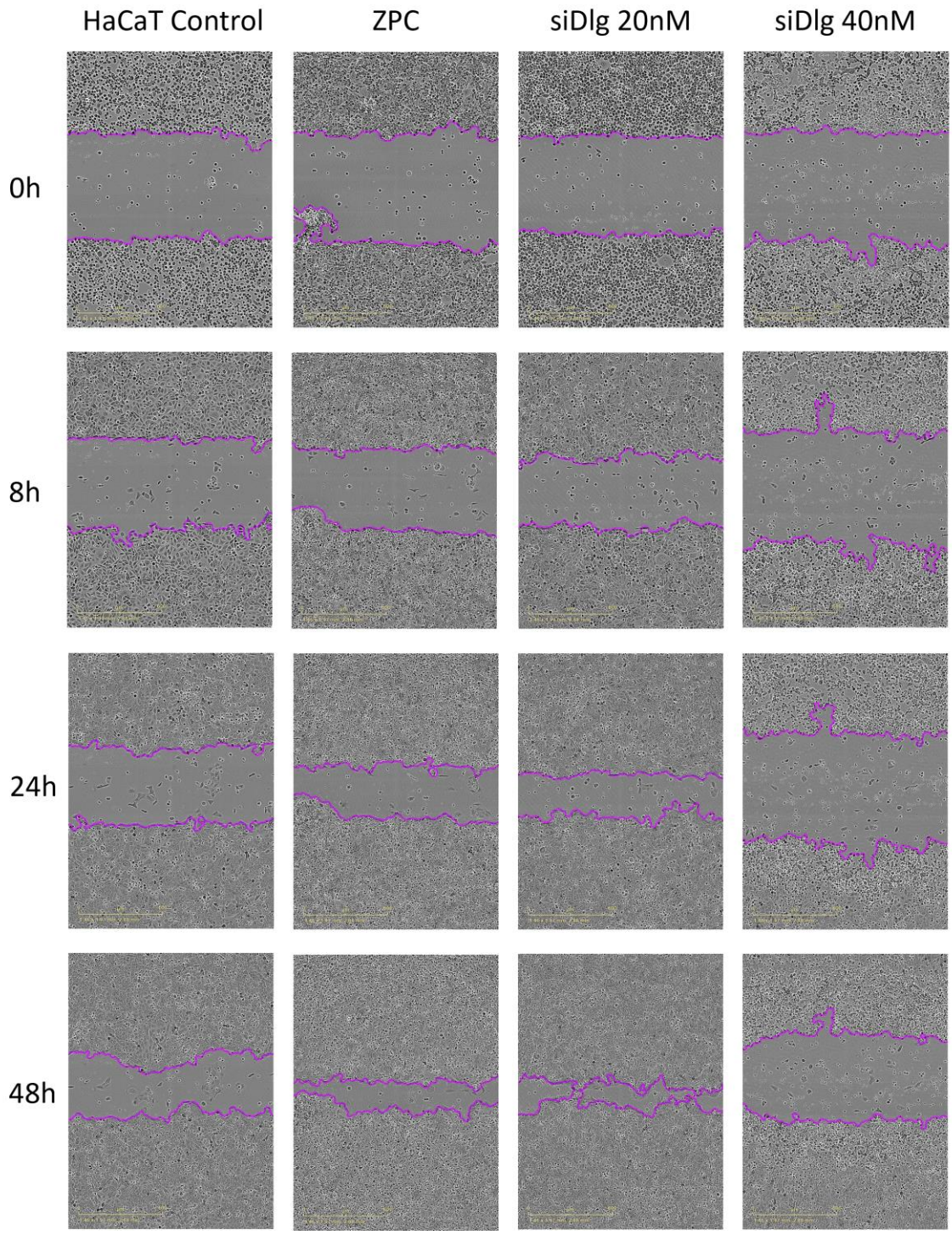

Figure 4.9: Representative images of $4x10^{-1}$µg/ml mitomycin C treated HaCaT cells filling wounds created by an Incucyte WoundMaker at different timepoints. Treatment groups are 100nM ZPC, 20 and 40nM siDlg1. HaCaT Control are treated only with mitomycin C for comparison. ZPC treatment group was made up of three biological replicates with three technical replicates of

each for a total of nine samples. HaCaT Control, 20 and 40nM siDlg groups were made up of six biological replicates made up of three technical replicates each for a total of 18 samples. Timepoints are shown on the left-hand side. Purple line highlights the wound area at each given timepoint as determined by the Incucyte analysis software. Scale bars=600μm.

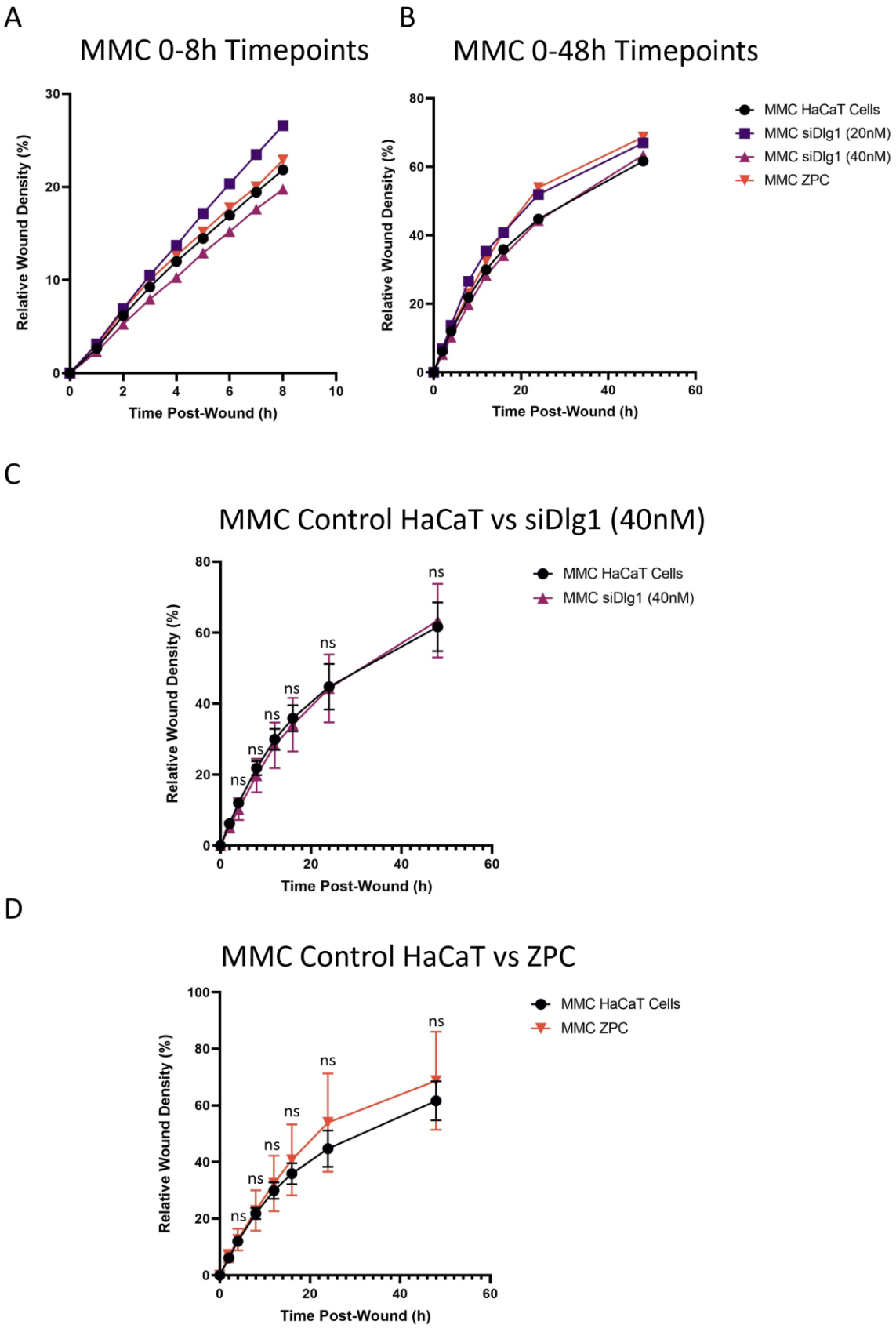

Figure 4.10: Quantification of $4x10^{-1}$µg/ml mitomycin C-treated HaCaT scratch wound assay. (A) RWD% of treatment groups at early timepoints (0-8h) **(B)** RWD% of treatment groups (0-48h). **(C)** RWD% showing no significant difference between Control HaCaT and siDlg1 (40nM). Graph shows mean±s.d. ns=p>0.05. Statistical significance was assessed using a Kruskal-Wallis test

followed by Dunn's post-hoc test. **(D)** RWD% showing ZPC had a higher relative wound density than Control HaCaT. Graph shows mean±s.d. ZPC treatment group was made up of three biological replicates with three technical replicates of each for a total of nine samples. HaCaT Control, 20 and 40nM siDlg groups were made up of six biological replicates made up of three technical replicates each for a total of 18 samples.

4.7 Cx43 and Dlg1 colocalise and are synergistic in live cells

While the results of the previous section indicated that Dlg1 plays an important positive role during the normal wound healing process of keratinocytes, there is little knowledge about the dynamics of Cx43/Dlg1 complex movement and function during wound healing. For instance, it is unknown whether Cx43 is capable of maintaining localisation at the plasma membrane if Dlg1 is not also localised to the same area, or if differences in the complex are observed in the cells of the wound edge compared to cells further away from the wound area. To address these questions, HEK293 cells were transfected with plasmids containing the sequence for fluorescently-tagged Cx43 (mCherry) or Dlg1 (GFP) and a scratch wound assay was performed, followed by live cell imaging of the wound area at intervals of 10 minutes using a Zeiss Axio Observer Z1 microscope **(Figure 4.11A, video files are also available for all figures in this section, attached to thesis)**. HEK293 cells were used in this section due to their improved transfection efficiency compared to HaCaT cells. HEK293 cells were observed to proliferate and migrate into the wound area, with the wound fully closing around the final timepoint of 66h. Transfection efficiency in this experiment was high, with both Cx43-mCherry and Dlg1-GFP being widely expressed (~80%, clearest in figures without brightfield channel) and many cells co-expressing the two proteins together. Removal of the brightfield channel to better visualise Cx43 and Dlg1 revealed extensive colocalisation between the two proteins in co-expressing cells, however no clear differences in Cx43/Dlg1 expression were observed in cells of the wound-edge compared to cells distal from the wound **(Figure 4.11B)**. Further evaluation of Cx43 and Dlg1 localisation through focusing on the right-hand wound edge showed Cx43 puncta, which were observed predominantly at the cell membrane and sites of cell-cell contact **(Figure 4.12A,B)**, with rapid alteration in cellular localisation between timepoints. Cx43 was also observed in the nucleus. In contrast, Dlg1 was shown to be far more diffuse and localised to both the cytoplasm and the cell membrane, with more subtle changes in localisation between timepoints. Importantly, Dlg1 almost invariably colocalised with Cx43 at sites of cell-cell

contact in co-expressing cells, with very little movement of Cx43 alone to these areas. This further emphasises the importance of Dlg1 in controlling gap junctional communication.

An interesting observation during the live cell experiment was that Cx43 and Dlg1 often localised to cell protrusions resembling filopodia/tunnelling nanotubes (TNTs) **(Figure 4.13A, B)**. These structures are actin-rich and play important roles in the processes of cell migration and direct cell-cell communication over larger distances, meaning they are involved in the wound healing process (Mattila and Lappalainen, 2008; Zurzolo, 2021). Cx43 localised to the ends of these protrusions, with Dlg1 also being present in the full-length of the structures **(Figure 4.13A, B)**. Intriguingly, this may suggest that Dlg1 is involved in establishment and/or maintenance of Cx43 in filopodia/tunnelling nanotubes.

Cx43 and Dlg1 were additionally observed during the process of cell division **(Figure 4.14A, B)**. In this example, Cx43 was originally localised mainly to a cellular protrusion at the leading-edge of the cell, while Dlg1 was instead widely distributed throughout the cytoplasm, as well as in the leading-edge protrusion. The cell then migrated forwards towards the direction of the protrusion (and the wound area), while simultaneously the protrusion contracted in the direction of the main cell body, eventually resulting in a rounded cell with Cx43 remaining localised to the leading-edge. A pool of Dlg1 also appeared to localise to the nucleus during this process. As the cell underwent cytokinesis, a pool of Cx43 was observed at the cleavage furrow between the two forming daughter cells. Following conclusion of cell division, the two proteins were redistributed to their original sites. This shows that the localisation of both Cx43 and Dlg1 are altered during the process of cell proliferation.

A

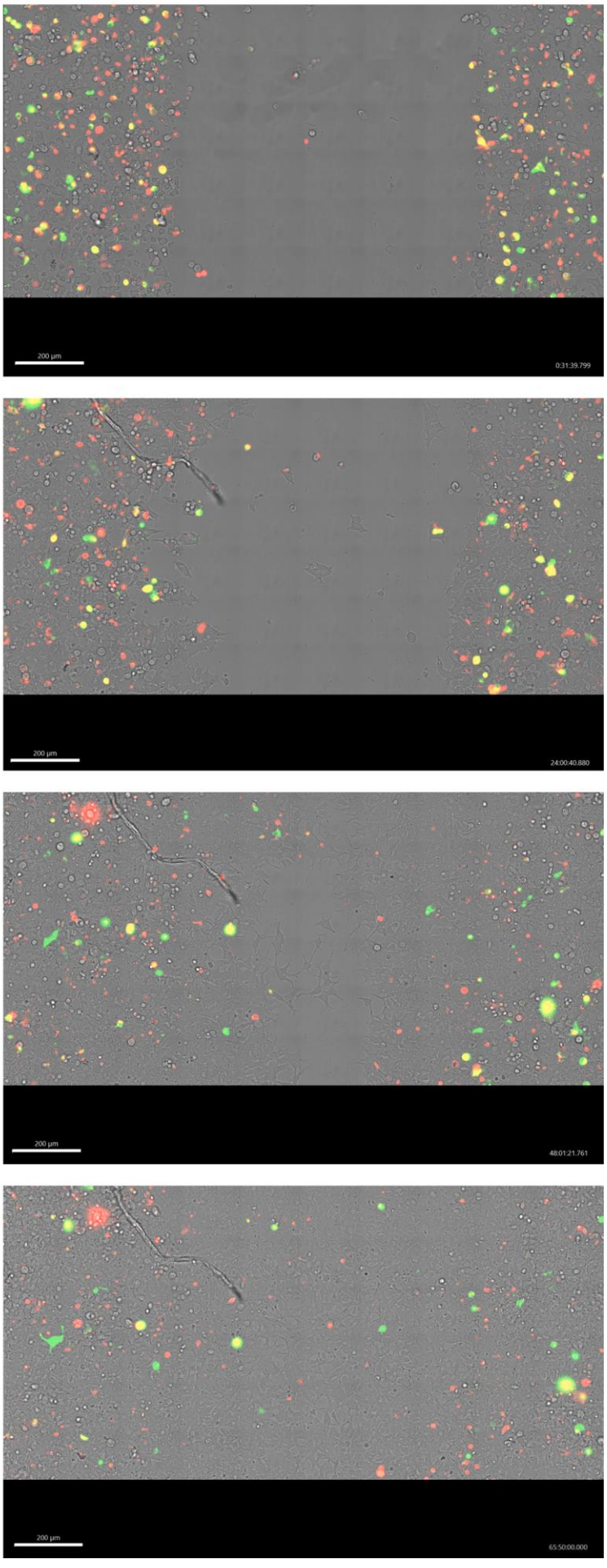
0h
200 µm
0:31:39.799
24h
200 µm
24:00:40.880
48h
200 µm
48:01:21.761
66h
200 µm
65:50:00.000

B

0h

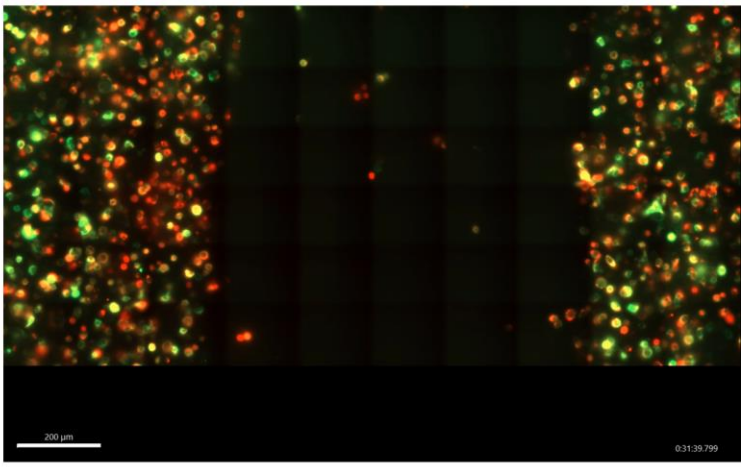

24h

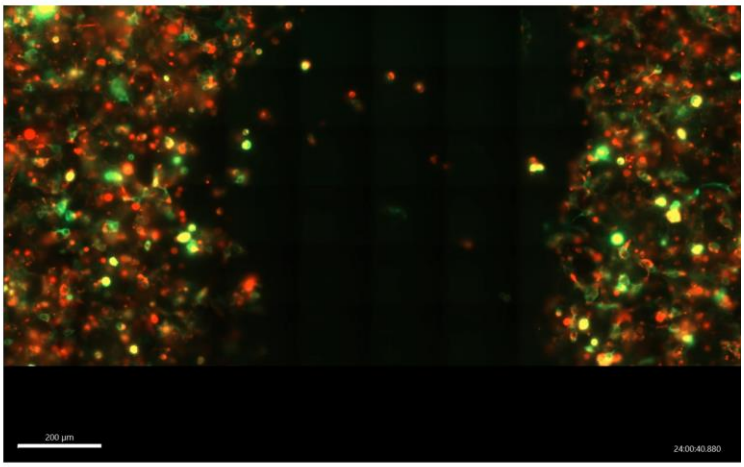

48h

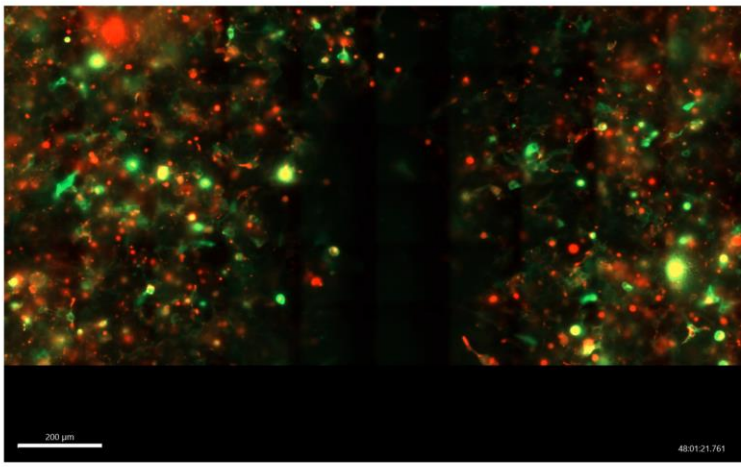

66h

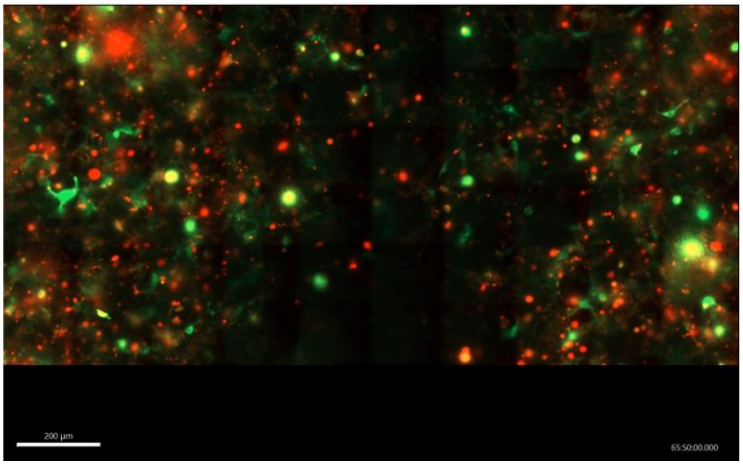

Figure 4.11: **Live cell scratch wound of HEK293 cells transfected with Cx43-mCherry and Dlg1-GFP. (A)** Images showing Cx43-mCherry (red channel), Dlg1-GFP (green channel) and brightfield channel in HEK293 cells over the course of scratch wound healing (0, 24, 48 and final 66h timepoints). Timepoint is shown to the left-hand side of images. Colocalisation was detected between the two proteins in co-transfected cells (yellow signal). Cells were imaged in 10 minute intervals over a period of 66h. Scale bar=200μm. **(B)** Images as shown in **(A)** without brightfield channel to allow better visualisation of Cx43 and Dlg1.

A

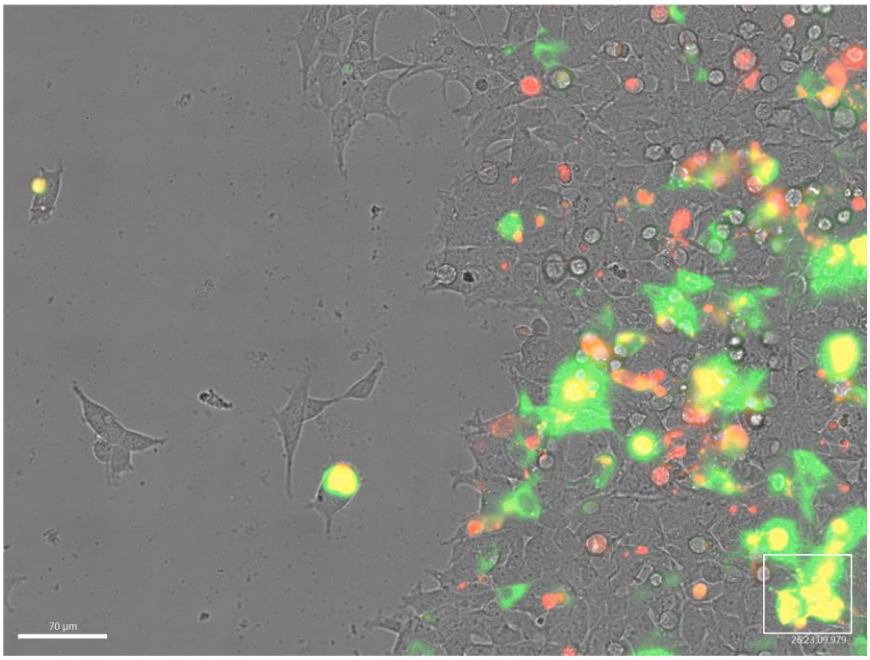

B

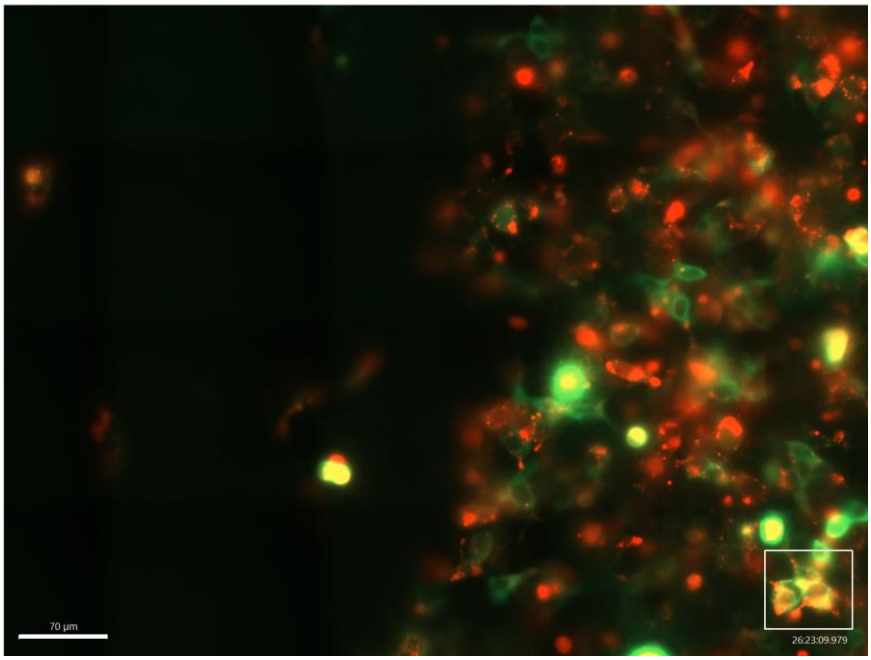

Figure 4.12: Zoomed live cell scratch wound of HEK293 cells transfected with Cx43-mCherry and Dlg1-GFP. (A) Movie showing Cx43-mCherry (red channel), Dlg1-GFP (green channel) and brightfield channel in HEK293 cells over the course of scratch wound healing. Image is zoomed in to allow visualisation of Cx43 and Dlg1 subcellular localisation. Area of extensive colocalisation (yellow signal) is highlighted by a white box in the bottom right-hand corner. Cells were imaged in 10 minute intervals over a period of 66h. Timestamp is shown in the bottom right-hand corner. Scale bar=70µm. **(B)** Image as shown in **(A)** without brightfield channel to allow better visualisation of Cx43 and Dlg1.

A

1

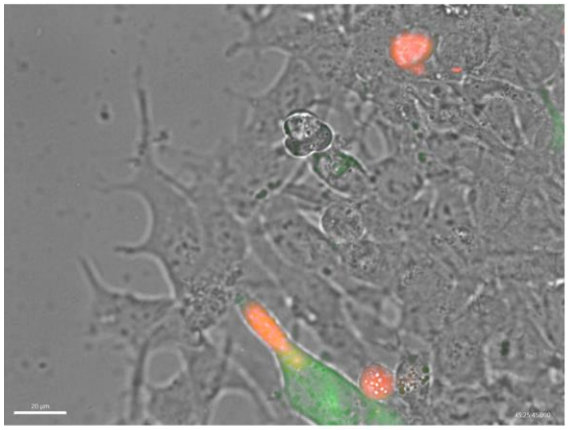

2

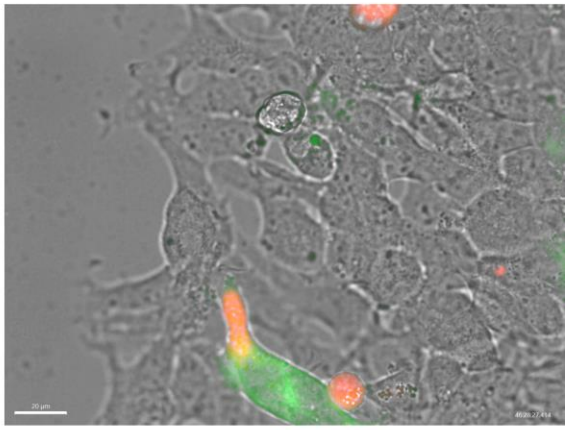

3

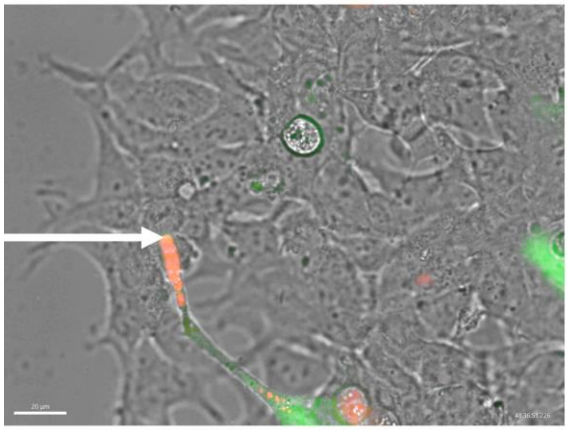

4

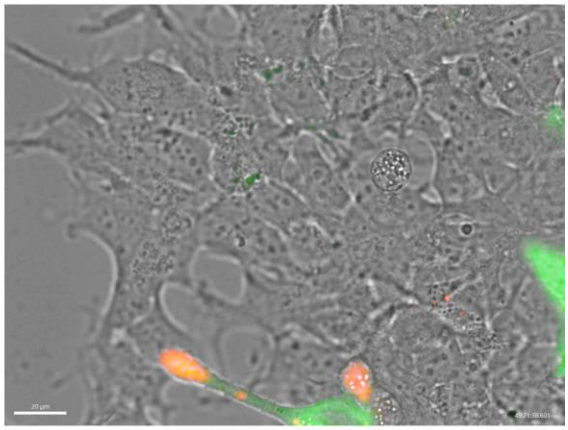

5

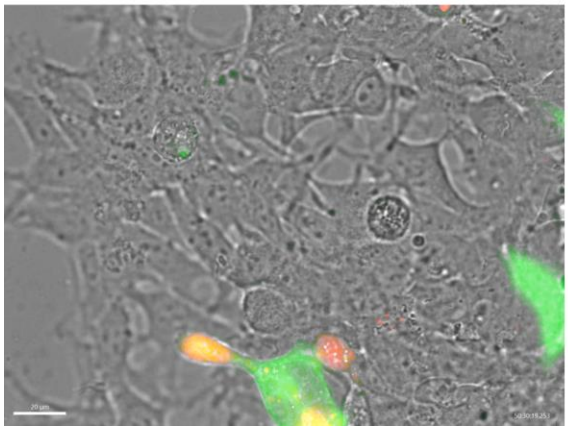

6

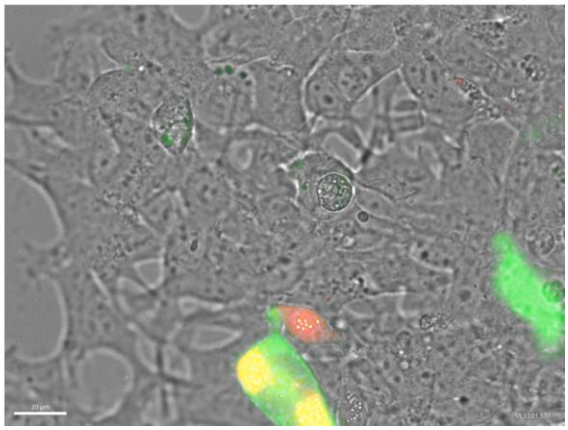

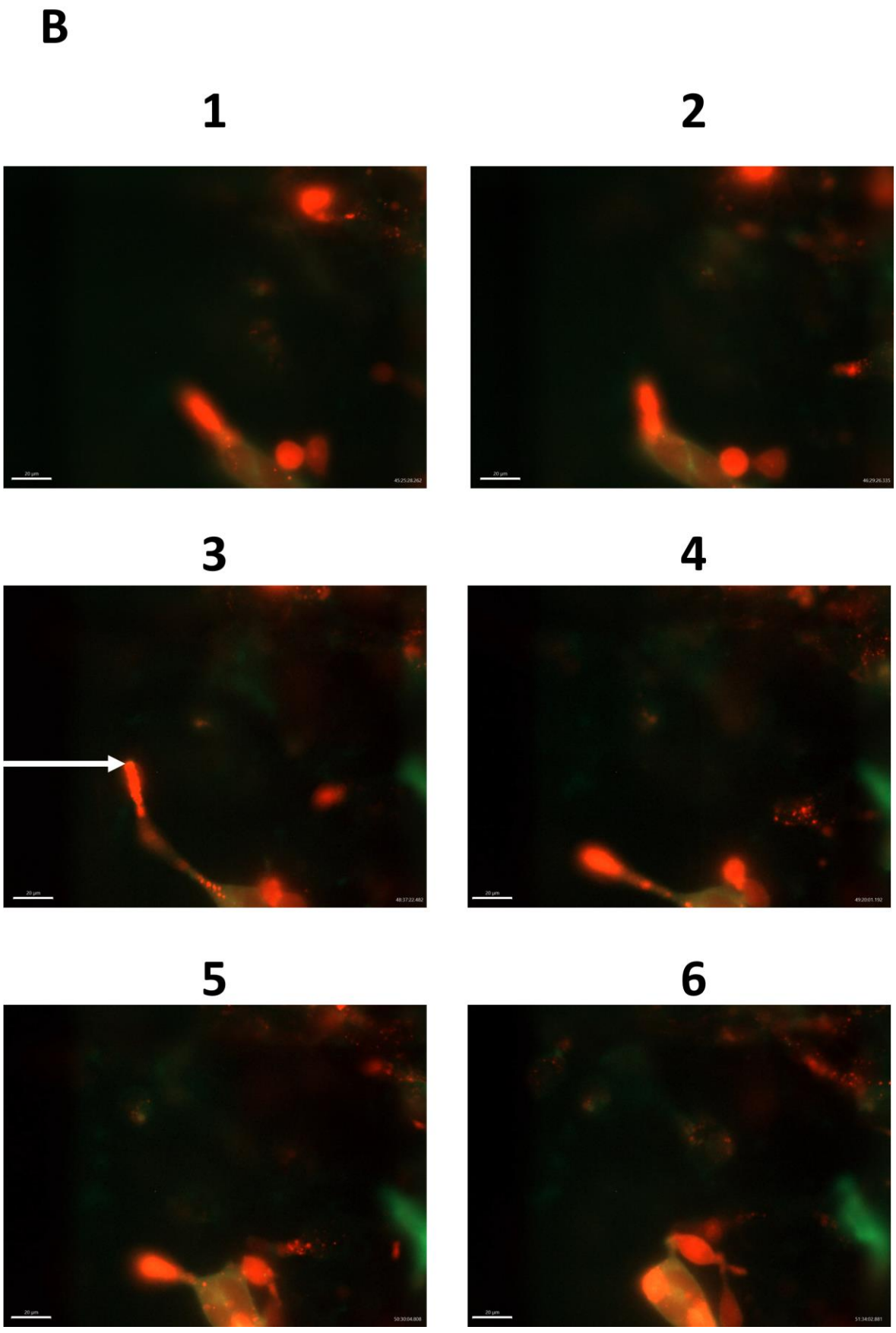

Figure 4.13: Zoomed live cell scratch wound of HEK293 cells transfected with Cx43-mCherry and Dlg1-GFP showing filopodium containing Cx43 and Dlg1. (A) Images showing Cx43-mCherry (red channel), Dlg1-GFP (green channel) and

brightfield channel in HEK293 cells. Numbering of images shows sequence of events. Arrow in panel 3 points to the tip of a potential tunnelling nanotube. Images are zoomed in to allow visualisation of Cx43 and Dlg1 subcellular localisation. Cells were imaged in 10 minute intervals over a period of 66h. Timestamp is shown in the bottom right-hand corner. Scale bar=20µm. **(B)** Images as shown in **(A)** without brightfield channel to allow better visualisation of Cx43 and Dlg1.

A

1

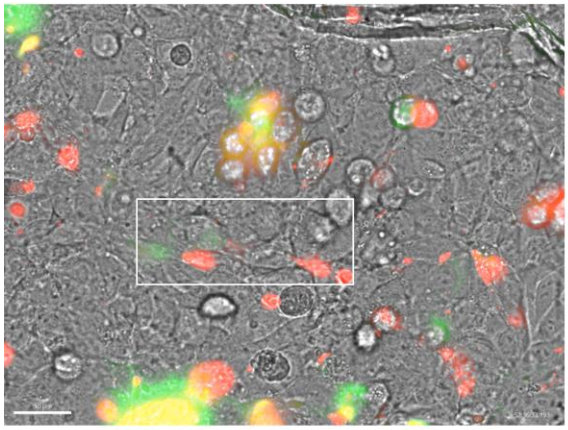

2

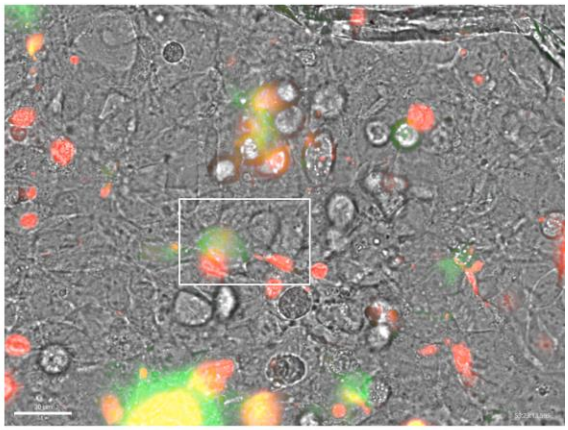

3

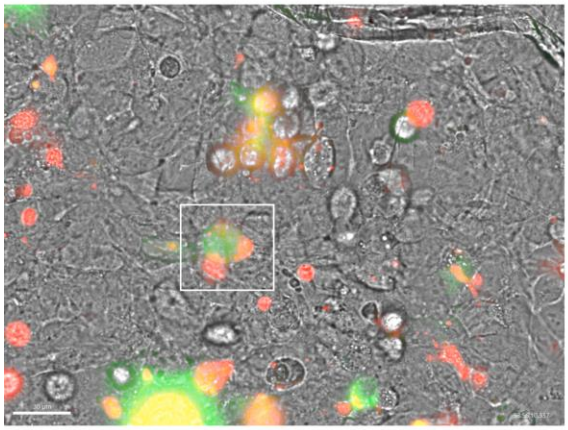

4

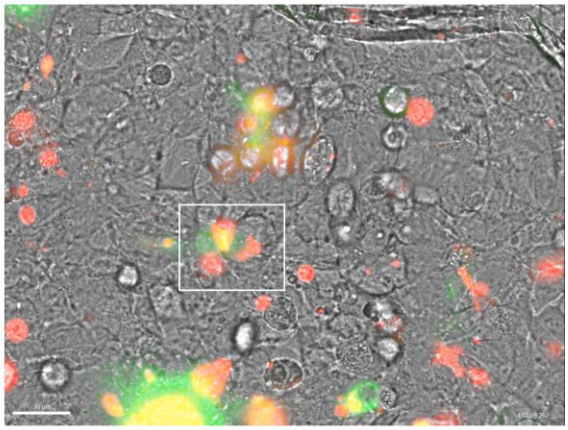

5

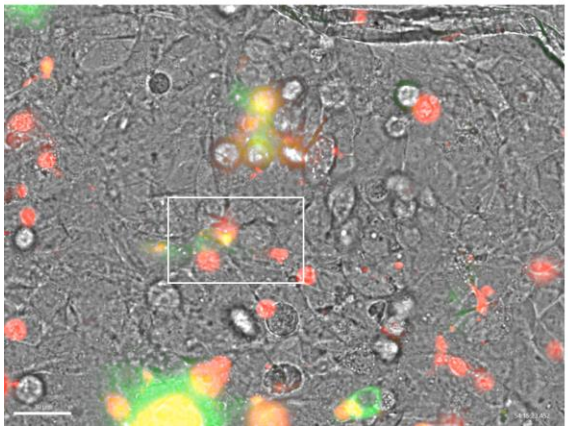

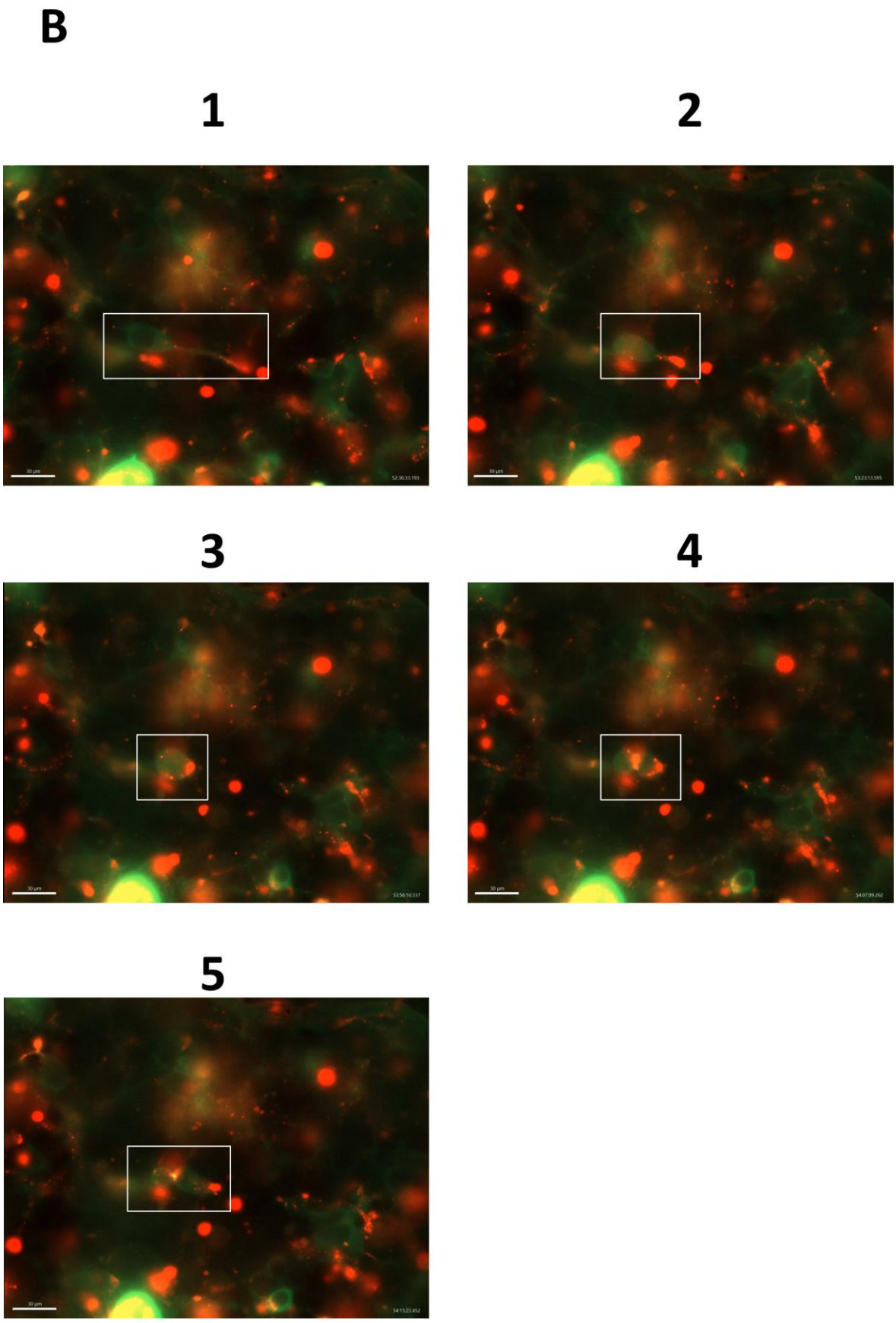

Figure 4.14: Zoomed live cell scratch wound of HEK293 cells transfected with Cx43-mCherry and Dlg1-GFP showing a dividing cell. (A) Images showing Cx43-mCherry (red channel), Dlg1-GFP (green channel) and brightfield channel in HEK293 cells. Numbering of images shows sequence of events. Dividing cell is

indicated by a white box. Images are zoomed in to allow visualisation of Cx43 and Dlg1 subcellular localisation. Cells were imaged in 10 minute intervals over a period of 66h. Timestamp is shown in the bottom right-hand corner. Scale bar=30μm. **(B)** Images as shown in **(A)** without brightfield channel to allow better visualisation of Cx43 and Dlg1.

4.8 Cx43 and Dlg1 interact in keratinocytes/dermal cells/adipocytes in non-diabetic and diabetic skin tissue

Given the importance of Cx43 and Dlg1 in *in vitro* studies, it was important to clarify the localisation of the two proteins in the skin. To address this, formalin-fixed paraffin-embedded (FFPE) samples of non-diabetic human abdominal skin tissue were obtained with ethical permission from three separate patients and stained for the two proteins in immunofluorescence experiments **(Figure 4.15A)**. Cx43 localised mainly to the cell membrane of keratinocytes, with some cytoplasmic and nuclear staining observed. Similarly, Dlg1 was mainly localised at the cell membrane and in the cytoplasm/nucleus. Both proteins were expressed in all layers of the skin (including the cornified layer), with the most pronounced staining in the spinous and granular layers. Colocalisation between the two proteins was clear at the plasma membrane of cells in the lower layers of the epidermis, suggesting the interaction is conserved *in vivo* in human epidermal keratinocytes.

In addition to epidermal keratinocytes, both proteins were detected in dermal cells and adipose tissue **(Figure 4.15A,B)**, with colocalisation between the two proteins observed. This provides evidence that the interaction between Cx43 and Dlg1 takes place in a number of different cell types *in vivo*.

As discussed previously in **Chapter 1**, diabetes is associated with impaired wound healing, where Cx43 is upregulated at the cell membrane of cells at the wound edge (Brandner *et al.*, 2004). To determine whether any changes in the Cx43 and Dlg1 interaction take place in diabetic tissue, FFPE abdominal skin samples from unwounded regions were obtained from three diabetic patients and stained for the two proteins **(Figure 4.16A)**. Levels and localisation of Cx43 and Dlg1 were similar to non-diabetic tissue, with both proteins mainly expressed at the cell membrane with some cytoplasmic staining. While staining in the other layers of the epidermis was consistent with the non-diabetic

samples, less staining of both Cx43 and Dlg1 were observed in the cornified layer of diabetic skin. In addition, one diabetic sample clearly displayed more nuclear Cx43 staining compared to all other samples (diabetic and non-diabetic) **(Figure 4.16A Lower Panel)**. As with the non-diabetic tissue, Cx43 and Dlg1 were additionally observed and colocalised in both dermal cells and adipocytes **(Figure 4.16A,B)**, further emphasising the importance of this interaction in other cell types. Taken together, these data warrant further investigation of the Cx43/Dlg1 interaction during the process of wound healing, particularly in primary keratinocytes isolated from diabetic and non-diabetic biopsies.

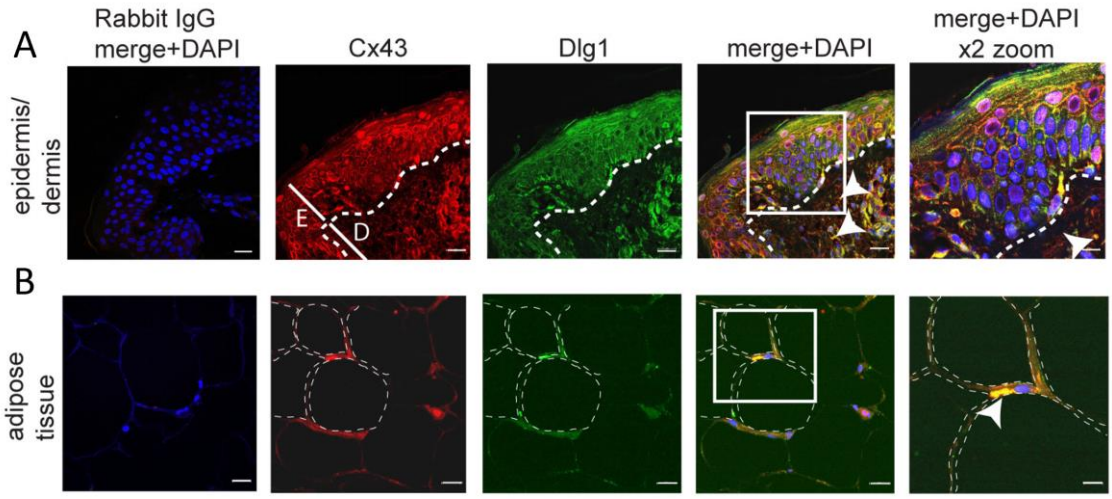

Figure 4.15: Cx43 and Dlg1 coloclalise *in vivo* in human skin tissue. (A) Immunofluorescent staining of Cx43 (red) and Dlg1 (green) in an FFPE skin block. Blue staining denotes cell nuclei. A merge image of rabbit IgG negative control is shown on the left-hand side. White dashed line illustrates the boundary between epidermis, E, and dermis, D. Sites of colocalisation between Cx43 and Dlg1 in the dermis are highlighted with white arrows. Areas enclosed by white boxes are shown enlarged 2x on the right-hand side. Images are representative of three tissue blocks from different patients, with the experiment repeated three times for each. **(B)** Cx43 (red) and Dlg1 (green) colocalise in adipocytes of the same FFPE tissue blocks. Blue staining denotes cell nuclei. Fat deposits outlined with white dotted lines. Obvious site of colocalisation highlighted with white arrow. Scale bars=20μm in regular images and 10μm in zoomed images.

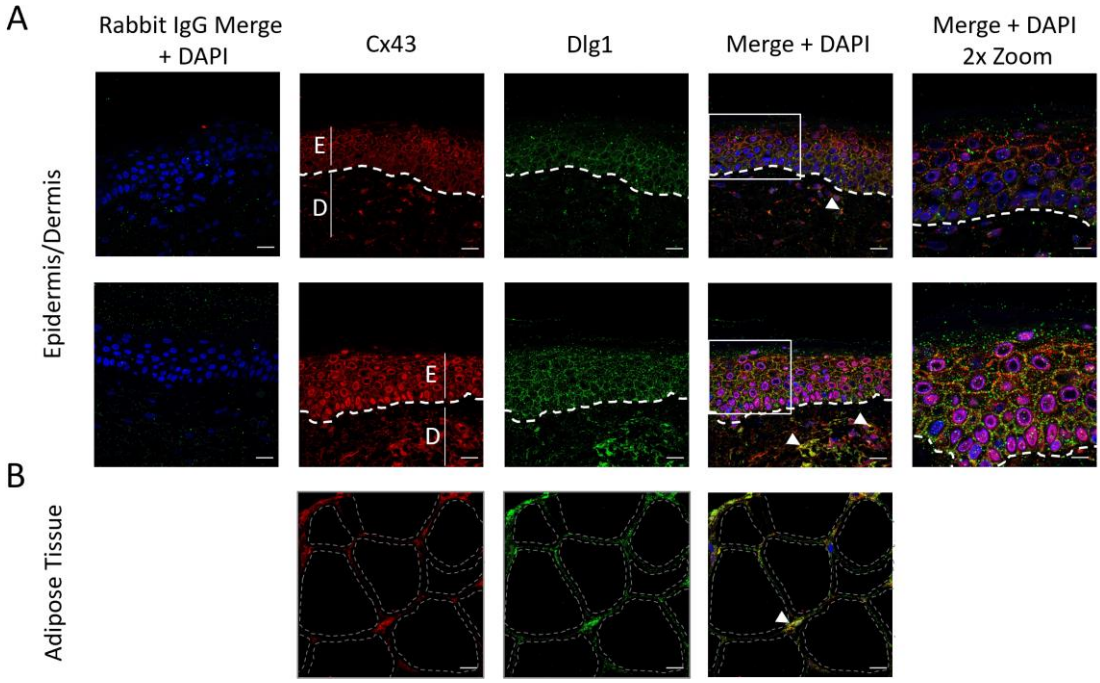

Figure 4.16: Cx43 and Dlg1 coloclalise *in vivo* in human diabetic skin tissue. (A) Immunofluorescent staining of Cx43 (red) and Dlg1 (green) in FFPE skin blocks from two separate diabetic patients. Blue staining denotes cell nuclei. A merge image of rabbit IgG negative control is shown on the left-hand side. White dashed line illustrates the boundary between epidermis, E, and dermis, D. Sites of colocalisation between Cx43 and Dlg1 in the dermis are highlighted with white arrows. Areas enclosed by white boxes are shown enlarged 2x on the right-hand side. Note the increased nuclear staining of Cx43 in the lower of the two samples. Images are representative of three tissue blocks from different patients, with the experiment repeated three times for each. **(B)** Cx43 (red) and Dlg1 (green) colocalise in adipocytes of the same FFPE tissue blocks. Blue staining denotes cell nuclei. Fat deposits outlined with grey dotted lines. Obvious site of colocalisation highlighted with white arrow. Scale bars=20μm in non-zoom images and 10μm in zoomed images.

4.9 Discussion

The skin serves a fundamental role in protecting the body from the external environment. Within the epidermis, Cx43 performs a vital function by forming direct intercellular contacts to permit the sharing of ions, metabolites, secondary messengers and microRNAs between adjacent cells. By comparison Dlg1 remains vastly understudied in the skin. Therefore, one of the main aims of this investigation was to clarify the effect of Dlg1 knockdown in wound healing studies (including roles in cell migration versus cell proliferation), as well as establish whether the Cx43/Dlg1 interaction is conserved in human skin.

Firstly, to address whether Dlg1 played any significant role in the wound healing process, scratch wound assays using HaCaT cells were performed. The results of this provided evidence that Dlg1 functions as a positive component of the natural wound healing process and therefore depletion of Dlg1 via siRNA inhibits wound healing. A cumulative inhibitory effect was observed when treating with 20nM and 40nM siDlg1, with the 40nM treatment group being significantly impaired in wound healing compared to control samples. This infers that HaCaT cells can compensate for loss of a certain level of Dlg1 protein (perhaps through related polarity proteins such as Scribble), but at higher concentrations this becomes inhibitory. In contrast to this, ZPC, which is a stable analogue of the GAP27 mimetic peptide, improved wound healing relative to control cells as previously reported in primary human keratinocytes (Faniku, 2018).

Through experiments on unwounded HaCaT cells, it was revealed that both 20nM and 40nM siDlg1 treatment significantly inhibited cell proliferation, which may have been responsible for the reduced wound healing rates of siDlg1-treated cells. Indeed, MMC treatment to remove the contribution of cell proliferation to wound healing resulted in abolition of the significant difference between control HaCaT and 40nM siDlg1-treated cells observed in the previous scratch wound assay. The inclusion of ZPC as a positive control was key for this experiment, as GAP27 increases cell migration to improve wound healing rates (Faniku *et al.*,

2018), meaning there should be a roughly equal difference between control HaCaT and ZPC treated groups regardless of MMC treatment. This was indeed the case in this study, although this effect was not found to be significant, which is likely due to reduced sample numbers of ZPC-treated cells compared to the other groups. A higher concentration of ZPC may also have further improved wound healing rates, as other experiments utilising different concentrations of ZPC (100nM and 100μM) found that both concentrations increased wound healing rates compared to mock-treated cells, with a dose-response effect being observed (Martin, unpublished data).

The effect of 40nM siDlg1 treatment in non-MMC groups was significant for the timepoints representing the middle stages of healing (4h-24h), with the maximum effect at 24h post-wounding (48h post-siRNA treatment in this experiment). The early timepoints being unaffected by siDlg1 treatment agrees with existing literature, which proposes that cell migration, not cell proliferation, is the major driver of reepithelialisation during the time immediately following wounding (Falanga, 2005), a process which seemed unaffected by Dlg1 knockdown. The slight convergence of the treatment groups at the 48h timepoint of the experiment may reflect either the final stages of wounding being less reliant on the presence of Dlg1 protein or, more likely, the loss of the transient effect caused by ZPC and siRNA in the treatment groups.

The results of the scratch wound assay in this investigation differ slightly from a previous study on Dlg1 in wound healing, where depletion of Dlg1 via siRNA resulted in a 20% decrease in wound healing due to inhibition of cell migration (O'Neill *et al.*, 2011). However, several key differences exist between the methodologies employed in the two studies. Firstly, the cell line used by O'Neill and colleagues was H1703 cells, a squamous lung cancer cell line. Dlg1 is multifaceted in cancer progression, being a suspected tumour suppressor which is targeted by several oncogenic viruses (Sun *et al.*, 2015; Suzuki *et al.*, 1999), while also promoting cancer in other scenarios (Frese *et al.*, 2006). This virtually precludes the comparison of the two investigations, as Dlg1 is likely to play different roles in the cell depending on cancer status (+ve or -ve) as well as

cancer type. Other distinctions include the use of MMC in all experiments, which means any effect of siDlg1 on cell proliferation is obscured, as well as the different timescales used in the experiments (scratch wound made 72h after siRNA transfection as opposed to 24h after in this study). While the data presented in this study do not suggest a significant role for Dlg1 in cell migration during wound healing, it would be useful to quantify migration rates and directionality of individual untreated and siDlg1-treated cells in future experiments to confirm the absence of an effect, for example through live cell tracking experiments.

The inhibition of wound healing following siDlg1 treatment was surprising given the status of Dlg1 as a suspected tumour suppressor in untransformed cells, which would infer depletion of Dlg1 would increase proliferative capacity of cells and promote wound closure. This result is even more puzzling given that knockdown of Dlg1 removes a portion of Cx43 from the plasma membrane, thereby preventing hemichannels and gap junctions which are widely accepted to restrict cell migration in several animal models and clinical trials (Ghatnekar *et al.*, 2009, 2015; Kretz *et al.*, 2003). This leads to the conclusion that removal of Dlg1 must affect other pathways to such an extent that it outweighs any positive benefit conferred by partial depletion of Cx43 on the plasma membrane. Results from **Chapter 3** showed no apparent effect of Dlg1 depletion on formation of either tight or adherens junctions. Therefore, these data suggest that the decrease in proliferation in this experiment is caused by partial loss of an important function during cell division or knock-on effects of loss of Dlg1 as a scaffolding and signal transduction protein. For example, knockdown of Dlg1 would prevent its interaction with SGEF (RhoG-specific guanine nucleotide exchange factor), with this complex normally functioning to enhance RhoG activity and thereby promote cell proliferation and migration (Krishna Subbaiah *et al.*, 2012). Dlg1 is also recruited to the midbody between daughter cells during cell division and loss of Dlg1 in these circumstances can result in arrest during cytokinesis, which may partially explain the anti-proliferative effect of siDlg1-treatment (Unno, Hanada and Chishti, 2008).

Overall, the data presented here do not suggest Dlg1 as an attractive therapeutic target in terms of improving wound healing rates, which is likely attributable to its many different interactions with other proteins as a critical cell polarity and scaffolding protein. This however does not eliminate the potential benefit of targeting the Cx43/Dlg1 interaction using small molecule inhibitors. Such inhibitors would require careful design in order to specifically target the interaction of Cx43 and Dlg1, which would allow Dlg1 to maintain its other roles while reducing Cx43 at the plasma membrane, theoretically improving wound healing rates in conditions such as diabetic foot ulcers.

To further investigate the dynamics of Cx43 and Dlg1 during the wound-healing process, the proteins were also visualised in a live-cell scratch wound experiment. Throughout the process of wound healing, Cx43 was mainly localised to the leading-edge of cells, where it was consistently accompanied by Dlg1. This is consistent with the involvement of Cx43 in correct establishment of a leading-edge in migrating cells, with knockdown resulting in disorganised cell movement (Matsuuchi and Naus, 2013). Some Cx43 was also observed in the nucleus. As Cx43 was produced with an mCherry tag on the C-terminus, the previously discussed six N-terminally truncated internally-translated isoforms of Cx43 were likely detected in this experiment in addition to full-length Cx43. This means the nuclear Cx43 signal could be due to GJA1-11k, which has previously been shown to localise to the nucleus and inhibit cell proliferation by stalling G_0/G_1 progression in HEK293FT cells (Epifantseva *et al.*, 2020). Importantly, there was no clear difference in Cx43 and Dlg1 expression or localisation in cells of the wound-edge compared to cells distal to the wound. Given the extensive data on the downregulation of Cx43 at cells of the wound edge (Mori *et al.*, 2006; Brandner *et al.*, 2004), this is likely to be an artefact of overexpression of the two proteins in these cells.

Observation of Cx43 and Dlg1 during cell division revealed that both proteins changed in localisation over the course of this process. Cellular protrusions containing both Cx43 and Dlg1 retracted, with a pool of Dlg1 relocating to the nucleus, which is in agreement with previous studies (Massimi *et al.*, 2008). Cx43 was also apparent between the two newly-formed daughter cells, which is

suggested to occur through a mechanism whereby gap junctions are internalised during mitosis as connexosomes and are rapidly recycled to the cell membrane following cell division (Vanderpuye, Bell and Murray, 2016).

Both Cx43 and Dlg1 were localised to cellular protrusions in the live cell experiment, which may represent filopodia or tunnelling nanotubes. Cx43 is understood to participate in long-range gap junctional communication via TNTs (Okafo, Prevedel and Eugenin, 2017) and is present in filopodia, likely due to its association with actin (Ambrosi *et al.*, 2016; Ochalski *et al.*, 1995). Further to this, the Cx43 C-terminus has been shown to promote filopodia formation through a channel-independent mechanism (Kameritsch *et al.*, 2015). Dlg1 plays a role in actin polymerisation (Round *et al.*, 2005) and is associated with filopodia (Sharma *et al.*, 2006; Iizuka-Kogo, Shimomura and Senda, 2005) and lamellipodia (Xavier *et al.*, 2004). While Dlg1 has not previously been identified in TNTs, due to its association with other actin-based cellular protrusions it is likely Dlg1 is also present in these structures. These results intriguingly suggest that Dlg1 may regulate Cx43 signalling in cellular protrusions in addition to conventional gap junction signalling, with these playing an important role during the process of wound healing. It would be interesting to investigate this further and observe whether depletion of Dlg1 results in changes to these structures.

To address issues of standardisation between scratch wound assays, a 3D-printed wound mask was designed and evaluated. In general, the mask reduced overall variation in wounds, though in most cases this was not a significant difference. Benefits of the wound mask include its ease of use, accessibility of necessary equipment, low cost of consumables and the opportunity for standardisation between labs through sharing of the mask blueprint. Several attempts have previously been made by different research groups and commercial companies to mitigate problems associated with scratch wound assays. For example, Sartorius has developed a wound making tool (which was used in this study), consisting of a metal board with pins for use with a 96-well plate (‘Incucyte ® 96-Well Scratch Wound Cell Migration and Invasion Assays User Manual Contents’, Accessed 29.7.23). The board is positioned so that the 96 pins are above the wells of the

plate and a button is pressed in order to move the pins across the plate, generating a cell-free area. This resolves many of the issues associated with conventional scratch wound assays, such as the angle of wound creation and force applied through the wound instrument, as well as removing a lot of human biases through use of software to automatically quantify wound areas. However, while this results in more standardised wounds across the plate, there is a high cost associated with the wounder and the pins can degrade from use over time, limiting its applicability in an assay where low cost is one of the most attractive features. Other cell removal techniques employ the use of lasers (Tamada *et al.*, 2007) and magnets (Fenu *et al.*, 2019) to generate wounds. In particular, the magnet-based approach is attractive as it resulted in less variation than the wound mask used in this study and would only be slightly more expensive to produce, with less equipment needed for the initial setup. Whichever method is used, the importance of a low-cost, easy-use tool for standardisation across labs remains vital to ensure valid comparisons between scratch wound data.

Finally, immunofluorescent staining of formalin-fixed paraffin-embedded human abdominal skin tissue blocks revealed that Cx43 and Dlg1 localise mainly to the plasma membrane of cells in the epidermis of human skin. Both proteins were observed in all layers of the epidermis, with the highest proportion of staining being in the spinous and granular layers. This is partially in agreement with other studies on Cx43, where expression has been reported to be highest in the spinous layer with some granular and basal layer expression, while being entirely absent from the cornified layer (Salomon *et al.*, 1994; Guo *et al.*, 1992). The localisation of Dlg1 at the plasma membrane of cells in this study mirrors the findings of Laprise and colleagues in human intestinal cells, where Dlg1 was located at the plasma membrane and played a critical role in adherens junctions formation (Laprise *et al.*, 2004). Dlg1 expression in the various sublayers of the normal human epidermis has not been studied previously, however as a key polarity protein it is widely expressed and thus would be expected to be present in most sublayers of the epidermis.

In this study, as with previous studies on the interaction between Cx43 and Dlg1 (MacDonald *et al.*, 2012; Sun *et al.*, 2015), a high degree of colocalisation was observed between the two proteins. This strongly suggests that the proteins interact *in vivo* in human skin, as has been found previously at the cell membrane in cervical mucosal epithelial tissue (Sun *et al.*, 2015). It is crucial for future studies to further confirm this finding through a more robust experimental technique, ideally a proximity ligation assay (PLA) or co-immunoprecipitation experiment following separation of the dermis from epidermis in fresh skin tissue samples. Due to the colocalisation in these samples, it is proposed that the Cx43/Dlg1 interaction serves a similar purpose in healthy primary human keratinocytes as in HaCaT epithelial cells, where Dlg1 controls plasma membrane localisation of Cx43 and gap junctional communication **(Chapter 3)**.

In addition to the plasma membrane staining, Cx43 and Dlg1 were also found in the cytoplasm and the nucleus. The expression pattern of Dlg1 is known to vary depending on stage of the cell cycle, being localised to the nucleus in the G_1 and M phases (Narayan, Massimi and Banks, 2009). The apparent nuclear staining of Cx43 was also interesting, as this may denote GJA1-11k, a truncated form of the Cx43 C-terminus produced through alternative translation. Though expression in the skin has not yet been confirmed, as the Rivedal antibody used in this experiment targets the C-terminal end of Cx43 (amino acids 363-381) (Rivedal *et al.*, 1996), the six alternatively translated isoforms of Cx43 (including GJA1-11k) are likely to be detected in addition to full-length Cx43. Studies to confirm the expression of GJA-11k, for example through mass spectrometry, could prove beneficial and lead to characterisation of this isoform and its role in the skin.

Expression and colocalisation of Cx43 and Dlg1 in this investigation was not limited to keratinocytes, as both proteins were also detected and colocalised in dermal cells and adipocytes. In accordance with previous findings, less Cx43 was found in the dermis compared to the epidermis (Salomon *et al.*, 1994; Guo *et al.*, 1992), which was also true of Dlg1. While the staining of Cx43 in the dermis did not display the clear punctate staining typical of gap junctions (as are seen

in keratinocytes), cultured human dermal fibroblasts have shown distinctive punctate staining at the cell membrane and communicate via gap junctions (Wright *et al.*, 2009). It may be that due to the lower abundance of gap junctions compared to keratinocytes and the effects of the sectioning process, punctate staining was difficult to observe, as has been reported previously (Guo *et al.*, 1992; Ko *et al.*, 2000). The communication of dermal fibroblasts via gap junctions, coupled with the observed colocalisation between Cx43 and Dlg1 may point to a conserved role for the Cx43/Dlg1 complex in epidermal and dermal cells, where Dlg1 is crucial in maintaining plasma membrane localisation of Cx43. It is important to note that the Cx43/Dlg1 interaction may also be involved in other noncanonical roles of Cx43 cell signalling, such as tunnelling nanotubes and extracellular vesicles (Ribeiro-Rodrigues *et al.*, 2017), which dermal cells may utilise more extensively than tightly-packed epidermal keratinocytes. In adipocytes, Cx43 and Dlg1 had a similar expression pattern to epidermal cells, with both being expressed at the cell membrane. Cx43 is known to be the major connexin in adipocytes and contributes to adipose tissue inflammation, which is a driver of insulin resistance (Ron *et al.*, 2022). While Dlg1 protein expression or localisation have not previously been studied in adipocytes, the findings of this investigation are supported by RNA sequencing data which suggests Dlg1 mRNA is present in these cells (Genotype-Tissue Expression (GTEx) Common Fund Project, Accessed 29.7.23). Further studies on the role of Cx43 and Dlg1 (separately and as a complex) in both dermal cells and adipocytes would prove useful in building a picture of the function and importance of the Cx43/Dlg1 interaction in the skin as a whole.

An important component of this investigation was the comparison of Cx43 and Dlg1 in non-diabetic and diabetic skin tissue. Diabetes as a condition has widespread effects which impact the affected individual on both an organismal and cellular level. This includes impaired wound healing, which frequently leads to the development of diabetic foot ulcers (DFUs) which are associated with high costs to the healthcare system and increased mortality (Becker *et al.*, 2012). Several studies have previously addressed Cx43 in DFUs, where it is found to be upregulated at cells of the wound edge and impair the proper progression of healing (Brandner *et al.*, 2004; Sutcliffe *et al.*, 2015). In this study, little

difference was observed between diabetic and non-diabetic skin tissue in terms of Cx43 and Dlg1 staining. This difference between the two studies is likely due to the tissue in this investigation being uninvolved in wounding, whereas Brandner and colleagues studied wound-edge tissue. Similarly, no apparent differences between staining in dermal cells and adipocytes were noted between non-diabetic and diabetic samples. As with the non-diabetic skin, Cx43 and Dlg1 were expressed and colocalised in all layers of the epidermis, with the exception being that no staining was observed in the cornified layer of the diabetic samples. This difference is likely not the result of actual Cx43/Dlg1 staining but instead either due to tissue autofluorescence (as has been noted for the cornified layer previously) (Coutinho *et al.*, 2003) or potential detachment and loss of the cornified layer at some point during the staining process.

An interesting finding was that some Cx43 localised to the nucleus of both non-diabetic and diabetic cells, but that a large increase in nuclear staining was observed in one of the three diabetic skin samples. While this could be an artefact caused by nonspecific staining of the epidermis, this staining could also represent GJA1-11k. This could suggest an upregulation of GJA1-11k in keratinocytes of some diabetic patients, which could feasibly contribute to impairment of the wound healing process through inhibition of cell cycle progression. Strong nuclear Cx43 staining has been reported in some types of cancer and is associated with poor prognosis (Aasen *et al.*, 2019b), meaning nuclear Cx43 may be a marker of disrupted tissue homeostasis. A quantitative analysis including more skin samples for each group is required to confirm whether there is increased expression of GJA1-11k in diabetic samples and the effect this may have on wound healing.

As this study used tissue from unwounded areas, it would be worthwhile to conduct a similar study with skin tissue proximal to wound areas/DFUs. While there was no obvious difference in Cx43 and Dlg1 colocalisation in this study, performing a PLA on these samples would have the added benefit of allowing quantification of the number of interactions between Cx43 and Dlg1 per cell in the epidermis/dermis, a metric that could give important insight into potential differences between diabetic and non-diabetic tissues. PLA, as well as scratch

wound assays utilising primary human keratinocytes derived from fresh skin samples were originally planned to be carried out as part of this study, however delays in the shipping of PLA products, as well as COVID-related delays in the acquisition of skin tissue meant this was not feasible within the timeframe of the PhD. It is therefore advised that these experiments are carried out as part of future studies to determine if Dlg1 performs a similar role during wound healing in primary keratinocytes and to compare the Cx43/Dlg1 interaction in diabetic and non-diabetic tissue.

Chapter 5: The Interaction of Cx43 and Dlg1

5.1 Introduction

5.1.1 Protein Structure of the Cx43 C-terminus and Dlg1

As described previously, the ~150 amino acid long cytoplasmic C-terminal tail of Cx43 (~aa232-382, predicted by analysis of rat Cx43 sequence) allows interaction with many different proteins and pathways (see **Chapter 1, Section 1.7** for examples) (Leithe *et al.*, 2018; Yeager and Gilula, 1992). Through nuclear magnetic resonance (NMR) spectroscopy, the C-terminus of Cx43 has previously been reported to be largely unstructured, with two potential α-helices forming between aa315-326 and aa340-348 (Sorgen *et al.*, 2004). The disorder in this region is consistent with Cx43 being highly adaptable to facilitate interactions with a diverse range of proteins (Aasen *et al.*, 2018). In this way, the Cx43 C-terminus conformation may be rapidly altered on binding to proteins or through post-translational modifications such as phosphorylation **(Figure 5.1)**, permitting alterations in function due to changes in the cellular environment. For example, interaction of the c-Src protein with the SH3-binding domain of Cx43 induces conformational changes which inhibit the interaction of ZO-1 PDZ2 domain with the extreme end of the Cx43 C-terminus (Sorgen *et al.*, 2004).

While the crystal structure for Dlg1 as a full protein is yet to be solved, several individual Dlg1 domains have been successfully crystallised, including the PDZ2 domain (Von Ossowski *et al.*, 2006) and the GUK domain (aa732-926) (Mori *et al.*, 2013), as well as the SH3/HOOK/GUK domains together (Zhu *et al.*, 2012). These domains are known to be generally well-conserved between members of the MAGUK family (Te Velthuis *et al.*, 2007). Other experimental approaches have also yielded important information on the relative positions of Dlg1 domains within the protein as a whole. For example, an investigation into Dlg1

and other MAGUK proteins utilising fluorescent resonance energy transfer (FRET) indicated that supertertiary structure is similar between MAGUK family members and the domains are partitioned into two main units based on relative proximity **(Figure 5.2)** (McCann *et al.*, 2012). Sequential PDZ domains in **Figure 5.2** are labelled as 1, 2 and 3. As with Cx43, Dlg1 interactions are regulated by post-translational modifications and conformational changes arising from binding to other interaction partners (Roberts, Delury and Marsh, 2012). Indeed, phosphorylation of Dlg1 residues S158 and S442 by cyclin dependent kinases (CDKs) 1 and 2 has been shown to regulate Dlg1 localisation and function during different stages of the cell cycle (Narayan *et al.*, 2009). Additionally, the ability of Dlg1 to interact with other proteins is further regulated through intramolecular interactions (Qian and Prehoda, 2006). An example of this is the association of the SH3 domain with the GUK domain, which is mediated by the HOOK region and blocks the canonical SH3-binding pocket of MAGUKs. Interaction of specific protein partners with HOOK alters the conformation of the protein and removes this blockage, which is thought to subsequently allow interaction of other partners with the SH3 domain in order to facilitate larger complex formation (Zhu *et al.*, 2012).

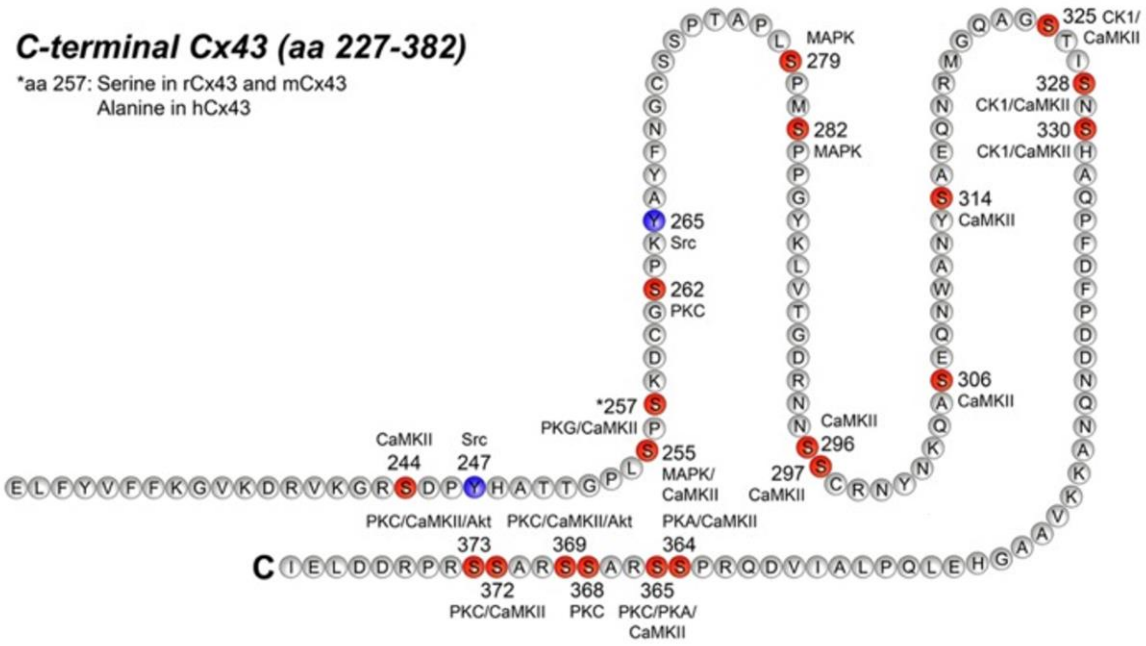

Figure 5.1: Phosphorylation sites of the Cx43 C-terminal tail. Individual residues of the Cx43 C-terminal tail (aa227-382) are denoted by circles containing a single letter amino acid abbreviation. Phosphorylation sites are highlighted by numbering of specific residues and proteins promoting phosphorylation at these sites are shown. CaMKII= calcium/calmodulin-dependent kinase II, Src=Src kinase, PKG=protein kinase G, PKC=protein kinase C, MAPK=MAP kinase, CK1=casein kinase 1, PKA=protein kinase A, Akt=Akt kinase. Adapted from Axelsen *et al.*, 2013.

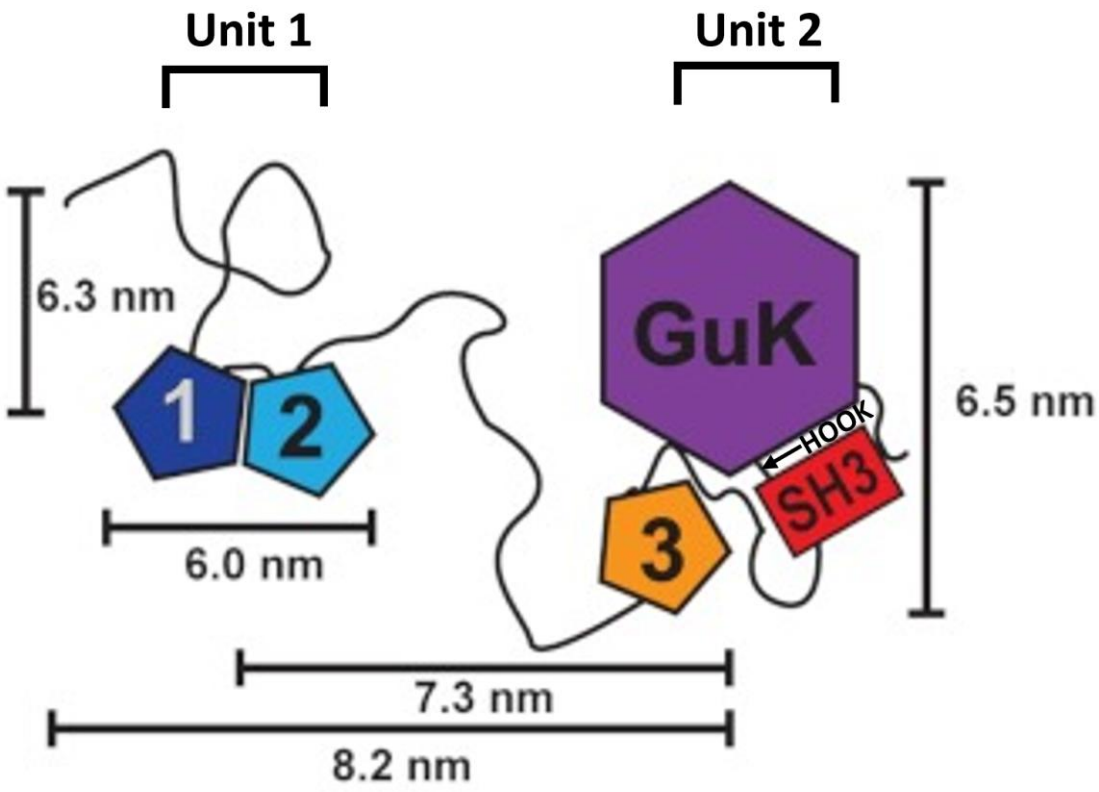

Figure 5.2: Cartoon depiction of the supertertiary structure of a MAGUK protein, PSD-95, as determined by FRET. 1, 2 and 3 represent the PDZ domains of PSD-95. SH3=SH3 domain, GUK=guanylate kinase domain. The HOOK domain is located between the SH3 and GUK domains and is indicated with an arrow. Lines with bars represent measured distances between domains. PDZ domains 1 and 2 cluster together to one side of the protein, while PDZ3, SH3, HOOK and GUK domains cluster to the other side. Adapted from McCann *et al.*, 2012.

5.1.2 The Interaction Interface of Cx32 and Dlg1

In addition to Cx43, Dlg1 is known to interact with the C-terminus of at least one other connexin protein, Cx32 (Duffy *et al.*, 2007; Stauch, Kieken and Sorgen, 2012). As with Cx43, the Cx32 C-terminal tail is largely unstructured, however some residues are able to form α-helices under certain conditions. These residues include the shared binding site for Calmodulin and Dlg1, with Calmodulin being shown to induce α-helical structure in the Cx32 C-terminus upon binding. While this change in structure was not detected in Cx32 on binding to Dlg1, the authors concluded that induction of a smaller α-helix would be difficult to detect and therefore it is possible that this change is also initiated on binding to Dlg1. The region of Dlg1 which interacts with the Cx32 C-terminus was originally shown to be within the SH3/HOOK/partial GUK (pGUK) domains, with further investigation demonstrating that the GUK domain is the minimum region required for interaction (Stauch *et al.*, 2012).

5.1.3 Previous Studies on the Cx43/Dlg1 Interaction

Due to the interaction of the Cx43 extreme C-terminus with the second PDZ domain of a different MAGUK protein, ZO-1 (Giepmans and Moolenaar, 1998; Toyofuku *et al.*, 1998), it was originally proposed that Cx43 may bind Dlg1 in a similar fashion. However, previous investigations by the Graham group showed that interaction between the two proteins does not require the terminal five amino acids of Cx43. Instead, the Cx43 C-terminus interacts with both the C- and N-termini of Dlg1 through a different mechanism which does not involve the PDZ domains (MacDonald *et al.*, 2012). Further unpublished work by the group utilising Cx43 C-terminal deletion mutants suggested that a Dlg1 binding site is contained within residues 348-377 of the Cx43 C-terminus, however this is unlikely to be the solitary binding site as wild-type levels of interaction with Dlg1 were not maintained in coimmunoprecipitation (co-IP) experiments using this mutant. The interaction was also found to be heavily reliant on phosphorylation status at several different sites (Dong, 2021). These include

residues S255, S262, S279, S368 and S373 which all showed decreased affinity for Dlg1 when mutated to alanine residues, which mimics unphosphorylated serine (Chen and Cole, 2015). In contrast, the same mutation of residue S282 increased Cx43/Dlg1 binding almost twofold, suggesting that various phosphorylation sites can modulate the Cx43/Dlg1 interaction in different ways (Dong, 2021).

A prerequisite for the development of safe and effective compounds targeting a specific protein-protein interaction is knowledge of the molecular interface at which the interaction takes place. Results from the previous chapter identified Dlg1 as an important component of the normal wound healing process **(Chapter 4)** and therefore it is not currently recommended as a singular therapeutic target for improving wound healing rates. The heavily context-dependent roles of Dlg1 in cancer as a pro- or anti-tumorigenic protein also further complicate the viability of Dlg1 as a therapeutic target (Roberts *et al.*, 2012). However, future design of inhibitors which specifically target the interaction between Cx43 and Dlg1 remain an attractive prospect due to their envisioned ability to disrupt Cx43 signalling at the plasma membrane, an effect which has previously been shown to improve wound healing rates in a clinical setting (Montgomery *et al.*, 2018). Therefore, in this chapter the potential molecular determinants of Cx43/Dlg1 interaction were studied in greater detail. In particular, the use of AlphaFold Colab protein modelling software (Jumper *et al.*, 2021) as a predictor of 3D structure of the Cx43/Dlg1 complex, as well as pre-existing data on both the interaction of Cx43/Dlg1 and Cx32/Dlg1 were combined to inform design of experimental testing of potential binding sites. This chapter details design and expression of recombinant proteins that can be utilised in the future to determine sites of Cx43/Dlg1 interaction, as well as to comprehensively address the role of phosphorylation in regulation of the interaction.

Aims:

- Generate AlphaFold Colab models of Cx43 C-terminus and Dlg1 singularly and as a complex for general structure analysis and the identification of potential regions of interaction between the two proteins.

- Produce recombinant protein expression vectors for regions of interest identified through AlphaFold complex model.
- Verify if predicted interaction sites are determinants of Cx43/Dlg1 binding through protein-protein interaction studies.
- Determine the effect of phosphorylation on Cx43/Dlg1 binding through interaction studies utilising various phospho-mimetic mutations at relevant sites of the Cx43 C-terminus.

5.2 Cx43 and Dlg1 AlphaFold Models are Consistent with Existing Literature

To better understand the individual structures of Cx43 and Dlg1, separate models were generated for each protein using an online AlphaFold Colab server https://colab.research.google.com/github/sokrypton/ColabFold/blob/main/beta/AlphaFold2_advanced.ipynb (Jumper *et al.*, 2021). Consistent with the literature, the Cx43 AlphaFold model possessed four clustered α-helical domains representing the transmembrane domains of the protein **(Figure 5.3, all AlphaFold models are also available as video files attached to thesis)**. The model was coloured according to the UniprotKB annotation system **(Table 5.1)** (Vasudevan *et al.*, 2011). When oriented to mimic the insertion of these domains into the plasma membrane, two short extracellular loop regions joining the transmembrane domains were apparent. One of these loops contained a small α-helical region, while the other formed two small ß-strand motifs. On the other hand, the N- and C-termini, as well as the cytoplasmic loop, were localised to the cytoplasmic side of the protein. The cytoplasmic loop was mainly composed of two large α-helices, while also containing two small unstructured regions. As has been reported previously, the ~150aa C-terminal region of the protein was largely disordered (Sorgen *et al.*, 2004), with some α-helical structure leading on from the adjacent transmembrane domain and an additional α-helical region observed between aa297-325.

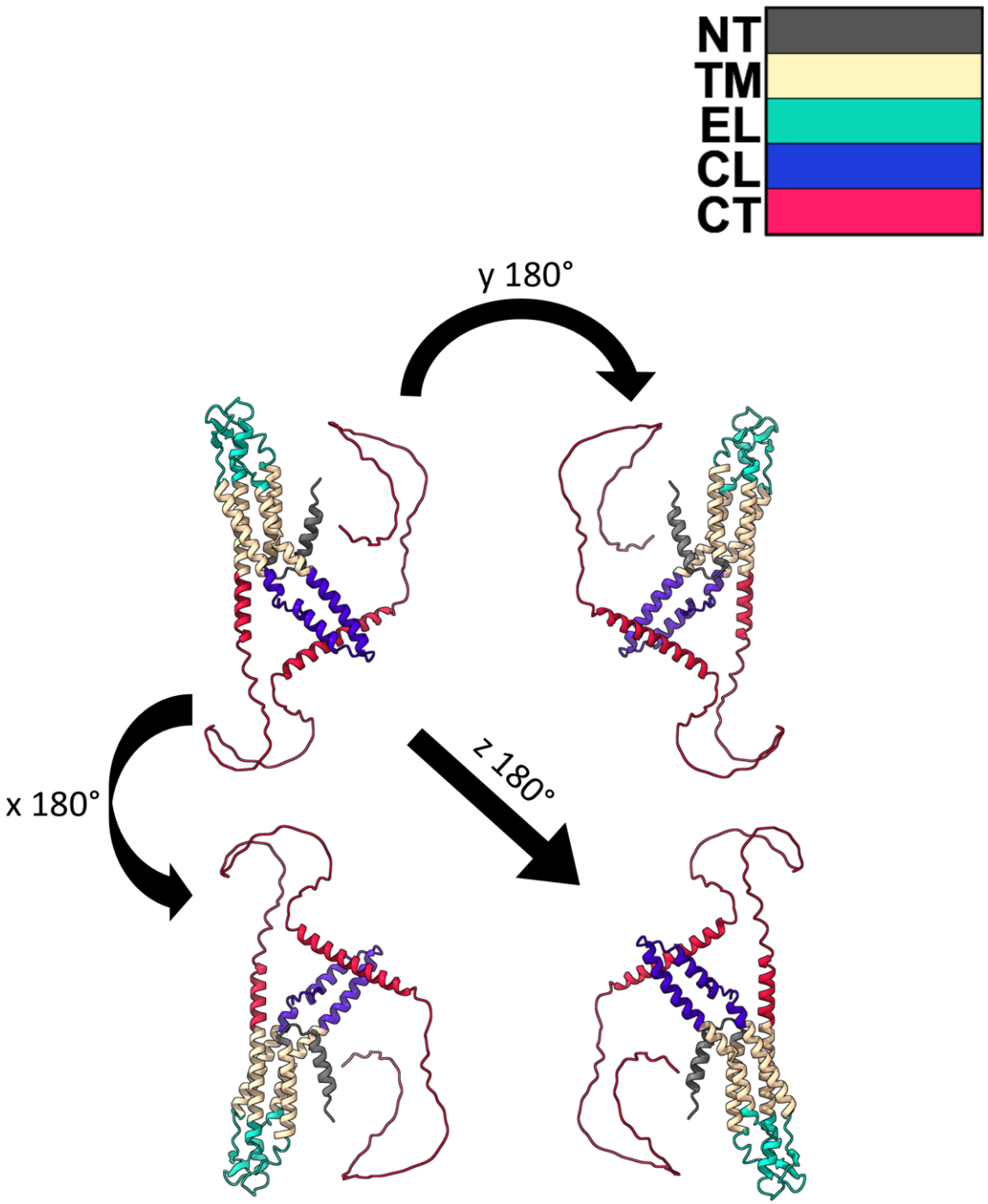

Figure 5.3: AlphaFold predictive model of human Cx43. Cx43 full-length=382aa. Rotations around the x, y and z axes are shown. Different regions are colour coded. Grey=NT=N-terminus, cream=TM=transmembrane domain, turquoise=EL=extracellular loop, dark blue=CL=cytoplasmic loop and crimson=CT=C-terminus. Helices and arrow structures represent α-helices and ß-sheets respectively. Several orientations of the protein are shown by rotating the model.

As with the Cx43 model, the Dlg1 AlphaFold model was largely in agreement with previous studies modelling Dlg1 and other MAGUK proteins **(Figure 5.4)**. This model was again coloured according to the UniprotKB annotation system **(Table 5.2)**. Three PDZ domains were observed, as well as a single L27, SH3, HOOK and GUK domain. Of note, the PDZ1 and PDZ2 domains clustered together to one side of the protein as a unit, while the other domains clustered as a second unit that was relatively distant from the first. Several linker regions were observed, particularly between the L27-PDZ1 domains and the PDZ2-PDZ3 domains. These regions were unstructured, which may confer flexibility to aid the role of Dlg1 as a scaffolding protein. The HOOK region (which is located between the SH3 and GUK domains) also consisted mostly of an unstructured loop, with a β-strand motif between aa703-710. Interestingly, this β-strand formed hydrogen bonds with another β-strand towards the C-terminal end of the protein in the amino acid residues following the GUK domain (aa895-899). This type of intramolecular interaction is likely involved in clustering of the domains and regulation of protein function.

Table 5.1: Cx43 structural features as predicted by the UniprotKB annotation system

Feature of Cx43	Cx43 Amino Acid Residues
N-terminus	1-23
Transmembrane Domain 1	24-44
Extracellular Loop 1	45-76
Transmembrane Domain 2	77-97
Cytoplasmic Loop	98-155
Transmembrane Domain 3	156-176
Extracellular Loop 2	177-207
Transmembrane Domain 4	208-228
C-terminus	229-382

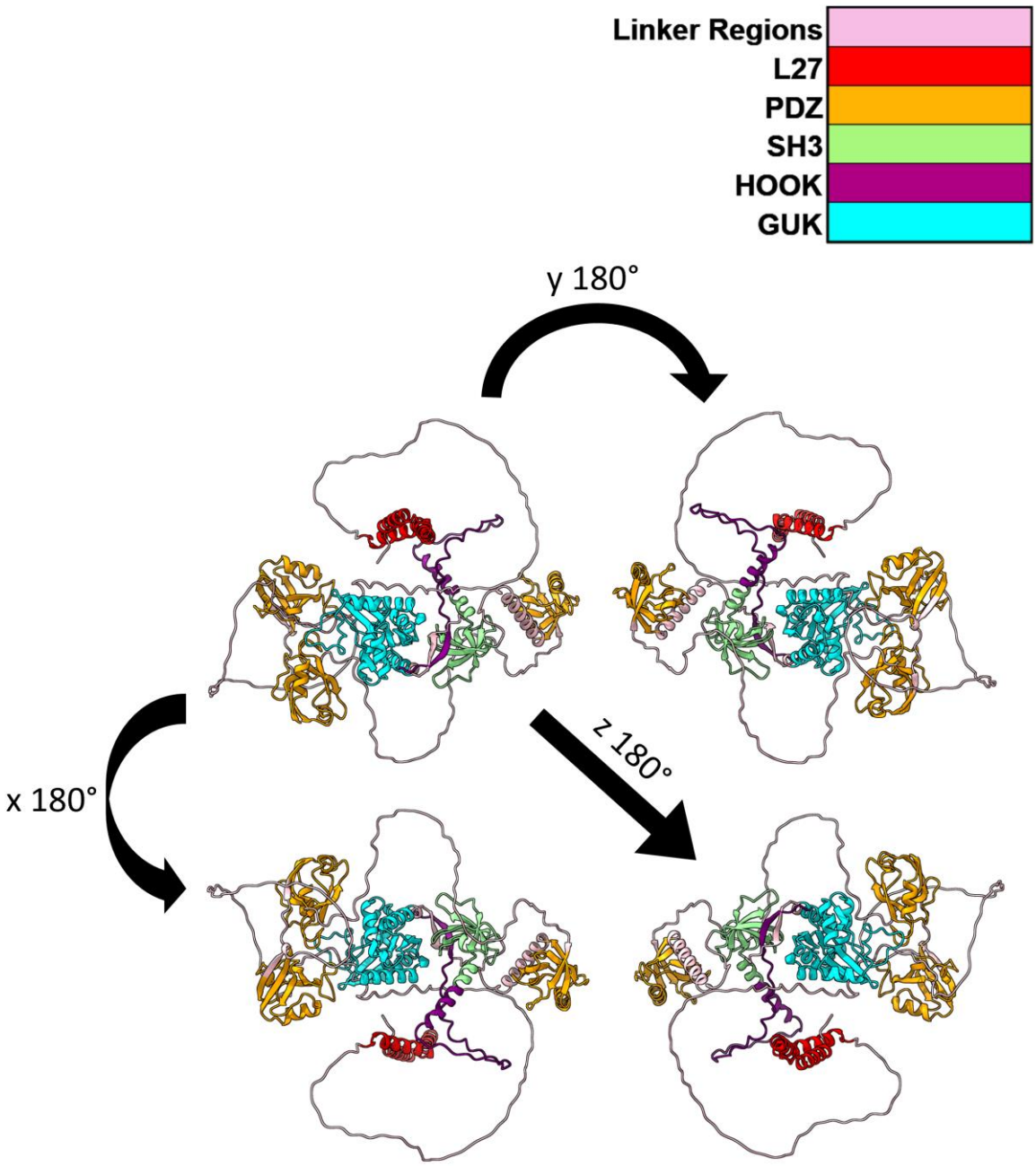

Figure 5.4: AlphaFold predictive model of human Dlg1. Dlg1 full-length=904aa. Rotations around the x, y and z axes are shown. Different regions are colour coded. Pink=linker regions, red=L27 domain, orange=PDZ domain, lime green=SH3 domain, purple=HOOK domain and cyan=GUK domain. Helices and arrow structures represent α-helices and ß-sheets respectively. PDZ1 and 2 clustered to one side of the protein while the rest of the domains clustered to the other. Several orientations of the protein are shown by rotating the model.

Table 5.2: Dlg1 structural features as predicted by the UniprotKB annotation system

Feature of Dlg1	Dlg1 Amino Acid Residues
L27 Domain	4-64
PDZ1 Domain	224-310
PDZ2 Domain	319-405
PDZ3 Domain	466-546
SH3 Domain	581-651
HOOK Region	662-693
GUK Domain	714-889

5.3 An AlphaFold Model of the Cx43/Dlg1 Interaction Predicts Three Distinct Dlg1 Binding Regions in the Cx43 C-terminal Tail

Following the separate Cx43 and Dlg1 models, a model of the two proteins as a complex was generated as above in order to determine any potential binding sites between the proteins. As Dlg1 was previously shown to interact with the C-terminus of Cx32 through its SH3/HOOK/pGUK domains (aa569-764) (Duffy *et al.*, 2007), this sequence, along with the C-terminus of Cx43 (aa232-382) was used as input to assess if a similar interaction could take place. In the complex model, the Cx43 C-terminus adopted a similar structure to the full-length protein model **(Figure 5.5A)**. One main α-helix was formed between aa66-89, which corresponds to aa297-320 of the full-length Cx43 and was almost identical to the α-helix-forming residues identified in the original model (aa297-325). However, two further regions of secondary structure were observed which were not present in the original full-length Cx43 model. These included a further very small α-helix formed towards the end of the C-terminus at aa146-149 (aa377-380 full-length) and a β-strand region between aa34-38 (aa265-269 full-length). The structure of Dlg1 was also similar in the complex to the original full model, with the SH3 and HOOK domains in an almost identical configuration **(Figure 5.5A)**. However, the structure of the GUK domain was mostly lost in the complex

model, which likely reflects the inclusion of only the first section of this domain in the input sequence.

Three individual regions of interaction with Dlg1 were identified within the Cx43 C-terminal tail **(Figure 5.5B)**. A summary of these interaction sites is shown in **Table 5.3** and the Cx43 residues involved can be seen in the context of the full-length Cx43 model in **Figure 5.6**. The interaction sites are subsequently referred to as sites A, B and C. Contact sites were identified between all three included domains of Dlg1 and the Cx43 C-terminus, indicating that the SH3, HOOK and GUK domains all may be involved in interaction with Cx43 **(Figure 5.5B)**. Of the three interaction sites within the Cx43 C-terminus, site A (262-278), which included the ß-strand region between 265-269, contained the most contact sites. Hydrogen bonds were predicted to form between the Cx43 C-terminus site A and the Dlg1 HOOK domain, as well as between site C (aa141-148) and the Dlg1 GUK domain. Interestingly, the sites of the Cx43 C-terminus which contained additional secondary structure compared to the full-length model were also sites of contact with Dlg1, which may suggest that binding of Dlg1 induces conformational changes in these areas. A surface model of the complex was also produced, as this can often provide valuable biological context to a given complex, including how interaction of certain proteins is likely to obscure other protein binding sites **(Figure 5.7)**. Surface models are also important in aiding rational drug design to disrupt protein-protein interactions. Here, the surface model suggested that the Cx43 C-terminus fits in a groove between the SH3/HOOK domains and the GUK domain.

Confidence of the AlphaFold complex model was assessed using two metrics, predicted local distance difference test (pLDDT) and predicted aligned error (PAE). pLDDT gives a measure of the per-residue confidence score for the model, ranging from a score of 0 for low confidence to 100 for extremely high confidence. On the other hand, PAE relates to the confidence in the placement of domains relative to other domains in a 3D space and is graded on a scale of 0 (low error) to 30 (high error) (Jumper *et al.*, 2021; Guo *et al.*, 2022). Contacts

between the two proteins can also be assessed according to PAE scores **(Figure 5.5B)**. Additional renders of the Cx43/Dlg1 interaction model which are coloured according to pLDDT and PAE are shown in **Figure 5.8A** and **Figure 5.8B** respectively. For pLDDT values, per-residue confidence for the Dlg1 SH3/HOOK/pGUK domains tended to be higher than the Cx43 C-terminus **(Figure 5.8A)**. Both proteins showed higher pLDDT values in domains and regions with secondary structure, while lower values were observed in unstructured linker regions. The main α-helix of the Cx43 C-terminus did not have as high a pLDDT value as other regions displaying secondary structure. When considering PAE, confidence in domain packing and bonds was highest at the Cx43 C-terminus interaction site A, where there was high confidence that the C-terminus had been placed correctly relative to the Dlg1SH3/HOOK domains **(Figure 5.8B)** and PAE values of contacts tended to be <~10 **(Figure 5.5B)**. Less certainty was observed for interaction sites B and C, where AlphaFold was not confident in the relative placement of the interacting regions **(Figure 5.8B)**, with PAE values of contacts of sites B and C with Dlg1 being ~20 and ~15 or less respectively **(Figure 5.5B)**.

Table 5.3: AlphaFold predicted interaction sites between the Cx43 C-terminus and Dlg1 SH3/HOOK/pGUK domains

Interaction Site Name	Cx43 C-terminus Interaction Site	Corresponding Full Length Cx43 Interaction Site	Dlg1 SH3/HOOK/pGUK Interaction Sites	Corresponding Full Length Dlg1 Interaction Sites
A	aa31-47	aa262-278	aa17-19, 44, 61, 136-150	aa585-587, 612, 629, 704-718
B	aa71-86	aa302-317	aa3, 41, 131	aa571, 609, 699
C	aa141-148	aa372-379	aa157-192	aa725-760

A

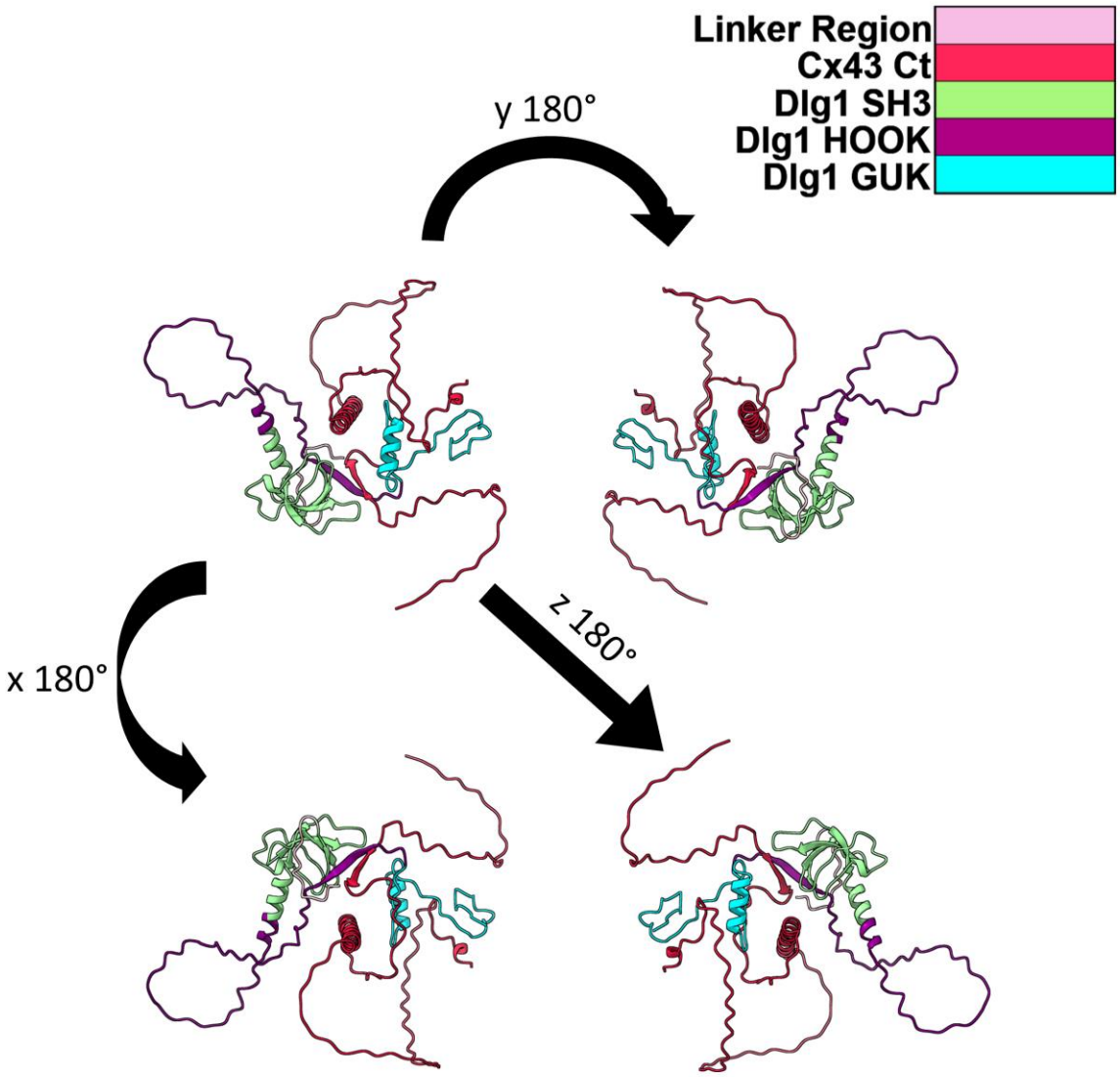
Linker Region
Cx43 Ct
Dlg1 SH3
Dlg1 HOOK
Dlg1 GUK
y 180°
x 180°
z 180°

B

Site A (Cx43 aa262-278)

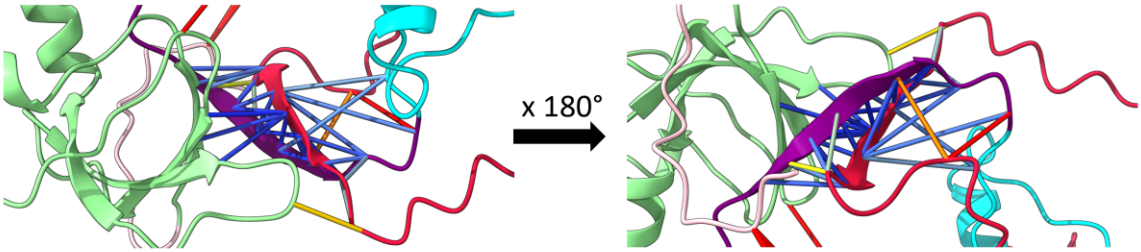

Site B (Cx43 aa302-317)

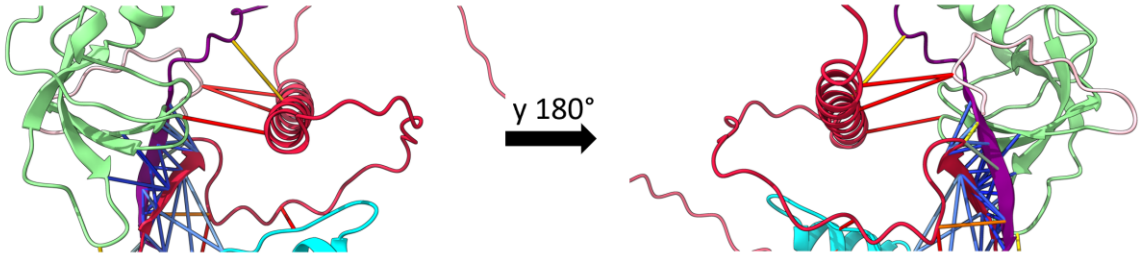

Site C (Cx43 aa372-379)

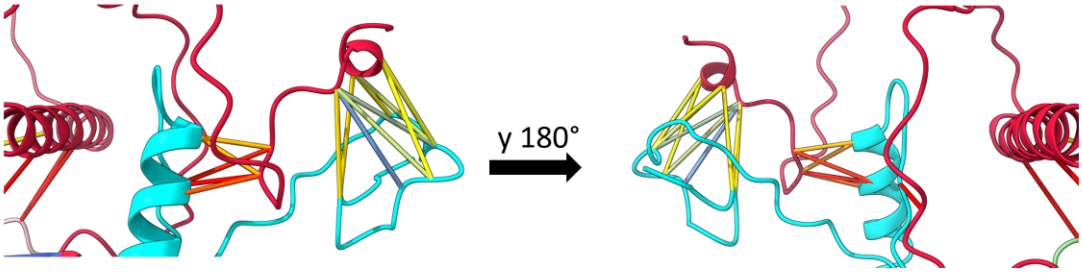

Figure 5.5: AlphaFold predictive model of the Cx43 C-terminus/Dlg1 SH3/HOOK/pGUK complex. (A) Model showing the proximity of the Cx43 C-terminus/Dlg1 SH3/HOOK/pGUK. Cx43 C-terminus=aa232-382, Dlg1 SH3/HOOK/pGUK=aa569-764. Rotations around the x, y and z axes are shown. Different regions are colour coded. Pink=linker regions, crimson=Cx43 C-terminus, lime green=SH3 domain, purple=HOOK domain and cyan=GUK domain. Helices and arrow structures represent α-helices and ß-sheets respectively. **(B)** Model showing three main regions of contact between the Cx43 C-terminus and Dlg1SH3/HOOK/pGUK in more detail. Domains are coloured as in **(A)**. Degree and axis of rotation are shown between images. Contacts are represented by solid lines between the proteins which are coloured according to predicted aligned error (PAE) values. Dark blue=low PAE=high confidence, yellow and orange=higher PAE=less confidence. Maximum length for contacts=4Å.

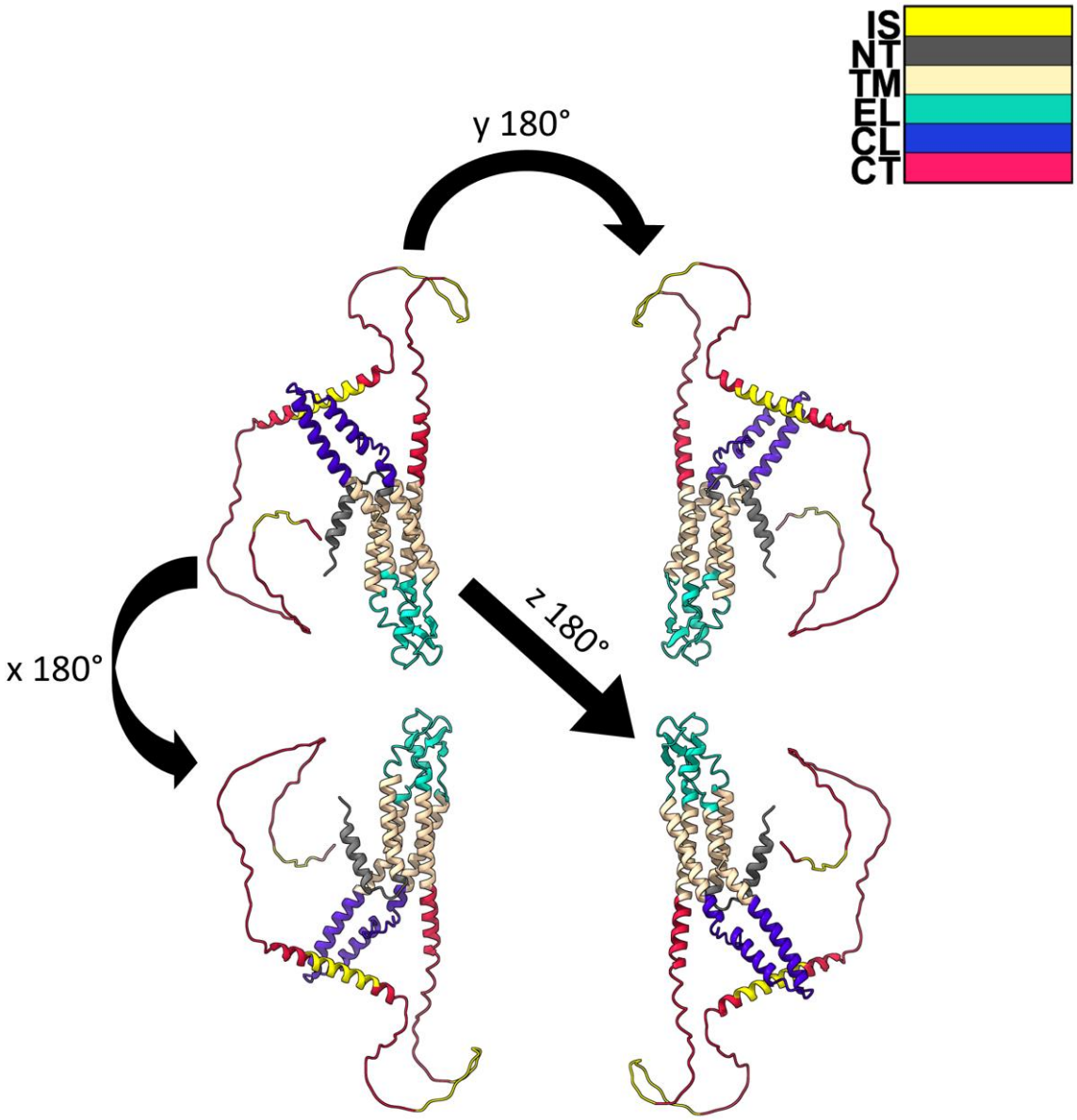

Figure 5.6: Full-length AlphaFold model of Cx43 showing the predicted sites of interaction with Dlg1. Cx43 full-length=382aa. Rotations around the x, y and z axes are shown. Different regions are colour coded. Yellow=interaction sites, grey=NT=N-terminus, cream=TM=transmembrane domain, turquoise=EL=extracellular loop, dark blue=CL=cytoplasmic loop and crimson=CT=C-terminus. Interaction sites are A:262-278, B:302-317 and C:372-379. Helices and arrow structures represent α-helices and β-sheets respectively. The protein is oriented as if it were inserted into the plasma membrane.

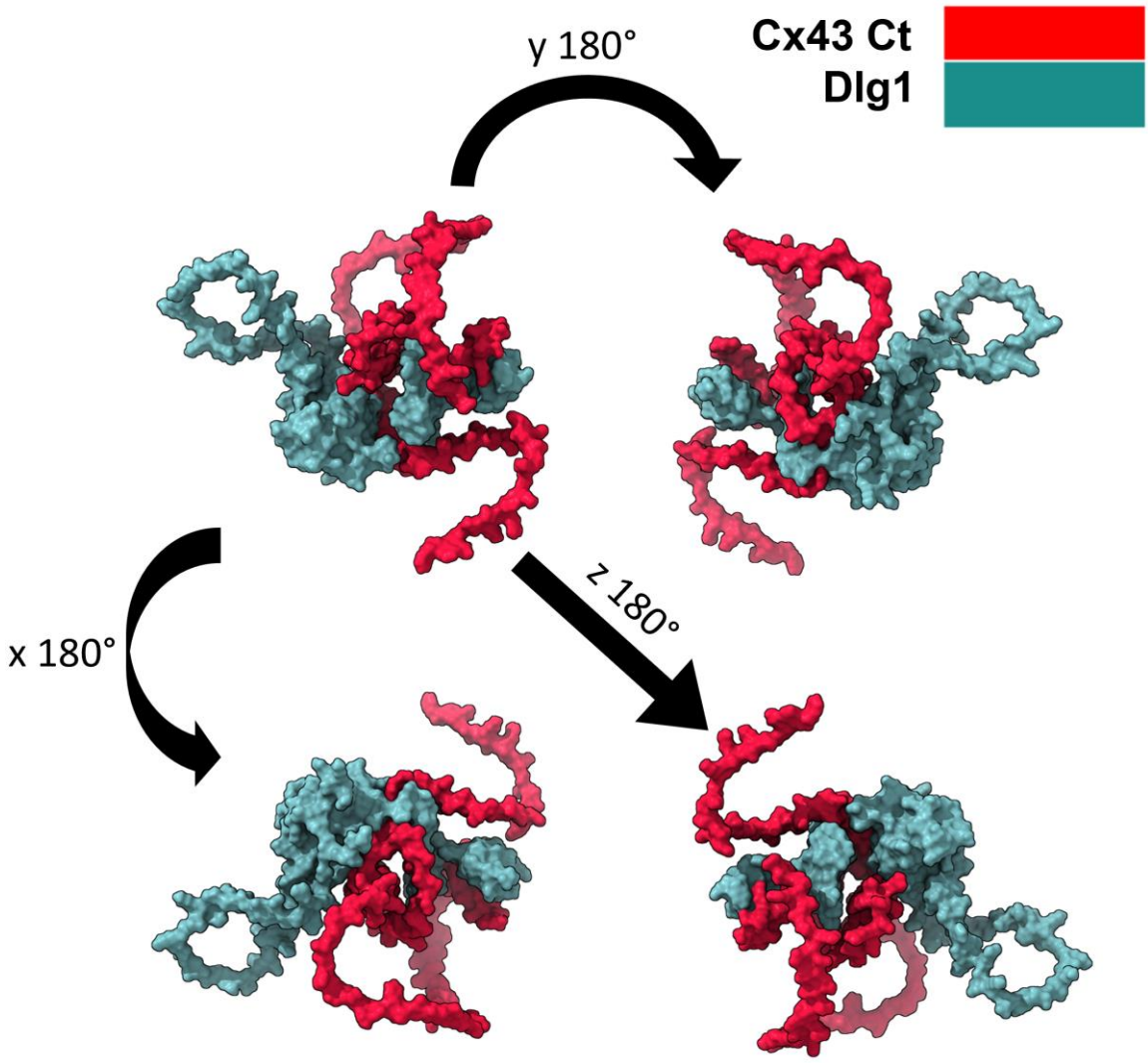

Figure 5.7: Surface of the Cx43 C-terminus/Dlg1 SH3/HOOK/pGUK complex. Model shows the Cx43 C-terminus in red and Dlg1 SH3/HOOK/pGUK in teal. Cx43 C-terminus=aa232-382, Dlg1 SH3/HOOK/pGUK=aa569-764. Rotations around the x, y and z axes are shown. The Cx43 C-terminus is predicted to fit in a groove between the SH3/HOOK domains and the GUK domain.

A

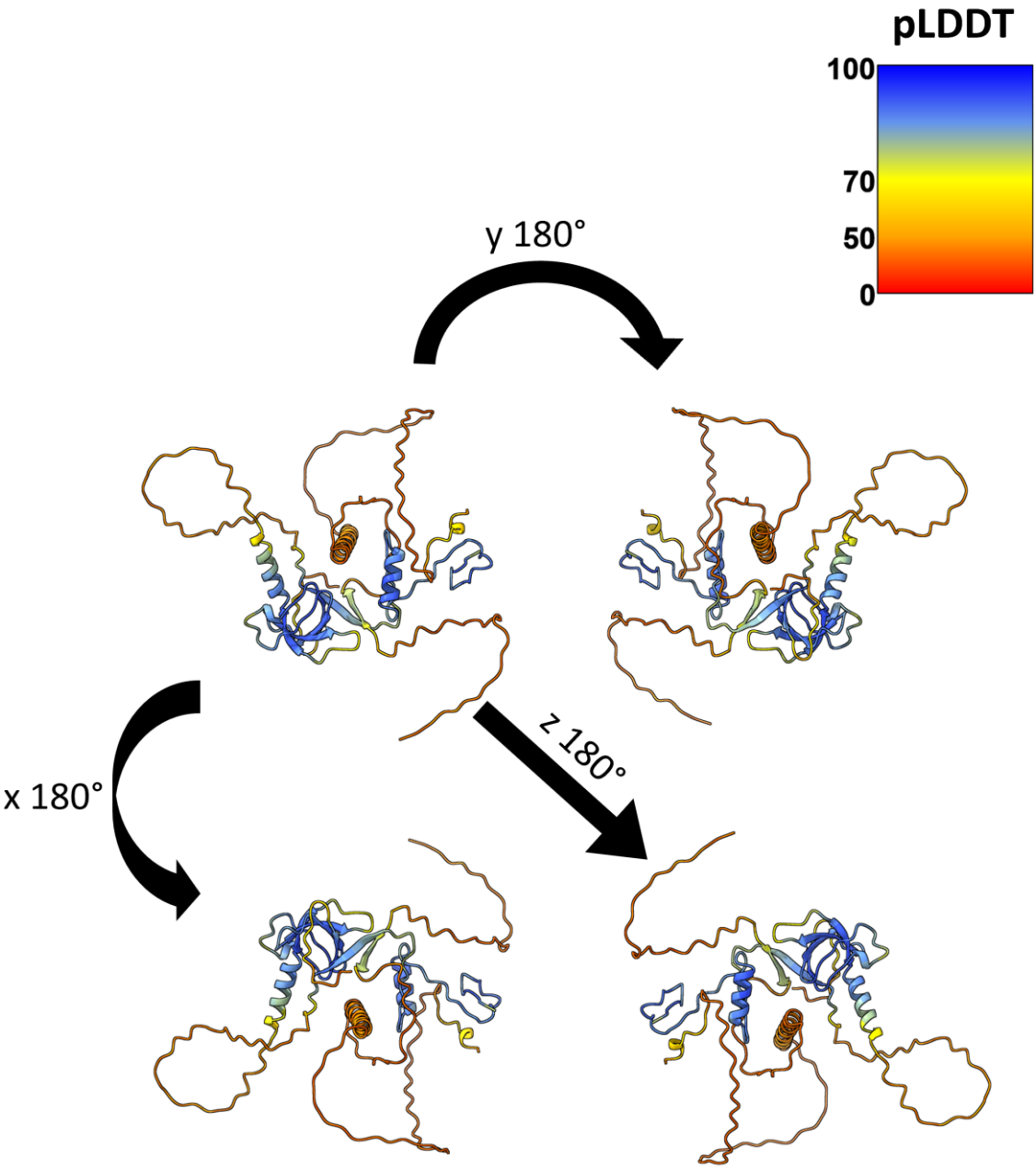

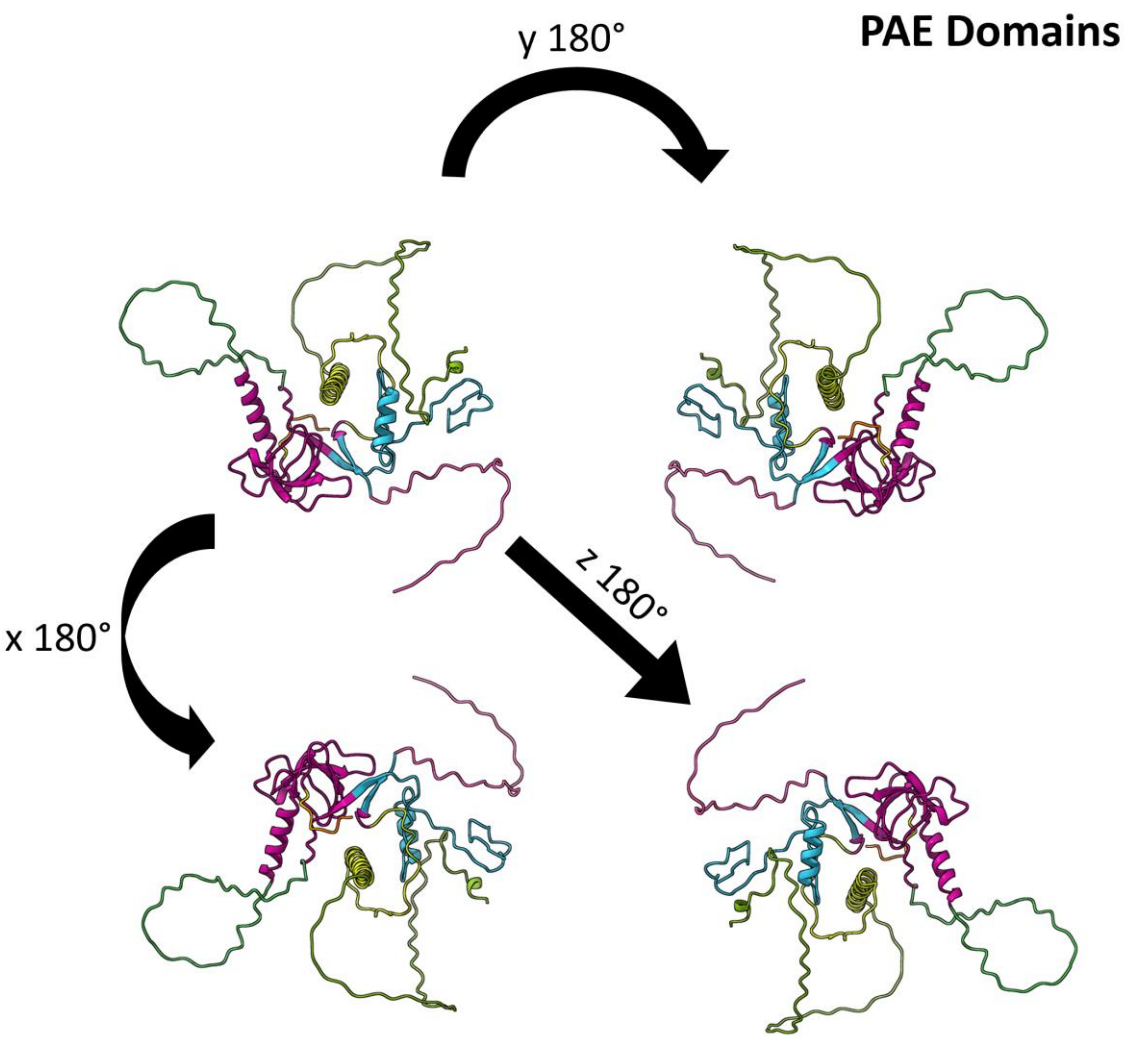

Figure 5.8: Evaluation of the Cx43 C-terminus/Dlg1 SH3/HOOK/pGUK model confidence. (A) Model showing the Cx43/Dlg1 complex coloured by pLDDT values. pLDDT is a per-residue confidence score, high pLDDT=more confidence in correct positioning of residue. Blue colour=high confidence, red colour=low confidence. Helices and arrow structures represent α-helices and ß-sheets respectively. **(B)** Model showing the Cx43/Dlg1 complex coloured by PAE domains. Regions of one colour are thought to be in the correct position relative to other areas of the same colour, while areas of different colours are less likely to be in the correct relative positions.

5.4 Expression of Recombinant Cx43 C-terminus and Dlg1 SH3/HOOK/GUK Proteins

To experimentally test the accuracy of the Cx43/Dlg1 AlphaFold complex model, the human sequences for the Cx43 C-terminus (aa232-382) and Dlg1SH3/HOOK/pGUK (aa569-764) were cloned into the bacterial pGEX-2T plasmid vector **(Figure 5.4)**. This expression system was chosen due to expected high protein yield. ZO-1 PDZ2 (aa150-312) was also cloned for use as a positive control in interaction studies since it interacts with the Cx43 C-terminus. All proteins were produced with a GST-tag fused to the N-terminal end of the protein for detection and purification. Successful cloning of each construct was confirmed by sequencing. Cx43 C-terminus, Dlg1SH3/HOOK/pGUK and ZO-1 PDZ2 constructs were then transformed into BL21 Gold *E.coli* cells for expression **(Figure 5.9)**. Empty pGEX-2T vector was included as a negative control which only expressed the GST-tag. Samples for each construct were induced at two different temperatures (20°C and 23°C) to optimise recombinant protein expression while limiting expression of native bacterial proteins. Samples without induction of recombinant protein expression were also included as negative controls. Of the three proteins, the Cx43 C-terminus was the most strongly expressed, with a clear band around the expected molecular weight of 43kDa (17kDa recombinant protein+26kDa GST-tag). Expression was most strongly induced by incubation of the *E. coli* cells at 23°C. A fainter band of a similar size was also observed in the uninduced control, which may suggest leaky expression of the protein. Dlg1SH3/HOOK/pGUK expression was not as strong as the Cx43 C-terminus, however there was a clear band in the 20°C and 23°C induced samples of around 55kDa not found in the uninduced sample. This band was slightly above the Dlg1SH3/HOOK/pGUK expected molecular weight of 49kDa and was most strong in the 23°C induced sample. ZO-1 PDZ2 produced the faintest bands of the three proteins and appeared to be more strongly expressed in the 20°C induced sample than the 23°C induced sample. The ZO-1 PDZ2 band was not observed in the uninduced sample and was around 49kDa in size, which is slightly above the predicted molecular weight of 45kDa.

From the results shown in **Figure 5.9**, it was clear that in addition to recombinant proteins, many other contaminating proteins were present in the samples and required removal prior to interaction studies. Therefore, additional purification steps were carried out on the sample containing Cx43 C-terminus recombinant protein. Glutathione affinity chromatography resulted in a much stronger Cx43 C-terminus protein band relative to the unbound protein fraction **(Figure 5.10A)**, which was included as a negative control to assess total protein in the sample and binding of the protein of interest to the glutathione beads. The majority of the Cx43 C-terminus protein was observed in fractions 8 and 9, with some contaminating protein bands also visible, particularly at lower molecular weights. Therefore, protein fractions 8 and 9 were pooled and further purified by size exclusion chromatography (SEC) **(Figure 5.10B)**. This resulted in highly pure Cx43 C-terminus protein bands in fractions 1, 2 and 3, with fractions 3 and 4 containing the majority of the Cx43 C-terminus protein. While other protein bands were detectable in fractions 1, 2 and 3, these were relatively minimal and therefore these samples were retained for further use. Subsequent fractions, while still containing Cx43 C-terminus protein, were contaminated with higher concentrations of other proteins and were discarded. Unfortunately, mitigating circumstances of the COVID19 pandemic 2020-2021 and shipping delays in some of the required products meant that Dlg1 SH3/HOOK/pGUK and ZO-1 PDZ2 were unable to be purified and used in further experiments.

Mutagenesis of the Cx43 C-terminus to delete interaction sites A, B and C was also attempted to determine whether these regions were necessary for interaction with Dlg1, however mutagenesis PCRs were unsuccessful **(Table 5.4)**.

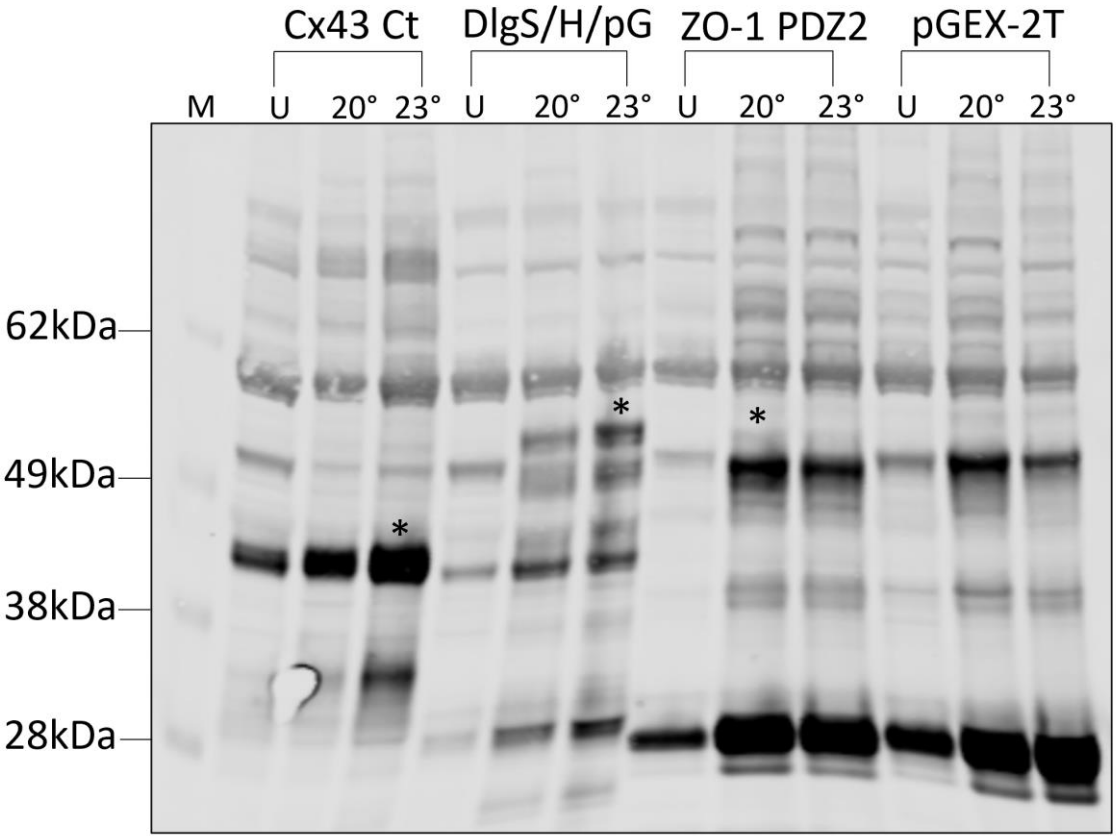

Predicted Molecular Weights (inc. GST):
Cx43Ct- 43kDa
DlgSH3/HOOK- 49kDa
ZO-1 PDZ2- 45kDa
pGEX-2T (just GST) 26kDa

Figure 5.9: Anti-GST western blot shows successful expression of the Cx43 C-terminus, DlgSH3/HOOK/pGUK and ZO-1 PDZ2 recombinant proteins in BL21 Gold *E.coli* cell extracts. DlgS/H/pG=DlgSH3/HOOK/pGUK. M=molecular weight markers, U=uninduced control supernatant, 20°=induced and incubated at 20°, 23°C=induced and incubated at 23°. Sizes of molecular weight markers are shown on the left-hand side in kilodaltons (kDa). Predicted molecular weights of recombinant proteins are shown in the table below the blot. Recombinant protein bands are highlighted with asterisks. Two different temperatures were tested to optimise expression of recombinant proteins.

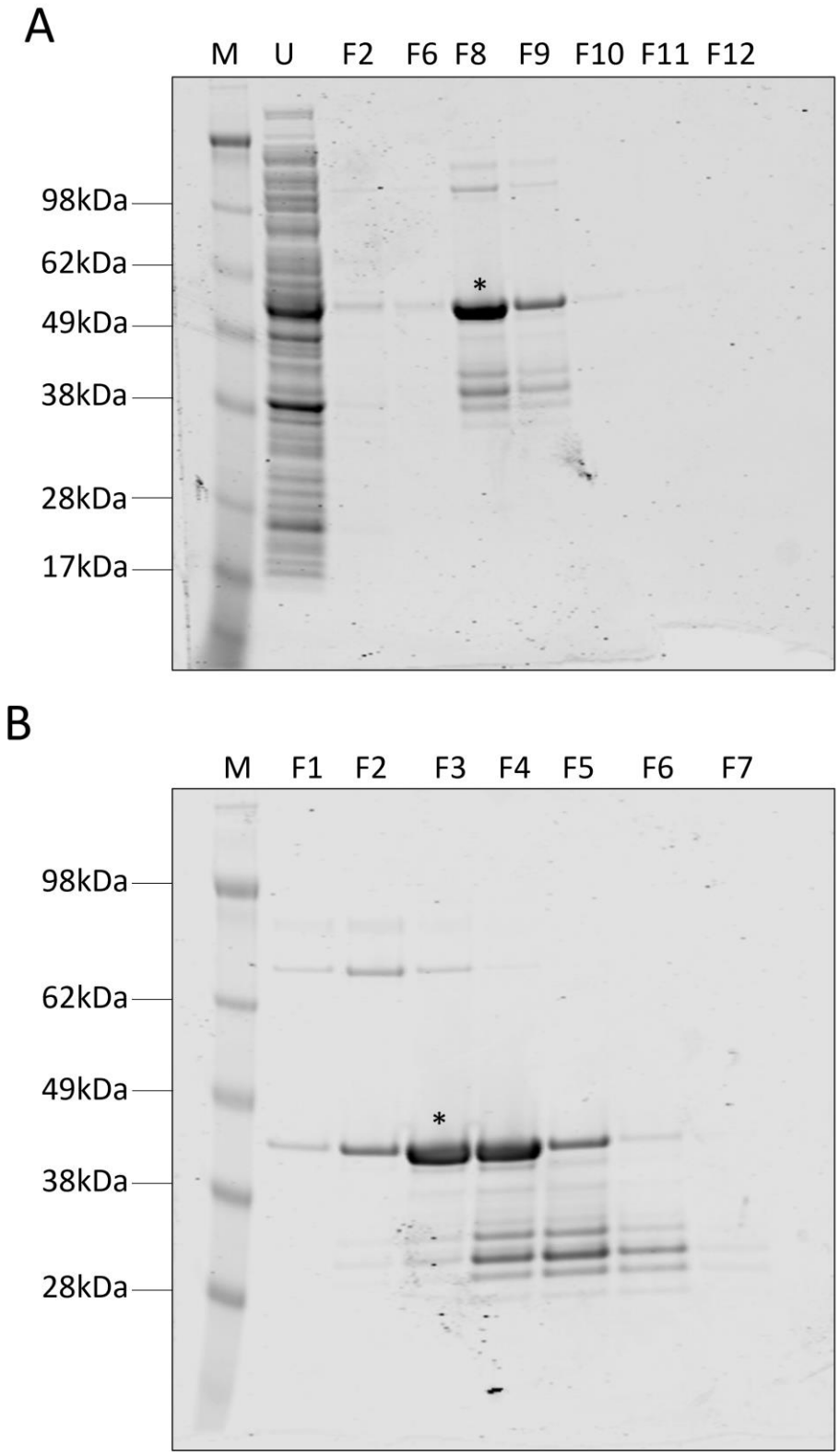

Figure 5.10: Coomassie staining of gels show purification of Cx43 C-terminus recombinant protein. (A) Glutathione-affinity chromatography of Cx43 C-terminus from BL21 Gold *E.coli* cell lysate. Cx43 C-terminus protein band is indicated by an asterisk. M=molecular weight markers, U=unbound protein which passed through the column, F=fraction number. Sizes of molecular weight markers are shown on the left-hand side in kilodaltons (kDa). Fractions F8 and F9 were concentrated and used in size exclusion chromatography (SEC). **(B)** SEC of Cx43 C-terminus. Fractions F1, F2 and F3 were retained for use in protein interaction experiments.

Table 5.4: pGEX-2T plasmid constructs for expression in BL21 Gold *E.coli* cells and subsequent interaction studies

Expression Construct	Notes
Cx43 C-terminus (aa232-382)	Expressed in BL21 Gold *E.coli*
Cx43 C-terminus Deletion A (Δ263-274)	Unsuccessful mutagenesis PCR
Cx43 C-terminus Deletion B (Δ302-310)	Unsuccessful mutagenesis PCR
Cx43 C-terminus Deletion C (Δ372-379)	Unsuccessful mutagenesis PCR
Dlg1SH3/HOOK/pGUK (aa569-764)	Expressed in BL21 Gold *E.coli*
ZO-1 PDZ2 (aa150-312)	Expressed in BL21 Gold *E.coli*

5.5 Design and Expression of Cx43 C-terminal Phospho-mimetic Mutants and a Further Deletion Mutation

Experimental work in this section was carried out by a master's student, Sanzida Islam Bristi, under my direct supervision.

Phosphorylation of certain Cx43 residues is known to play a critical part in the regulation of function and protein-protein interactions (Aasen *et al.*, 2018). Previous work by the Graham group resulted in the generation of six mutated Cx43 C-terminus sequence plasmids (Dong, 2021). Each of these mutants contained a single amino acid change of a serine residue to an alanine residue. Alanine and phenylalanine mimic unphosphorylated serine and tyrosine respectively and can therefore be used to test the effect of phosphorylation on protein-protein interactions (Chen and Cole, 2015). Co-IP experiments utilising these mutants showed varied residue-specific effects of Cx43 phosphorylation on interaction with Dlg1 (Dong, 2021). However, the impact of mutations at these sites that mimic phosphorylated residues, instead of unphosphorylated residues, remained to be addressed. Therefore, site-directed mutagenesis was carried out

on the existing mammalian expression vector pFLAG3xCMV10 Cx43 C-terminus plasmid to mutate the same serine residues to glutamic acid, which mimics phosphorylated serine/tyrosine (Chen and Cole, 2015). As the AlphaFold Cx43/Dlg1 complex model predicted an additional phosphorylation site, Y265, as part of interaction site A **(Table 5.1)**, further mutants Y265F and Y265E were designed to test whether phosphorylation at this site modulates Cx43/Dlg1 interaction. A deletion mutant of the main α-helical region of the Cx43 C-terminus was also prepared to test whether removal of these residues affected Cx43/Dlg1 interaction. This mutant was similar to deletion B (Δaa302-310) in the previous section but was expanded to include the entire α-helical region, as opposed to only residues predicted to interact with Dlg1. A summary of the expression constructs generated is shown in **Table 5.5**. Successful mutagenesis was confirmed by sequencing as before.

Following sequencing, constructs were transfected into HEK293 cells for expression **(Figure 5.11)**. Mammalian cells were used for recombinant protein expression in this section to be consistent with previous studies and to more closely mimic the native conditions of the Cx43/Dlg1 interaction (Chapple *et al.*, 2006). HEK293 cells in particular were chosen due to their high transfection efficiency and high levels of recombinant protein production. All proteins were tagged with 3x FLAG tag on the C-terminal end of the protein for detection. Results of an anti-FLAG western blot showed a strong protein band in the lane containing the Cx43 C-terminus wild-type construct at ~19kDa, which was the expected size of the recombinant protein **(Figure 5.11)**. This band was not present in the -ve control sample which was extract from HEK293 cells transfected with empty pMaxGFP plasmid (Lonza Biosciences, Basel Switzerland). Bands of similar molecular weight were seen for almost all of the substitution mutations as expected, however the S368E sample produced no band at this size, indicating the protein was not expressed. Interestingly, a further strong protein band was observed slightly above the recombinant protein band in the S282E sample, which may be the result of phosphorylation. Similar weaker bands were also present in other samples such as S255E. The Cx43 C-terminus deletion D (Δaa296-330) sample showed a band at a slightly lower

molecular weight (~15kDa) compared to the other samples, which reflects the deletion of the main α-helix. With successful expression confirmed, these recombinant proteins can be used further in the future to study Cx43/Dlg1 interaction using techniques such as co-IP and micro-scale thermophoresis (MST). Preliminary co-IP experiments comparing wild-type Cx43 C-terminus with deletion D Cx43 have suggested the α-helix-forming residues 296-330 may be important for interaction with Dlg1 (data not shown), however additional experiments are required to confirm this finding.

Table 5.5: pFLAG3xCMV10 plasmid constructs for expression in HEK293 cells and subsequent interaction studies

Expression Construct	Notes
Cx43 C-terminus (aa236-382)	Expressed in HEK293 cells
Cx43 C-terminus Deletion D (Δ296-330)	Expressed in HEK293 cells
S255E	Expressed in HEK293 cells
S262E	Expressed in HEK293 cells
S279E	Expressed in HEK293 cells
S282E	Expressed in HEK293 cells
S368E	Unsuccessful expression in HEK293 cells
S373E	Expressed in HEK293 cells
Y265E	Unsuccessful mutagenesis PCR
Y265F	Expressed in HEK293 cells

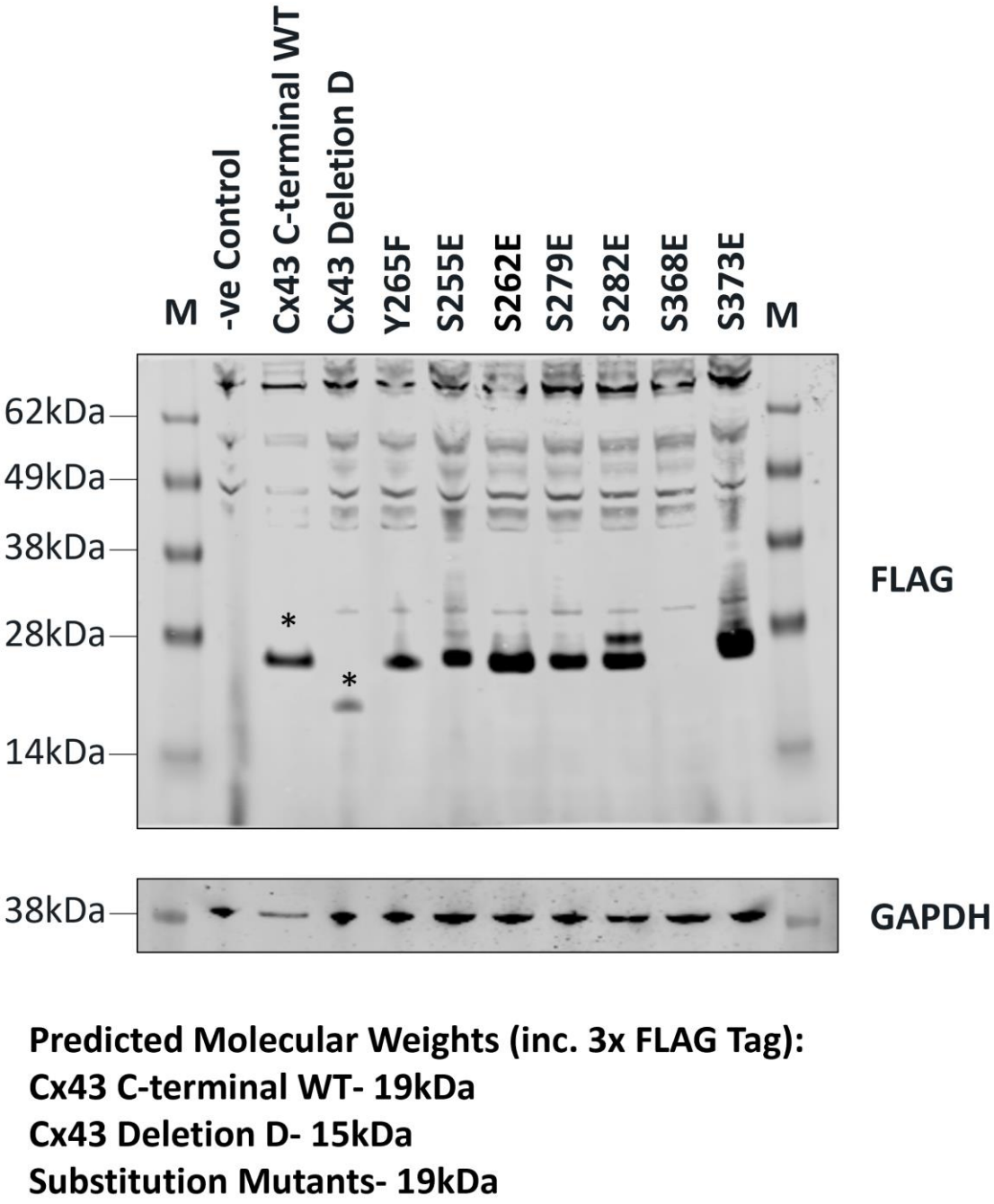

Figure 5.11: Anti-FLAG western blot shows successful expression of the Cx43 C-terminus and mutant recombinant proteins in HEK293 cell extracts. M=molecular weight markers, WT=wild-type. –ve Control=GFPMax-transfected HEK293 cell extract. Sizes of molecular weight markers are shown on the left-hand side in kilodaltons (kDa). GAPDH was included as a protein loading control. Predicted molecular weights of recombinant proteins are shown in the table below the blot. Example recombinant protein bands are highlighted by asterisks.

5.6 Discussion

In this chapter, the structures of human Cx43 and Dlg1 were predicted both separately and as a complex using AlphaFold Colab (Jumper *et al.*, 2021). The proposed structures of the two proteins separately were largely in agreement with experimentally determined structures. The Cx43 C-terminus was mainly disordered as has been previously reported, however small differences were observed in secondary structure between this model and earlier studies. In particular, the AlphaFold model predicted two α-helical regions, with one following on from the final transmembrane domain and the other from residues 297-325. The second α-helical sequence from residues 297-325 includes one of the α-helical regions determined by NMR spectroscopy, which was composed of amino acids 315-326 (Sorgen *et al.*, 2004). However, Sorgen and colleagues also demonstrated a second α-helical region existed from residues 340-348, which was not observed in this study. Prediction of the structure of the Cx43 C-terminal residues 255-382 by a further protein folding service, Phyre2, suggested two smaller α-helical regions between positions 308-312 and 316-319 (Leithe *et al.*, 2018), with only a very small α-helical region between 347-348 instead of the larger, experimentally determined α-helix from NMR studies. As has been discussed previously, the Cx43 C-terminus is thought to be mainly unstructured in order to allow flexibility and the adoption of secondary structure on interaction with other protein partners or changes in environmental conditions. While proteins with large unstructured regions tend to produce lower confidence models (Ruff and Pappu, 2021), the differences in the secondary structure of predicted and experimental models potentially reflect different conformations adopted by the protein depending on environmental conditions such as pH, which has previously been shown to affect Cx43 C-terminus function (Morley, Taffet and Delmar, 1996).

As has been described previously for Dlg1 and other MAGUK proteins (McCann *et al.*, 2012), the Dlg1 model could be divided into two main units, with one containing the PDZ1 and PDZ2 domains and the other containing the L27, PDZ3,

SH3, HOOK and GUK domains. Domains within each unit were in relative proximity to each other but more distant from domains in the other unit. Of particular interest was an intramolecular interaction between ß-strands formed by the HOOK region and a linker region directly following the GUK domain. In *Drosophila*, the contacts formed between these regions mediate the interaction of the SH3 and GUK domains, which has important implications in terms of protein-protein interactions and Dlg1 function (Newman and Prehoda, 2009). For example, the binding of several interaction partners of Dlg1, such as the synaptic protein GukHolder, has been previously shown to be regulated through the intramolecular interaction of these regions (Wu *et al.*, 2000; Qian and Prehoda, 2006). Disruption of this interaction through truncation of the linker region following the GUK domain resulted in unregulated complex formation, preventing Dlg1 performing its normal role in asymmetric cell division. This highlights the importance of intramolecular interactions in Dlg1 function (Newman and Prehoda, 2009).

When the Cx43 C-terminus and Dlg1SH3/HOOK/pGUK domains were modelled together as a complex, three distinct regions of interaction were predicted within the Cx43 C-terminus. These were Site A between residues 262-278 (involving a ß-strand), Site B between 302-317 (involving the main α-helix) and Site C between 372-379 (involving a small second α-helix). Of the three sites, Site A contained the most contact sites with Dlg1 and also possessed the highest confidence in individual contacts, as well as the placement of the two proteins relative to each other (as determined by PAE scores). Interestingly, while the ß-strand region of Site A was not observed in either previous NMR experiments (Sorgen *et al.*, 2004) or the individual AlphaFold model of the Cx43 C-terminus produced in this study, a ß-strand in this exact region was predicted with high confidence through the Phyre2 model of the Cx43 C-terminus (Leithe *et al.*, 2018). As mentioned above, adoption of this conformation may rely on the presence of certain interaction partners or be dependent on environmental factors. The most striking difference between the Dlg1 individual model and the model of the two proteins together was the replacement of the intramolecular interaction between the HOOK and linker region of Dlg1 with an almost identical interaction between the HOOK region and site A of the Cx43 C-terminus. As the

sequence of Dlg1 in this model contained only part of the GUK domain, the intramolecular interaction of these regions was not possible in the complex model. This may suggest that, as with other proteins, interaction of Cx43 and Dlg1 is regulated through Dlg1 intramolecular interaction in these regions, particularly due to the high confidence in this section of the model. It would be interesting to investigate whether the interaction is still predicted to take place in the presence of the full C-terminal end of Dlg1 (569-904).

Previous studies by the Graham group have demonstrated that the Cx43 C-terminus interacts with both the N- and C-termini of Dlg1 (MacDonald *et al.*, 2012) and that a binding site is contained within residues 348-377 of Cx43 (Dong, 2021). However, this site is unlikely to be the sole determinant of interaction as expression of this region alone does not maintain wild-type levels of binding (Dong, 2021). Of the interacting regions identified in this study, only Site C is partially within residues 348-377. This indicates that Sites A and B may be responsible for the difference observed between wild-type and mutant binding to Dlg1, although only the C-terminal end of Dlg1 was considered in this investigation and thus there are likely additional Cx43 binding sites yet to be identified. The latter section of Site C (372-379) includes some of the amino acids shown to interact with ZO-1. As interaction with Dlg1 was maintained in GST-pulldown experiments with mutant Cx43 protein containing a truncation of the terminal 5 amino acids of the C-terminus (MacDonald *et al.*, 2012), Site C is likely not essential for interaction with Dlg1.

To experimentally test the accuracy of the AlphaFold complex model, several expression constructs were designed and transformed into bacterial cells. While coimmunoprecipitation has commonly been utilised in the Graham group previously for protein-protein interaction studies, it is unable to give kinetic data which can give valuable biological context to the nature of a given protein-protein interaction, such as its stability. Therefore, techniques such as surface plasmon resonance (SPR), which can determine association and dissociation constants, were attractive for this study. As SPR protein consumption is greater relative to traditional co-IP experiments, a bacterial cell line was utilised for

optimal protein expression. While time-constraints meant protein-protein interaction experiments were not possible in this investigation, these recombinant proteins may prove useful in future studies of the Cx43/Dlg1 interaction.

In addition to bacterial expression vectors, mammalian expression vectors were designed for the Cx43 C-terminus, as well as a deletion of the main predicted α-helix (including interaction Site B) and several phospho-mutants. These constructs were designed to complement existing serine to alanine mutants of the Cx43 C-terminus (Dong, 2021), with the addition of a further two mutants at Y265 due to this being part of interaction site A. The additional protein bands observed in the S282E sample and, to a lesser degree, other samples such as S255E was interesting, as this may indicate phosphorylation of the recombinant proteins. This could be due to phosphorylation of the mutated glutamic acid residue, which while mimicking phosphorylated serine has also recently been shown to be capable of being phosphorylated itself in humans (Hardman *et al.*, 2019). Alternatively, the extra protein bands may reflect phosphorylation of sites other than the mutated residue. The processes of both forward trafficking and internalisation of Cx43 from the cell membrane have been shown to be controlled by sequential phosphorylation events. For example, phosphorylation of S282 is associated with gap junction closure and is often followed by phosphorylation of Y247, which promotes gap junction internalisation (Solan and Lampe, 2014). This suggests that mimicking phosphorylation at one site of the Cx43 C-terminus can promote phosphorylation of other sites. It is planned in the future to use techniques such as micro-scale thermophoresis, which involves fluorescent tagging of one protein partner and monitoring of its movement through a thermal gradient, which changes depending on protein binding status (Jerabek-Willemsen *et al.*, 2014), in conjunction with traditional co-IP techniques to address the role of phosphorylation and individual Cx43 residues in Dlg1 binding.

The predicted interaction sites of Cx43 and Dlg1 from the AlphaFold model have several implications for the lifecycle of Cx43. In particular, interaction site A of

Cx43 includes the ß-strand forming residues ^{265}YAYF^{268}, which together form a key regulatory site involved in internalisation and degradation of Cx43. Motifs of this kind are conserved between many membrane proteins and function as a general target for proteins promoting internalisation (Bonifacino and Traub, 2003). For example, the adapter protein complex-2 (AP-2), interacts with the Cx43 ^{265}YAYF^{268} site, as well as ^{286}YKLV^{289} to promote internalisation via a process similar to clathrin-mediated endocytosis (Fong, Kells and Falk, 2013). Substitution or deletion mutations at either of these sites disrupted interaction with AP-2 and drastically reduced endocytosis of Cx43 gap junctions, demonstrating the importance of these sites for Cx43 internalisation. Site A is additionally significant for interaction of Cx43 with c-Src. c-Src is a tyrosine kinase and functions as an important regulator of gap junctional Cx43 by binding aa274-283 and phosphorylating Y265, subsequently leading to internalisation of Cx43 (González-Sánchez *et al.*, 2016; Giepmans *et al.*, 2001a). This is similarly achieved by the Rous sarcoma virus protein v-Src, which may also cause indirect phosphorylation at additional Cx43 sites (Zhou, Kasperek and Nicholson, 1999). The overlap of both the AP-2 and c-Src interaction sites with those predicted for Dlg1 suggests that binding of these proteins to Cx43 are mutually exclusive.

Interaction Sites A (262-278) and B (302-317) of the Cx43 C-terminus are also very similar to the interacting regions previously demonstrated for Drebrin, which interacts with Cx43 at residues 264-275, 282-290 and 299-321 (Ambrosi *et al.*, 2016). Due to the significant overlap in these regions, it is suggested that Dlg1 and Drebrin may directly compete for binding to Cx43. This is an intriguing idea, as Drebrin is an actin-binding protein which has been shown to stabilise Cx43 at the plasma membrane (Butkevich *et al.*, 2004), which is also a role that Dlg1 may perform (as discussed in **Chapter 3**). This opens the possibility that Drebrin and Dlg1 have similar roles in the Cx43 lifecycle. The two proteins may perform the same role independently in separate cell types, or alternatively carry out identical roles in the Cx43 lifecycle at separate stages of the cell cycle. It is also possible that they function cooperatively in different parts of the lifecycle and one protein 'hands-over' Cx43 to the other.

Finally, interaction Site C (372-379) of the Cx43 C-terminus overlaps with the region which binds 14-3-3 proteins (370-376) (Park *et al.*, 2007). 14-3-3 proteins have been demonstrated to be involved in both Cx43 forward trafficking to the plasma membrane (Batra *et al.*, 2014) and endocytosis of gap junction channels (Smyth *et al.*, 2014), with this effect being specific to Cx43 as other connexin proteins lack this site (Park *et al.*, 2007). This again may suggest mutual exclusion of binding between Cx43 and Dlg1/14-3-3. The potential competition between Dlg1 and 14-3-3 proteins is also relevant to HPV infection, as high-risk HPV E6 protein interacts with 14-3-3ζ via its PDZ-binding domain when phosphorylated (Boon and Banks, 2013). As this is also the mode of interaction between E6 and Dlg1 (Thomas *et al.*, 2008), with E6, Dlg1 and Cx43 being shown to exist as a complex (Sun *et al.*, 2015), it may be that E6 can also interact indirectly with Cx43 through 14-3-3ζ. The consequences of this are currently unclear, as 14-3-3ζ is not targeted for degradation by E6 and instead seems to be involved in maintaining E6 levels (Boon and Banks, 2013). The implications of the interaction of Cx43 and Dlg1 for other Cx43 interaction partners are discussed further in **Chapter 6**.

Chapter 6: Discussion

Cx43 is a widely expressed protein which possesses channel-forming roles to allow direct intercellular communication between adjacent cells, as well as non-channel forming roles to modulate a wide range of other processes through interactions with other protein partners. Through these functions, Cx43 is involved in many fundamental processes and is essential for homeostasis in a variety of different contexts, with alteration to Cx43 expression and function being associated with numerous disease states (McLachlan *et al.*, 2008). Dlg1 is a cell polarity and signal transduction protein which is similarly crucial to homeostasis and interacts with Cx43 (MacDonald *et al.*, 2012). While this interaction is likely to take place in a variety of cell types given the wide expression profiles of the two proteins, their potential interaction in keratinocytes was of particular interest in this study due to the increased levels of Cx43 at the plasma membrane of wound-edge cells in chronic non-healing wounds (Brandner *et al.*, 2004). Wound care is currently responsible for a massive global physical health and economic burden, which is partly due to the lack of effective treatment options to improve wound closure rates. This is particularly concerning when considering that the rate of diabetes, which is heavily associated with the development of certain chronic wounds, is expected to rise sharply in the coming decades (Becker *et al.*, 2012). It is therefore essential to conduct further study on interactions like that between Cx43 and Dlg1, particularly as Cx43 has shown great promise as a therapeutic target in wound healing (Montgomery *et al.*, 2018). Such investigations may lead to the future development of therapeutics targeting these proteins or their interaction to improve wound healing rates.

One of the main aims of this investigation was to define the role of Dlg1 in the Cx43 lifecycle **(Chapter 3)**. Previous studies by the Graham group have shown that knockdown of Dlg1 results in decreased Cx43 protein levels and removes a large proportion of Cx43 from the plasma membrane (Dong, 2021), however the exact details of how Dlg1 functions in this pathway remained unclear. In this

study, depletion of Dlg1 caused a significant decrease in Cx43 protein levels but no change in Cx43 mRNA levels, meaning the role of Dlg1 is performed at a later stage of the lifecycle following protein synthesis. Further analysis through confocal microscopy experiments revealed that knock down of Dlg1 resulted in reduced Cx43 at the plasma membrane, as well as a reduction in association with a marker of the endoplasmic reticulum. In contrast, Cx43 colocalisation with a lysosomal marker was elevated and a dramatic increase in association with markers of the Golgi was observed. Experiments utilising an inhibitor of the lysosomal pathway further confirmed that increased lysosomal degradation of Cx43 takes place in siDlg1-treated cells. Gap junctional communication was also vastly reduced in cells where Dlg1 had been knocked down, suggesting Dlg1 controls gap junctional intercellular signalling through its role in the Cx43 lifecycle.

Overall, data from **Chapter 3** suggest two possible roles for Dlg1 in the Cx43 lifecycle: Dlg1 controls forward trafficking of Cx43 from the Golgi to the cell membrane, or Dlg1 stabilises Cx43 at the cell membrane and prevents endocytosis of Cx43 and subsequent retrograde transport to the Golgi. Both models are plausible and are supported by data presented in this study, as well as data from other groups. For example, Dlg1 promotes the polymerisation of actin and therefore could be involved in efficient targeting of Cx43 to adherens junctions (Round *et al.*, 2005). Dlg1 is also known to be involved in trafficking of several membrane proteins (including K^+ channels) to the plasma membrane in neurons, suggesting it may be able to perform a similar role for Cx43 (Fourie *et al.*, 2014). The involvement of Dlg1 in protein trafficking is known to include Dlg1-mediated recruitment of motor proteins, such as members of the kinesin family, to vesicles containing interaction partners following exit from the Golgi. In some cases, Dlg1 functions as part of a complex with a further MAGUK protein, CASK, to achieve forward trafficking of proteins (Walch, 2013). Dlg1 and CASK directly interact through their respective L27 domains (Lee *et al.*, 2002). Interestingly, CASK also directly interacts with Cx43 and is suggested to be involved in its forward trafficking given that it preferentially interacts with unphosphorylated Cx43 (Márquez-Rosado *et al.*, 2012). This raises the possibility

that Dlg1 and CASK function together to promote forward trafficking of Cx43 to the plasma membrane.

While the hypothesis that Dlg1 promotes forward trafficking of Cx43 is attractive due to its simplicity, it is disputed by certain data presented in this study. The results from the AlphaFold complex model of Cx43 and Dlg1 in **Chapter 5** revealed three prospective binding sites within Cx43: residues A 262-278, B 302-317 and C 372-379. The first of these, which contains the most contacts with Dlg1 of the three sites, directly overlaps with the region expected to bind to CASK (260-280) (Márquez-Rosado *et al.*, 2012). Therefore, if this model is correct, binding of Dlg1 and CASK to Cx43 is mutually exclusive and the three proteins could not exist in a complex like that described for some other proteins that Dlg1 controls (Walch, 2013). That both MAGUK proteins are expected to bind Cx43 in a similar way is interesting, as Cx43 residues 274-284 comprise the SH3-binding region (Iyyathurai *et al.*, 2018), which indeed formed contacts with the SH3 domain of Dlg1 in the AlphaFold model. This, in addition to conventional interactions with PDZ-domains, likely points to a further conserved mode of interaction between Cx43 and select members of the MAGUK family. Despite this, both proteins could also still function together in the trafficking pathway of Cx43 with a 'hand-over' step involved between them.

Interaction site C (372-379) of the AlphaFold model also overlapped with the binding region for 14-3-3 proteins (370-376), which are expressed in keratinocytes (Sambandam *et al.*, 2015) and are involved in forward trafficking of Cx43 (Batra *et al.*, 2014). While, as with CASK, this may suggest synergistic roles at different stages of the forward trafficking pathway, or conserved roles at different stages of the cell cycle, it could also indicate different roles for 14-3-3 proteins and Dlg1 in the Cx43 lifecycle. The strongest evidence to suggest that Dlg1 may not function in the forward trafficking of Cx43 to the plasma membrane comes from immunofluorescence experiments in this study, where little cytoplasmic colocalisation was observed between Cx43 and Dlg1. This suggests that interaction between the two proteins could be limited to sites of cell-cell contact rather than an earlier stage of the Cx43 trafficking pathway.

The other possible role of Dlg1 in the Cx43 lifecycle is in stabilisation of Cx43 at the plasma membrane. In this scenario, depletion of Dlg1 results in internalisation of Cx43 from the plasma membrane, after which it is likely that a certain pool of protein is degraded through the lysosomal pathway and the rest is recycled to the Golgi. This type of mechanism has been shown previously for E-cadherin when Scribble is knocked down (Lohia *et al.*, 2012). This model has several intriguing implications for Cx43. For example, it could be beneficial under certain circumstances for cells to retain a pool of internalised Cx43 that can be rapidly redelivered to the plasma membrane to enable quick changes in gap junctional signalling. This type of Cx43 recycling is already known to take place through connexosomes (Carette *et al.*, 2015) and retrograde trafficking of Cx43 to the Golgi could therefore represent an additional retention mechanism. An example of where this could be relevant is the M phase of cell division, where Dlg1 relocates to the cytoplasm and binds to mitotic spindle (Narayan *et al.*, 2009), while Cx43 also relocates to become intracellular (Vanderpuye *et al.*, 2016). In the following stage of cytokinesis, gap junctional communication is rapidly established between daughter cells, with both Cx43 and Dlg1 localising to the midbody. Further research is required to establish if there is increased association of Cx43 with the Golgi in certain stages of the cell cycle.

The idea that Dlg1 stabilises Cx43 at the cell membrane is supported in part by results from the AlphaFold complex model of the two proteins **(Chapter 5)**. As noted previously, the prospective interaction sites with Dlg1 within the Cx43 C-terminus include a key site regulating gap junction internalisation and degradation (^{265}YAYF^{268}), as well as regions which overlap with binding sites for Src, AP-2 and 14-3-3. Each of these proteins are associated with facilitating endocytosis of gap junctions from the plasma membrane, suggesting that Dlg1 may compete with them for binding to Cx43. A further regulatory protein which targets Cx43 in a Ca^{2+}-dependent manner is calmodulin, which binds to both the cytoplasmic loop and the C-terminus of Cx43 to facilitate channel closure (Zheng *et al.*, 2020). The calmodulin binding region of Cx43 is thought to be within residues 265-319, which means Dlg1 binding may also inhibit this interaction. Interestingly, the potential Dlg1 binding sites identified in this study directly overlap with two of the regions known to bind to Drebrin (residues 264-275, 282-

290 and 299-321), which has been shown to stabilise Cx43 at the plasma membrane (Ambrosi *et al.*, 2016). The two proteins could therefore function synergistically in stabilising Cx43 at the plasma membrane through steric inhibition of other protein partners which promote internalisation. This, along with the incomplete knockdown of Dlg1, may explain why a pool of Cx43 remains localised to the cell membrane under conditions where Dlg1 is depleted. The reason for this proposed functional redundancy is unknown but may be due to the two proteins: 1. Performing the same role in different cell types. 2. Performing the same role in different cell cycle stages 3. Functioning in sequential stages of the lifecycle with 'hand-over' from one protein to another. 4. Functioning together in the same cell type to allow multiple pathways to regulation of membranous Cx43. The finding that Cx43 had reduced colocalisation with EEA1 (a marker of early endosomes) in siDlg1-treated cells contradicts the idea of Dlg1 stabilising Cx43 at the cell membrane, as reduction of Dlg1 would be expected to increase the proportion of endosomal Cx43 prior to recycling to the Golgi. One explanation for this could be that depletion of Dlg1 leads to internalisation of Cx43 primarily as connexosomes before recycling to the Golgi, which could account for the lack of colocalisation with EEA1. Given the diffuse staining of EEA1 observed in this study, this work would benefit from confirmation of Cx43 colocalisation with a different marker of the endosomes.

Considering all the data, both proposed roles for Dlg1 in the Cx43 lifecycle are viable, with the added possibility that Dlg1 performs both of these functions. Additional experiments are required to determine which (if not both) of these models are correct. Further work should include analysis of Cx43 colocalisation with markers of recycling endosomes, which could facilitate Cx43 retrograde transport to the Golgi. Treatment of control and siDlg1-treated cells with an endocytosis inhibitor, such as dynasore, should also be performed to assess localisation of Cx43 under these conditions **(Figure 6.1)**. If there is an increase in Cx43 membrane localisation following dynasore treatment, it suggests that Cx43 forward trafficking is unaffected by Dlg1 depletion and therefore Dlg1 prevents internalisation of Cx43. If this is the case, kinetic data on the strength of the interaction between Cx43 and Dlg1 would give important context to the role of Dlg1, for example whether Dlg1 is likely to displace other proteins from

Cx43 to prevent internalisation or, conversely, whether Dlg1 itself is displaced to promote endocytosis. It is unclear whether Dlg1 could perform a similar role in the lifecycle of other connexin family members. As the sequence and length of the C-terminus of connexin proteins is responsible for much of the variation between different family members (Koval, 2006), it is likely that interaction with Dlg1 is limited to a few connexins. While Cx43 is an α-connexin, Cx32 (which also interacts with Dlg1) is a ß-connexin (Stauch *et al.*, 2012), demonstrating that interaction with Dlg1 is not restricted to a single connexin subfamily. If Dlg1 is found to regulate other connexin family members, interactions between these proteins could be novel therapeutic targets.

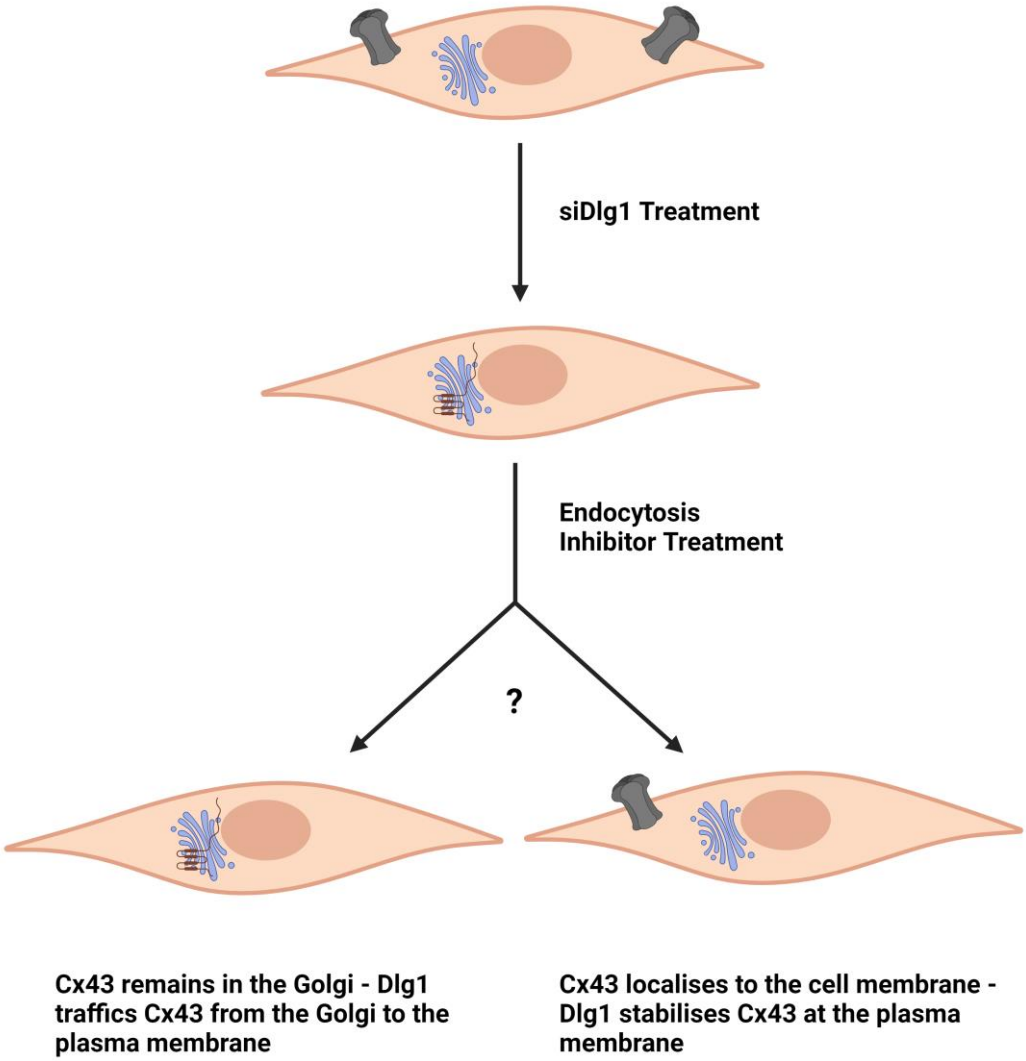

Figure 6.1: A potential experiment using an endocytosis inhibitor to differentiate between the different possible roles of Dlg1 in the Cx43 lifecycle. Figure shows the effects of siDlg1 treatment and possible effects of endocytosis inhibitor treatment on Cx43 localisation. Cx43 is shown either as hemichannels on the cell membrane in grey or a single intracellular Cx43 protein in brown. Cells are shown in beige and the Golgi apparatus is shown in blue. Treatment with siDlg1 removes Cx43 from the cell membrane and causes accumulation of Cx43 in the Golgi. Treatment with an endocytosis inhibitor can either lead to no change in Cx43 localisation (i.e. Cx43 remains in the Golgi) or Cx43 relocating to the cell membrane. If Cx43 remains in the Golgi, it is suggested that it is unable to reach the plasma membrane in the absence of Dlg1 and therefore Dlg1 controls forward trafficking of Cx43 to the plasma membrane. In contrast, if Cx43 is localised to the cell membrane in cells treated with an endocytosis inhibitor, it is suggested that Cx43 is capable of reaching the plasma membrane in the absence of Cx43 and therefore Dlg1 stabilises Cx43 at the cell membrane to prevent swift internalisation of Cx43 and subsequent recycling to the Golgi.

One of the most significant findings from this investigation was that depletion of Dlg1 impaired wound healing in HaCaT cells through reduced cell proliferation **(Chapter 4)**. This result was somewhat counterintuitive given that Dlg1 controls Cx43 cell membrane localisation (which is associated with stalled wound healing) and is a suspected tumour suppressor protein (Brandner *et al.*, 2004; Roberts *et al.*, 2012). This implies that Dlg1 performs other crucial functions in the cell which outweigh the benefit of removal of Cx43 from the cell membrane. For example, Dlg1 (together with CASK) is required for correct orientation of mitotic spindle during cell division in mammalian epithelial cells (Porter *et al.*, 2019). Disruption of this process could lead to incorrect cell division resulting in aneuploid cells, which may subsequently exhibit impaired cell division due to tumour suppressor mechanisms (Thompson and Compton, 2010). The decrease in cell proliferation observed in siDlg1-treated cells could additionally be linked to the functions of Dlg1 in cell polarity and signal transduction. Increased proliferation of Dlg1-depleted cells has been observed in several different cell types, including mouse B-cells (Dong *et al.*, 2019) and mouse lens epithelial cells (Nguyen *et al.*, 2003). This suggests cell-type specific effects of Dlg1, which may be reliant on differential expression of the various Dlg1 splice isoforms which have been proposed to have different functions (McLaughlin *et al.*, 2002). While limited other literature on the effect of Dlg1 in wound healing exists, one study found that knockdown of Dlg1 resulted in ~20% slower wound closure in a squamous lung cancer cell line due to decreased cell migration (O'Neill *et al.*, 2011). Data from this study indicated removal of Dlg1 has negligible effects on cell migration, suggesting promotion of migration may be a cancer cell specific effect. A quantitative analysis of cell migration and direction through live cell experiments would be beneficial in further proving this.

Overall, the results of this investigation suggest that specific targeting of Dlg1 in wound healing may restrict wound closure rates and therefore Dlg1 is not a suitable therapeutic target for epidermal wound healing. It is essential that similar studies are carried out in primary human keratinocytes to verify these results. Such research is especially relevant considering the finding that Cx43 and Dlg1 colocalise in keratinocytes of human abdominal skin sections of both non-diabetic and diabetic patients. While limited changes in the two proteins

were observed in diabetic skin compared to non-diabetic skin, further work is required to determine if disease states where Cx43 signalling is modified are associated with changes in Dlg1 levels, localisation or association with Cx43.

Despite removal of Dlg1 likely being detrimental to wound healing, the interaction between Cx43 and Dlg1 remains a promising therapeutic target. Development of a mimetic peptide to the binding sites of Cx43 with Dlg1 could prevent Cx43 plasma membrane localisation without drastically altering the important functions Dlg1 possesses. According to the AlphaFold model produced in this study, a mimetic peptide of the main Cx43 interaction region (residues 262-278) may have the additional benefit of preventing interaction with Drebrin, meaning that if these two proteins have overlapping functions in keratinocytes, a further reduction in Cx43 cell membrane localisation would be expected, which could correlate with improved wound closure. It is therefore crucial that future studies determine the accuracy of the Cx43/Dlg1 AlphaFold complex model through experimental analysis, as characterisation of interacting regions between the two proteins can inform mimetic peptide development, as has been the case for the successful Cx43-targeting peptide αCT1 (Montgomery *et al.*, 2018). This is currently planned to be performed using microscale thermophoresis (MST), which can measure binding affinity through determination of dissociation constant (Jerabek-Willemsen *et al.*, 2014). Furthermore, binding of small peptides is also able to be assessed, meaning individual prospective interacting regions can be generated and tested for binding to Dlg1. Initial experiments will involve testing of a peptide based on the sequence of interaction site B with full-length Dlg1 to provide information on whether the main α-helical region of the Cx43 C-terminus is important for Dlg1 binding. Preliminary results from co-IP experiments using wild-type Cx43 C-terminus and a deletion of site B expression constructs suggest that this site could be important for Dlg1 interaction (data not shown), however this experiment must be repeated to draw accurate conclusions.

Study of Cx43 and Dlg1 is complicated through several factors, including the channel/non-channel roles of Cx43, the existence of Cx43 internally-translated isoforms, Dlg1 splicing variants and post-translational modifications of the two

proteins. In particular, the role of phosphorylation is predicted to be important for Cx43 binding to Dlg1 given the plethora of ways in which it is already known to modulate Cx43 function and localisation (Solan and Lampe, 2014). The plasmids containing phospho-mimetic mutations of the Cx43 C-terminus will be useful in future experiments to determine how phosphorylation at specific sites affects interaction with Dlg1. Information from these experiments can be combined with existing data from mutants which mimic unphosophorylated residues to give a more comprehensive understanding of the role of phosphorylation in interaction of the two proteins (Dong, 2021). This may additionally give clues as to the function of the interaction, as phosphorylation at certain sites is associated with certain stages of the Cx43 lifecycle. Phosphorylation of Dlg1 is also likely to impact interaction with Cx43. Indeed, phosphorylation of Dlg1 at residue S232 by CaMKII has been shown to regulate its interaction with other proteins, such as the NR2A subunit of NMDA receptor in neuronal cells (Gardoni *et al.*, 2003). Furthermore, phosphorylation has previously been shown to control localisation of Dlg1 to the cell membrane (Massimi *et al.*, 2006).

As well as phosphorylation, Cx43 has been reported to undergo ubiquitination, SUMOylation, acetylation and S-nitrosylation (Leithe *et al.*, 2018). Though less research has focused on these modifications, ubiquitination has been suggested to regulate Cx43 gap junction turnover and sorting to either the autophagic or endolysosomal systems of degradation. For example, the NEDD4 ubiquitin ligase binds to Cx43 between residues 283-286 and promotes degradation via the autophagic pathway (Spagnol *et al.*, 2016), while interaction with Tsg101 instead targets Cx43 to the lysosomal pathway (Leithe *et al.*, 2009). Given that regulation of Cx43 is thought to involve a complex combination of phosphorylation and ubiquitination, it is highly likely that Dlg1 binding affects these processes in some way. Identification of specific sites of ubiquitination in the future will be significant in establishing how these systems synergise to regulate Cx43/Dlg1 interaction.

While the primary focus of this thesis has been on epidermal wound healing, the interaction between Cx43 and Dlg1 also has implications for viral infections. A growing number of viruses are being shown to cause downregulation of Cx43, including Zika virus (Li *et al.*, 2022), Borna disease virus (Köster-Patzlaff, Hosseini and Reuss, 2007) and SARS-CoV-2 (Raghavan, Kenchappa and Leo, 2021). Conversely, HIV causes upregulation of Cx43 through its Tat protein and also utilises gap junctions in tunnelling nanotubes to allow cell-cell spread of the virus (Berman *et al.*, 2016; Okafo *et al.*, 2017). Design of mimetic peptides to inhibit the interaction of Cx43 and Dlg1 may therefore also be applicable as drug treatments for viral infections which result in the upregulation of Cx43. Previously, the Graham group has focused on the relevance of Cx43/Dlg1 interaction in HPV-associated cancer progression, with the oncogenic E6 protein being responsible for degradation of Dlg1 and relocation of Cx43 from the cell membrane to the cytoplasm (Sun *et al.*, 2015). It is currently unknown whether targeting the Cx43/Dlg1 interaction could have therapeutic benefit in this scenario. In certain other types of cancer overexpression of Cx43 restores some level of growth control, such as in the human osteosarcoma U2OS cell line (Zhang *et al.*, 2001). While the majority of research on protein-protein interactions has focused on the use of interaction inhibitors, treatments can also be designed to instead stabilise interactions through binding to regions which are uninvolved in the interaction and altering the conformation of the protein (Lu *et al.*, 2020). This approach could be used to positively modulate Cx43 and Dlg1 interaction, particularly if the intramolecular interactions between Dlg1 SH3 and GUK domains are found to be a regulator of binding to Cx43. Agents which stabilise the Cx43/Dlg1 interaction could result in less degradation of Cx43 and inhibit cell proliferation in HPV-positive cervical cancer cells. On the other hand, as the interaction between E6 and Cx43 is thought to be mediated by Dlg1, it may be beneficial to inhibit Cx43/Dlg1 interaction to prevent degradation of Cx43 through an E6-mediated effect. Indeed, as Dlg1 was proposed to maintain a cytoplasmic pool of Cx43 in HPV-infected cells (MacDonald *et al.*, 2012), inhibition of this interaction may allow recycling of Cx43 to the plasma membrane.

In conclusion, this investigation has shown that Dlg1 plays an important role in the normal wound healing process in keratinocytes and therefore knock down impairs wound closure, suggesting Dlg1 in itself is not a viable therapeutic target to improve chronic wound healing rates. The function of Dlg1 in the normal lifecycle of Cx43 in keratinocytes has also been further characterised. This contributes to understanding of the complex Cx43 lifecycle. Furthermore, AlphaFold has been utilised to predict binding sites between the two proteins, which now require experimental testing to confirm. Identification of binding sites may lead to future development of agents to modulate the interaction of Cx43 and Dlg1 and improve wound healing rates.

References

Aasen, T, Hodgins, MB, Edward, M and Graham, S V. (2003), The relationship between connexins, gap junctions, tissue architecture and tumour invasion, as studied in a novel in vitro model of HPV-16-associated cervical cancer progression, *Oncogene*, 22, (39), Oncogene, pp. 7969–7980.

Aasen, T, Johnstone, S, Vidal-Brime, L, Lynn, KS and Koval, M (2018), Connexins: Synthesis, Post-Translational Modifications, and Trafficking in Health and Disease, *International Journal of Molecular Sciences*, 19, (5), Multidisciplinary Digital Publishing Institute (MDPI).

Aasen, T, Leithe, E, Graham, S V., Kameritsch, P, Mayán, MD, Mesnil, M, Pogoda, K and Tabernero, A (2019a), Connexins in cancer: bridging the gap to the clinic, *Oncogene*, Nature Publishing Group, pp. 4429–4451.

Aasen, T, Sansano, I, Montero, MÁ, Romagosa, C, Temprana-Salvador, J, Martínez-Marti, A, Moliné, T, Hernández-Losa, J and y Cajal, SR (2019b), Insight into the Role and Regulation of Gap Junction Genes in Lung Cancer and Identification of Nuclear Cx43 as a Putative Biomarker of Poor Prognosis, *Cancers*, 11, (3), Multidisciplinary Digital Publishing Institute (MDPI), p. 320.

Abdo, JM, Sopko, NA and Milner, SM (2020), The applied anatomy of human skin: A model for regeneration, *Wound Medicine*, 28, Elsevier, p. 100179.

Ai, Z, Fischer, A, Spray, DC, Brown, AMC and Fishman, GI (2000), Wnt-1 regulation of connexin43 in cardiac myocytes, *Journal of Clinical Investigation*, 105, (2), American Society for Clinical Investigation, p. 161.

Ambrosi, C, Ren, C, Spagnol, G, Cavin, G, Cone, A, Grintsevich, EE, Sosinsky, GE and Sorgen, PL (2016), Connexin43 Forms Supramolecular Complexes through Non-Overlapping Binding Sites for Drebrin, Tubulin, and ZO-1, *PLoS ONE*, 11, (6), PLOS.

Andolfi, C, Tiribelli, C and Pascut, D (2022), Recent Hints on the Dual Role of Discs Large MAGUK Scaffold Protein 5 in Cancers and in Hepatocellular Carcinoma, *Frontiers in Bioscience - Landmark*, 27, (5), Bioscience Research Institute, p. 164.

Anon (n.d.), Genotype-Tissue Expression (GTEx) Common Fund Project, viewed 29 July, 2023a, <https://www.bgee.org/experiment/SRP012682>.

Anon (n.d.), Incucyte ® 96-Well Scratch Wound Cell Migration and Invasion Assays User Manual Contents.

Aoki, K and Taketo, MM (2007), Adenomatous polyposis coli (APC): a multi-functional tumor suppressor gene, *Journal of Cell Science*, 120, (19), The Company of Biologists, pp. 3327–3335.

Asaba, N, Hanada, T, Takeuchi, A and Chishti, AH (2003), Direct interaction with a kinesin-related motor mediates transport of mammalian discs large tumor suppressor homologue in epithelial cells, *Journal of Biological Chemistry*, 278, (10), Elsevier, pp. 8395–8400.

Au, A, Shao, Q, White, KK, Lucaciu, SA, Esseltine, JL, Barr, K and Laird, DW (2020), Comparative Analysis of Cx31 and Cx43 in Differentiation-Competent Rodent Keratinocytes, *Biomolecules*, 10, (10), Multidisciplinary Digital Publishing Institute (MDPI), pp. 1–22.

Ávalos-Díaz, E and Esparza, RH (2013), Dermatological autoimmune diseases, El Rosario University Press.

Axelsen, LN, Calloe, K, Holstein-Rathlou, N-H and Nielsen, MS (2013), Managing the complexity of communication: regulation of gap junctions by post-translational modification, *Frontiers in Pharmacology*, 4, Frontiers Media SA.

Basheer, WA, Xiao, S, Epifantseva, I, Fu, Y, Kleber, AG, Hong, TT and Shaw, RM (2017), GJA1-20k Arranges Actin to Guide Cx43 Delivery to Cardiac Intercalated Discs, *Circulation research*, 121, (9), NIH Public Access, p. 1069.

Batra, N, Riquelme, MA, Burra, S and Jiang, JX (2014), 14-3-3θ facilitates plasma membrane delivery and function of mechanosensitive connexin 43 hemichannels, *Journal of Cell Science*, 127, (1), Company of Biologists, pp. 137–146.

van Bavel, C, Thiels, W and Jelier, R (2023), Cell shape characterization, alignment, and comparison using FlowShape, *Bioinformatics*, 39, (6), Oxford Academic.

Becker, DL, Thrasivoulou, C and Phillips, ARJ (2012), Connexins in wound healing; Perspectives in diabetic patients, *Biochimica et Biophysica Acta - Biomembranes*, Elsevier, pp. 2068–2075.

Berman, JW, Carvallo, L, Buckner, CM, Luers, A, Prevedel, L, Bennett, M V. and Eugenin, EA (2016), HIV-tat alters Connexin43 expression and trafficking in human astrocytes: Role in NeuroAIDS, *Journal of Neuroinflammation*, 13, (1), BioMed Central Ltd., pp. 1–11.

Berthoud, VM, Minogue, PJ, Laing, JG and Beyer, EC (2004), Pathways for degradation of connexins and gap junctions, *Cardiovascular Research*, 62, (2), Oxford Academic, pp. 256–267.

Beyer, EC, Paul, DL and Goodenough, DA (1987), Connexin43: a protein from rat heart homologous to a gap junction protein from liver, *The Journal of cell biology*, 105, (6 Pt 1), J Cell Biol, pp. 2621–2629.

Bilder, D, Li, M and Perrimon, N (2000), Cooperative regulation of cell polarity and growth by Drosophila tumor suppressors, *Science*, 289, (5476), American Association for the Advancement of Science, pp. 113–116.

Bonifacino, JS and Traub, LM (2003), SIGNALS FOR SORTING OF TRANSMEMBRANE PROTEINS TO ENDOSOMES AND LYSOSOMES *, *Annu. Rev. Biochem*, 72, pp. 395–447.

Boon, SS and Banks, L (2013), High-Risk Human Papillomavirus E6 Oncoproteins Interact with 14-3-3ζ in a PDZ Binding Motif-Dependent Manner, *Journal of Virology*, 87, (3), American Society for Microbiology (ASM), p. 1586.

Boukamp, P, Petrussevska, RT, Breitkreutz, D, Hornung, J, Markham, A and Fusenig, NE (1988), Normal keratinization in a spontaneously immortalized aneuploid human keratinocyte cell line, *Journal of Cell Biology*, 106, (3), J Cell Biol, pp. 761–771.

Boulton, AJM and Whitehouse, RW (2020), The Diabetic Foot, *Endotext*, MDText.com, Inc.

Brandmaier, A, Hou, SQ and Shen, WH (2017), Cell cycle control by PTEN, *Journal of molecular biology*, 429, (15), NIH Public Access, p. 2265.

Brandner, JM, Houdek, P, Hüsing, B, Kaiser, C and Moll, I (2004), Connexins 26, 30, and 43: Differences Among Spontaneous, Chronic, and Accelerated Human Wound Healing, *Journal of Investigative Dermatology*, 122, (5), Elsevier, pp. 1310–1320.

Bruzzone, S, Guida, L, Zocchi, E, Franco, L and Flora, A De (2001), Connexin 43 hemichannels mediate Ca2+-regulated transmembrane NAD+ fluxes in intact cells, *The FASEB Journal*, 15, (1), Wiley, pp. 10–12.

Butkevich, E, Hülsmann, S, Wenzel, D, Shirao, T, Duden, R and Majoul, I (2004), Drebrin Is a Novel Connexin-43 Binding Partner that Links Gap Junctions to the Submembrane Cytoskeleton, *Current Biology*, 14, (8), Cell Press, pp. 650–658.

Cabral-Pacheco, GA, Garza-Veloz, I, Rosa, CCD La, Ramirez-Acuña, JM, Perez-Romero, BA, Guerrero-Rodriguez, JF, Martinez-Avila, N and Martinez-Fierro, ML (2020), The Roles of Matrix Metalloproteinases and Their Inhibitors in Human Diseases, *International Journal of Molecular Sciences*, 21, (24), Multidisciplinary Digital Publishing Institute (MDPI), pp. 1–53.

Van Campenhout, CA, Eitelhuber, A, Gloeckner, CJ, Giallonardo, P, Gegg, M, Oller, H, Grant, SGN, Krappmann, D, Ueffing, M and Lickert, H (2011), Dlg3 Trafficking and Apical Tight Junction Formation Is Regulated by Nedd4 and Nedd4-2 E3 Ubiquitin Ligases, *Developmental Cell*, 21, (3), Elsevier, p. 479.

Carette, D, Gilleron, J, Denizot, JP, Grant, K, Pointis, G and Segretain, D (2015), New cellular mechanisms of gap junction degradation and recycling, *Biology of the Cell*, 107, (7), Wiley-Blackwell Publishing Ltd, pp. 218–231.

del Castillo, FJ, Cohen-Salmon, M, Charollais, A, Caille, D, Lampe, PD, Chavrier, P, Meda, P and Petit, C (2010), Consortin, a trans-Golgi network cargo receptor for the plasma membrane targeting and recycling of connexins, *Human Molecular Genetics*, 19, (2), Oxford University Press, p. 262.

Chang, M and Nguyen, TT (2021), Strategy for Treatment of Infected Diabetic Foot Ulcers, *Accounts of Chemical Research*, 54, (5), American Chemical Society, pp. 1080–1093.

Chapple, SDJ, Crofts, AM, Shadbolt, SP, McCafferty, J and Dyson, MR (2006), Multiplexed expression and screening for recombinant protein production in mammalian cells, *BMC Biotechnology*, 6, (1), BioMed Central, pp. 1–15.

Charles, CA, Tomic-Canic, M, Vincek, V, Nassiri, M, Stojadinovic, O, Eaglstein, WH and Kirsner, RS (2008), A GENE SIGNATURE OF NON-HEALING VENOUS ULCERS: POTENTIAL DIAGNOSTIC MARKERS, *Journal of the American Academy of Dermatology*, 59, (5), NIH Public Access, p. 758.

Chen, Z and Cole, PA (2015), Synthetic Approaches to Protein Phosphorylation, *Current opinion in chemical biology*, 28, NIH Public Access, p. 115.

Churko, JM and Laird, DW (2013), Gap junction remodeling in skin repair following wounding and disease, *Physiology*, 28, (3), American Physiological Society Bethesda, MD, pp. 190–198.

Cotrina, ML, Lin, JHC, Alves-Rodrigues, A, Liu, S, Li, J, Azmi-Ghadimi, H, Kang, J, Naus, CCG and Nedergaard, M (1998), Connexins regulate calcium signaling by controlling ATP release, *Proceedings of the National Academy of Sciences of the United States of America*, 95, (26), National Academy of Sciences, p. 15735.

Coutinho, P, Qiu, C, Frank, S, Tamber, K and Becker, D (2003), Dynamic changes in connexin expression correlate with key events in the wound healing process, *Cell Biology International*, 27, (7), Academic Press, pp. 525–541.

Di, WL, Rugg, EL, Leigh, IM and Kelsell, DP (2001), Multiple epidermal connexins are expressed in different keratinocyte subpopulations including connexin 31, *The Journal of investigative dermatology*, 117, (4), J Invest Dermatol, pp. 958–964.

Dinh, TL and Veves, A (2005), A review of the mechanisms implicated in the pathogenesis of the diabetic foot, *International Journal of Lower Extremity Wounds*, 4, (3), pp. 154–159.

Dong, L (2021), hDlg controls the trafficking of gap junction protein Cx43 in normal keratinocytes and human papillomavirus-positive tumour cells. PhD

Thesis. Glasgow University, viewed 25 November, 2023, <https://theses.gla.ac.uk/82160/7/2021DongLiPhD.pdf>.
Dong, X, Li, X, Liu, C, Xu, K, Shi, Y and Liu, W (2019), Discs large homolog 1 regulates B-cell proliferation and antibody production, *International Immunology*, 31, (12), Oxford Academic, pp. 759–770.
Donnelly, S, English, G, De Zwart-Storm, EA, Lang, S, Van Steensel, MAM and Martin, PE (2012), Differential susceptibility of Cx26 mutations associated with epidermal dysplasias to peptidoglycan derived from Staphylococcus aureus and Staphylococcus epidermidis, *Experimental Dermatology*, 21, (8), pp. 592–598.
Duffy, HS, Iacobas, I, Hotchkiss, K, Hirst-Jensen, BJ, Bosco, A, Dandachi, N, Dermietzel, R, Sorgen, PL and Spray, DC (2007), The Gap Junction Protein Connexin32 Interacts with the Src Homology 3/Hook Domain of Discs Large Homolog 1 *, *THE JOURNAL OF BIOLOGICAL CHEMISTRY*, 282, (13), pp. 9789–9796.
Dunham, B, Liu, S, Taffet, S, Trabka-Janik, E, Delmar, M, Petryshyn, R, Zheng, S, Perzova, R and Vallano, ML (1992), Immunolocalization and expression of functional and nonfunctional cell-to-cell channels from wild-type and mutant rat heart connexin43 cDNA., *Circulation Research*, 70, (6), pp. 1233–1243.
Dunn, CA, Su, V, Lau, AF and Lampe, PD (2012), Activation of Akt, Not Connexin 43 Protein Ubiquitination, Regulates Gap Junction Stability, *The Journal of Biological Chemistry*, 287, (4), American Society for Biochemistry and Molecular Biology, p. 2600.
Echetebu, CO, Ali, M, Izban, MG, MacKay, L and Garfield, RE (1999), Localization of regulatory protein binding sites in the proximal region of human myometrial connexin 43 gene, *Molecular Human Reproduction*, 5, (8), Oxford Academic, pp. 757–766.
Elfgang, C, Eckert, R, Lichtenberg-Fraté, H, Butterweck, A, Traub, O, Klein, RA, Hülser, DF and Willecke, K (1995), Specific permeability and selective formation of gap junction channels in connexin-transfected HeLa cells., *Journal of Cell Biology*, 129, (3), The Rockefeller University Press, pp. 805–817.
Epifantseva, I and Shaw, RM (2018), Intracellular Trafficking Pathways of Cx43 Gap Junction Channels, *Biochimica et biophysica acta*, 1860, (1), NIH Public Access, p. 40.
Epifantseva, I, Xiao, S, Baum, RE, Kléber, AG, Hong, TT and Shaw, RM (2020), An Alternatively Translated Connexin 43 Isoform, GJA1-11k, Localizes to the Nucleus and Can Inhibit Cell Cycle Progression, *Biomolecules 2020, Vol. 10, Page 473*, 10, (3), Multidisciplinary Digital Publishing Institute, p. 473.
Evans, WH, Bultynck, G and Leybaert, L (2012), Manipulating Connexin Communication Channels: Use of Peptidomimetics and the Translational Outputs, *The Journal of Membrane Biology*, 245, (8), Springer, p. 437.
Ezeonwumelu, IJ, Garcia-Vidal, E and Ballana, E (2021), JAK-STAT Pathway: A Novel Target to Tackle Viral Infections, *Viruses*, 13, (12), Multidisciplinary Digital Publishing Institute (MDPI).
Falanga, V (2005), Wound healing and its impairment in the diabetic foot, *The Lancet*, 366, (9498), Elsevier, pp. 1736–1743.
Faniku, C (2018), Connexin43 and Pannexin-1 as potential therapeutic targets for wound healing. PhD Thesis., Glasgow Caledonian University .
Faniku, C, O'Shaughnessy, E, Lorraine, C, Johnstone, SR, Graham, A, Greenhough, S and Martin, PEM (2018), The Connexin Mimetic Peptide

Gap27 and Cx43-Knockdown Reveal Differential Roles for Connexin43 in Wound Closure Events in Skin Model Systems, *International Journal of Molecular Sciences*, 19, (2), Multidisciplinary Digital Publishing Institute (MDPI).

Fenu, M, Bettermann, T, Vogl, C, Darwish-Miranda, N, Schramel, J, Jenner, F and Ribitsch, I (2019), A novel magnet-based scratch method for standardisation of wound-healing assays, *Scientific Reports 2019 9:1*, 9, (1), Nature Publishing Group, pp. 1–9.

Fong, JT, Kells, RM and Falk, MM (2013), Two tyrosine-based sorting signals in the Cx43 C-terminus cooperate to mediate gap junction endocytosis, *Molecular Biology of the Cell*, 24, (18), American Society for Cell Biology, p. 2834.

Fourie, C, Li, D and Montgomery, JM (2014), The anchoring protein SAP97 influences the trafficking and localisation of multiple membrane channels, *Biochimica et Biophysica Acta (BBA) - Biomembranes*, 1838, (2), Elsevier, pp. 589–594.

Frese, KK, Latorre, IJ, Chung, SH, Caruana, G, Bernstein, A, Jones, SN, Donehower, LA, Justice, MJ, Garner, CC and Javier, RT (2006), Oncogenic function for the Dlg1 mammalian homolog of the Drosophila discs-large tumor suppressor, *The EMBO Journal*, 25, (6), European Molecular Biology Organization, p. 1406.

Furmanová, K, Byška, J, Gröller, EM, Viola, I, Paleček, JJ and Kozlíková, B (2018), COZOID: Contact zone identifier for visual analysis of protein-protein interactions, *BMC Bioinformatics*, 19, (1), BioMed Central Ltd., pp. 1–17.

Gad, SE (2014), Mitomycin C, *Encyclopedia of Toxicology: Third Edition*, Academic Press, pp. 354–356.

Gao, RJ, Zhang, AM, Jia, QH, Dang, ZT, Tian, T, Zhang, JR, Cao, N, Tang, XC, Ma, KT, Li, L and Si, JQ (2021), The promoting role of Cx43 on the proliferation and migration of arterial smooth muscle cells for angiotensin II-dependent hypertension, *Pulmonary Pharmacology & Therapeutics*, 70, Academic Press, p. 102072.

García, IE, Prado, P, Pupo, A, Jara, O, Rojas-Gómez, D, Mujica, P, Flores-Muñoz, C, González-Casanova, J, Soto-Riveros, C, Pinto, BI, Retamal, MA, González, C and Martínez, AD (2016), Connexinopathies: A structural and functional glimpse, *BMC Cell Biology*, 17, (1), BioMed Central, pp. 71–87.

Garcia-Vega, L, O'shaughnessy, EM, Albuloushi, A and Martin, PE (2021), Connexins and the Epithelial Tissue Barrier: A Focus on Connexin 26, *Biology 2021, Vol. 10, Page 59*, 10, (1), Multidisciplinary Digital Publishing Institute, p. 59.

Gardiol, D, Kühne, C, Glaunsinger, B, Lee, SS, Javier, R and Banks, L (1999), Oncogenic human papillomavirus E6 proteins target the discs large tumour suppressor for proteasome-mediated degradation, *Oncogene 1999 18:40*, 18, (40), Nature Publishing Group, pp. 5487–5496.

Gardoni, F, Mauceri, D, Fiorentini, C, Bellone, C, Missale, C, Cattabeni, F and Di Luca, M (2003), CaMKII-dependent Phosphorylation Regulates SAP97/NR2A Interaction, *Journal of Biological Chemistry*, 278, (45), Elsevier, pp. 44745–44752.

Geimonen, E, Jiang, W, Ali, M, Fishman, GI, Garfield, RE and Andersen, J (1996), Activation of protein kinase C in human uterine smooth muscle induces connexin-43 gene transcription through an AP-1 site in the promoter sequence, *Journal of Biological Chemistry*, 271, (39), Elsevier, pp. 23667–23674.

Gemel, J, Simon, AR, Patel, D, Xu, Q, Matiukas, A, Veenstra, RD and Beyer, EC (2014), Degradation of a Connexin40 mutant linked to atrial fibrillation is accelerated, *Journal of molecular and cellular cardiology*, 74, NIH Public Access, p. 330.

Ghatnekar, GS, Grek, CL, Armstrong, DG, Desai, SC and Gourdie, RG (2015), The Effect of a Connexin43-Based Peptide on the Healing of Chronic Venous Leg Ulcers: A Multicenter, Randomized Trial, *Journal of Investigative Dermatology*, 135, (1), Nature Publishing Group, pp. 289–298.

Ghatnekar, GS, O'Quinn, MP, Jourdan, LJ, Gurjarpadhye, AA, Draugh, RL and Gourdie, RG (2009), Connexin43 carboxyl-terminal peptides reduce scar progenitor and promote regenerative healing following skin wounding, *Regenerative medicine*, 4, (2), NIH Public Access, p. 205.

Giepmans, BNG, Hengeveld, T, Postma, FR and Moolenaar, WH (2001a), Interaction of c-Src with gap junction protein connexin-43. Role in the regulation of cell-cell communication, *Journal of Biological Chemistry*, 276, (11), American Society for Biochemistry and Molecular Biology, pp. 8544–8549.

Giepmans, BNG and Moolenaar, WH (1998), The gap junction protein connexin43 interacts with the second PDZ domain of the zona occludens-1 protein, *Current Biology*, 8, (16), Cell Press, pp. 931–934.

Giepmans, BNG, Verlaan, I, Hengeveld, T, Janssen, H, Calafat, J, Falk, MM and Moolenaar, WH (2001b), Gap junction protein connexin-43 interacts directly with microtubules, *Current Biology*, 11, (17), Cell Press, pp. 1364–1368.

Giepmans, BNG, Verlaan, I and Moolenaar, WH (2009), Connexin-43 Interactions with ZO-1 and α- and ß-tubulin, *http://dx.doi.org/10.3109/15419060109080727*, 8, (4–6), Taylor & Francis, pp. 219–223.

Girão, H, Catarino, S and Pereira, P (2009), Eps15 interacts with ubiquitinated Cx43 and mediates its internalization, *Experimental Cell Research*, 315, (20), Academic Press, pp. 3587–3597.

Golebiewska, EM and Poole, AW (2015), Platelet secretion: From haemostasis to wound healing and beyond, *Blood Reviews*, 29, (3), Elsevier, p. 153.

Goliger, JA and Paul, DL (1995), Wounding Alters Epidermal Connexin Expression and Gap Junction-mediated Intercellular Communication, *Molecular Biology of the Cell*, 6, pp. 1491–1501.

Gonzalez, ACDO, Andrade, ZDA, Costa, TF and Medrado, ARAP (2016), Wound healing - A literature review, *Anais Brasileiros de Dermatologia*, 91, (5), Sociedade Brasileira de Dermatologia, p. 614.

González-Sánchez, A, Jaraíz-Rodríguez, M, Domínguez-Prieto, M, Herrero-González, S, Medina, JM, Tabernero, A, González-Sánchez, A, Jaraíz-Rodríguez, M, Domínguez-Prieto, M, Herrero-González, S, Medina, JM and Tabernero, A (2016), Connexin43 recruits PTEN and Csk to inhibit c-Src activity in glioma cells and astrocytes, *Oncotarget*, 7, (31), Impact Journals, pp. 49819–49833.

Goodenough, DA, Goliger, JA and Paul, DL (1996), Connexins, connexons, and intercellular communication, *Annual review of biochemistry*, 65, Annu Rev Biochem, pp. 475–502.

Graham, S V. (2017), The human papillomavirus replication cycle, and its links to cancer progression: a comprehensive review, *Clinical Science*, 131, (17), Portland Press, pp. 2201–2221.

Grant, BD and Donaldson, JG (2009), Pathways and mechanisms of endocytic recycling, *Nature Reviews Molecular Cell Biology 2009 10:9*, 10, (9), Nature Publishing Group, pp. 597–608.

Guest, JF, Fuller, GW and Vowden, P (2020), Cohort study evaluating the burden of wounds to the UK's National Health Service in 2017/2018: update from 2012/2013, *BMJ Open*, 10, (12), British Medical Journal Publishing Group, p. e045253.

Guo, H, Acevedo, P, Parsa, FD and Bertram, JS (1992), Gap-Junctional Protein Connexin 43 Is Expressed in Dermis and Epidermis of Human Skin: Differential Modulation by Retinoids, *Journal of Investigative Dermatology*, 99, (4), Elsevier, pp. 460–467.

Guo, HB, Perminov, A, Bekele, S, Kedziora, G, Farajollahi, S, Varaljay, V, Hinkle, K, Molinero, V, Meister, K, Hung, C, Dennis, P, Kelley-Loughnane, N and Berry, R (2022), AlphaFold2 models indicate that protein sequence determines both structure and dynamics, *Scientific Reports*, 12, (1), Nature Publishing Group, p. 10696.

Gupta, P, Uner, OE, Nayak, S, Grant, GR and Kalb, RG (2018), SAP97 regulates behavior and expression of schizophrenia risk enriched gene sets in mouse hippocampus, *PLoS ONE*, 13, (7), PLOS.

Hardman, G, Perkins, S, Brownridge, PJ, Clarke, CJ, Byrne, DP, Campbell, AE, Kalyuzhnyy, A, Myall, A, Eyers, PA, Jones, AR and Eyers, CE (2019), Strong anion exchange-mediated phosphoproteomics reveals extensive human non-canonical phosphorylation, *The EMBO Journal*, 38, (21), European Molecular Biology Organization.

Hay, RJ, Johns, NE, Williams, HC, Bolliger, IW, Dellavalle, RP, Margolis, DJ, Marks, R, Naldi, L, Weinstock, MA, Wulf, SK, Michaud, C, J.l. Murray, C and Naghavi, M (2014), The global burden of skin disease in 2010: An analysis of the prevalence and impact of skin conditions, *Journal of Investigative Dermatology*, 134, (6), Nature Publishing Group, pp. 1527–1534.

Hernandez, M, Shao, Q, Yang, XJ, Luh, SP, Kandouz, M, Batist, G, Laird, DW and Alaoui-Jamali, MA (2006), A histone deacetylation-dependent mechanism for transcriptional repression of the gap junction gene cx43 in prostate cancer cells, *Prostate*, 66, (11), pp. 1151–1161.

Hesketh, GG, Van Eyk, JE and Tomaselli, GF (2009), Mechanisms of Gap Junction Traffic in Health and Disease, *Journal of cardiovascular pharmacology*, 54, (4), NIH Public Access, p. 263.

Howard Evans, W and Leybaert, L (2009), Mimetic Peptides as Blockers of Connexin Channel-Facilitated Intercellular Communication, *http://dx.doi.org/10.1080/15419060801891034*, 14, (6), Taylor & Francis, pp. 265–273.

Hulkower, KI and Herber, RL (2011), Cell Migration and Invasion Assays as Tools for Drug Discovery, *Pharmaceutics*, 3, (1), Multidisciplinary Digital Publishing Institute (MDPI), p. 107.

Hunter, AW, Jourdan, J and Gourdie, RG (2003), Cell Communication & Adhesion Fusion of GFP to the Carboxyl Terminus of Connexin43 Increases Gap Junction Size in HeLa Cells Fusion of GFP to the Carboxyl Terminus of Connexin43 Increases Gap Junction Size in HeLa Cells, *Cell Communication and Adhesion*, 10, pp. 211–214.

Iizuka-Kogo, A, Shimomura, A and Senda, T (2005), Colocalization of APC and DLG at the tips of cellular protrusions in cultured epithelial cells and its dependency on cytoskeletons, *Histochemistry and Cell Biology*, 123, (1), Springer, pp. 67–73.

Iqbal, A, Jan, A, Wajid, MA and Tariq, S (2017), Management of Chronic Non-healing Wounds by Hirudotherapy, *World Journal of Plastic Surgery*, 6, (1), Iran Society of Plastic, Reconstructive and Aesthetic Surgeons, p. 9.
Iyyathurai, J, Wang, N, D'hondt, C, Jiang, JX, Leybaert, L and Bultynck, G (2018), The SH3-binding domain of Cx43 participates in loop/tail interactions critical for Cx43-hemichannel activity, *Cellular and molecular life sciences : CMLS*, 75, (11), NIH Public Access, p. 2059.
James, CD and Roberts, S (2016), Viral interactions with PDZ domain-containing proteins—An oncogenic trait?, *Pathogens*, 5, (1), MDPI AG, pp. 1–22.
Jerabek-Willemsen, M, André, T, Wanner, R, Roth, HM, Duhr, S, Baaske, P and Breitsprecher, D (2014), MicroScale Thermophoresis: Interaction analysis and beyond, *Journal of Molecular Structure*, 1077, Elsevier, pp. 101–113.
Johnson, RG, Meyer, RA, Li, XR, Preus, DM, Tan, L, Grunenwald, H, Paulson, AF, Laird, DW and Sheridan, JD (2002), Gap Junctions Assemble in the Presence of Cytoskeletal Inhibitors, but Enhanced Assembly Requires Microtubules, *Experimental Cell Research*, 275, (1), Academic Press, pp. 67–80.
Jordan, K, Chodock, R, Hand, AR and Laird, DW (2001), The origin of annular junctions: a mechanism of gap junction internalization, *Journal of Cell Science*, 114, (4), The Company of Biologists, pp. 763–773.
Jumper, J, Evans, R, Pritzel, A, Green, T, Figurnov, M, Ronneberger, O, Tunyasuvunakool, K, Bates, R, Žídek, A, Potapenko, A, Bridgland, A, Meyer, C, Kohl, SAA, Ballard, AJ, Cowie, A, Romera-Paredes, B, Nikolov, S, Jain, R, Adler, J, Back, T, Petersen, S, Reiman, D, Clancy, E, Zielinski, M, Steinegger, M, Pacholska, M, Berghammer, T, Bodenstein, S, Silver, D, Vinyals, O, Senior, AW, Kavukcuoglu, K, Kohli, P and Hassabis, D (2021), Highly accurate protein structure prediction with AlphaFold, *Nature 2021 596:7873*, 596, (7873), Nature Publishing Group, pp. 583–589.
Kameritsch, P, Kiemer, F, Beck, H, Pohl, U and Pogoda, K (2015), Cx43 increases serum induced filopodia formation via activation of p21-activated protein kinase 1, *Biochimica et Biophysica Acta (BBA) - Molecular Cell Research*, 1853, (11), Elsevier, pp. 2907–2917.
Kamibayashi, Y, Oyamada, M, Oyamada, Y and Mori, M (1993), Expression of gap junction proteins connexin 26 and 43 is modulated during differentiation of keratinocytes in newborn mouse epidermis, *The Journal of investigative dermatology*, 101, (6), J Invest Dermatol, pp. 773–778.
Kjenseth, A, Fykerud, TA, Sirnes, S, Bruun, J, Yohannes, Z, Kolberg, M, Omori, Y, Rivedal, E and Leithe, E (2012), The Gap Junction Channel Protein Connexin 43 Is Covalently Modified and Regulated by SUMOylation, *The Journal of Biological Chemistry*, 287, (19), American Society for Biochemistry and Molecular Biology, p. 15851.
Ko, K, Arora, P, Lee, W and McCulloch, C (2000), Biochemical and functional characterization of intercellular adhesion and gap junctions in fibroblasts, *American Journal of Physiology - Cell Physiology*, 279, (1 48-1), American Physiological Society, pp. 147–157.
Kobayashi, H and Fukuda, M (2013), Arf6, Rab11 and transferrin receptor define distinct populations of recycling endosomes, *Communicative & Integrative Biology*, 6, (5), Taylor & Francis.
Köster-Patzlaff, C, Hosseini, SM and Reuss, B (2007), Persistent Borna Disease Virus infection changes expression and function of astroglial gap junctions in vivo and in vitro, *Brain Research*, 1184, (1), Elsevier, pp. 316–332.
Koval, M (2006), Pathways and control of connexin oligomerization, *Trends in Cell Biology*, Elsevier, pp. 159–166.

Koval, M, Molina, SA and Burt, JM (2014), Mix and match: Investigating heteromeric and heterotypic gap junction channels in model systems and native tissues, *FEBS Letters*, 588, (8), John Wiley & Sons, Ltd, pp. 1193–1204.

Kretz, M, Euwens, C, Hombach, S, Eckardt, D, Teubner, B, Traub, O, Willecke, K and Ott, T (2003), Altered connexin expression and wound healing in the epidermis of connexin-deficient mice, *Journal of Cell Science*, The Company of Biologists Ltd, pp. 3443–3452.

Krishna Subbaiah, V, Massimi, P, Boon, SS, Myers, MP, Sharek, L, Garcia-Mata, R and Banks, L (2012), The Invasive Capacity of HPV Transformed Cells Requires the hDlg-Dependent Enhancement of SGEF/RhoG Activity, *PLoS Pathogens*, 8, (2), PLOS, p. 1002543.

Krzyszczyk, P, Schloss, R, Palmer, A and Berthiaume, F (2018), The Role of Macrophages in Acute and Chronic Wound Healing and Interventions to Promote Pro-wound Healing Phenotypes, *Frontiers in Physiology*, 9, (MAY), Frontiers Media SA, p. 419.

Laird, DW (2006), Life cycle of connexins in health and disease, *Biochemical Journal*, Portland Press Ltd, pp. 527–543.

Laird, DW and Lampe, PD (2018), Therapeutic strategies targeting connexins, *Nature reviews. Drug discovery*, 17, (12), NIH Public Access, p. 905.

Laird, DW, Puranam, KL and Revel, J-P (1991), Turnover and phosphorylation dynamics of connexin43 gap junction protein in cultured cardiac myocytes, *Biochem. J*, 273, pp. 67–72.

Lampe, PD, TenBroek, EM, Burt, JM, Kurata, WE, Johnson, RG and Lau, AF (2000), Phosphorylation of Connexin43 on Serine368 by Protein Kinase C Regulates Gap Junctional Communication, *The Journal of Cell Biology*, 149, (7), The Rockefeller University Press, p. 1503.

Landén, NX, Li, D and Ståhle, M (2016), Transition from inflammation to proliferation: a critical step during wound healing, *Cellular and Molecular Life Sciences*, 73, (20), Springer, p. 3861.

Langlois, S, Maher, AC, Manias, JL, Shao, Q, Kidder, GM and Laird, DW (2007), Connexin levels regulate keratinocyte differentiation in the epidermis, *Journal of Biological Chemistry*, 282, (41), Elsevier, pp. 30171–30180.

Laprise, P, Viel, A and Rivard, N (2004), Human Homolog of Disc-large Is Required for Adherens Junction Assembly and Differentiation of Human Intestinal Epithelial Cells, *Journal of Biological Chemistry*, 279, (11), American Society for Biochemistry and Molecular Biology Inc., pp. 10157–10166.

Lauf, U, Giepmans, BNG, Lopez, P, Braconnot, S, Chen, SC and Falk, MM (2002), Dynamic trafficking and delivery of connexons to the plasma membrane and accretion to gap junctions in living cells, *Proceedings of the National Academy of Sciences of the United States of America*, 99, (16), National Academy of Sciences, pp. 10446–10451.

Lee, S, Fan, S, Makarova, O, Straight, S and Margolis, B (2002), A Novel and Conserved Protein-Protein Interaction Domain of Mammalian Lin-2/CASK Binds and Recruits SAP97 to the Lateral Surface of Epithelia, *Molecular and Cellular Biology*, 22, (6), Taylor & Francis, p. 1778.

Leithe, E, Kjenseth, A, Sirnes, S, Stenmark, H, Brech, A and Rivedal, E (2009), Ubiquitylation of the gap junction protein connexin-43 signals its trafficking from early endosomes to lysosomes in a process mediated by Hrs and Tsg101, *Journal of Cell Science*, 122, (21), The Company of Biologists, pp. 3883–3893.

Leithe, E, Mesnil, M and Aasen, T (2018), The connexin 43 C-terminus: A tail of many tales, *Biochimica et Biophysica Acta (BBA) - Biomembranes*, 1860, (1), Elsevier, pp. 48–64.
Leithe, E and Rivedal, E (2004a), Epidermal growth factor regulates ubiquitination, internalization and proteasome-dependent degradation of connexin43, *Journal of Cell Science*, 117, (7), The Company of Biologists, pp. 1211–1220.
Leithe, E and Rivedal, E (2004b), Ubiquitination and down-regulation of gap junction protein connexin-43 in response to 12-O-tetradecanoylphorbol 13-acetate treatment, *The Journal of biological chemistry*, 279, (48), J Biol Chem, pp. 50089–50096.
Leykauf, K, Salek, M, Bomke, J, Frech, M, Lehmann, WD, Dürst, M and Alonso, A (2006), Ubiquitin protein ligase Nedd4 binds to connexin43 by a phosphorylation-modulated process, *Journal of Cell Science*, 119, (17), The Company of Biologists, pp. 3634–3642.
Li, K, Chi, Y, Gao, K, Yan, Q, Matsue, H, Takeda, M, Kitamura, M and Yao, J (2013), Connexin43 Hemichannel-Mediated Regulation of Connexin43, *PLOS ONE*, 8, (2), Public Library of Science, p. e58057.
Li, S, Armstrong, N, Zhao, H, Cruz-cosme, R, Yang, H, Zhong, C, Fu, W, Wang, W, Yang, D, Xia, N, Cheng, T and Tang, Q (2022), Zika Virus Infection Downregulates Connexin 43, Disrupts the Cardiomyocyte Gap Junctions and Induces Heart Diseases in A129 Mice, *Journal of Virology*, 96, (21), American Society for Microbiology (ASM).
Li, X, Pan, JH, Song, B, Xiong, EQ, Chen, ZW, Zhou, ZS and Su, YP (2012), Suppression of CX43 expression by miR-20a in the progression of human prostate cancer, *Cancer Biology and Therapy*, 13, (10), Taylor & Francis, pp. 890–898.
Li, X, Su, V, Kurata, WE, Jin, C and Lau, AF (2008), A novel connexin43-interacting protein, CIP75, which belongs to the UbL-UBA protein family, regulates the turnover of connexin43, *Journal of Biological Chemistry*, 283, (9), Elsevier, pp. 5748–5759.
Lobmann, R, Ambrosch, A, Schultz, G, Waldmann, K, Schiweck, S and Lehnert, H (2002), Expression of matrix-metalloproteinases and their inhibitors in the wounds of diabetic and non-diabetic patients, *Diabetologia*, 45, (7), Springer, pp. 1011–1016.
Loewenstein, WR, Nakas, M and Socolar, SJ (1967), Junctional Membrane Uncoupling : Permeability transformations at a cell membrane junction, *The Journal of General Physiology*, 50, (7), The Rockefeller University Press, p. 1865.
Lohia, M, Qin, Y and Macara, IG (2012), The Scribble Polarity Protein Stabilizes E-Cadherin/p120-Catenin Binding and Blocks Retrieval of E-Cadherin to the Golgi, *PLoS ONE*, 7, (11), PLOS, p. 51130.
Lu, H, Zhou, Q, He, J, Jiang, Z, Peng, C, Tong, R and Shi, J (2020), Recent advances in the development of protein–protein interactions modulators: mechanisms and clinical trials, *Signal Transduction and Targeted Therapy 2020 5:1*, 5, (1), Nature Publishing Group, pp. 1–23.
Lue, RA, Marfatia, SM, Branton, D and Chishti, AH (1994), Cloning and characterization of hdlg: the human homologue of the Drosophila discs large tumor suppressor binds to protein 4.1., *Proceedings of the National Academy of Sciences of the United States of America*, 91, (21), National Academy of Sciences, p. 9818.

MacDonald, AI, Sun, P, Hernandez-Lopez, H, Aasen, T, Hodgins, MB, Edward, M, Roberts, S, Massimi, P, Thomas, M, Banks, L and Graham, S V. (2012), A functional interaction between the MAGUK protein hDlg and the gap junction protein connexin 43 in cervical tumour cells, *Biochemical Journal*, 446, (1), pp. 9–21.

MacLeod, AS and Mansbridge, JN (2016), The Innate Immune System in Acute and Chronic Wounds, *Advances in Wound Care*, 5, (2), Mary Ann Liebert, Inc., p. 65.

Makino, K, Kuwahara, H, Masuko, N, Nishiyama, Y, Morisaki, T, Sasaki, JI, Nakao, M, Kuwano, A, Nakata, M, Ushio, Y and Saya, H (1997), Cloning and characterization of NE-dlg: a novel human homolog of the Drosophila discs large (dlg) tumor suppressor protein interacts with the APC protein, *Oncogene 1997 14:20*, 14, (20), Nature Publishing Group, pp. 2425–2433.

Márquez-Rosado, L, Singh, D, Rincón-Arano, H, Solan, JL and Lampe, PD (2012), CASK (LIN2) interacts with Cx43 in wounded skin and their coexpression affects cell migration, *Journal of Cell Science*, 125, (3), Company of Biologists, pp. 695–702.

Marshall, CD, Hu, MS, Leavitt, T, Barnes, LA, Lorenz, HP and Longaker, MT (2018), Cutaneous Scarring: Basic Science, Current Treatments, and Future Directions, *Advances in Wound Care*, 7, (2), Mary Ann Liebert, Inc., p. 29.

Martin, P (1997), Wound healing - Aiming for perfect skin regeneration, *Science*, 276, (5309), American Association for the Advancement of Science, pp. 75–81.

Martin, PEM, Blundell, G, Ahmad, S, Errington, RJ and Evans, WH (2001), Multiple pathways in the trafficking and assembly of connexin 26, 32 and 43 into gap junction intercellular communication channels, *Journal of Cell Science*, 114, (21), The Company of Biologists, pp. 3845–3855.

Marziali, F, Valdano, MB, Avalos, CB, Moriena, L, Cavatorta, AL and Gardiol, D (2017), Interference of HTLV-1 Tax Protein with Cell Polarity Regulators: Defining the Subcellular Localization of the Tax-DLG1 Interaction, *Viruses*, 9, (12), Multidisciplinary Digital Publishing Institute (MDPI).

Massimi, P, Narayan, N, Cuenda, A and Banks, L (2006), Phosphorylation of the discs large tumour suppressor protein controls its membrane localisation and enhances its susceptibility to HPV E6-induced degradation, *Oncogene 2006 25:31*, 25, (31), Nature Publishing Group, pp. 4276–4285.

Massimi, P, Narayan, N, Thomas, M, Gammoh, N, Strand, S, Strand, D and Banks, L (2008), Regulation of the hDlg/hScrib/Hugl-1 tumour suppressor complex, *Experimental Cell Research*, 314, (18), Academic Press, pp. 3306–3317.

Massimi, P, Zori, P, Roberts, S and Banks, L (2012), Differential Regulation of Cell-Cell Contact, Invasion and Anoikis by hScrib and hDlg in Keratinocytes, *PLoS ONE*, 7, (7), PLOS.

Masson-Meyers, DS, Andrade, TAM, Caetano, GF, Guimaraes, FR, Leite, MN, Leite, SN and Frade, MAC (2020), Experimental models and methods for cutaneous wound healing assessment, *International Journal of Experimental Pathology*, 101, (1–2), John Wiley & Sons, Ltd, pp. 21–37.

Matsuuchi, L and Naus, CC (2013), Gap junction proteins on the move: Connexins, the cytoskeleton and migration, *Biochimica et Biophysica Acta (BBA) - Biomembranes*, 1828, (1), Elsevier, pp. 94–108.

Mattila, PK and Lappalainen, P (2008), Filopodia: molecular architecture and cellular functions, *Nature Reviews Molecular Cell Biology 2008 9:6*, 9, (6), Nature Publishing Group, pp. 446–454.

Mazzalupo, S, Wong, P, Martin, P and Coulombe, PA (2003), Role for keratins 6 and 17 during wound closure in embryonic mouse skin, *Developmental Dynamics*, 226, (2), John Wiley & Sons, Ltd, pp. 356–365.
McCann, JJ, Zheng, L, Rohrbeck, D, Felekyan, S, Kühnemuth, R, Sutton, RB, Seidel, CAM and Bowen, ME (2012), Supertertiary structure of the synaptic MAGuK scaffold proteins is conserved, *Proceedings of the National Academy of Sciences of the United States of America*, 109, (39), National Academy of Sciences, pp. 15775–15780.
McLachlan, E, Plante, I, Shao, Q, Tong, D, Kidder, GM, Bernier, SM and Laird, DW (2008), ODDD-Linked Cx43 Mutants Reduce Endogenous Cx43 Expression and Function in Osteoblasts and Inhibit Late Stage Differentiation, *Journal of Bone and Mineral Research*, 23, (6), John Wiley & Sons, Ltd, pp. 928–938.
McLaughlin, M, Hale, R, Ellston, D, Gaudet, S, Lue, RA and Viel, A (2002), The distribution and function of alternatively spliced insertions in hDlg, *Journal of Biological Chemistry*, 277, (8), Elsevier, pp. 6406–6412.
McNeil, E, Capaldo, CT and Macara, IG (2006), Zonula Occludens-1 Function in the Assembly of Tight Junctions in Madin-Darby Canine Kidney Epithelial Cells, *Molecular Biology of the Cell*, 17, (4), American Society for Cell Biology, p. 1922.
Meraviglia, V, Azzimato, V, Colussi, C, Florio, MC, Binda, A, Panariti, A, Qanud, K, Suffredini, S, Gennaccaro, L, Miragoli, M, Barbuti, A, Lampe, PD, Gaetano, C, Pramstaller, PP, Capogrossi, MC, Recchia, FA, Pompilio, G, Rivolta, I and Rossini, A (2015), Acetylation mediates Cx43 reduction caused by electrical stimulation, *Journal of Molecular and Cellular Cardiology*, 87, Academic Press, pp. 54–64.
Misinzo, G, Delputte, PL and Nauwynck, HJ (2008), Inhibition of Endosome-Lysosome System Acidification Enhances Porcine Circovirus 2 Infection of Porcine Epithelial Cells, *Journal of Virology*, 82, (3), American Society for Microbiology, pp. 1128–1135.
Montgomery, J, Ghatnekar, GS, Grek, CL, Moyer, KE and Gourdie, RG (2018), Connexin 43-based therapeutics for dermal wound healing, *International Journal of Molecular Sciences*, MDPI AG, p. 1778.
Mori, K, Iwao, K, Miyoshi, Y, Nakagawara, A, Kofu, K, Akiyama, T, Arita, N, Hayakawa, T and Nakamura, Y (1998), Identification of brain-specific splicing variants of the hDLG1 gene and altered splicing in neuroblastoma cell lines, *Journal of human genetics*, 43, (2), J Hum Genet, pp. 123–127.
Mori, R, Power, KT, Wang, CM, Martin, P and Becker, DL (2006), Acute downregulation of connexin43 at wound sites leads to a reduced inflammatory response, enhanced keratinocyte proliferation and wound fibroblast migration, *Journal of Cell Science*, 119, (24), The Company of Biologists, pp. 5193–5203.
Mori, S, Tezuka, Y, Arakawa, A, Handa, N, Shirouzu, M, Akiyama, T and Yokoyama, S (2013), Crystal structure of the guanylate kinase domain from discs large homolog 1 (DLG1/SAP97), *Biochemical and Biophysical Research Communications*, 435, (3), Academic Press, pp. 334–338.
Morley, GE, Taffet, SM and Delmar, M (1996), lntramolecular Interactions Mediate pH Regulation of Connexin43 Channels, *Biophysical Journal*, 70, pp. 1294–1302.
Murray, PJ and Wynn, TA (2011), Protective and pathogenic functions of macrophage subsets, *Nature reviews. Immunology*, 11, (11), NIH Public Access, p. 723.

Nadarajah, B, Jones, AM, Evans, WH and Parnavelas, JG (1997), Differential Expression of Connexins during Neocortical Development and Neuronal Circuit Formation, *Journal of Neuroscience*, 17, (9), Society for Neuroscience, pp. 3096–3111.
Nakagawa, T, Futai, K, Lashuel, HA, Lo, I, Okamoto, K, Walz, T, Hayashi, Y and Sheng, M (2004), Quaternary structure, protein dynamics, and synaptic function of SAP97 controlled by L27 domain interactions, *Neuron*, 44, (3), Elsevier, pp. 453–467.
Narayan, N, Massimi, P and Banks, L (2009), CDK phosphorylation of the discs large tumour suppressor controls its localisation and stability, *Journal of Cell Science*, 122, (1), The Company of Biologists, pp. 65–74.
Newman, RA and Prehoda, KE (2009), Intramolecular Interactions Between the Src Homology 3 Guanylate Kinase Domains of Discs Large Regulate Its Function in Asymmetric Cell Division, *Journal of Biological Chemistry*, 284, (19), Elsevier, pp. 12924–12932.
Nguyen, MM, Nguyen, ML, Caruana, G, Bernstein, A, Lambert, PF and Griep, AE (2003), Requirement of PDZ-Containing Proteins for Cell Cycle Regulation and Differentiation in the Mouse Lens Epithelium, *Molecular and Cellular Biology*, 23, (24), Taylor & Francis, p. 8970.
Ochalski, PAY, Sawchuk, MA, Hertzberg, EL and Nagy, JI (1995), Astrocytic gap junction removal, connexin43 redistribution, and epitope masking at excitatory amino acid lesion sites in rat brain, *Glia*, 14, (4), pp. 279–294.
Ofran, Y and Rost, B (2003), Predicted protein–protein interaction sites from local sequence information, *FEBS Letters*, 544, (1–3), John Wiley & Sons, Ltd, pp. 236–239.
Okafo, G, Prevedel, L and Eugenin, E (2017), Tunneling nanotubes (TNT) mediate long-range gap junctional communication: Implications for HIV cell to cell spread, *Scientific Reports 2017 7:1*, 7, (1), Nature Publishing Group, pp. 1–9.
Oliva, C and Sierralta, J (2018), MAGUK, *Encyclopedia of Signaling Molecules*, Springer, Cham, pp. 2918–2924.
O'Neill, AK, Gallegos, LL, Justilien, V, Garcia, EL, Leitges, M, Fields, AP, Hall, RA and Newton, AC (2011), Protein Kinase Cα Promotes Cell Migration through a PDZ-Dependent Interaction with its Novel Substrate Discs Large Homolog 1 (DLG1), *The Journal of Biological Chemistry*, 286, (50), American Society for Biochemistry and Molecular Biology, p. 43559.
Opneja, A, Kapoor, S and Stavrou, EX (2019), Contribution of Platelets, the Coagulation and Fibrinolytic Systems to Cutaneous Wound Healing., *Thrombosis research*, 179, NIH Public Access, p. 56.
Von Ossowski, I, Oksanen, E, Von Ossowski, L, Cai, C, Sundberg, M, Goldman, A and Keinänen, K (2006), Crystal structure of the second PDZ domain of SAP97 in complex with a GluR-A C-terminal peptide, *The FEBS Journal*, 273, (22), John Wiley & Sons, Ltd, pp. 5219–5229.
Oyamada, M, Takebe, K and Oyamada, Y (2013), Regulation of connexin expression by transcription factors and epigenetic mechanisms, *Biochimica et Biophysica Acta (BBA) - Biomembranes*, 1828, (1), Elsevier, pp. 118–133.
Ozog, MA, Bernier, SM, Bates, DC, Chatterjee, B, Lo, CW and Naus, CCG (2004), The Complex of Ciliary Neurotrophic Factor-Ciliary Neurotrophic Factor Receptor α Up-Regulates Connexin43 and Intercellular Coupling in Astrocytes via the Janus Tyrosine Kinase/Signal Transducer and Activator of Transcription Pathway, *Molecular Biology of the Cell*, 15, (11), American Society for Cell Biology, p. 4761.

Pace, NP, Benoit, V, Agius, D, Grima, MA, Parascandalo, R, Hilbert, P and Borg, I (2019), Two novel GJA1 variants in oculodentodigital dysplasia, *Molecular Genetics & Genomic Medicine*, 7, (9), Wiley-Blackwell.

Park, DJ, Wallick, CJ, Martyn, KD, Lau, AF, Jin, C and Warn-Cramer, BJ (2007), Akt phosphorylates connexin43 on Ser373, a 'Mode-1' binding site for 14-3-3, *Cell Communication and Adhesion*, 14, (5), pp. 211–226.

Peracchia, C (2004), Chemical gating of gap junction channels: Roles of calcium, pH and calmodulin, *Biochimica et Biophysica Acta (BBA) - Biomembranes*, 1662, (1–2), Elsevier, pp. 61–80.

Pettersen, EF, Goddard, TD, Huang, CC, Meng, EC, Couch, GS, Croll, TI, Morris, JH and Ferrin, TE (2021), UCSF ChimeraX: Structure visualization for researchers, educators, and developers, *Protein Science : A Publication of the Protein Society*, 30, (1), Wiley-Blackwell, p. 70.

Vande Pol, SB and Klingelhutz, AJ (2013), Papillomavirus E6 oncoproteins, *Virology*, 445, (1–2), Academic Press, pp. 115–137.

Pollok, S, Pfeiffer, AC, Lobmann, R, Wright, CS, Moll, I, Martin, PEM and Brandner, JM (2011), Connexin 43 mimetic peptide Gap27 reveals potential differences in the role of Cx43 in wound repair between diabetic and non-diabetic cells, *Journal of Cellular and Molecular Medicine*, 15, (4), Wiley-Blackwell, p. 861.

Porter, AP, White, GRM, Mack, NA and Malliri, A (2019), The interaction between CASK and the tumour suppressor Dlg1 regulates mitotic spindle orientation in mammalian epithelia, *Journal of Cell Science*, 132, (14), Company of Biologists Ltd.

Puranam, KL, Laird, DW and Revel, JP (1993), Trapping an Intermediate Form of Connexin43 in the Golgi, *Experimental Cell Research*, 206, (1), Academic Press, pp. 85–92.

Qian, Y and Prehoda, KE (2006), INTERDOMAIN INTERACTIONS IN THE TUMOR SUPPRESSOR DISCS LARGE REGULATE BINDING TO THE SYNAPTIC PROTEIN GUKHOLDER, *The Journal of biological chemistry*, 281, (47), NIH Public Access, p. 35757.

Qin, H, Shao, Q, Igdoura, SA, Alaoui-Jamali, MA and Laird, DW (2003), Lysosomal and proteasomal degradation play distinct roles in the life cycle of Cx43 in gap junctional intercellular communication-deficient and -competent breast tumor cells, *Journal of Biological Chemistry*, 278, (32), American Society for Biochemistry and Molecular Biology Inc., pp. 30005–30014.

Qiu, C, Coutinho, P, Frank, S, Franke, S, Law, L-Y, Martin, P, Green, CR and Becker, DL (2003), Targeting Connexin43 Expression Accelerates the Rate of Wound Repair, *Current Biology*, 13, pp. 1697–1703.

Radstake, WE, Gautam, K, Van Rompay, C, Vermeesen, R, Tabury, K, Verslegers, M, Baatout, S and Baselet, B (2023), Comparison of in vitro scratch wound assay experimental procedures, *Biochemistry and Biophysics Reports*, 33, Elsevier, p. 101423.

Raghavan, S, Kenchappa, DB and Leo, MD (2021), SARS-CoV-2 Spike Protein Induces Degradation of Junctional Proteins That Maintain Endothelial Barrier Integrity, *Frontiers in Cardiovascular Medicine*, 8, Frontiers, p. 687783.

Rawlings, JS, Rosler, KM and Harrison, DA (2004), The JAK/STAT signaling pathway, *Journal of Cell Science*, 117, (8), The Company of Biologists, pp. 1281–1283.

Reissner, C and Missler, M (2014), MAGUKs end a tale of promiscuity, *Proceedings of the National Academy of Sciences of the United States of America*, 111, (49), National Academy of Sciences, p. 17350.

Reuver, SM and Garner, CC (1998), E-cadherin mediated cell adhesion recruits SAP97 into the cortical cytoskeleton, *Journal of Cell Science*, 111, (8), The Company of Biologists, pp. 1071–1080.
Rhett, JM, Jourdan, J and Gourdie, RG (2011), Connexin 43 connexon to gap junction transition is regulated by zonula occludens-1, *Molecular Biology of the Cell*, 22, (9), The American Society for Cell Biology , pp. 1516–1528.
Ribeiro-Rodrigues, TM, Martins-Marques, T, Morel, S, Kwak, BR and Girão, H (2017), Role of connexin 43 in different forms of intercellular communication - gap junctions, extracellular vesicles and tunnelling nanotubes, *Journal of Cell Science*, 130, (21), Company of Biologists Ltd, pp. 3619–3630.
Richards, TS, Dunn, CA, Carter, WG, Usui, ML, Olerud, JE and Lampe, PD (2004), Protein kinase C spatially and temporally regulates gap junctional communication during human wound repair via phosphorylation of connexin43 on serine368, *The Journal of Cell Biology*, 167, (3), The Rockefeller University Press, p. 555.
Rivedal, E, Mollerup, S, Haugen, A and Vikhamar, G (1996), Modulation of gap junctional intercellular communication by EGF in human kidney epithelial cells, *Carcinogenesis*, 17, (11), Carcinogenesis, pp. 2321–2328.
Roberts, S, Calautti, E, Vanderweil, S, Nguyen, HO, Foley, A, Baden, HP and Viel, A (2007), Changes in localization of human discs large (hDlg) during keratinocyte differentiation is associated with expression of alternatively spliced hDlg variants.
Roberts, S, Delury, C and Marsh, E (2012), The PDZ protein discs-large (DLG): the 'Jekyll and Hyde' of the epithelial polarity proteins, *The FEBS Journal*, 279, (19), John Wiley & Sons, Ltd, pp. 3549–3558.
Ron, S, Ron, I, Rathaus, M, Livne, R and Tirosh, A (2022), 1395-P: The Role of Adipocyte Connexin-43 in Mediating Adipose Tissue Inflammation and Dysfunction in Obesity, *Diabetes*, 71, (Supplement_1), American Diabetes Association.
Round, JL, Tomassian, T, Zhang, M, Patel, V, Schoenberger, SP and Miceli, MC (2005), Dlgh1 coordinates actin polymerization, synaptic T cell receptor and lipid raft aggregation, and effector function in T cells, *The Journal of Experimental Medicine*, 201, (3), The Rockefeller University Press, p. 419.
Ruff, KM and Pappu, R V. (2021), AlphaFold and Implications for Intrinsically Disordered Proteins, *Journal of Molecular Biology*, 433, (20), Academic Press, p. 167208.
Sabio, G, Cerezo-Guisado, MI, Del Reino, P, Iñesta-Vaquera, FA, Rousseau, S, Arthur, JSC, Campbell, DG, Centeno, F and Cuenda, A (2010), p38γ regulates interaction of nuclear PSF and RNA with the tumour-suppressor hDlg in response to osmotic shock, *Journal of Cell Science*, 123, (15), Company of Biologists, p. 2596.
Saidi Brikci-Nigassa, A, Clement, MJ, Ha-Duong, T, Adjadj, E, Ziani, L, Pastre, D, Curmi, PA and Savarin, P (2012), Phosphorylation controls the interaction of the connexin43 C-terminal domain with tubulin and microtubules, *Biochemistry*, 51, (21), American Chemical Society, pp. 4331–4342.
Salomon, D, Masgrau, E, Vischer, S, Ullrich, S, Dupont, E, Sappino, P, Saurat, JH and Meda, P (1994), Topography of Mammalian Connexins in Human Skin, *Journal of Investigative Dermatology*, 103, (2), Elsevier, pp. 240–247.
Sambandam, SAT, Kasetti, RB, Xue, L, Dean, DC, Lu, Q and Li, Q (2015), 14-3-3σ regulates keratinocyte proliferation and differentiation by modulating Yap1

cellular localization, *The Journal of investigative dermatology*, 135, (6), NIH Public Access, p. 1621.
Schilrreff, P and Alexiev, U (2022), Chronic Inflammation in Non-Healing Skin Wounds and Promising Natural Bioactive Compounds Treatment, *International Journal of Molecular Sciences 2022, Vol. 23, Page 4928*, 23, (9), Multidisciplinary Digital Publishing Institute, p. 4928.
Schindelin, J, Arganda-Carreras, I, Frise, E, Kaynig, V, Longair, M, Pietzsch, T, Preibisch, S, Rueden, C, Saalfeld, S, Schmid, B, Tinevez, JY, White, DJ, Hartenstein, V, Eliceiri, K, Tomancak, P and Cardona, A (2012), Fiji: an open-source platform for biological-image analysis, *Nature Methods 2012 9:7*, 9, (7), Nature Publishing Group, pp. 676–682.
Schultz, GS, Chin, GA, Moldawer, L and Diegelmann, RF (2011), Principles of Wound Healing, *Diabetic Foot Problems*, University of Adelaide Press, pp. 395–402.
Scott, H, Dong, L, Stevenson, A, MacDonald, AI, Srinivasan, S, Massimi, P, Banks, L, Martin, PE, Johnstone, SR and Graham, S V. (2023), The human discs large protein 1 interacts with and maintains connexin 43 at the plasma membrane in keratinocytes, *Journal of Cell Science*, 136, (11), The Company of Biologists.
Seaman, MNJ (2012), The retromer complex – endosomal protein recycling and beyond, *Journal of Cell Science*, 125, (20), Company of Biologists, p. 4693.
Segretain, D and Falk, MM (2004), Regulation of connexin biosynthesis, assembly, gap junction formation, and removal, *Biochimica et Biophysica Acta - Biomembranes*, 1662, (1–2), Biochim Biophys Acta, pp. 3–21.
Sharma, M, Leung, L, Brocardo, M, Henderson, J, Flegg, C and Henderson, BR (2006), Membrane localization of adenomatous polyposis coli protein at cellular protrusions: Targeting sequences and regulation by β-catenin, *Journal of Biological Chemistry*, 281, (25), Elsevier, pp. 17140–17149.
Shaw, RM, Fay, AJ, Puthenveedu, MA, von Zastrow, M, Jan, YN and Jan, LY (2007), Microtubule Plus-End-Tracking Proteins Target Gap Junctions Directly from the Cell Interior to Adherens Junctions, *Cell*, 128, (3), Elsevier B.V., pp. 547–560.
Shearer, LJ and Petersen, NO (2019), Distribution and Co-localization of endosome markers in cells, *Heliyon*, 5, (9), Elsevier, p. e02375.
Shirao, T and Sekino, Y (2017), General introduction to Drebrin, *Advances in Experimental Medicine and Biology*, 1006, Springer New York LLC, pp. 3–22.
Singh, D and Lampe, PD (2003), Identification of connexin-43 interacting proteins, *Cell Communication and Adhesion*, 10, (4–6), Taylor and Francis Inc., pp. 215–220.
Smyth, JW, Hong, TT, Gao, D, Vogan, JM, Jensen, BC, Fong, TS, Simpson, PC, Stainier, DYR, Chi, NC and Shaw, RM (2010), Limited forward trafficking of connexin 43 reduces cell-cell coupling in stressed human and mouse myocardium, *The Journal of Clinical Investigation*, 120, (1), American Society for Clinical Investigation, p. 266.
Smyth, JW and Shaw, RM (2013), Autoregulation of Connexin43 Gap Junction Formation by Internally Translated Isoforms, *Cell Reports*, 5, (3), Cell Press, pp. 611–618.
Smyth, JW, Zhang, SS, Sanchez, JM, Lamouille, S, Vogan, JM, Hesketh, GG, Hong, T, Tomaselli, GF and Shaw, RM (2014), A 14-3-3 Mode-1 Binding Motif Initiates Gap Junction Internalization during Acute Cardiac Ischemia, *Traffic (Copenhagen, Denmark)*, 15, (6), NIH Public Access, p. 684.

Solan, JL and Lampe, PD (2009), CONNEXIN 43 PHOSPHORYLATION – STRUCTURAL CHANGES AND BIOLOGICAL EFFECTS, *The Biochemical journal*, 419, (2), NIH Public Access, p. 261.

Solan, JL and Lampe, PD (2018), Spatio-temporal regulation of connexin43 phosphorylation and gap junction dynamics, *Biochimica et Biophysica Acta (BBA) - Biomembranes*, 1860, (1), Elsevier, pp. 83–90.

Solan, JL and Lampe, PD (2014), Specific Cx43 phosphorylation events regulate gap junction turnover in vivo, *FEBS letters*, 588, (8), NIH Public Access, p. 1423.

Song, MS, Salmena, L and Pandolfi, PP (2012), The functions and regulation of the PTEN tumour suppressor, *Nature Reviews Molecular Cell Biology 2012 13:5*, 13, (5), Nature Publishing Group, pp. 283–296.

Sorgen, PL, Duffy, HS, Sahoo, P, Coombs, W, Delmar, M and Spray, DC (2004), Structural Changes in the Carboxyl Terminus of the Gap Junction Protein Connexin43 Indicates Signaling between Binding Domains for c-Src and Zonula Occludens-1* □ S, JBC Papers in Press.

Sotelo, NS, Valiente, M, Gil, A and Pulido, R (2012), A functional network of the tumor suppressors APC, hDlg, and PTEN, that relies on recognition of specific PDZ-domains, *Journal of Cellular Biochemistry*, 113, (8), John Wiley & Sons, Ltd, pp. 2661–2670.

Spagnol, G, Kieken, F, Kopanic, JL, Li, H, Zach, S, Stauch, KL, Grosely, R and Sorgen, PL (2016), Structural Studies of the Nedd4 WW Domains and Their Selectivity for the Connexin43 (Cx43) Carboxyl Terminus *.

Spagnol, G, Trease, AJ, Zheng, L, Gutierrez, M, Basu, I, Sarmiento, C, Moore, G, Cervantes, M and Sorgen, PL (2018), Connexin43 Carboxyl-Terminal Domain Directly Interacts with ß-Catenin, *International Journal of Molecular Sciences*, 19, (6), Multidisciplinary Digital Publishing Institute (MDPI).

Stauch, K, Kieken, F and Sorgen, P (2012), Characterization of the Structure and Intermolecular Interactions between the Connexin 32 Carboxyl-terminal Domain and the Protein Partners Synapse-associated Protein 97 and Calmodulin, *The Journal of Biological Chemistry*, 287, (33), American Society for Biochemistry and Molecular Biology, p. 27771.

Sterling, J, Stanley, M, Gatward, G and Minson, T (1990), Production of human papillomavirus type 16 virions in a keratinocyte cell line., *Journal of Virology*, 64, (12), American Society for Microbiology (ASM), p. 6305.

Stout, RF, Snapp, EL and Spray, DC (2015), Connexin Type and Fluorescent Protein Fusion Tag Determine Structural Stability of Gap Junction Plaques, *The Journal of Biological Chemistry*, 290, (39), American Society for Biochemistry and Molecular Biology, p. 23497.

Su, V, Hoang, C, Geerts, D and Lau, AF (2014), CIP75 (connexin43-interacting protein of 75 kDa) mediates the endoplasmic reticulum dislocation of connexin43, *Biochemical Journal*, 458, (1), Portland Press, pp. 57–67.

Su, WH, Mruk, DD, Wong, EWP, Lui, WY and Cheng, CY (2012), Polarity Protein Complex Scribble/Lgl/Dlg and Epithelial Cell Barriers, *Advances in experimental medicine and biology*, 763, NIH Public Access, p. 149.

Suarez-Arnedo, A, Figueroa, FT, Clavijo, C, Arbeláez, P, Cruz, JC and Muñoz-Camargo, C (2020), An image J plugin for the high throughput image analysis of in vitro scratch wound healing assays, *PLOS ONE*, 15, (7), Public Library of Science, p. e0232565.

Sun, P, Dong, L, MacDonald, AI, Akbari, S, Edward, M, Hodgins, MB, Johnstone, SR and Graham, S V. (2015), HPV16 E6 controls the gap junction protein Cx43 in cervical tumour cells, *Viruses*, 7, (10), MDPI AG, pp. 5243–5256.

Sutcliffe, JES, Chin, KY, Thrasivoulou, C, Serena, TE, O'Neil, S, Hu, R, White, AM, Madden, L, Richards, T, Phillips, ARJ and Becker, DL (2015), Abnormal connexin expression in human chronic wounds, *British Journal of Dermatology*, 173, (5), Oxford Academic, pp. 1205–1215.

Suzuki, T, Ohsugi, Y, Uchida-Toita, M, Akiyama, T and Yoshida, M (1999), Tax oncoprotein of HTLV-1 binds to the human homologue of Drosophila discs large tumor suppressor protein, hDLG, and perturbs its function in cell growth control, *Oncogene 1999 18:44*, 18, (44), Nature Publishing Group, pp. 5967–5972.

Tadvalkar, G and Pinto da Silva, P (1983), In vitro, rapid assembly of gap junctions is induced by cytoskeleton disruptors, *The Journal of cell biology*, 96, (5), J Cell Biol, pp. 1279–1287.

Tamada, M, Perez, TD, Nelson, WJ and Sheetz, MP (2007), Two distinct modes of myosin assembly and dynamics during epithelial wound closure, *The Journal of Cell Biology*, 176, (1), The Rockefeller University Press, p. 27.

Thomas, M, Dasgupta, J, Zhang, Y, Chen, X and Banks, L (2008), Analysis of specificity determinants in the interactions of different HPV E6 proteins with their PDZ domain-containing substrates, *Virology*, 376, (2), Academic Press, pp. 371–378.

Thomas, M, Myers, MP, Massimi, P, Guarnaccia, C and Banks, L (2016), Analysis of Multiple HPV E6 PDZ Interactions Defines Type-Specific PDZ Fingerprints That Predict Oncogenic Potential, *PLoS Pathogens*, 12, (8), PLOS.

Thompson, SL and Compton, DA (2010), Proliferation of aneuploid human cells is limited by a p53-dependent mechanism, *The Journal of Cell Biology*, 188, (3), The Rockefeller University Press, p. 369.

Totland, MZ, Rasmussen, NL, Knudsen, LM and Leithe, E (2020), Regulation of gap junction intercellular communication by connexin ubiquitination: physiological and pathophysiological implications, *Cellular and Molecular Life Sciences*, 77, (4), Springer, p. 573.

Toyofuku, T, Akamatsu, Y, Zhang, H, Kuzuya, T, Tada, M and Hori, M (2001), c-Src regulates the interaction between connexin-43 and ZO-1 in cardiac myocytes, *Journal of Biological Chemistry*, 276, (3), Elsevier, pp. 1780–1788.

Toyofuku, T, Yabuki, M, Otsu, K, Kuzuya, T, Hori, M and Tada, M (1998), Direct association of the gap junction protein connexin-43 with ZO-1 in cardiac myocytes, *Journal of Biological Chemistry*, 273, (21), Elsevier, pp. 12725–12731.

Unno, K, Hanada, T and Chishti, AH (2008), Functional involvement of human discs large tumor suppressor in cytokinesis, *Experimental cell research*, 314, (17), NIH Public Access, p. 3118.

Vanderpuye, OA, Bell, CL and Murray, SA (2016), REDISTRIBUTION OF CONNEXIN 43 DURING CELL DIVISION, *Cell biology international*, 40, (4), NIH Public Access, p. 387.

Vasudevan, S, Vinayaka, CR, Natale, DA, Huang, H, Kahsay, RY and Wu, CH (2011), Structure-Guided Rule-Based Annotation of Protein Functional Sites in UniProt Knowledgebase, *Methods in Molecular Biology*, 694, Humana Press Inc., pp. 91–105.

Te Velthuis, AJW, Admiraal, JF and Bagowski, CP (2007), Molecular evolution of the MAGUK family in metazoan genomes, *BMC Evolutionary Biology*, 7, (1), BioMed Central, pp. 1–10.

Vinken, M (2015), Introduction: Connexins, pannexins and their channels as gatekeepers of organ physiology, *Cellular and Molecular Life Sciences*, Birkhauser Verlag AG, pp. 2775–2778.
Vinken, M (2016), Regulation of connexin signaling by the epigenetic machinery, *Biochimica et biophysica acta*, 1859, (2), Europe PMC Funders, p. 262.
Walch, L (2013), Emerging Role of the Scaffolding Protein Dlg1 in Vesicle Trafficking, *Traffic*, 14, (9), John Wiley & Sons, Ltd, pp. 964–973.
Wang, FF, Li, Y and Liu, HC (2019), Suppression of connexin 43 expression by miR-106a promotes melanoma cell proliferation, *European review for medical and pharmacological sciences*, 23, (3), Eur Rev Med Pharmacol Sci, pp. 911–917.
Wang, N, De Bock, M, Decrock, E, Bol, M, Gadicherla, A, Vinken, M, Rogiers, V, Bukauskas, FF, Bultynck, G and Leybaert, L (2013), Paracrine signaling through plasma membrane hemichannels, *Biochimica et biophysica acta*, 1828, (1), NIH Public Access, p. 35.
Wang, YW, Ren, JH, Xia, K, Wang, SH, Yin, TF, Xie, DH and Li, LH (2012), Effect of mitomycin on normal dermal fibroblast and HaCat cell: an in vitro study, *Journal of Zhejiang University. Science. B*, 13, (12), Zhejiang University Press, p. 997.
Warn-Cramer, BJ, Cottrell, GT, Burt, JM and Lau, AF (1998), Regulation of Connexin-43 Gap Junctional Intercellular Communication by Mitogen-activated Protein Kinase, *Journal of Biological Chemistry*, 273, (15), Elsevier, pp. 9188–9196.
Wickett, R and Visscher, O (2006), Structure and function of the epidermal barrier, *American Journal of Infection Control*, 34, (10), Mosby, pp. S98–S110.
Wilgus, TA, Roy, S and McDaniel, JC (2013), Neutrophils and Wound Repair: Positive Actions and Negative Reactions, *Advances in Wound Care*, 2, (7), Mary Ann Liebert, Inc., p. 379.
Woods, DF and Bryant, PJ (1989), Molecular cloning of the lethal(1)discs large-1 oncogene of Drosophila, *Developmental Biology*, 134, (1), Academic Press, pp. 222–235.
Woods, DF, Hough, C, Peel, D, Callaini, G and Bryant, PJ (1996), Dlg protein is required for junction structure, cell polarity, and proliferation control in Drosophila epithelia, *The Journal of Cell Biology*, 134, (6), The Rockefeller University Press, p. 1469.
Wright, CS, Pollok, S, Flint, DJ, Brandner, JM and Martin, PEM (2012), The connexin mimetic peptide Gap27 increases human dermal fibroblast migration in hyperglycemic and hyperinsulinemic conditions in vitro, *Journal of Cellular Physiology*, 227, (1), John Wiley & Sons, Ltd, pp. 77–87.
Wright, CS, Van Steensel, MAM, Hodgins, MB and Martin, PEM (2009), Connexin mimetic peptides improve cell migration rates of human epidermal keratinocytes and dermal fibroblasts in vitro, *Wound Repair and Regeneration*, 17, (2), John Wiley & Sons, Ltd, pp. 240–249.
Wu, H, Reissner, C, Kuhlendahl, S, Coblentz, B, Reuver, S, Kindler, S, Gundelfinger, ED and Garner, CC (2000), Intramolecular interactions regulate SAP97 binding to GKAP, *EMBO Journal*, 19, (21), Oxford University Press, pp. 5740–5751.
Wu, H, Reuver, SM, Kuhlendahl, S, Chung, WJ and Garner, CC (1998), Subcellular targeting and cytoskeletal attachment of SAP97 to the epithelial lateral membrane, *Journal of Cell Science*, 111, (16), The Company of Biologists, pp. 2365–2376.

Xavier, R, Rabizadeh, S, Ishiguro, K, Andre, N, Ortiz, JB, Wachtel, H, Morris, DG, Lopez-Ilasaca, M, Shaw, AC, Swat, W and Seed, B (2004), Discs large (Dlg1) complexes in lymphocyte activation, *The Journal of Cell Biology*, 166, (2), The Rockefeller University Press, p. 173.

Xu, Q, Kopp, RF, Chen, Y, Yang, JJ, Roe, MW and Veenstra, RD (2012), Gating of connexin 43 gap junctions by a cytoplasmic loop calmodulin binding domain, *American Journal of Physiology - Cell Physiology*, 302, (10), American Physiological Society, p. C1548.

Yamakawa, S and Hayashida, K (2019), Advances in surgical applications of growth factors for wound healing, *Burns & Trauma 2019 7:1*, 7, (1), BioMed Central, pp. 1–13.

Yeager, M and Gilula, NB (1992), Membrane topology and quaternary structure of cardiac gap junction ion channels, *Journal of Molecular Biology*, 223, (4), Academic Press, pp. 929–948.

Yi, ZC, Wang, H, Zhang, GY and Xia, B (2007), Downregulation of connexin 43 in nasopharyngeal carcinoma cells is related to promoter methylation, *Oral Oncology*, 43, (9), Pergamon, pp. 898–904.

Zhang, X-F and Cui, X (2017), Connexin 43: Key roles in the skin, *Biomedical Reports*, 6, (6), Spandidos Publications, p. 605.

Zhang, Y and Skolnick, J (2004), Scoring function for automated assessment of protein structure template quality, *Proteins: Structure, Function and Genetics*, 57, (4), pp. 702–710.

Zhang, YW, Morita, I, Ikeda, M, Ma, KW and Murota, S (2001), Connexin43 suppresses proliferation of osteosarcoma U2OS cells through post-transcriptional regulation of p27, *Oncogene 2001 20:31*, 20, (31), Nature Publishing Group, pp. 4138–4149.

Zheng, L, Chenavas, S, Kieken, F, Trease, A, Brownell, S, Anbanandam, A, Sorgen, PL and Spagnol, G (2020), Calmodulin Directly Interacts with the Cx43 Carboxyl-Terminus and Cytoplasmic Loop Containing Three ODDD-Linked Mutants (M147T, R148Q, and T154A) that Retain α-Helical Structure, but Exhibit Loss-of-Function and Cellular Trafficking Defects, *Biomolecules*, 10, (10), Multidisciplinary Digital Publishing Institute (MDPI), pp. 1–23.

Zhou, JZ and Jiang, JX (2014), Gap junction and hemichannel-independent actions of connexins on cell and tissue functions – An update, *FEBS letters*, 588, (8), NIH Public Access, p. 1186.

Zhou, L, Kasperek, EM and Nicholson, BJ (1999), Dissection of the Molecular Basis of pp60 v-src Induced Gating of Connexin 43 Gap Junction Channels, *The Journal of Cell Biology*, 144, (5), pp. 1033–1045.

Zhu, J, Shang, Y, Chen, J and Zhang, M (2012), Structure and function of the guanylate kinase-like domain of the MAGUK family scaffold proteins, *Frontiers in Biology 2012 7:5*, 7, (5), Springer, pp. 379–396.

Zihni, C, Mills, C, Matter, K and Balda, MS (2016), Tight junctions: from simple barriers to multifunctional molecular gates, *Nature Reviews Molecular Cell Biology 2016 17:9*, 17, (9), Nature Publishing Group, pp. 564–580.

Zubek, J, Tatjewski, M, Boniecki, A, Mnich, M, Basu, S and Plewczynski, D (2015), Multi-level machine learning prediction of protein–protein interactions in Saccharomyces cerevisiae, *PeerJ*, 3, (7), PeerJ, Inc.

Zurzolo, C (2021), Tunneling nanotubes: Reshaping connectivity, *Current Opinion in Cell Biology*, 71, Elsevier Current Trends, pp. 139–147.